QUANTUM INVESTIGATION OF LASER COOLING AND TRAPPING OF POLARITON AND POLARON IN NANOSTRUCTURES

Clautaire Mwebi Ekengoue

REPUBLIQUE DU CAMEROUN

PAIX-TRAVAIL-PATRIE

****

UNIVERSITE DE DSCHANG

****

ECOLE DOCTORALE

REPUBLIC OF CAMEROON

PEACE-WORK-FATHERLAND

****

UNIVERSITY OF DSCHANG

****

POST GRADUATE SCHOOL

DSCHANG SCHOOL OF SCIENCES AND TECHNOLOGY

Unité de Recherche de Matière Condensée, d'Electronique et de Traitement de Signal (URMACETS)

TOPIC:

QUANTUM INVESTIGATION OF LASER COOLING AND TRAPPING OF POLARITON AND POLARON IN NANOSTRUCTURES

Thesis defended publicly in fulfilment of the requirements for the award of a
Doctorate/Ph.D in Physics
Option: Condensed Matter and Nanomaterials

By
MWEBI EKENGOUE Clautaire
Register number: **CM04-09SCI1009**
Master of Sciences (**MSc**) degree in physics (Condensed Matter)

Under the direction of:

LUKONG Cornelius FAI
Professor

And

the co-direction of:

KENFACK SADEM Christian
Associate Professor

Year 2021

CERTIFICATION

I, the undersigned, **MWEBI EKENGOUE Clautaire**, Registration Number: **CM04-09SCI1009**, hereby certify that this thesis entitled "**Quantum investigation of laser cooling and trapping of polariton and polaron in nanostructures**" is the fruit of my personal research carried out in the « Unité de Recherche de Matière Condensée, d'Electronique et de Traitement de Signal (UR-MACETS) » at the University of Dschang under the direction of Prof. **LUKONG Cornelius FAI** and the co-direction of Prof. **KENFACK SADEM Christian**, in partial fulfillment for the award of the Philosophy Doctorate (PhD) degree in Physics (Option: **Condensed Matter and Nanomaterials**).

This thesis is authentic and has not been previously submitted for a degree or Diploma in any other University

The AUTHOR

M. MWEBI EKENGOUE Clautaire

The CO-DIRECTORS

LUKONG Cornelius FAI
Professor
University of Dschang

KENFACK SADEM Christian
Associate Professor
University of Dschang

DEDICATION

To

EKENGOUE Family *and particularly my lovely sister* ***ETANKI EKENGOUE Charlotte***

ACKNOWLEGEMENTS

The completion of this work ownes very much to many people.

Firstly, I would like to express my sincere gratitude to the Director of this thesis, **Prof. LUKONG Cornelius FAI** for his constant guidance and encouragement without which this work would not have been possible;

Of course, the most important person for the research during my Ph.D years is my supervisor, Co-Director of the present thesis, **Prof. KENFACK SADEM Christian**. We have had a close collaboration always running smoothly. Even though he has been busy as any Senior lecturer, I have never felt as standing still on the same old spot, the help has always been there. Not only when we have worked directly together, he has always been a resource and helpful hand, giving comments and suggestions. Particularly, he has been a spring of inspiration for me and has broadening my horizons in physics;

I am greatful to **Prof. FOTUE Alain Jervé** for his guidance, teaching and collaboration in this research work;

I am also grateful for the many teachers I have had the pleasure to meet along the way, in the Dschang University and particularly within the Physics Department. Special thanks to them. They have made this journey more interesting;

Many thanks to **Prof. UMAKANT D. Rapol**, Associate Professor at the Indian Institute of Science, Education and Resarch (IISER), Pune (India), for his perfect collaboration and guidance. He always answers my questions and makes everythinks to bring a helpful hand thereby contributing to the amelioration of the quality of this research work;

I have had the joy to work with some other people during these years, and they are warmly thanked here: **Dr. EDMOND DANGA Jeremi**, **Dr. MBOGNOU FOBASSO Florette**, **Dr. EKOSSO Christelle**, **M. GUEPNANG Valère**, **M. NGUEMASSON NGALE Charles** and all other lab collaborators who are not named here;

I am grateful to LEKOMO family, especially Father **LEKOMO François** and wife **FOUENGO Marie Noël**, and their children **KOUEMINI MATENKEU Millagros**, **METENEKEU Aimée**, **MEDJOUNDEM YMELE** Williams and **NDIMO Prudence Flora**

without forgetting my friend **KEMGANG LEKOMO Hypolite**, for accepting me as their soon when I was writing the present thesis.

My huge family deserves all possible gratitude, cheering me along climbs and descents. My mother and father, my sisters and brothers**: EKENGOUE Gabriel, KAMENI Madeleine**, **NGWESSE Clovis**, **ESSOUNSOL Marceline**, **MOUNKWA Micheline**, **ETANKI Charlotte**, **MWETEING Floriane**, **ESSELEM Delano**, **MBESSE Ledoux** and **EMAMBO Ginette**. Thanks to my nieces and nephews for their kind attention.

Finally, I presnt my deep gratitude goes to my friends and colleagues, particularly the African Scientific Association for Innovative and Entrepreneurship **(ASAIE)** members for their collaboration and engagement.

Many thanks, to all those who contributed directly or indirectly to the success of this PhD thesis project.

TABLE OF CONTENTS

ABSTRACT

Nowadays, exciton polaritons that arise through the strong coupling between excitons and photons are major candidates to demonstrate a wide array of fundamental phenomena and potential applications that range from Bose-Einstein-like condenstation to analogue Hamiltonian simulators and chip-scale interferometers. In the present thesis, we investigate the effect of surrounding environment on the dynamic of laser cooled and trapped polariton and polaron in nanostructures. We consider the system of interest as a TLS with ground state $|g\rangle$ and first excited state $|e\rangle$. We begin our analysis studying the dynamical behavior of a system of laser cooled and trapped polariton within semi-classical approach. Later, we introduce a magnetic field which we consider as a trap and perform the Vonn Neumann entropy. We found that the probability of finding cooled and trapped polariton in the excited state and energy of the system is controlled by the surrounding environment. Based on the matrix representation of the system's Hamiltonian, we identified and formulated the Landau Zener problem in cooling and trapping of polariton. Motivated by the fact that (i) polaron can be considered as TLS, (2i) polaron are fermions which satisfied the Fermi-Dirac statistics and (3i) polaritons became intermediate particles due to laser cooling and trapping process thereby satisfying Fermi-Dirac statistics althougth they are bosons, we extended our study to polaron. Due to their physical properties, we found interesting the use of two dimensional (2D) transition metal dichalcogenides (TMDs) materials of MX_2 types as new playground for laser cooling and trapping of polariton as well as polaron. Using Landau-Zener-Stückelberg Interferometry theory (LZSIT) in one hand and both the quantum mechanical Schrödinger approach (QMSA) and the improved wigner-Brillouin theory (IWBT) on the other hand, we investigated Landau energy levels (LELs) and transition probabilities in both diabatic and adiabatic basis of the laser cooled and trapped polariton and polaron. We showed that the effect of surrounding environment on the dynamic of laser cooled and trapped polariton and polaron is considerably reduced in 2D TMDs materials of our choice as compared to that of nanostructures. In addition, laser cooling and trapping phenomenon is highly appreciated in 2D TMDs material $MoSe_2$ which stands therefore as appropriate candidate for quantum implementation and simulation nanodevices.

Keywords: polariton, polaron, surrounding environment, laser cooling and trapping, transition metal dichalcogenides, Landau-Zener-Stückelberg.

TITLE IN FRENCH

INVESTIGATION QUANTIQUE DU REFROIDISSEMENT ET DU PIEGEAGE LASER DU POLARITON ET DU POLARON DANS LES NANOSTRUCTURES

RESUME

De nos jours, les exciton-polaritons résultant de l'interaction excitons photons sont des entités atomiques permettent de mettre en evidence plusieurs phénomènes physiques et leurs potentielles applications allant de la condensation de Bose-Einstein aux simulateurs d'Hamiltoniens analogiques et interféromètres quantiques. La présente thèse a porté en l'étude de l'effet de l'environnement sur la dynamique du polariton et du polaron refroidis et piégés par la lumière laser dans les nanostructures. Nous avons considéré notre système d'intérêt comme un système à deux niveaux avec un état fondamental $|g\rangle$ et un premier état excite $|e\rangle$. L'étude commence par l'analyse de comportements de la dynamique du polariton refroidi et piégé par laser dans une approche semi-classique. Par la suite, nous avons introduit dans le système un champ magnétique faible, considéré comme un confinement, et avons évalué l'entropie de Vonn Neumann. Nous avons montré que la probabilité de trouver le polariton refroidi et piégé dans l'état excité ainsi que l'énergie du système sont contrôlées par l'environnement extérieur. Sur la base de la représentation matricielle du Hamiltonien du système, nous avons identifié et formulé le problème de Landau Zener dans le refroidissement et le piégeage laser du polariton. Motivé par le fait que (i) le polaron peut être considéré comme un système à deux niveaux, (2i) le polaron est un fermion qui satisfait la statistique de Fermi-Dirac et (3i) le polaritons refroidi et piégé par la lumière laser est considéré comme une particule intermédiaire, satisfaisant la statistique de Fermi-Dirac bienqu'étant un boson, nous avons étendu notre étude au polaron. En raison de leurs propriétés physiques, nous avons trouvé intéressant l'utilisation de dichalcogénures métaux de transition (DMTs) bidimensionnels (2D) de types MX_2 comme nouvel environnement pour le refroidissement et le piégeage laser du polariton et du polaron. Sous la base d'une part de la théorie de l'interférométrie de Landau-Zener-Stückelberg et d'autre part l'approche de la mécanique quantique de Schrödinger et la théorie de Wigner-Brillouin améliorée, nous avons étudié les niveaux d'énergie de Landau et les probabilités de transition dans les bases diabatique et adiabatique du polariton et polaron refroidi et piégé par la lumière laser. Nous avons montré que l'effet de l'environnement extérieur sur la dynamique du polariton et du polaron refroidi et piégé par laser est considérablement réduit dans les DMTs 2D de notre choix par rapport à celui des nanostructures. De plus, le phénomène de refroidissement et de piégeage laser des entités atomiques est très apprécié dans le DMT 2D $MoSe_2$ qui se présente donc comme le

matériau approprié pour l’implémentation des ordinateurs quantiques et les nanodispositifs de simulation.

Mots clés: polariton, polaron, environnement extérieur, refroidissement et piégeage laser, dichalcogénures métaux de transition, Landau-Zener-Stückelberg.

LIST OF ABREVIATIONS

2D	Two Dimensional
3D	Three Dimensionnal
A	
AIA	Adiabatic Impulse Aproximation
B	
BEC	Bose-Einstein Condensation
C	
CAD	Computer Aided Design
CVD	Chemical Vapor Deposition
D	
DBR	Distributed Bragg Reflector
DDPT:	Dykhne-Davis-Pechukas Theory
DMRGT	Density-Matrix Renormalization-Group Techniques
DNA	Deoxyribonucleic Acid
DPSS	Diode-Pumped Solid State
DUV	Deep Ultra Violet
E	
EDT	Exact Diagonalization Techniques
EM	Electromagnetic
EMW	Electromagnetic Wave
ET	Electron Transfer
F	
FC	Finesse Coefficient
FC	Flow cytometry
FCS	Fluorescence Correlation Spectroscopy
FIR	Far Infrared
FORT:	Far-Off-Resonance dipole Trap
G	
GaAs	Gallium Arsenide
GLM	Global-Local Method
GLZI	Geometric Landau-Zener Interferometry
GPT	Gross-Pitaevskii Theory

I

IP	Ioffe-Pritchard
ISO	International Organization for Standardization
IWBT	Improved Wigner-Brillouin Theory

J

JCH	Jaynes-Cummings Hamiltonian
JCLZH	Jaynes-Cummings Landau Zener Hamiltonian
JCM	Jaynes-Cummings Model

L

LASER	Light Amplification by Stimulated Emission of Radiation
LEM	Liquid Exfoliation Method
LL	Landau Level
LLP	Lee-Low Pines
LZ	Lansau Zener
LZS	Landau-Zener-Stückelberg
LZSI	Landau-Zener-Stückelberg Interferometry

M

MEM	Mechanical Exfoliation Method
MOCVD	Metal-Organic Chemical Vapor Deposition
MOT	Magneto-Optical Trap
MW	Microwave
MZ	Mach-Zehnder

N

NIR	Near infrared

O

OCP	Organic Compound Precursors
ODE	Ordinary Differential Equation
OM	Optical Molasse

P

PA	Perturbation Approach
PCF	Parabolic Cylinder Function

Q

QMCC	Quantum Monte Carlo Calculations
QUEST	Quasi-Electrostatic Trap
R	
RM	Rabi Model
RWA	Rotating Wave Approximation
S	
SC	Semiclassical
SD	Schmidt Decomposition
SE	Schrödinger Equation
SL	Stereolithography
SW	Standing Wave
T	
TDSE	Time Dependent Schrödinger Equation
TEM	Transverse Electromagnetic
TFT	Thin Film Transistors
TISE	Time-Independent Schrödinger Equation
TLS	Two-level System
TMD	Transition Metal Dichalcogenide
TW	Travelling Wave
U	
UL	Lower Polariton
UP	Upper Polariton
UV	Ultra Violet
W	
WGM	Whispering-Gallery Modes
WKM	Wentzel-Kramers-Brillouin

LIST OF TABLES

LIST OF FIGURES

GENERAL INTRODUCTION

Nowadays, with the rapid development of optical techniques (Zhang et al., 2012), many experiments are accomplished with polaritons and polarons in a controlled manner using laser radiation. The ability of light to exert pressure on matter, known as laser cooling and trapping (Shore and Knight, 1993; Shimizu and Sasada, 1998) has becomes of particular interest in physical science and applications. The idea that light exerts pressure on matter arose when Keppler (1619) suggested that it was the pressure of sunlight that made comet tails stream away from the sun (Minogin and Letokhov, 1987). Investigations of the actions of light on matter have yielded many important results. The light force acting on the matter has been divided into two main forces. The first one is the scattering force which drives the atomic particle in the direction of radiation propagation (Menz et al., 2019). The second one is the dipole force which pushes the atomic particle toward extrema of the radiation intensity distribution.

The understanding of the dynamic of light-matter (polariton and polaron) interaction has ended up to a wide range of nanotechnologies, which has attracted a lot of research works and created opportunities for numerous of applications. These include sensing (Chung et al., 2011), imaging (Zhang and Liu, 2008), subwavelength aperture transmission (Barnes et al., 2003), nano-photon detectors (Luo et al., 2015; Tang et al., 2008), nanoscale optical trapping (Novotny et al., 1997; Ye et al., 2013) and optical non linearities (Nahata et al., 2003). Laser cooled and trapped polaritons and polarons have been found as appropriate candidate for quantum computation implementation. Unfortunately, a number of processes and particularly the surrounding effect of environment limit both polaritons and polarons lifetime thereby yields decoherence problem.

Quantum decoherence, sometimes called dynamical decoherence or environment induced decoherence (Paz and Zurek, 2001; Zureck, 2003; Schlosshauer, 2004) is the most significant obstacle of expanding quantum technology (Roszak et al., 2015). It appears as a result of an interaction of the quantum system of interest with an environment (Joos et al., 2003; Schlosshauer, 2007). In general, perfect isolation of a real physical system is not possible. Even the simplest quantum system, like the spin of an electron, may be in weak though continuous interaction with the environment. In laser cooling and trapping of polariton or polaron, several potential sources of decoherence include fluctuation in the ion trap potential (Schneider and

Milburn, 1998), quantum jump to auxiliary electronic levels (Meekhof et al., 1996), the instabilities of the trap drive frequency and voltage amplitude (Monroe et al., 1995; Roos et al., 1999).

Several theoretical approaches have been proposed to overcome limitations due to surrounding environment. The first concrete decoherence models and numerical estimates of decoherence rates were worked out by Joos and Zeh (1985) and Zurek (1986). Zurek (1986) introduced a broader audience of physicists to decoherence theory. Such dissemination and maturing of decoherence theory came at a perfect time, as the period saw the blossoming of quantum information (Berthiaume and Brassard, 1992; Bernstein and Vazirani, 1993 ; Simon, 1994), as well as experimental advances in the creation of superpositions of mesoscopically and macroscopically distinct states (van der Wal et al., 2000). In quantum computation, the quantum states relevant to quantum information processing and Schrödinger-cat-type experiments require the insights of decoherence theory. Conversely, the new experiments served as a fertile ground for testing the predictions of decoherence theory. Accordingly, these developments led to a rapid rise in interest and research activity in the field of decoherence. Today, decoherence has becomes a central topic of modern quantum mechanics and is studied intensively both theoretically and experimentally in several research field allowing complete analysis of atomic particles in interaction in order to provide possibility for successful implementation of quantum computers.

In condensed Matter and Nanomaterials Laboratory at the University of Dschang, important efforts are made in solving the decoherence effets. Kenmoe et al. (Kenmoe et al., 2015) demonstrate that some specific problem of LZ transitions in a qubit coupled to an environment (problem known as dissipative) can be marched onto the frame of original problem without dissipation. By using a variational method of Pekar type, Kenfack et al. (2015) studied the transition probability and decoherence time of levitating polaron in helium film thickness. Fotue et al. (2020) by utilizing the modified Lee Low and Pines variationnal method, they used the symmetric quantum dot as main confinement of bipolarons quasiparticules in order to encrase their their stability and reduce the environmental decoherence effect. Vubangsi et al. (2021) studied the effect of surrounding environment, a compositional gradient, on the quantum mechanical properties of semiconductor heterostructures using a model anharmonic oscillator with asymptotically decreasing effective mass. Pernel Nguenang et al. (2021) investigate the

influence of surrounding environment, here the external voltage or driving terms, on the energy level of a simple Josephson-junction circuit. Other interesting research works carried by many other young research and experts based on quantum decoherence are encountered in the Condensed Matter and Nanomaterial Laboratory at the Universty of Dschang.

Surprisingly, theoretical investigaion based on laser cooling and trapping of atomic entities like polaritons and polarons by several authors did not considered the surrounding effect of environment, the target element in successfull realization of quantum computers (Shimizu and Sasada, 1998). An observation which attracted our attention thereby standing as our motivation to investigate decoherence probleme in cooling and trapping of polariton and polaron. In many cases, the interaction between light and matter can be reduced to the concept of the two-level system (TLS). A TLS is not only the key element in various fields of contemporary physics, like radiation-matter interactions and collision physics, but also the fundamental building block of modern applications ranging from quantum control to quantum information processing. The TLS interacting with the periodically driven fields is an important prototype of a large number of quantum phenomena in nearly every subfield of optics and physics (Allen and Eberly, 1997). We considered the resulted laser cooled and trapped polariton and polaron as TLS, with ground state $|g\rangle$ and first excited state $|e\rangle$. From the rotating wave approximation (RWA) and using classical electromagnetism formulas, cooled and trapped polariton's most important parameters including force, torque, transition probability of finding the system in the excited state and total energy are carefully determined. Withing the previous theoretical analysis, the Hamiltonian of laser cooled and trapped polariton is formulated in it matrix form. Yield the prediction of the possibility to formulate Landau-Zener (LZ) problem in laser cooling and trapping of polariton.

According to a variety of physical areas, LZ processes play an important role, e.g., in artificial atoms (Zenesini et al., 2009) and also Bose-Einstein condensates in optical lattices (You and Nori, 2011), which can behave like controllable quantum TLSs (Buluta et al., 2011 ; Shevchenko et al., 2010). LZ and so far Landau-Zener-Stückelberg (LZS) problems have been studied by several groups (Oliver et al., 2005 ; Sillanpää et al., 2006 ; Wilson et al., 2007 ; Izmalkov et al., 2008 ; Shytov, 2004). The standard LZ problem for an isolated TLS can be solved exactly. For some many-level systems, the LZ transition probability can also be calculated exactly for some initial states (Saito, 2006). LZ transitions controlled by classical field have been

demonstrated by Wubs et al. (2005). In a quantum photon field, Keeling and Gurarie (2008) found that varying the LZ sweep rate produces collapses and revivals of the coherent field amplitude. In addition, it has always been expected that polaritons are ultimately quantum particles theoretically capable of entanglement. This means that, within the LZ theory, it could be possible to predict other important physical phenomena due to laser cooling and trapping of polaritons with application in quantum phase transition, quantum computing, optoélectronic and interferometry to cite a few. Thus, LZ model is a reasonable and unique model to describe laser cooling and trapping of polariton and so far polaron in order to capture the essential physics and provide great insight on the mathematical analysis related to the development of nanoscale devices using cooled and trapped polaritons and polarons.

While a tremendous progress in the development of quantum technologies is apparent, it is still unclear which material platform is the most suitable for the realization of future quantum computers (Nielsen, 2010). Number of theoretical as well as practical research works [(Bechtold et al., 2015; Xue et al., 2020) have demonstrated the use of semiconductors materials in the development of the above mentioned quantum devices. Nevertheless, their crystalline structures are enriched by a variety of intrinsic defects, such as vacancies, adatoms, grain boundaries and substitutional impurities (Hu, 2019), leading to scattering phenomena including scalabilities and decoherence effects (Barreiro et al., 2011) which limit the performance of quantum operation. These defects motivate the search for new materials and techniques to make a great variety of novel experiments feasible.

Recently, two-dimensional (2D) transition metal dichalcogenides (TMDs) materials (Bhimanapati et al., 2015) stand as a diagnostic tool for understanding quantum dynamics, yielding a robust scenario for readout fidelity (Choi et al., 2017; Koshelev et al., 2018). In fact, 2D TMDs materials are totally different and novel systems that bear exciting similarities with graphene (Montambaux, 2018). Due to their fascinating properties such as (i) their unique optoelectronic features in the monolayer limit, (2i) the flexibility of their excitonic binding energies and (3i) their high oscillator strength, they possess advantages of being unique candidate which serve as new playgrounds for measuring and testing physical phenomena that may not be reachable in their precursors (graphene). These include the possibility of probing geometrical properties of the wave functions, of manipulating edge states, of performing interference

experiments in reciprocal space and of controlling crossing and avoided crossing points of energy levels in electronic spectrum of 2D material (Montambaux, 2018). The above mentioned properties and thereby applications constitute our raison of choosing 2D TMDs materials as appropriate candidate which can allow successful implementation of quantum computation devices.

The main objective of the present thesis is to investigate the effect of surrounding environment on the dynamic of laser cooled and trapped polariton and polaron in nanostructures. To get to the main objective, specific objectives include:

- Investigate the effect of surrounding environment in laser cooling and trapping of polariton and polaron,
- Formulate Landau-Zener problem in cooling and trapping of polariton for robust control of polariton's dynamic throght Landau-Zener-Stückelberg Majorana interferometry (LZSMI) theory and predict other important physical phenomena due to laser cooling and trapping of polariton,
- Investigate LELs and transition probabilities in both diabatic and adiabatic basis of laser cooled and trapped polariton embedded in 2D TMDs materials using LZSMIT,
- Investigate LELs of laser cooled and trapped polaron embedded in 2D TMDs material under the influence of triangular quantum well potential using both QMSA and IWBT.

The entire thesis is organized in three main chapters. Chapter one is devoted to literature review on light matter interaction. In particular, we provide a brief overview on the coherent dynamic of polariton and polaron considered as TLS focusing on the diabatic and adiabatic basis. Further, we provide generalities on the analytical solvable models always used in theoretical analysis in light-matter interaction processes, thereby spreading the day-to-day evolurion of laser cooling and trapping polariton and polaron phenomena. At the end, a generality on the quantum description of polariton and polaron in microcavities is presented. We consider monolayer 2D TMDs, and focus on their composition or construction, synthesis methods and applications. An overview is also carried out on nanomaterials and quantum wells.

Chapter two presents mathematical tools and methods used in the whole thesis. As a typical mathematical tool, the classical electromagnetism allow complete understanding of the origin of

radiation force and torque applied to atomic particle in presence of radiation field. Practical investigation of laser cooling and trapping phenomena originate decoherence state of the system. Quantum investigation of decoherecnce effet leads to the utilization of the RWA based on the JCM. The efficient theoretical description of the above mentioned system requires the transition to the reasonable model which describes laser cooling and trapping of atomic particles process in order to capture the essential physics. In the framework of LZ (LZSI) theory based on Whittaker method that uses Weber's differential equation base on parabolic cylinder functions, LZS transition probabilities and total energy are investigated. In this same chapter, analytical results obtained through our analysis are also presented.

Chapter three is devoted to numerical results achieved. Here, graphical representation of particular parameters of interest which are transition probabilities, total energy of the system, entropy and LELs are depicted versus various some parameters of interest in different coupling states of the laser cooled and trapped polaritons and polarons with surrounding environment.

The present thesis ends with a general conclusion thereby presenting a brief summary of the thesis with concluding remarks, and outlines the perspectives for future research works and applications.

CHAPTER ONE

LITTERATURE REVIEW

Introduction

The interaction of a single dipole with a monochromatic radiation field presents an important theoretical problem in Physic (Fortier, 2007). Electromagnetic (EM) interaction can be used to act on atomic particles, to manipulate them, to control their various degrees of freedom. With the development of laser sources, the field of laser cooling and trapping of atomic particle has considerably expanded during the last few years (Chu, 1998; Cohen-Tannoudji, 1998; Phillips, 1998). Methods have been developed to trap atoms, to cool them to very low temperatures.

The importance of laser cooling to Physics has been recognized by the Nobel Prize committee three times in the last decade. The first recognition has been attributed to Chu, Cohen-Tannoudji and Phillips in the year 1998 for their research work entitled 'for the development of methods to cool and trap atoms with laser light' (Chu, 1998; Cohen-Tannoudji, 1998; Phillips, 1998). In 2001, the second recognition was awarded to Cornell, Ketterle and Wieman for the achievement of BEC in dilute gases of alkali atoms and for early fundamental studies of properties of the condensates (Cornell and Wieman, 2002; Ketterle, 2002). And finally, Glauber, Hall and Hänsch received the third recognition for their contribution to quantum theory of optical coherence and their contribution to the develop ent of laser-based precision spectroscopy including the optical frequency comb technique (Cornell and Wieman, 2002; Ketterle, 2002). Up to dates, due to laser cooling and trapping techniques, experiments with atomic particles with single photons are now carried out regularly in a handful of laboratories around the world (Fortier, 2007) and number of applications and development of laser cooling and trapping techniques continues to expand.

The aim of this chapter is to present an overview on laser cooling and trapping of atomic particles. We will focus on two important aspects: (i) the coherent dynamic of atomic particles interacting with radiation field (considered here as TLS) and (2i) generalities on laser cooling and trapping of atomic particles. In this chapter, an overview of monolayers 2D TMDs is also

presented, since these 2D materials have been found as attractive milieu for realization of laser cooling and trapping of atomic particles phenomena.

I.1. Coherent dynamic of two-level systems

I.1.1. The two-level systems

In quantum mechanics, a TLS, also known as a two-state system is a quantum system that can exist in any quantum superposition of two independent quantum states (Griffiths, 2004). The quantum TLS (Figure 1) is usually called qubit in quantum information and computation and represents the individual unit of classical information which takes one of the two independent possible values $\{0,1\}$ (Preskill, 2015). A TLS has many important applications in many research fields such as nuclear magnetic resonance, laser optics and so on. Many physical phenomena can be modeled to as a TLS problem (Basdevant, 2016). The advantage of TLS is that the wavefunction can be expressed in term of two coupled ordinary first-order differential equations. The general solution of these equations is a linear combintion of two Floquet modes whose functional forms are known. Another advantage of developping theory using TLS is that the model is mathematically less challenging than the continuum wave mechanics approach, requiring only basic linear algebra instead of calculus and differential equations.

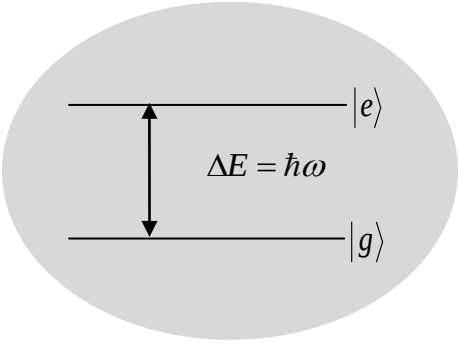

Figure 1. Modelling of an atomic transition in term of two-level system

I.1.2. The Fock space

A Fock space is an infinite-dimensional vector space and is a natural tool for quantum field theory. It is of fundamental importance since it represents typical state space for gases of

particles, thermal baths, etc. This Mathematical construction is used to construct the quantum states of a multi-particle systems from a single particle system (LeBlanc, 2012). The Fock space has been named in 1932 (Fock, 1932). The creation and annihilation operators are used to account for the introduction and removal of particles, allowing the description of a system with a variable number of particles (LeBlanc, 2012). The Fock space is an algebraic construction used in quantum mechanics to construct the quantum states space of a variable or unknown number of identical particles from a single particle Hilbert space H (Reed and Simon, 1975). Informally, a Fock space is the sum of a set of Hilbert spaces representing zero particle states, one particle states, two particle states, and so on.

I.1.2.1. The diabatic basis

We begin this section by given a brief definition of the diabatic state. This is an electronic state that does not change character as a function of molecular geometry. Diabatic state provides a framework for obtaining quantitative predictions about electron transfer (ET) dynamics. Qualitatively, in contrast to adiabatic, a diabatic electronic state is one that does not change its physical character as one moves along a reaction coordinate. Diabatic electronic states play an important role in a variety of research fields. Therfore, diabatic electronic states are often used in chemistry for the construction of potential energy surfaces (Kim et al., 2000), in spectroscopy for the assignment of vibronic transitions and rationalization of the rates of interstate transitions (Ichino et al., 2006). The impotance of the diabatic electronic states is also relevant in electronic since they typically have a small derivative coupling, simplifying the description of electronic transitions (Müller and Stock, 1997 ; Butler, 1998) and in scattering theory as they connect to clearly-defined product channels (Cohen and Micha, 1992 ; Tully, 2000 ; Mahapatra et al., 2001). Finally, diabatic states play a qualitative role in our understanding of molecular bonding (Aqvist and Warshel, 1993), ET (Sidis, 1992) and proton tunnelling (Kuznetsov and Ulstrup, 1999).

I.1.2.2. The adiabatic basis

Another canonical choice for the basis consists of the eigenstates of the Hamiltonian in the adiabatic basis. The adiabatic basis is usually a particularly good choice when the diabatic basis is not, namely, in the case when the external field is changing slowly. Thus, the dynamics is called adiabatic and its solution can be approximated with the adiabatic states. Often this

corresponds to the parameter region of strong coupling. This adiabatic basis transformation also has fundamental role in both the Dykhne-Davis-Pechukas theory (DDPT) (Laloe, 2012) and in the plane-curve representation of time-dependent two-level problems

I.2. Laser

I.2.1. History

In 1704, Newton characterized light as a stream of particles. The Young's interference experiment in 1803 and the discovery of the polarity of light convinced other scientists of that time that light was emitted in the form of waves. Maxwell theoretically formulated the concept of EM radiation, of which light is an example in 1880. At the turn of the 20th century, the black body radiation phenomenon challenged the waveform light theory. Additional work undertaken by Hertz on the photoelectric effect and Planck on the formulation of the distribution of the radiation emitted by a black body or perfect absorber of radiant energy complemented further the understanding of light propagation. The significance of Planck's constant in this context is that radiation such as light, is emitted, transmitted and absorbed in discrete energy packets or quanta, determined by the frequency of the radiation and the value of Planck's constant. The observations that the number of electrons released in the photoelectric effect is proportional to the intensity of the light and that the frequency or wavelength of light determines the maximum kinetic energy of the electrons, indicated a kind of interaction between light and matter that could not be explained in terms of classical physics. In 1905, Albert Einstein explains that light can be regarded alternatively as composed of discrete particles (photons), equivalent to energy quanta. In explaining the photoelectric effect, Einstein assumed that a photon could penetrate matter, where it would collide with an atom. Since all atoms have electrons, an electron would be ejected from the atom by the energy of the photon, with great velocity. Einstein also predicted in 1917 that, when there exists the population inversion between the upper and lower energy levels among the atom systems, it was possible to realize amplified stimulated radiation, which is laser light. Stimulated EM radiation emission has the same frequency (wavelength) and phase (coherence) as the incident radiation.

I.2.2. Definition and properties

The term laser is an acronym for light amplification by stimulated emission of radiation (Gould, 1959; Taylor, 2000). Lasers are devices that produce intense beams of light. The wavelength (color) of laser light is extremely pure (monochromatic) when compared to other sources of light, and all of the photons (energy) that make up the laser beam have a fixed phase relationship (coherence) with respect to one another. Light from a laser typically has verylow divergence (directionality). It can travel over great distances or can be focused to a very small spot with a brightness which exceeds that of the sun (high collimated). It comes that, properties of laser light include (i) coherence, (2i) collimation, (3i) monochromaticity and (4i) directionality. In the former, photons are emitted in phase. Phase is the position of a point in time on a waveform cycle. Collimation corresponds to the phenomenon in which photons travel in parallel, and therefore diverge very little as they propagate away from the laser device. It is this collimation that results in the narrow beam diameter of laser. Monochromaticity consists of one specific wavelength or single colour of light while the later, that is uniform polarization, is the electric field of the photons usually oscillates in a specific direction perpendicular to the direction of the beam.

I.2.3. Components, design and types of typical laser system

A laser consists of three main components as illustrated in Figure 2 above. These consist of (i) excitation source, which supplies the necessary energy, (2i) lasing medium or gain medium, which determines the wavelength of the laser produced and (3i) optical resonator, which contains the lasing medium with two parallel mirrors on either side, thus, causing the photons to pass repeatedly back and forth between the two. One of the mirrors is partially transparent, allowing some of the photons to exit the device to form the laser beam. This is termed the output coupler. Since the discovery of the laser, literally thousands of types of lasers have been discovered. Lasers can be broadly classified into four categories including gas discharge lasers (Dzyubenko et al., 2017), semiconductor diode lasers (Arrigoni et al., 2009), optically pumped lasers (Taylor, 2000), and other. Lastly is a category which includes chemical lasers (Minucci and Olivia, 1993), gas-dynamics lasers (Minucci and Olivia, 1993), x-ray lasers (Hecht, 2008), combustion lasers and others developed primarily for military applications.

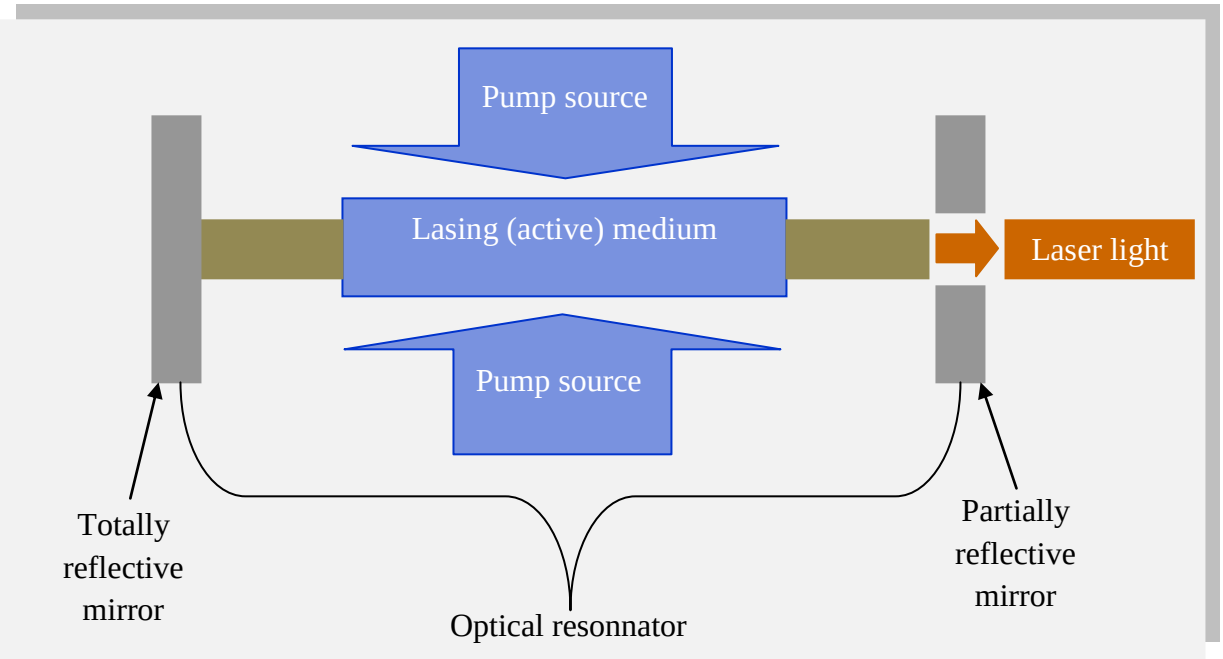

Figure 2. Graphical design and components of typical laser device

I.2.4. Applications of laser light

Lasers have become so much a part of daily life that many people may not realize how ubiquitous they are. Laser applications are so numerous and can be classified between industrial applications, scientific applications and clinical and medical applications.

I.2.4.1. Industrial applications

High-power lasers have long been used for cutting and welding materials. Today the frames of automobiles are assembled using laser welding robots. Complex cardboard boxes are made with laser-cut dies, and lasers are routinely used to engrave numbers and codes on a wide variety of products. Some less well-known applications include 3D stereolithography (SL) and photolithography (PL). The former, also known as stereolithography apparatus, optical fabrication, photo-solidification, or resin printing is a form of 3D printing technology used for creating models, prototypes, patterns, and production parts in a layer by layer fashion using photochemical processes by which light causes

chemical monomers and oligomers to cross-link together to form polymers (Patent, 1986). Other industrial laser applications include marketing, scribing and non contact measurement.

Laser marketing is a process where lasers are used extensively in production to apply indelible, human and machine readable marks and codes to a wide variety of products and packaging (Klavins et al., 2019; Greats impressions, 2013). Typical applications include marking semiconductor wafers for identification and lot control, removing the black overlay on numeric display pads, engraving gift items, and scribing solar cells and semiconductor wafers. Information can be placed in direct text (letters, numbers, and images) or encrypted (barcode or QR code). Laser scribing (Nisar et al., 2013) is similar to laser marking, except that the scan pattern is typically rectilinear (Figure 3), and the goal is to create microscoring along the scan lines so that the substrate can be easily broken apart (Jenne et al., 2020). A wide variety of materials, including metal, wood, glass, silicon and rubber are amenable to laser scribing. Each material has different absorption and thermal characteristic, and some even have directional preferences due to crystalline structure. Consequently, the type of laser used depends, to some extent, on the material to be marked. Other considerations are the size of the pattern, the speed of the scan, cosmetic quality, and cost. Noncontact measurement is another industrial laser application. There are many types of laser-based noncontact measurement techniques in use today including scatter measurement (Lipi et al., 2012; Sicker et al., 2016), polarimetry (Bornhop and Dotson, 2006; Mishchenko et al., 2011), ellipsometry and interferometric measurement (Bunch and Hellemans, 2004).

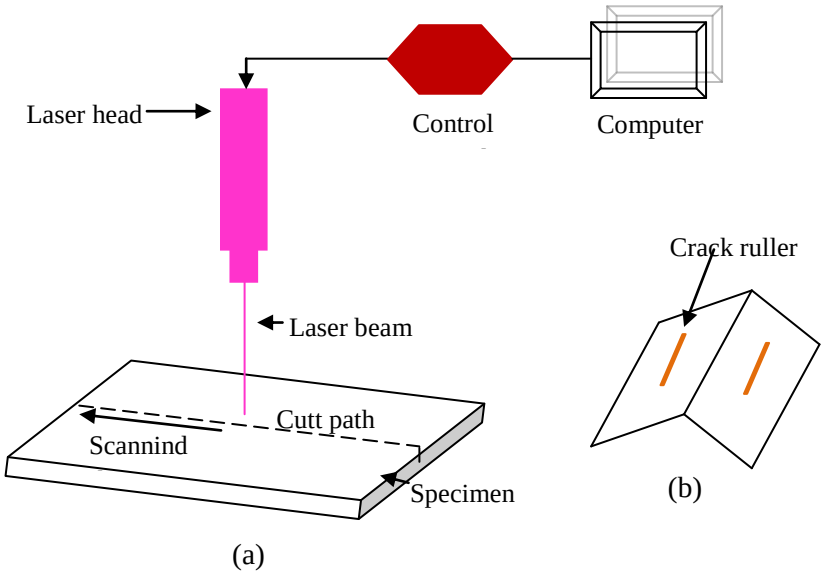

Figure 3. Laser scribe and break method. Laser scribing (a) and mechanical breaking with the help of crack rullers (b). [as investigated by Nisar et al.(2013)].

I.2.4.2. Scientific applications

In the field of science and technology, lasers are used extensively in the scientific laboratory for a wide variety of spectroscopic and analytic tasks. Of particular interest are confocal scanning microscopy and time-resolved spectroscopy (TRS). The later is a technique used to observe phenomena that occur on a very short time scale. This technique has been used extensively to understand biological processes such as photosynthesis, which occur in picoseconds or less. Scanning microscopy, another interesting laser scientific application, is used to build up a 3D image of a biological sample. Annother interesting laser scientific and technological application is the microarray scanning (MS). In deoxyribonucleic acid (DNA) research, a microarray is a matrix of individual DNA molecules attached, in ordered sets of known sequence, to a substrate which is approximately the size of a microscope slide.

I.2.4.3. Clinical and medical applications

One of the earliest applications of lasers in medicine was photocoagulation, using an argon-ion laser to seal off ruptured blood vessels on the retina of the eye. The laser beam passed

through the lens and vitreous humor in the eye and focused on the retina, creating scar tissue that effectively sealed the rupture and staunched the bleeding. Today, lasers are used extensively in analytical instrumentation, ophthalmology, cellular sorting, and of course, to correct vision. Flow cytometry (FC) is a technique used for measuring single cells. Not only it is a key research tool for cancer and immunoassay disease research, but it is also used in the food industry for monitoring natural beverage drinks for bacterial content or other disease causing microbes. In a basic cytometer, the cells flow, one at a time, through a capillary or flow cell where they are exposed to a focused beam of laser light. Lasers are used in a variety of surgical and dental procedures from cutting tissue, vaporizing tumors, removing tattoos, removing plaque, removing cavities, removing hair and follicles, resurfacing of skin and of course, correcting vision. In many ways, medical applications are like materials processing applications. In some cases material is ablated. In others tissue is cut or welded, and in yet others, photochemical changes are caused in blood vessels to encourage shrinkage and absorption. Understanding tissue absorption characteristics and reaction to wavelength and power are keys. Cosmetic treatment of wrinkles, moles, warts, and discolorations is often accomplished with near infrared and infrared lasers. Lasers are also used to treat macular degeneration, an overgrowth of veins and scar tissue in the retinal region, a condition associated with advancing age.

I.3. Polaritons

I.3.1. Definition, schematization and types

Polaritons (Figure 4) are the eigenmodes of systems consisting of strong interaction between semiconductor excitons, coulomb bound electron-hole pairs, and cavity photons (Tao et al., 2016).

Usually, one indicates the type of the crystal excitation which participates in the formation of polaritons by adding prefixes. Therefore, it is distinguishable several types of polaritons, including exciton polaritons (Pekar, 1958), Plasmon polaritons (Ebbesen et al., 1998), optical phonon polaritons, intersubbands polaritons (Manceau et al., 2017), Bragg polaritons (Klingshirn 2012), plexcitons, Mangnon polaritons and cavity polaritons (Ebbesen et al., 1998). The quasiparticles, which appear as a result of interaction between an EM field and the resonances of magnetic permeability, are known as magnetic polaritons.

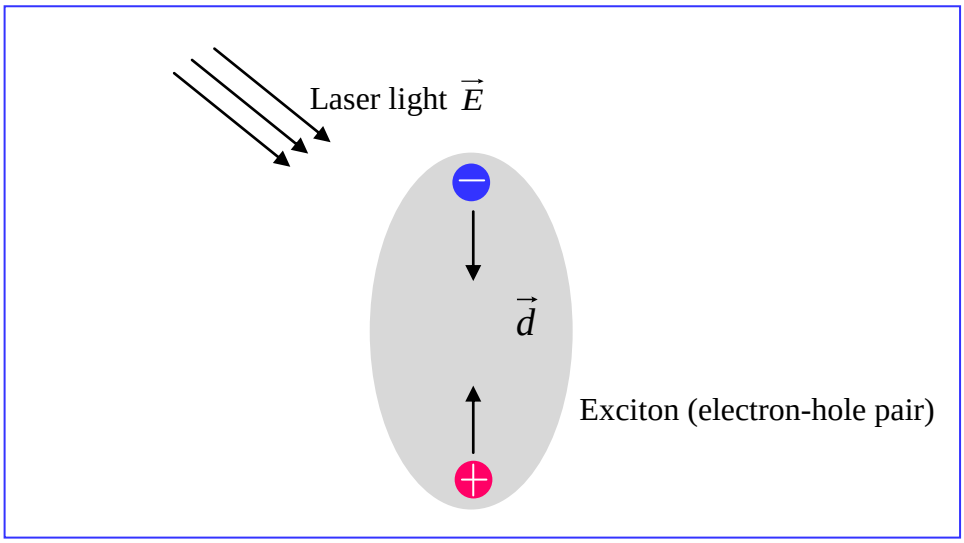

Figure 4. Schematic representation of exciton-photon interaction or polariton formation.

I.3.2. Properties

Polaritons inherit the properties of both photons and medium excitations. This mixed character of polaritons leads to many interesting physical properties. In regard of their properties, polariton are found to be squeezed with respect to state of certain intrinsic photon-exciton mixed bosons. In general, squeezing is time periodic during a polariton period. The problem of examining squeezing effect of polariton in homogeneous dielectric medium has been independently investigated by Abram (1987) and Glauber and Lewenstein (1989). Artoni and Birman (1990) interpreted the effect firstly as sudden transition and secondly as quantum correlation in polariton states between intrinsic photon-exciton mixed bosons of opposite wave vectors.

I.4. Polarons

I.4.1. Definition, schematization and types

Polarons are quasiparticles which describe interactions between free electrons and induced polarization resulting from electrons/ions or electrons/atoms coupling in solid materials (Landau, 1993; Landau, 1948). There are a number of polaron-type quasiparticles that result from other interactions, such as a spin polaron (electron interacting with atomic magnetic moments)

(Devreese, 2008; Kaminski and Sarma, 2002), a piezopolaron and so on. For more about various types of polarons, readers should refer to Devreese (2008). A polaron may be large (Devreese, 2008) or small (Devreese, 2008), depending on how its radius compares to the lattice constant. Other than size, the most important differences between large and small polarons are in their electrical transport: large polarons tend to have band-like transport, while small polarons usually undergo hopping transport. Two polarons of like charge can bind into a bipolaron (Figure 6) (Devreese, 2008), and two polarons of opposite charge can bind into a polaronic exciton.

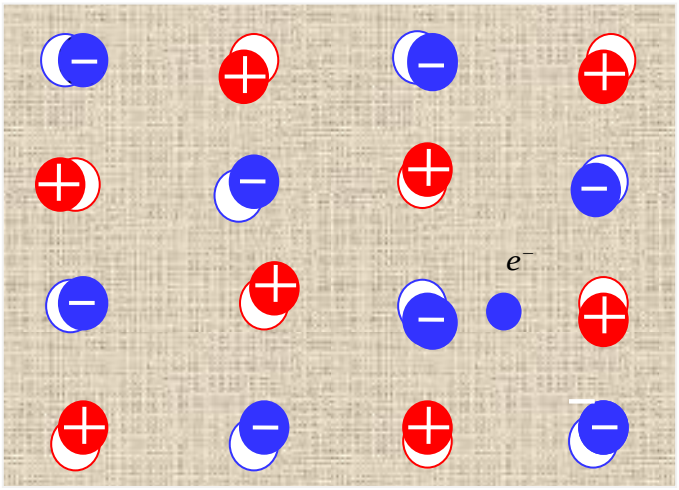

Figure 5. Artist view of a Polaron. A conduction electron in an ionic crystal or a polar semiconductor repels the negative ions and attracts the positive ions. A self-induced potential arises, which acts back on the electron and modifies its physical properties.[As indicated by Devreese (2003)]

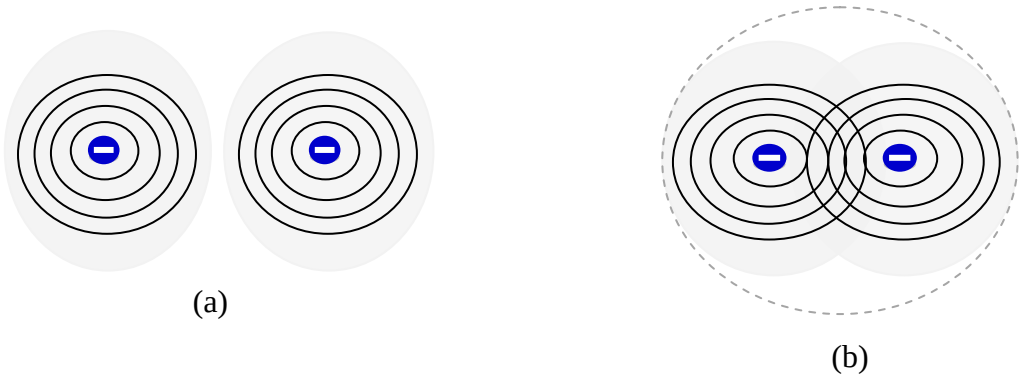

Figure 6. Cartoon illustrating bipolaron formation. a) Two separated polarons each in its own polarisation well. b) Bipolaron where two electrons are localized in the same potential well (Devreese, 2008).

I.4.2. Properties

We presented above majors differences between small polaron or Holstein polaron (Holstein-Hubbard model) and large polaron or Fröhlich polaron. The polaron character is well pronounced only for strong-coupling. In regard of their properties, polaronic entities are characterized by their binding (or self-) energy, their effective mass and their characteristic response to external electric and magnetic fields (Devreese, 2005).

I.5. Laser cooling and trapping of polaritons and polarons

I.5.1. Historical review

The field of laser cooling and trapping of atomic particles has blossomed during the last decade (Chu, 1995). The first experiments were carried out with ions following the idea of Wineland and Dehmelt (1975) although the possibility of laser cooling atoms was suggested at the same time by Hansch and Schawlow (1975). Ions can be trapped for long periods in ultra-high vacuum and then cooled down at nearest zero temperature. Whereas, for neutral atoms, trapping was not achieved until after the pioneering experiments in which an atomic beam was slowed using light forces (Foot, 1991). Since then, laser cooling and trapping of atomic particles has became a very active and increasingly visible field of research and this was highlighted by the Nobel prize in physics in 1997, awarded to Chu, Cohen-Tannoudji, and Phillips, and by the realization of BEC and the corresponding Nobel prize in 2001 to Cornell, Ketterle, and Wieman (Kaiser et al., 2003). Most of the research work has been focused towards understanding the atomic physics of laser cooling and trapping processes themselves (Foot, 1991). Thus, in the issue on mechanical effects of light (1985) (Meystre and Stenholm, 1985), several contributions focused on light forces on two-level atomic transitions, with mainly theoretical papers and a few experiments testing general principles. Just a few years later, 1989, a second special issue on laser cooling and trapping of atoms proved how active this field had become. Here several contributions presented experimental results on cooling of atoms and ions, while theory papers analyzed the effect on the atomic motion caused by the coupling between the atom's complex internal structure and light fields (Andrews and Bradshaw, 2016).

I.5.2. Interaction of polariton and polaron with a quasi-resonant light beam: the light force

According to the momentum conservation, when a photon is absorbed its momentum $\vec{p} = \hbar\vec{k}$ is transferred to the atom (Figure 7) retaining both its magnitude and direction [Figure 7 (a, b)]. This tiny momentum kick due to absorption of a single photon alters the velocity of an atom by recoil velocity $v_{rec} = \frac{\hbar k}{m} \approx 1 cm/s$ which can be compared with typical velocities of a few $100 m/s$ in room temperature atoms. The absorption is followed by spontaneous emission with a natural lifetime $\tau = 1/\gamma$ of the excited state, where γ is its decay rate (or width), and thus the atom recoils once more. Since the spontaneous emission is isotropic, the recoil of the atom associated with this process is in a random direction, thus there is no net change of momentum on average. Thus overall the change of the atomic momentum is solely the effect of absorption (Figure 7c). In laser cooling experiments, atoms in an atomic beam are slowed by the light force from resonant scattering of a counter propagating laser beam. Each absorbed photon gives the atom a kick in the direction opposite to its motion and the emitted photons go in all directions, so the net effect of many photons is a force on the atom which slows it down.

If we cool the further atomic particle by applying the laser cooling process in all three dimensions using a configuration of three orthogonal standing waves along the cartesian axes, all from the same laser, then the interaction of an atomic beam with a counter propagating laser beam slows the atomic particle down and can produces a cloud of stopped atoms with a velocity spread much less than at room temperature. When the laser frequency is detuned below the atomic resonance frequency, the Doppler effect shifts an atom closer to resonance with whichever beam the atom is moving towards. Thus, the resultant force damps the velocity. This force slows the atom down whichever direction it moves in. So in the intersection of the laser beams the light exerts a frictional or damping force on the atoms.

Accompanying the cooling process by the scattering force, there is always some diffusion or heating which limits the lowest temperature which can be reached. The diffusion arises from the recoil of the atom from the spontaneous photons which can be modelled by a random walk in momentum space with step length equal to the photon momentum $\hbar k$.

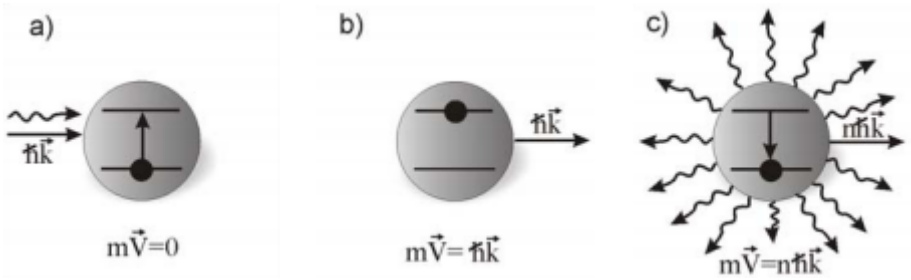

Figure 7. A simplified depiction of the light pressure acting on the two-level atom. (a) the resonant photon approaches an atom of mass m in its ground state and in rest; (b) as a result of absorption the atom, now in the excited state, gains a momentum kick, $m\vec{v} = \hbar\vec{k}$; (c) recoil momentum due to the isotropic spontaneous emission averages out over many absorption/emission cycles thus, after n cycles the atom gains momentum $m\vec{v} = n\hbar\vec{k}$ along the propagation direction of incoming photons. The wavy arrow is for photon, the thick one for momentum [Kowalski et al. (2010)].

I.5.3. Typology of laser cooling of two-level systems

I.5.3.1. Doppler cooling

Doppler cooling is a mechanism which can be used to slow the motion of atoms. The term is sometimes used synonymously with laser cooling, although laser cooling includes other techniques. The so-called Doppler cooling is the simplest cooling mechanism which has been initially proposed by Hänsch and Schawlow (1975) for free atoms and by Wineland and Dehmelt (1975) for trapped atomic particles. Doppler cooling involves light with frequency tuned slightly below an electronic transition in an atomic particle. Doppler cooling occurs when atoms are irradiated with counterpropagating laser waves detuned below resonance. Owing to the Doppler effect, a moving atomic particle will tend to absorb photons into the laser wave counterpropagating its velocity rather than into the copropagating wave. Therefore, it encounters a force opposed to its velocity and becomes cooled (Castin et al., 1989; Phillips and Metcalf, 1982).

I.5.3.2. Sub-doppler cooling

Sub-Doppler cooling is a mechanism that can be used to cool a substance to a temperature lower than the Doppler cooling limit. The Sub-Doppler laser cooling has been a well established and widespread technique since the late 1980s (Lett et al., 1988). The cooling process consists in using light polarization gradients and optical pumping to cool down atoms below the Doppler temperature limit $T_{DL} = \frac{\hbar\Gamma}{2K_B}$ (Dalibard and Cohen-Tannoudji, 1989), where K_B is the Boltzmann constant and Γ is the natural linewidth.

I.5.3.3. Subrecoil cooling

Sub-recoil cooling is a cooling process which results in a delocalization of atoms in the laser wave (Lawall et al., 1995). Subrecoil cooling corresponds to a situation where the de Broglie wavelength λ_{DB} of the atoms is larger than the wavelength λ_L of the laser used to cool them. The spatial extent of the wave packets describing the center of mass of the atom can no longer be neglected and a full quantum treatment of atomic motion is needed (Lawall et al., 1995).

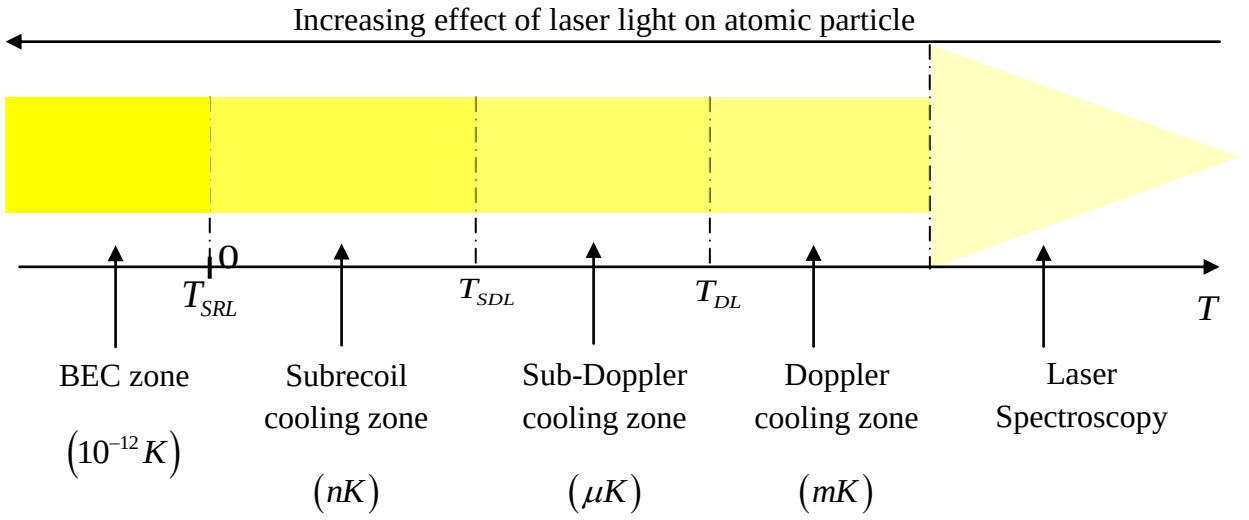

Figure 8. A few important landmarks in the temperature scale corresponding to various temperature selection or cooling types.

I.6. Trapping techniques

I.6.1. Optical trapping

The motion of a TLS in a spatially inhomogeneous laser field is generally governed by the dipole gradient force, the radiation pressures force and the momentum diffusion (Balykin et al., 2000). For an atom slowly moving in a far-detuned laser field the optical excitation is low. As a result, the radiation pressure force originating from the absorption of the laser light and the heating caused by the momentum diffusion are small. Accordingly, the motion of a cold atom in a far-detuned inhomogeneous laser field at not too long interaction time is basically governed by the dipole gradient force. The minima of the potential produced by the dipole gradient force in a far-detuned laser field can thus be used for optical trapping of cold atoms at time intervals limited by the heating due to the momentum diffusion (Balykin et al., 2000). Conceptually, the simplest optical trap for cold atoms can consist of a single focused laser beam formed by a TEM Gaussian laser mode (Balykin et al., 2000).

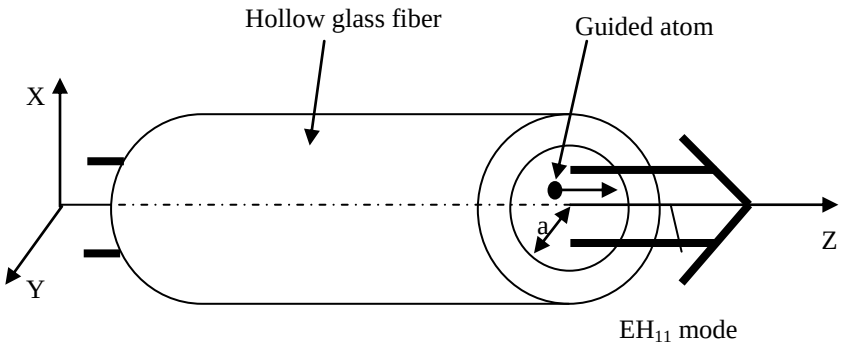

Figure 9. Scheme of an atom waveguide based on the optical mode EH_{11} propagating in the dielectric waveguide (left) and the optical potential for atoms (right) (Ol'shanii et al., 1993; Balykin et al., 2000).

I.6.2. Magnetic trapping

Magnetic trapping of atomic particles was proposed at least as early as 1960 (Heer, 1963). Despite considerable development in the theory of magnetic trapping (Goluband and Pendlebury, 1979; Kugler et al., 1978), the successful trapping of cold neutrons (Kugler et al., 1978) and serious attempts to trap atoms (Martin, 1975), no such trapping has been reported until the first

observation of magnetically trapped neutral atoms by Migdall and co-workers in the year 1985 (Migdall et al., 1985). In general, all static magnetic traps use nonuniform stationary magnetic fields for trapping atoms. The most important static magnetic trap of the first kind is the so-called spherical quadrupole trap proposed by Paul (Niehues, 1976). In this trap, two opposite circular currents produce a static magnetic field in the form of a spherical quadrupole (Figure 10a). The radii of the circular currents are taken to be approximately $\frac{4}{5}$ of the distance between the planes of the currents in order that the trap can have the same potential well depth along and across the symmetry axis (Balykin et al., 2000).

The magnetic bottle constitutes another type of magnetic trap of particular interest in this section. A magnetic bottle is an arrangement that permits to confine charged particles. A particle inside a magnetic bottle makes a circular motion following magnetic field lines which have a sort of cylindrical symmetry as it's shown in figure 10b. Based on figure 10b, trapping atomic particles can be as simple as putting a gas of atoms in a storage vessel that has walls that inhibit sticking. However, EM fields can also be configured to confine atoms with much less perturbation to their internal structure and minimal heating from the surrounding environment.

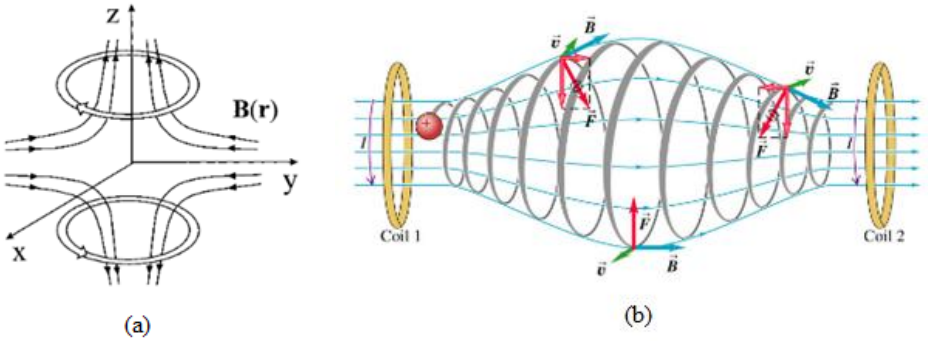

Figure 10. Magnetic field in a sphericalquadrupole magnetic trap generated by two Helmholtz coils (a) [Balykin et al. (2000)] and magnetic bottle atoms trap (b).

Another interesting type of magnetic trap to be mentioned in the present thesis is the usually called Ioffe-Pritchard (IP) trap (Figure 11) (Cavazos, 2015; Bolpasi et al., 2012). The original configuration for the IP trap consists of 4 straight, current carrying bars which create a confining quadrupole field in the radial direction. A pair of coils known as pinch coils (PI) are

also used to add a curvature to the field in the axial direction and therefore to provide the axial confinement.

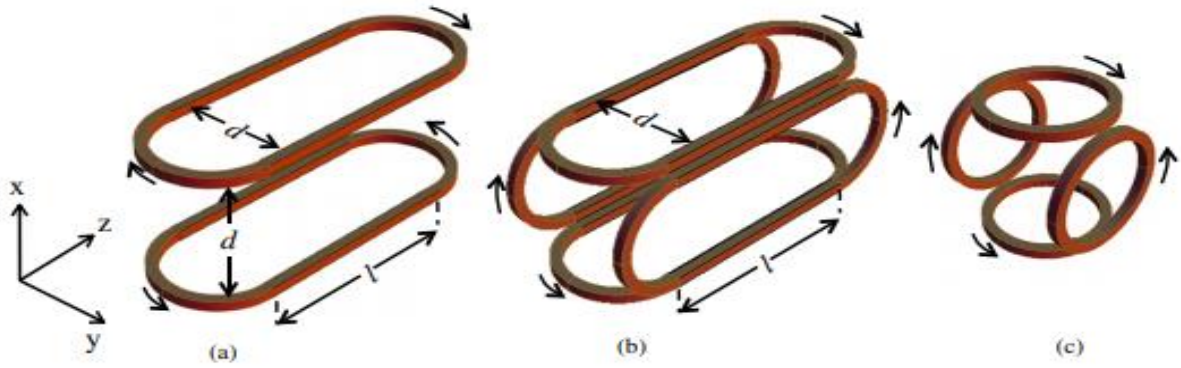

Figure 11. (a) One pair of Ioffe racetracks of length l and width d used to create the 2D linear quadrupole field. (b) The corresponding case of two pairs of racetracks with the same dimensions. (c) Racetrack coils of zero length as presented in this paper. The The arrows indicate the direction of the current [Bolpasi et al.(2012)].

I.6.3. Magneto-optical trapping (MOT)

Magneto-optical trapping is a trapping technique that uses 3D magneto-optical trap. This (Figure 12) is an apparatus that uses laser cooling with magneto-optical trapping in order to produce samples of cold trapped neutral atoms at temperatures as low as several microkelvins, two or three times the recoil limit (Kowalski et al., 2010). By combining the small momentum of a single photon with a velocity and spatially dependent absorption cross section and a large number of absorption-spontaneous emission cycles, atoms with initial velocities of hundreds of metres per second can be slowed to tens of centimetres per second. In a three dimensional (3D) optical molasses (OM) arrangement, three pairs of mutually orthogonal and counterpropagating laser beams intersect in a vacuum chamber containing vapor of the studied element. The laser beams, tuned below the resonance, create a viscous region where the inhibiting force is exerted on the atoms. However, the radiation pressure itself does not allow for their spatial confinement. The atoms are still able to move slowly in any direction and eventually they diffuse out of the region. In order to both cool and confine atoms, the force has to be additionally position-dependent. Operation of the MOT is based on manipulations of the external and internal degrees

of freedom of atoms by means of carefully prepared optical and magnetic fields (Cohen-Tannoudji, 1997).

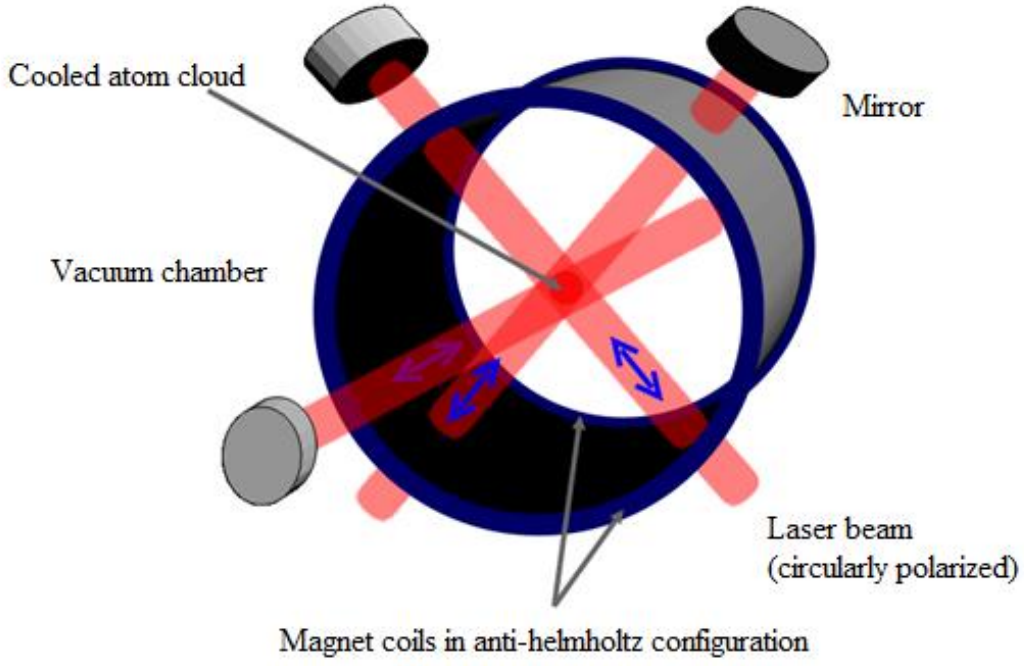

Figure 12. An experimental setup of a magneto-optical trap. The laser field is produced by three pairs of counter-propagating laser beams with circular polarizations (Krieger, 2006).

I.7. Bose-Einstein condensation of two-level systems

I.7.1. Historical review of Bose-Einstein condensation

BEC (Bose, 1924; Einstein, 1924; Einstein, 1925) was observed in 1995 in a remarkable series of experiments on vapors of Rubidium ($^{87}R_b$) (Figure 13) (Anderson et al., 1995) and Sodium ($^{23}N_a$) (Davis et al., 1995) in which the atoms were confined in magnetic traps and cooled down to extremely low temperatures, of the order of fractions of microkelvins. The first evidence for condensation emerged from time-of-flight measurements. The atoms were left to expand by switching off the confining trap and then imaged with optical methods. A sharp peak in the velocity distribution was then observed below a certain critical temperature, providing a clear signature for BEC. In the same year, first signatures of the occurrence of BEC in vapors of lithium were also reported (Bradley et al., 1995). The experimental and theoretical research on

this unique phenomenon predicted by quantum statistical mechanics is much older and has involved different areas of physics [for an interdisciplinary review of BEC, readers should refer to Griffin et al. (1995)]. In particular, from the very beginning, superfluidity in helium was considered by London (1938) as a possible manifestation of BEC. Evidence for BEC in Helium later emerged from the analysis of the momentum distribution of the atoms measured in neutron-scattering experiments (Sokol, 1995).

A rather massive amount of work has been done in the last couple of years, both to interpret the initial observations and to predict new phenomena. In the presence of harmonic confinement, the many-body theory of interacting Bose gases gives rise to several unexpected features (Dalfovo and Giorgini, 1999). This opens new theoretical perspectives in this interdisciplinary field, where useful concepts coming from different areas of physics such as atomic physics, quantum optics, statistical mechanics, and condensed-matter physics are now merging together. The natural starting point for studying the behavior of these systems is the theory of weakly interacting bosons which, for inhomogeneous systems, takes the form of the Gross-Pitaevskii theory (GPT). This is a mean-field approach for the order parameter associated with the condensate. It provides closed and relatively simple equations for describing the relevant phenomena associated with BEC. In particular, it reproduces typical properties exhibited by superfluid systems, like the propagation of collective excitations and the interference effects originating from the phase of the order parameter. The theory is well suited to describing most of the effects of two-body interactions in these dilute gases at zero temperature and can be naturally generalized to also explore thermal effects (Dalfovo and Giorgini, 1999).

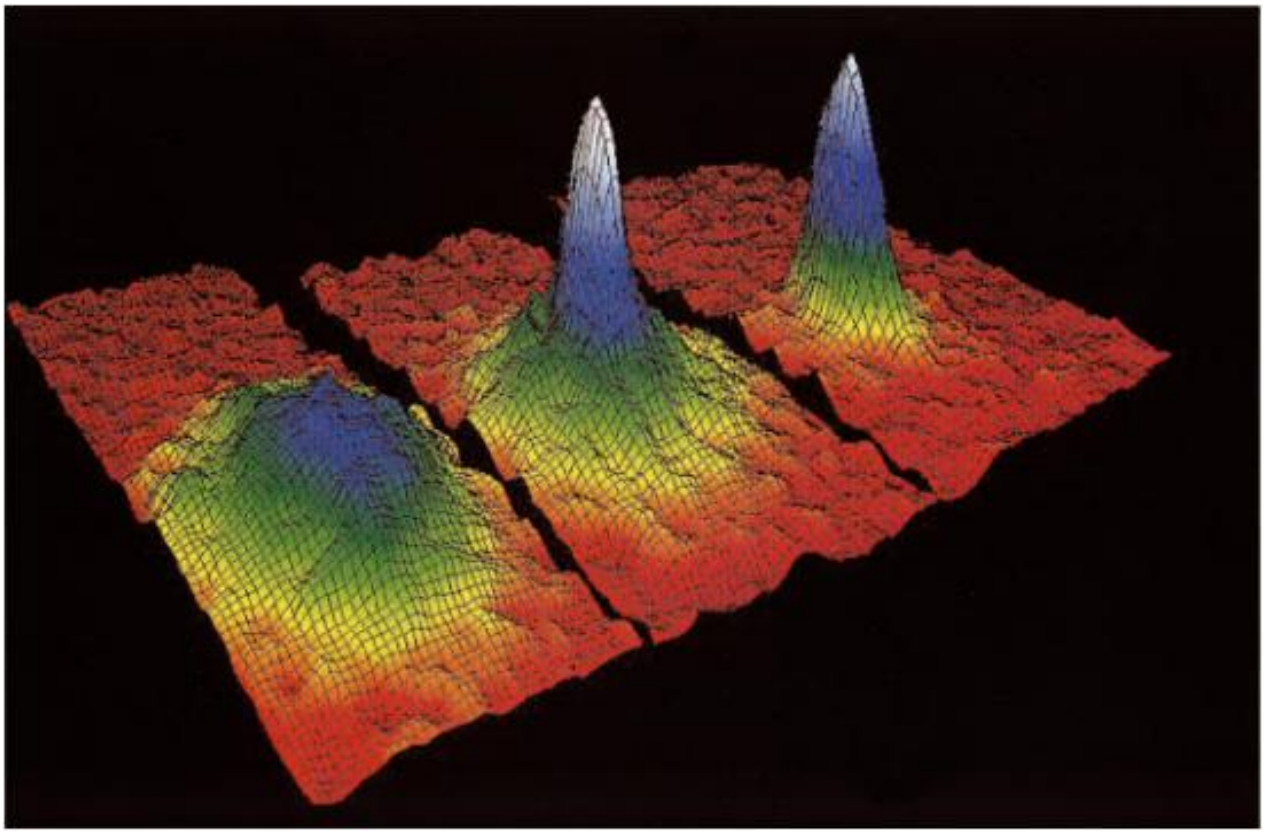

Figure 13. (Color) Images of the velocity distribution of rubidium atoms in the experiment by Anderson et al. (1995), taken by means of the expansion method. The left frame corresponds to a gas at a temperature just above condensation; the center frame, just after the appearance of the condensate; the right frame, after further evaporation leaves a sample of nearly pure condensate. The field of view is 200 mm3270 mm, and corresponds to the distance the atoms have moved in about 1/20 s. The color corresponds to the number of atoms at each velocity, with red being the fewest and white being the most. From Cornell (1996), in Dalfovo and Giorgini (1999).

I.7.2. Experimental realization of Bose-Einstein condensation

In 1995, a series of spectacular experimental developments changed the face of physics forever (Stickney, 2007). In this year the first true BEC was created by Eric Cornell and Carl Wieman in Boulder, Colorado. Later that year Wolfgang Ketterle also created a BEC in Cambridge, Massachusetts. Two technical developments made this possible. The first was the advent of laser cooling and trapping in the mid 1980's (Stickney, 2007) (Figure 14). The second was the development of magnetic trapping and RF-forced evaporative cooling. The combination of these two experimental techniques allowed physicists to cool a gas from hundreds of degrees Kelvin to a few nano Kelvin without using any conventional cryogenic techniques.

Figure 14. An atom chip [From Stickney (2007)]

I.7.3. Applications of Bose-Einstein condensates

The overall phenomenon of BEC is closely related to superconductivity and that application would trump everything else. The primary application of atomic BEC systems is in basic research areas at the moment, and will probably remain so for the foreseeable future. BEC is a tool for lithography, but that's not likely to be a real commercial application any time soon, because the throughput is just too low. Recently, an arbitrary pattern nanolithography system using interferometry of BECs has been proposed, since atomic interferometry using BEC has been demonstrated under various configurations (Debs et al., 2011; Muntinga et al., 2013), thus paving the way for the feasibility of the concept.

One of the hottest areas in BEC at the moment is the use of Bose condensates (and the related phenomenon of degenerate Fermi gases) to simulate condensed matter systems. One can easily makes an optical lattice from an interference pattern of multiple laser beams that looks to the atoms rather like a crystal lattice in a solid looks to electrons: a regular array of sites where the particles could be trapped, with all the sites interconnected by tunneling. The big advantage BEC/ optical lattice systems have over real condensed matter systems is that they are more easily tunable. Possibilities for easily variations of the lattice spacing, the strength of the interaction

between atoms, and the number density of atoms in the lattice, allowing possibilities to explore a range of different parameters with essentially the same sample, which is very difficult to do with condensed matter systems where one needs to grow all new samples for every new set of values in exploration.

There is a great deal of work using BEC systems to explore condensed matter physics. essentially making cold atoms look like electrons. The fiew years old review article, by Immanuel Bloch, Jean Dalibard, and Wilhelm Zwerger (Bloch et al., 2008) covers a lot of this work. There is also a good deal of interest in BEC for possible applications in precision measurement. At the moment, some of the most sensitive detectors ever made for things like rotation, acceleration, and gravity gradients come from atom interferometry, using the wavelike properties of atoms to do interference experiments that measure small shifts induced by these effects. One area of interest is high precision measurement schemes, for which BECs are particularly well suited because they are extremely cold and have laser like coherence properties. More information based on this BEC application can be found in the papers of Dunningham et al. (2005), Hardesty (2016) and Ball (2014). The other really hot area of BEC research is in looking for ways to use BEC systems for quantum information processing. In most of the experimental implementations of quantum computation up to now, a qubit is represented by a single or a few particles (Shi, 1999). But representing qubits in terms of macroscopic quantum coherence of a many-body system, such as superconducting state or BEC may have various advantages, including the simplification of the operations, easier manipulation, and being robust against some microscopic details and thus reduces errors. While quantum computation based on Josephson-junction (Ioffe it et al., 1999; Mooij et al., 1999) involves superconducting states, atomic Bose-Einstein condensates are more controllable at present day.

I.8. Nanostructures

I.8.1. Definition

Nanostructured materials are the fundamental components of nanoscience and nanotechnology. There have been several definitions given for nanostructures in recent years. Different organizations have differences in opinion when defining nanostructures. Thus, a single internationally accepted definition for nanostructures does not exist. For us to properly define

nanomaterials, we have to define nanoscale dimensions first. Generally, the International Organization for Standardization (ISO) defines a nanostructured material as a material with any external nanoscale dimension or having internal nanoscale surface structure. Similarly, the European Commission describes nanostructures as a manufactured or natural material that possesses unbounded, aggregated or agglomerated particles with external dimensions between 1-100 nm size ranges. Generally, the use of different definitions across various jurisdictions acts as a major hindrance to regulatory efforts as it causes legal hesitation in utilizing regulatory techniques for identical nanostructures. Nanoparticles, quantum dots, nanoplates, nanofibers, nanowires, and other related terms have also been defined based on the ISO definition (Bleeker et al., 2013).

I.8.2. Classification of nanostructures

I.8.2.1. Classification of nanostructures based on dimension

Nanostructures are structures between 1 and 100 nm in size that are made up of carbon, composite, metal, metal oxide, organic, or inorganic material. Nanostructures differ in shape, dimension, and size. Many nanostructures and nanomaterials have been reported and it is expected that their diversity will increase in the near future. Depending on their dimensions, nanostructures are classified into one of four categories (Ramrakhiani, 2012):

- 0D, where length, height, and breadth parameters are fixed at a single point, for instance at a dot,
- 1D, where only one parameter exists, for instance grapheme,
- 2D, where parameters of length and breadth exist, for instance carbon nanotubes, transition metal dichalcogenides (TMDs),
- 3D, where all three parameters exists, for instance Pd and ZnO NPs.

Generally, electrons in 0D nanostructures are trapped in a dimensionless space while 1D nanostructures have electrons that can be moved along the (x)-axis no more than 100 nm. Accordingly, 2D and 3D nanostructures have electrons that can be moved along the (x, y)-axis and (x, y, z)-axis, respectively (Ramrakhiani, 2012).

I.8.2.2. Classification of nanostructures based on material composite

Nanostructures have different shapes, sizes, structures and origins. They can be spherical, conical, spiral, cylindrical, tubular, flat, hollow, or irregular in shape and be from 1 to 100 nm in size. Most nanostructured materials can be generally classified into four material-based categories: organic, inorganic, composite and carbon-based.

I.8.3. Properties of nanostructures

Properties are essentially about cause and effect. A material left completely undisturbed doesn't display its properties. However, if we probe something, the response will reveal the characteristic properties of the object. More accurately, however, we should specify its reflectance, hardness, heat capacity and so on as precisely defined properties that can be measured in a specific setup. All the materials- may be metals, semiconductors or insulators. Thus geometrical structure, chemical bonds, ionization potential, electronic properties, optical properties, mechanical strength, melting point, magnetic properties etc. are all affected by the particle sizes.

I.8.3.1. Mechanical properties of nanostructures

Mechanical properties include elastic, inelastic (plastic, fracture, or viscoelastic), and strength. Elastic and inelastic properties are needed to predict deformation from an applied load in the elastic and inelastic regimes, respectively. The strength property is needed to predict the allowable operating limit. Some of the properties of interest are hardness, elastic modulus, bending strength (fracture stress), fracture toughness and fatigue strength. Micro/nanostructures have some surface topography and local scratches dependent upon the manufacturing process. Surface roughness and local scratches may compromise the reliability of the devices and their effect needs to be studied.

Lot of techniques are used to measure mechanical properties of nanostructures materials. These include tensile tests and bending tests (Johansson et al., 1988), resonant structure tests for measurement of elastic properties (Johansson et al., 1988), fracture toughness tests (Wilson et

al., 1995), and fatigue tests (Komai et al., 1998). Most recently, a few researchers have measured mechanical properties of nanoscale structures using atomic force microscopy (AFM) (Sundararajan Bhushan, 2002) and nanoindentation (Li et al., 2003). For stress and deformation analyses of simple geometries and boundary condition, analytical models are more appropriate. For analysis of complex geometries, numerical models are used. The conventional finite element method (FEM) can be used down to a few tens of nanometers, although its applicability is questionable at the nanoscale. FEM has been also used for simulation and prediction of residual stresses and strains induced in MEMS devices during fabrication (Hsu and Sun, 1998), to perform fault analysis in order to study MEMS faulty behavior (Kolpekwar et al., 1998), to compute mechanical strain resulting from the doping of silicon, and to analyze micromechanical experimental data (Wilson and Beck, 1996) and nanomechanical experimental data. FEM analysis of nanostructures has been carried out to analyze the effect of types of surface roughness and scratches on stresses in nanostructures (Bhushan and Agrawal, 2003).

I.8.3.2. Thermal properties of nanostructures

It is found that melting point is lowered with decreasing particle size. It may be reduced to half of the original. The specific heat and thermal expansion may increase up to 50% or more with reducing particle size.

I.8.3.3. Optical properties of nanostructures

Enhanced luminescence with fast response has been observed by decreasing size of nanocrystals. This is because of changes in electronic structure and useful in fast response devices with emission of desired color. Nanoparticles may be used in lasers also since these can operate at lower threshold. Confinement of photons and phonons in nanoparticles also affect the Raman spectra. Nonlinear optical properties are also observed in semiconductor clusters in glass or polymer matrix.

I.8.3.4. Magnetic properties of nanostructures

Saturation magnetization values of nanoparticles are smaller but coercive values are much larger than their polycrystalline counterparts. This is due to their high surface to volume ratio and increased effective anisotrophy. Curie temperature of ferromagnetic materials decreases with decreasing size of nanoparticles, and hence the substance remains paramagnetic even below usual Curie temperature showing super paramagtetism. In nanocrystalline phase, each particle is a single ferromagnetic domain.

I.8.3.5. Electrical properties of nanostructures

Electrical properties are affected by the size in nanometer range. Electrical conductivity is reduced by decreasing the size of nanocrystals. Ferroelectric materials become non-ferroelectric at reduced sizes (20 nm).

I.8.4. Synthesis of nanostructures

Various syntheisis methods found in both physical and chemical area of science are presented in Table 1. Figure 15 illustrate the general synthesis process of nanostructures as mentionned by Meera Ramrakhiani (2012).

Table 1. Physical and chemical synthesis methods of nanostructures materials. **Source.** Meera Ramrakhiani (2012)

Area of science	Synthesis methods
Physical methods	➢ Consolidation ➢ Gas aggregation of monomer ➢ Inert gas evaporation ➢ Sputtering ➢ Ion beam method ➢ Ball milling

Chemical methods	➢ Lithography ➢ Chemical precipitation and capping ➢ Sol-gel method ➢ Micro-emulsion ➢ Condensed phase synthesis ➢ Reduction technique ➢ Electro-chemical deposition

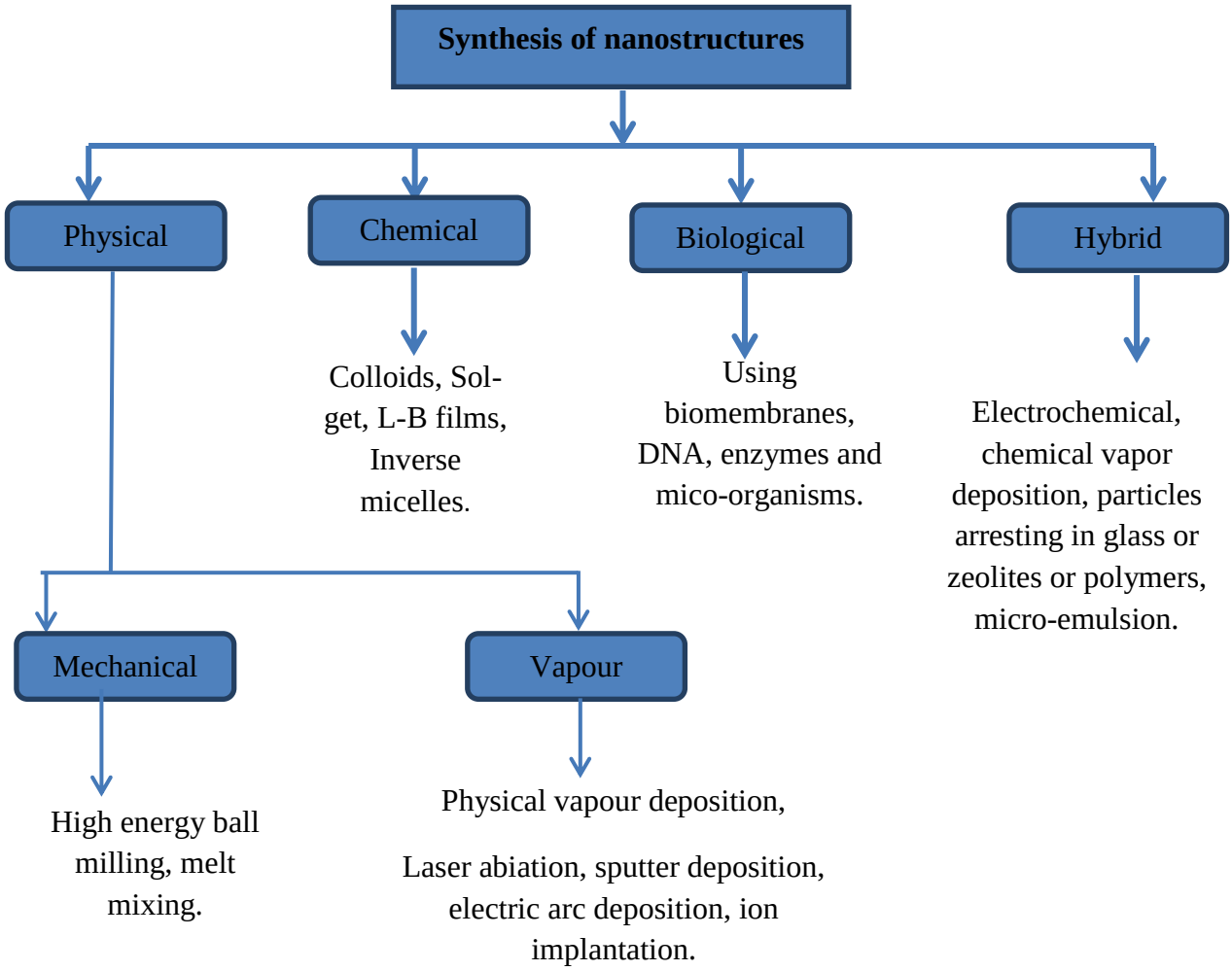

Figure 15. General process of nanostructures synthesis. **Source.** Ramrakhiani (2012)

I.8.5. Characterization of nanostructures

In order to understand the inter-relationship between structure and properties, nanocrystalline materials need to be characterized on both atomic and nanometer scales. The characteristic of above involves determining the shapes and sizes of nanoparticles and understanding of the inter-particle interactions. This information is important both from the scientific and the industrial application point of view. A number of experimental techniques have been employed to yield structural information on nanocrystalline materials. These include 'direct' microscopic techniques such as (i) atomic force microscopy, (2i) transmission electron microscopy, (3i) scanning electron microscopy and (4i) field ion microscopy. In addition to these, many indirect techniques are also used to obtain the information about the nanomaterials structures. A few indirect techniques are (i) absorption spectra, (2i) diffraction of X-rays, electrons or neutrons, (3i) Rutherford back scattering, (4i) Raman spectroscopy, (5i) Auger electron spectroscopy and (6i) Photoluminescence and Photoluminescence excitation. X-ray diffraction patterns for various sizes of nanocrystals show that the peaks are broadened as the crystal size is reduced. The absorption edge or peak is shifted towards higher energy side by reducing the size indicating the widening of the forbidden energy gap of the material. These techniques are complementary to each other. Depending on the system to be studied, one technique may be better than the other.

I.8.6. Quantum well

I.8.6.1. Definition and schematization

Quantum wells are 2D structures for which the bound states are characterized by standing waves in the confined directions and running in the other two. More precisely, a quantum well is a potential well with only discrete energy values. The classic model used to illustrate a quantum well is depicted in Figure 16 below.

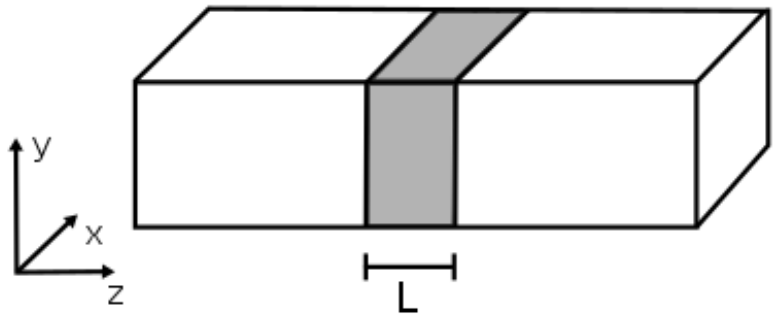

Figure 16. Simple illustration of a quantum well potential. Source. Irnova (2018).

I.8.6.2. Fabrication

There are 3 main approaches to growing a quantum well material system: lattice-matched, strain-balanced, and strained (Sayed and Bedair, 2019). In the former, the well and the barrier have a similar lattice constant as the underlying substrate material (Sayed and Bedair, 2019). With this method, the bandgap difference there is minimal dislocation but also a minimal shift in the absorption spectrum. In a strain-balanced system, the well and barrier are grown so that the increase in lattice constant of one of the layers is compensated by the decrease in lattice constant in the next compared to the substrate material. The choice of thickness and composition of the layers affect bandgap requirements and carrier transport limitations. This approach provides the most flexibility in design, offering a high number of periodic QWs with minimal strain relaxation (Sayed and Bedair, 2019). A strained system is grown with wells and barriers that are not similar in lattice constant. A strained system compresses the whole structure. As a result, the structure is only able to accommodate a few quantum wells (Sayed and Bedair, 2019).

I.8.6.3. Quantum well models

I.8.6.3.1. The infinite quantum well model

The simplest model of a quantum well system is the infinite well model (Fox and Ispasoiu, 2006). The walls/barriers of the potential well are assumed to be infinite in this model. This approximation is rather unrealistic, as the potential wells created in quantum wells are

generally of the order of a few hundred milli-electronvolts, which is far smaller than the infinitely high potential assumed. However, as a first approximation, the infinite well model serves as a simple and useful model that provides some insight into the physics behind quantum wells (Fox and Ispasoiu, 2006).

I.8.6.3.2. The finite quantum well model

The finite quantum well model provides a more realistic model of quantum wells. Here the walls of the well in the heterostructure are modeled using a finite potential V_0, which is the difference in the conduction band energies of the different semiconductors. Since the walls are finite and the electrons can tunnel into the barrier region. Therefore the allowed wave functions will penetrate the barrier wall.

I.8.7. Applications of nanostructures

Because of the very fine grain sizes, nanocrystalline materials exhibit a variety of properties that are different and often considerably improved in comparison with those of conventional coarse-grained polycrystalline materials. The fascinating field of nanotechnology has wide range of applications. Use of nanoscale materials may improve the performance of presently available devices. The nano-version of Silica, Titanium dioxide, Clays, Powdered metals, polymers and chemical products will be established in near future. New materials with difference performance characteristics may also be developed from nanostructured materials. On the other hand some new products have come up such as nanotubes, bucky balls, dendrimers, and quantum dots to cite a fiew. which are at research level.

I.8.7.1. Tougher and harder cutting tools

Cutting tools made of nanocrystalline materials, such as Tungsten carbide, Tantalum carbide, and Titanium carbide, are much harder, much more wear-resistant, erosion-resistant, and last longer than their conventional (large-grained) counterparts. They also enable the manufacturer to machine various materials much faster, thereby increasing productivity and

significantly reducing manufacturing costs. Also, for the miniaturization of microelectronic circuits, the industry needs microdrills with enhanced edge retention and far better wear resistance. Since nanocrystalline carbides are much stronger, harder, and wear-resistant, they are currently being used in these microdrills.

I.8.7.2. Ductile, machinable ceramics

Ceramics are very hard, brittle, and difficult to machine. These characteristics of ceramics have discouraged the potential users from exploiting their beneficial properties. However, with a reduction in grain size, these ceramics have increasingly been used. Zirconia, a hard, brittle ceramic, has even been rendered superplastic. However, these ceramics must possess nanocrystalline grains to be superplastic. In fact, nanocrystalline ceramics, such as Silicon nitride (Si_3N_4) and Silicon carbide (SiC), have been used in such automotive applications as high-strength springs, ball bearings, and valve lifters, because they possess good formability and machinabilty combined with excellent physical, chemical, and mechanical properties. They are also used as components in high-temperature furnaces.

I.8.7.3. Phosphors for high-definition TV and flat-panel displays

The resolution of a television or a monitor depends greatly on the size of the pixel. These pixels are essentially made of materials called "phosphors," which glow when struck by a stream of electrons inside the cathode ray tube. The resolution improves with a reduction in the size of the pixel, or the phosphors. Nanocrystalline Zinc selenide, Zinc sulfide, Cadmium sulfide, and Lead telluride synthesized by the sol-gel technique are candidates for improving the resolution of monitors. The use of nanophosphors is envisioned to reduce the cost of these displays so as to render high-definition televisions and personal computers affordable to be purchased by an average household. Also, the flat-panel displays constructed out of nanomaterials possess much higher brightness, contrast and fast response than the conventional ones owing to their enhanced electrical and magnetic properties.

I.8.7.4. Optical filters and attenuators

Optical transparency of nanocrystalline ceramics can be controlled by grain size. By changing the size, optical filters for different colors can be made. These are also useful for sunscreens and so on.

I.8.7.5. Lasers with low threshold current

Double heterostructure lasers made from quantum well and quantum dots can be operated at extra low threshold current, which are used in compact disk players optical communications etc.

I.8.7.6. Elimination of pollutants

Nanocrystalline materials possess extremely large grain boundaries relative to their grain size. Hence, nanomaterials are very active in terms of their chemical, physical, and mechanical properties. Due to their enhanced chemical activity, nanomaterials can be used as catalysts to react with such noxious and toxic gases as carbon monoxide and nitrogen oxide in automobile catalytic converters and power generation equipment to prevent environmental pollution arising from burning gasoline and coal.

I.8.7.7. High-power magnets

The strength of a magnet is measured in terms of coercivity and saturation magnetization values. These values increase with a decrease in the grain size and an increase in the specific surface area (surface area per unit volume of the grains) of the grains. It has been shown that magnets made of nanocrystalline yttrium-samarium-cobalt grains possess very unusual magnetic properties due to their extremely large surface area. Typical applications for these high-power rare-earth magnets include quieter submarines, automobile alternators, land-based power generators, and motors for ships, ultra-sensitive analytical instruments, and magnetic resonance imaging in medical diagnostics.

I.9. 2D Transition metal dichalcogenides

I.9.1. Definition, composition and types

Transition metal dichalcogenides (TMDs) are 2D nanostructures materials of the type MX_2, where M is a transition metal atom (such as Mo or W) and X is a chalcogen atom (usually S, Se or Te). The first element corresponds to groups $4-10$ of the transition metal series. Generally, TMDs materials containing group $4-7$ transition elements have a layered structure, while those with group $8-10$ transition metals have non-layered structures (Han et al., 2015). Depending on their chemical compositions and structural configurations, atomically thin 2D materials can be categorized as metallic, semi-metallic, semiconducting, insulating, or superconducting. Unlike graphene, many 2D TMDs are semiconductor in nature.

I.9.2. Synthesis of 2D transition metal dichalcogenides

There are many different techniques used for the development of 2D TMDs materials. These consist of:

- mechanical exfoliation method (MEM),
- liquid exfoliation method (LEM),
- sulfurization (or selenization)
- vaporization of metal oxide with chalcogen precursor,
- chemical vapor deposition,
- metal-organic chemical vapor deposition (MOCVD).

MEM: MEM is typically adopted to prepare single-layer TMDs samples. Within this method, the single crystal TMDs samples prepared by the mechanical exfoliation method are of good quality, and can be used for studying their basic properties (Yin et al., 2012; Li et al, 2012) by optical microscopy, atomic force microscopy, scanning tunneling microscopy, transmission electron microscopy and so on. However, the size of the TMDs materials prepared by the MEM is quite small approximately on the tens of microns scale, posing a limitation to real device applications.

CVD: CVD method is the most effective way to achieve large area growth. This method can be divided into two types: the sulfurization (or selenization) of metal thin films and vapor phase reaction of metal oxides with chalcogen precursor. The CVD is one of the most effective methods to achieve large area growth of atomically thin 2D TMDs for the successful device applications. The simplest form of CVD to grow 2D TMDs is the co-evaporation of metal oxides and chalcogen precursors that lead to vapor phase reaction followed by the formation of a stable 2D TMD over a suitable substrate. The growth mechanism of CVD method differs in each synthesis process as the materials forming process also depends on (1) properties of substrate, (2) temperature and (3) atomic gas flux (for further informations, redears should refer to (Lee, et al., 2012).

MOCVD: MOCVD is similar to a conventional CVD except those metal-organic or organic compound precursors (OCP) are used as the source materials. In MOCVD reaction, the desired atoms are combined with complex organic molecules and flown over a substrate where the molecules are decomposed by heat and the target atoms are deposited on the substrate atom by atom. The quality of films can be engineered by varying the composition of atoms at atomic scale, which results in the desired thin film with high crystallinity. The advantages of MOCVD in 2D TMDs growth are: (i) it can achieve large-scale and uniform growth of 2D TMDs, (ii) it provides a precise control over both metal and chalcogen precursors and thereby controls the composition and morphology of 2D TMDs (Kang, et al., 2015). In addition, the MOCVD method is versatile, highly scalable, and provides significant stoichiometric control over the films, but the use of toxic precursors, slow film growth rate and high production cost set it back for the widespread use.

I.9.3. Properties of transition metal dichalcogenides

Among several properties that possesses TMDs, the most important are Mechanical and optical properties. The strength of the strongest single layer membranes is 11% of their Young's modulus, corresponding to the upper theoretical limit, which indicates that the material is highly crystalline and almost defect-free. This results show that single-layer MoS_2 could be suitable for a variety of applications, such as reinforcing elements in composites and for the fabrication of flexible electronic devices (Bertolazzi et al., 2011). The various electronic properties of TMDs

arise from the filling of the non-bonding d bands from the group $4-10$ species. When the orbitals are partially occupied, the TMDs display metallic properties, whereas when they are fully occupied, they exhibit semiconducting ones. The influence of the chalcogen atoms on the electronic structure is minor compared with that of the metal atoms. However, it is observed that the broadening of the d bands decreases the bandgap by increasing the atomic number of the chalcogen (Chhowalla et al., 2013). The bulk TMDs material has an indirect bandgap according to both the theoretical calculations and experimental results (Cong et al., 2014; Li et al., 2007; Lee et al., 2012; Li et al., 2012).

I.9.4. Applications of transition metal dichalcogenides

2D TMDs materials are considered attractive for diverse applications including electronics [Radisavljevic et al. (2011); Wang et al. (2012); , optoelectronics (Yin et al., 2012; Lee et al., 2012; Zhong et al., 2010), sensing (He et al., 2012; Li et al., 2012a; He et al., 2012b) and energy devices (Du et al., 2010) (Figure 18).

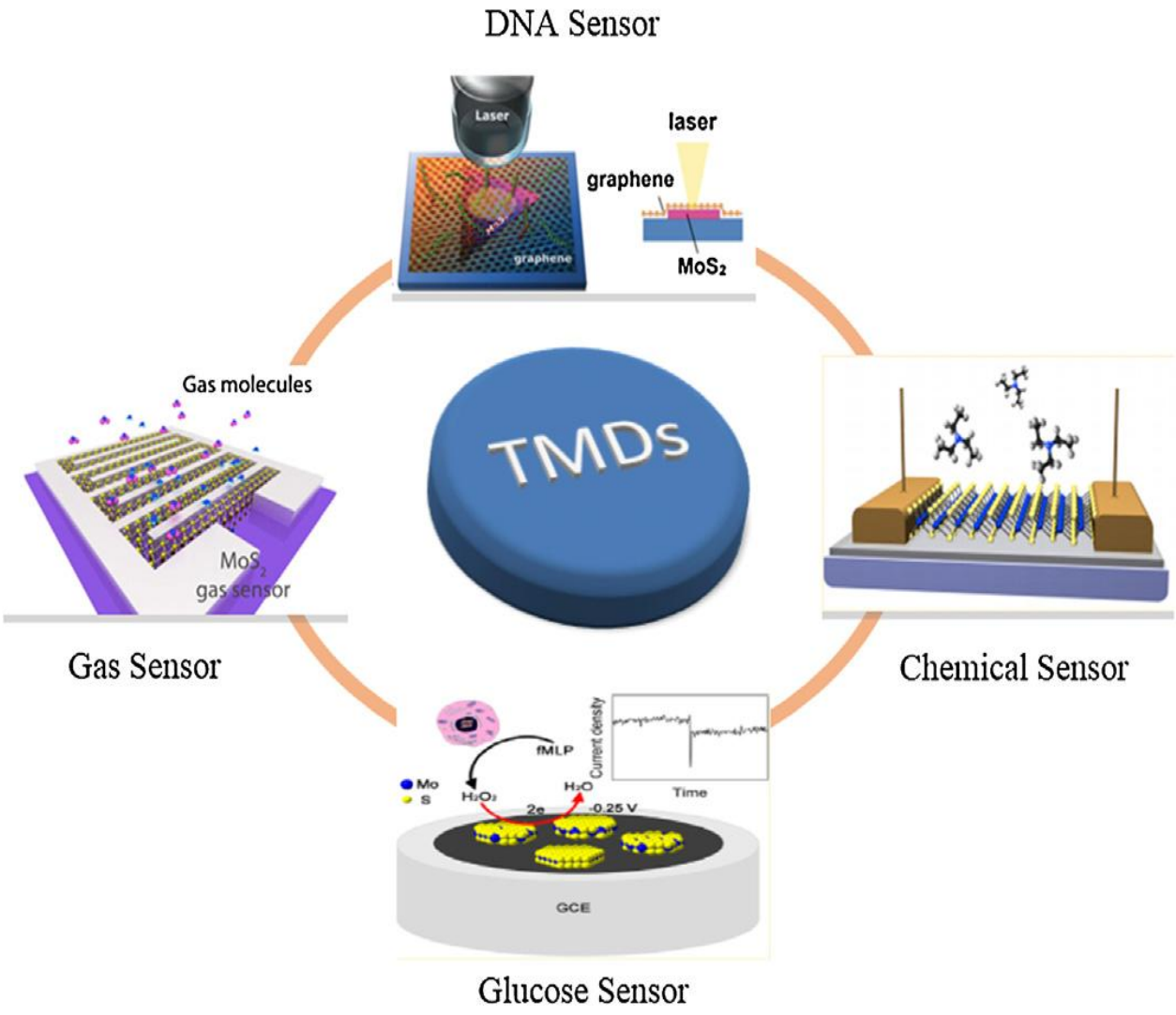

Figure 17. Various gas, chemical and biosensors constructed using 2D TMDs materials like MoS2, WS2, etc. [Reprinted with permission from Perkins et al. (2013), American Chemical Society, American Chemical Society (Loan, et al., 2014), John Wiley and Sons (Cho, et al., 2015), Nature Publishing Group].

Conclusion

This chapter focused on generalities on quantum population transfer in atomic particles and particularly two-level system while interacting with laser light. We begin with coherent dynamic of atomic particles (TLS) where specific mathematical models and basis of theoretical investigations are presented. Further, a review on laser cooling and trapping of atomic particles is presented. Of course, concepts and techniques for both cooling and trapping phenomena are presented, and thus an important landmark in the temperature scale corresponding to various

temperatures selection or cooling types is depicted, followed by important applications. Finally, we present a large literature review on nanostructures and particularly 2D TMDs materials thereby reporting their applications.

CHAPTER TWO

METHODS AND MODELS

Introduction

The physics of light-matter interactions is a rapidly developing interdisciplinary research area, combining methods and phenomena both from condensed matter physics and quantum optics (Shahnazaryan, 2017). The background, challenges and complete overview based on laser cooling and trapping of atomic particles have been carefully discussed in the previous chapter. There, a perefect classification of different laser cooling types and trapping systems are discussed with illustrations. BEC with applications as similar as 2D TMDs materials with properties also constitute part of the previous section. The present chapter for instance, presents some mathematical tools and methods that are useful in assessing effect of surrounding environment in laser cooling and trapping of atomic entities and particularly polaritons and polarons, so as to achieve our main objective. To make things easier for readers, we divided the chapter in three main sections. The first section presents some mathematical solvable models such as Rabi, Jaynes-Cummings and Landau-Zener models. This is for readers to have a lucid idea on mathematical approach and theoretical formulation made in the present thesis. The second section presents methods and models with analytical results based on the semiclassical approach of laser cooling and trapping of TLS in general and particularly polaritons and polarons. The main purpose of this section is to clarify for readers the origin of the force and torque in laser cooling and trapping phenomena. The last section is devoted to the presentation of quantum mechanical approach of laser cooled and trapped polariton and polariton. This section is the main section where we developed our model and thus possesses important mathematical methods and formalism which allow robust control of the dynamic of laser cooled and trapped polariton and polaron.

II.1. Mathematical solvable models

II.1.1. Rabi and Jaynes-Cummings models

The Rabi model (RM) (Rabi, 1936) is the semi-classical version of the model which describes the simplest interaction between a TLS with laser light. The quantized version of the Rabi model was investigated by Jaynes and Cummings in 1963 (Jaynes and Cummings, 1963). The model represents the only model where rotating wave approximation (RWA) can be apply. The initial goal of Jaynes and Cummings while introducing such a model was to study the relationship between the quantum theory of radiation and the corresponding semi-classical (SC) theory. The Jaynes-Cummings Hamiltonian (JCH) is expressed in Eq.1, where a and a^+ are the destruction and creation operators for a single bosonic mode of frequency ω , $\sigma_\pm = \frac{1}{2}\left(\sigma_1 \pm i\sigma_2\right)$ are pseudo-spin operators defined so as to satisfy the commutation relations $\left[\sigma_+, \sigma_-\right] = \sigma_3$ and $\left[\sigma_3, \sigma_\pm\right] = \pm 2\sigma_\pm$ with level splitting 2Δ, and g denotes the coupling parameter which control the light matter interaction.

$$H_{JC} = \Delta\sigma_3 + \omega a^+ a + g\left(a^+ + a\right)\sigma_1 \qquad (1).$$

The Jaynes Cummings Model (JCM) has been very successfully applied to understand a range of experimental phenomena, such as vacuum Rabi mode splitting (VRMS) (Shimizu and Sasada, 1998) and quantum Rabi oscillation (QRO). In fact, the model is easy to solve, allowing the physical properties of the model to be readily obtained and compared with a large number of experiments. The basic physics explored in the JCM includes Rabi oscillations, collapses and revivals of quantum state populations, quadrature squeezing, entanglement, Schrödinger cat states and photon anti-bunching. Circuit quantum electrodynamics (QED), two-dimensional electron gases and trapped ions supported by the concepts of quantum metamaterials and quantum simulations (Pedernales et al., 2015) have emerged as platforms for faithful representations of abstract models, quite analogous to the possibilities established by the advent of cold atom physics. The impact on practical applications is even greater. This is because the TLS appearing in the SC and quantum Rabi models is a qubit which is the building block of quantum information technologies with the ultimate goal to realize quantum simulations and quantum computations. The RM forms the connecting link in the interplay of mathematics, physics, and technology.

II.1.2. Landau-Zener model

Landau–Zener model (LZM) is an analytic solution to the equations of motion governing the transition dynamics of a TLS, with a time-dependent Hamiltonian varying such that the energy separation of the two states is a linear function of time (Landau, 1932; Zener, 1932; Stûckelberg, 1932; Majorana, 1932). The Schrödinger equation (SE) for a TLS can be reduced to a second order complex ODE. One common strategy for its solution is to try to transform the equation into a form for which the solutions are known. The model functions describing the time-dependence of the external field are typically assumed to be analytic. They are of such form that the ODE belongs to the class of hypergeometric differential equations, basically the most general class of ODEs in mathematical physics for which the solutions are currently well characterized. Focusing ourselves on the second order ODE for amplitude, the two-level SE consists of two coupled differential equations, first-order in time with probability amplitudes which can be coupled. Yield a single second ODE for either one of the probability amplitudes. Giving the ground state $|g\rangle$, the ODE obtained with the real-symmetric traceless Hamiltonian of the form Eq.2 is given by relation Eq.3, and similar equation holds for excited state $|e\rangle$ but with energy $\varepsilon(t)$ replace by $-\varepsilon(t)$. LZ model is obtained from Eq.2 given that energy $(\varepsilon(t))$ and coupling $(V(t))$ are expressed as $\varepsilon(t)=\varepsilon_0 t$ and $V(t)=V_0$. ε_0 and V_0 are again real constants. This gives a model for the time-dependencies of the system.

$$H(t)=\begin{pmatrix}\varepsilon(t) & V(t)\\ V(t) & -\varepsilon(t)\end{pmatrix} \qquad (2),$$

$$\ddot{C}_1(t)-\frac{\dot{V}(t)}{V(t)}\dot{C}(t)+\left[i\dot{\varepsilon}(t)-i\varepsilon(t)\frac{\dot{V}(t)}{V(t)}+\varepsilon^2(t)+V^2(t)\right]C_1(t)=0 \qquad (3).$$

II.1.3. The Schmidt decomposition

The Schmidt decomposition (SD), named after its originator Erhard Schmidt, refers to a particular way of expressing a vector in the tensor product of two inner product spaces. It is a widely employed tool of quantum theory which plays a key role for distinguishable particles in

scenarios such as entanglement characterization, theory of measurement and state purification (Sciara et al., 2017).

We begin with a review. We recall the notation of the intrinsically symmetric particle-based approach introduced by Lo Franco and Compagno (2016). Hereafter, we mean by symmetric states or symmetric Hilbert space, the symmetric or antisymmetric behavior of the system states depending on the bosonic or fermionic nature of the particles, respectively. The overall state of two identical particles, one in the state $|\phi\rangle$ and other in state $|\psi\rangle$, is completely characterized by enumerating the one-particle states and represented as $|\phi,\psi\rangle$. Two particles in $|\phi,\psi\rangle$ are not independent and their overall state is a whole which cannot be written as a tensorial product of one-particle states, i.e. $|\phi,\psi\rangle \neq |\phi\rangle \otimes |\psi\rangle$. However, a nonseparable external symmetric product of one-particle states can be introduced as $|\phi,\psi\rangle := |\phi\rangle \times |\psi\rangle$. Analogously, we have $\langle\phi,\psi| := \left(|\phi\rangle \otimes |\psi\rangle\right)^{+} = \langle\phi| \times \langle\psi|$. The probability amplitude of finding the two particles in $|\varphi,\varsigma\rangle$ if they are in $|\phi,\psi\rangle$, is obtained by the symmetric two-particle scalar product defined by Lo Franco and Compagno (2016) in terms of one-particle amplitudes Eq.4. This probability amplitude immediately shows that the generic state $|\phi,\psi\rangle$ is symmetric, i.e. $|\phi,\psi\rangle = \eta|\psi,\phi\rangle$. The state $|\phi,\psi\rangle$ spans a linear symmetric two-particle Hilbert space $H_{\eta}^{(2)}$. A symmetric inner product between state spaces of different dimensionality can also be introduced (Lo Franco and Compagno, 2016) as indicated in Eq.5.

$$\langle\varphi,\varsigma|\phi,\psi\rangle = \langle\varphi|\phi\rangle\langle\varsigma|\psi\rangle + \eta\langle\varphi|\psi\rangle\langle\varsigma|\phi\rangle \tag{4}.$$

$$\langle\psi_k|\cdot|\phi,\psi\rangle \equiv \langle\psi_k|\phi,\psi\rangle = \langle\psi_k|\phi|\psi\rangle\rangle + \eta\langle\psi_k|\psi\rangle|\phi\rangle \tag{5}.$$

In the above equations, the quantity η is a constant which can takes the value $\eta = 1$ for bosons and $\eta = -1$ for fermions. In $H_{\eta}^{(2)}$, it is possible to choose an orthonormal two-particle basis $\{|i,j\rangle\}$, $|i\rangle$ and $|j\rangle$ being single-particle states, where an arbitrary state of two identical particles

can be expressed as $\left|\Psi^{(2)}\right\rangle = \sum_{ij} c_{ij} \left|i, j\right\rangle$. From Eq.5, one then gets the reduced (single-particle) density matrix via partial trace (Lo Franco and Compagno, 2016) as given in Eq.6. Here $\rho = \sum_j \left\langle j\right|\Psi^{(2)}\left\rangle\right\langle\Psi^{(2)}\left|j\right\rangle$.

$$\rho^{(1)} = \frac{1}{2}\sum_j \left\langle j\right|\Psi^{(2)}\left\rangle\right\langle\Psi^{(2)}\left|j\right\rangle = \frac{1}{2} Tr^{(1)}\rho \tag{6}.$$

We emphasize that now partial trace depends on the single-particle basis being local or nonlocal. It then comes the following theorem: 'within a symmetric two-particle Hilbert space $H_{\eta}^{(2)}$, a pure state of two d-level identical particles $\left|\Psi\right\rangle$ can always be written in the (SD) Eq.7. The Schmidt coefficients λ_i are the square roots of the eigenvalues of the reduced density matrix and the states $\left\{\left|i\right\rangle\right\}$ its eigenstates. The state $\left|\vec{i}\right\rangle$ belongs to the basis $\left\{\left|i\right\rangle\right\}$ and the symmetric two-particle basis $\left\{\left|i, \vec{i}\right\rangle\right\}$ is the Schmidt basis.

$$\left|\Psi\right\rangle = \frac{1}{\sqrt{2}}\sum_i \sqrt{\lambda_i}\left|i, i\right\rangle, \left(\lambda_i \succ 0, \sum_i \lambda_i = 1\right) \tag{7}.$$

II.2. Semiclassical approach of laser cooling and trapping of two-level systems

II.2.1. Dipole approximation of the force and corresponding torque

Early in 1619, Johannes Kepler suggested that the mechanical effect of light might be responsible for the deflection of the tail of comets entering our solar system. Also, the classical Maxwell theory showed in 1873 that the radiation field carries with it momentum and that "light pressure" is exerted on illuminated objects. Later, in 1905, Einstein introduced the concept of the photon and showed that energy transfer between light and matter occurs in discrete quanta (Dion et al., 2016). Force and torque were found to be of great importance in microscopic events, and particularly in laser cooling and trapping of TLS. The net force acting on a charge q at position

R moving with the velocity V when it is interacting with the EM field E and B is entirely determined by the help of classical Lorentz equation (Eq.8).

$$F_q(r) = q[E(R) + V \times B(R)]. \quad (8).$$

A quantized TLS is well described by a dipole. To derive the EM force acting on a dipole, we consider two oppositely charged particles $+q$ and $-q$ with masses m placed at $d + \frac{R}{2}$ and $d - \frac{R}{2}$ respectively. That is separated by a tiny distance $|d|$, and illuminated by an arbitrary EM field E and B, as shown in Figure 18. The resultant force on the two charges is expressed by Eq.9. In both Eq.8 and Eq.9, R is for the center of mass coordinates. The two particles are bound to each other by a dipole momentum.

$$F = F_q(R + \frac{d}{2}) + F_{-q}(R - \frac{d}{2}). \quad (9).$$

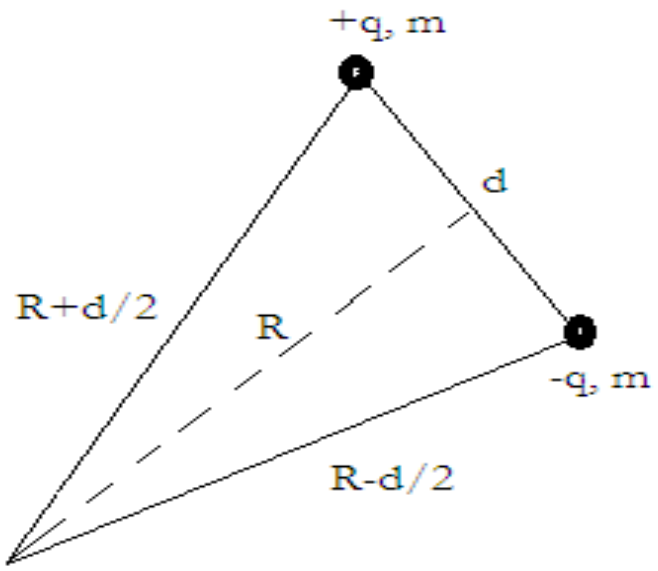

Figure 18. Graphical representation of the system use to derive mechanical force and torque when an atom interacts with light in the dipole approximation.

When the field is almost constant within the distance of $|d|$, we can expand Eq.9 in powers series of d and truncate the higher term beyond the second order. It comes the following:

$$F_q\left(R+\frac{d}{2}\right)=F_q\left(R\right)+\frac{d}{2}F_q^{'}\left(R\right)+\frac{d^2}{8}F_q^{"}\left(R\right)=F_q\left(R\right)+\frac{d}{2}\nabla_R F_q\left(R\right)+\frac{d^2}{8}\Delta_R F_q\left(R\right) \quad (10),$$

$$F_{-q}\left(R-\frac{d}{2}\right)=F_{-q}\left(R\right)-\frac{d}{2}F_{-q'}\left(R\right)+\frac{d^2}{8}F_{-q}^{"}\left(R\right)=F_{-q}\left(R\right)-\frac{d}{2}\nabla_R F_{-q}\left(R\right)+\frac{d^2}{8}\Delta_R F_{-q}\left(R\right) \quad (11).$$

The substitution of Eq.10 and Eq.11 into Eq.9 and taking into account Eq.8, conducts to the following expression of the mechanical force.

$$F=\frac{d}{2}\left[\nabla_R F_q\left(R\right)-\nabla_R F_{-q}\left(R\right)\right]=d\nabla_R qE+d\nabla_R V\times B=d\nabla_R qE+d\nabla_R \dot{R}\times B \quad (12),$$

where $V=\frac{dR}{dt}=\dot{R}$.

Taking into consideration some mathematical formulas, such as the derivation of a product of two functions u and v, and also introducing the third derivative term so as to obtain $\frac{dx}{dy}=\frac{dx}{dt}\frac{dt}{dy}$ (for functions x and y for example) (Djelouah, 2013), then the expression of the force F gives Eq.13 where the dots denote the differentiation with respect to time.

$$F=\left(\mu\cdot\nabla\right)E+\dot{\mu}\dot{R}^{-1}E+\dot{\mu}\times B+\dot{R}\times\left(\mu\cdot\nabla\right)B \quad (13).$$

In Eq.13 above, the parameter μ represents the dipole moment and expressed explicitly by $\mu=qd$. It time derives expression is $\dot{\mu}$ and one can easily obtains $\dot{\mu}=\frac{d\mu}{dt}$. Jeffry (2002) shown that the sinusoidal plane wave constitutes the particular solution of the wave equation if the relation that follows, call dispersion relation, $k=\frac{\omega}{c}$ is verified. Again, Fujii (2014) also shows that $\vec{k}\cdot\vec{E}=0$ for a plane wave. Since $E=cB$, one can write, $\vec{k}\cdot\vec{B}=0$. The final expression of the force acting on a dipole electric moment takes the form of Eq.14.

$$F=\left(\mu\cdot\nabla\right)E+\dot{\mu}\times B+\dot{R}\times\left(\mu\cdot\nabla\right)B=F^{in\,\mathrm{hom}\,o}+F^{Lorentz}+F_{moving}^{in\,\mathrm{hom}\,o}. \quad (14).$$

In Eq.14, to the right hand side, the first term $F^{in\,\mathrm{hom}\,o}$ represents the inhomogeneous field-force, the second $F^{Lorentz}$ the Lorentz force and the third $F_{moving}^{in\,\mathrm{hom}\,o}$ can be consider as the inhomogeneous

field-force on the moving dipole moment which perceives the magnetic field in the reference frame as the electric field due to the Lorentz transformation.

Besides the force, an EM field E and B can also carry angular momentum which exerts a mechanical torque on an irradiated structure. This torque can be calculated from classical electromagnetism, as similar as we did for the mechanical force. The mechanical torque N acting on the charges in the electric dipole moment, for respective charges q at $R+\frac{d}{2}$ and $-q$ at $R-\frac{d}{2}$ is given in Eq.15.

$$N=\frac{d}{2}\times\left[F_q\left(R+\frac{d}{2}\right)-F_{-q}\left(R-\frac{d}{2}\right)\right]. \tag{15}$$

Performing similar expansions as in Eq.10 and Eq.11, and taking the difference, yield Eq.16.

$$F_q\left(R+\frac{d}{2}\right)-F_{-q}\left(R-\frac{d}{2}\right)=2q\left(E+V\times B\right)+\frac{d^2}{4}\nabla_R\left[d\nabla_R q\left(E+V\times B\right)\right] \tag{16}$$

Taking into account considerations of the above section and from the plane electromagnetic wave $\nabla\cdot E=0$ and $\nabla\cdot B=0$, it comes Eq.17 below.

$$d\nabla_R q\left(E+V\times B\right)=\left(\mu\cdot\nabla\right)E+\dot{\mu}\times B+\dot{R}\times\left(\mu\cdot\nabla\right)B. \tag{17}$$

Therefore,

$$F_q\left(R+\frac{d}{2}\right)-F_{-q}\left(R-\frac{d}{2}\right)=2qE+2qV\times B+\dot{\mu}\times\left(\frac{d}{4}\nabla\right)B \tag{18}$$

And the net mechanical torque, acting on the dipole which interacts with light expressed in Eq.17 takes the form of Eq.19.

$$N=\mu\times E+\mu\times(\dot{R}\times B)+\frac{d}{2}\left[\dot{\mu}\times\left(\frac{d}{4}\nabla\right)B\right] \tag{19}$$

To the right hand side of Eq.19, the first term is a torque on the dipole moment in the electric field, the second term is the contribution from the Lorentz transformation of the magnetic field

and the third one is another torque from the Lorentz torque induced by the inhomogeneous magnetic field. The parameter μ still represents the dipole moment and expressed explicitly by $\mu = qd$ with time derivative $\dot{\mu}$. If we apply Eq.19 to an interaction between laser light and an atom, and specifying a monochromatic radiation with an angular frequency ω_l , then the wavelength λ of the laser light is much larger than the dimensions of the atomic TLS $|d|$. As already said in the first part for a plane wave, when E and B are the fields of an identical electromagnetic wave (EMW), the amplitude satisfies $|E| = c|B|$.

The proper use of Eq.13 and Eq.19 requires additional approximations. In a semi classical treatment, the system is considered as sitting at point R, with a well defined velocity V. The position and the momentum must be replaced by their corresponding operators and the atom is described by a wave packet of spatial extension ΔR and linear momentum extension Δp (Xiao-Guang and Chang-Pu, 1996). But, since both position and linear momentum seems to be small compared to the wave length, then one can apply the point like description. For such an approach to be valid, two essential conditions must be simultaneously fulfilled (Xiao-Guang and Chang-Pu, 1996):

i. the dimensions of the atom must be small compared to the laser optical wavelength λ,
ii. the displacement velocity of the atom must be smaller compared to that of light (laser light).

Moreover, like has suggested Jeffry (2002), the velocity of the system is much smaller than that of light c. So, from i and ii, it comes $\lambda \prec\prec c$ and $|d| \prec\prec \Gamma$ respectively. The second inequality conducts to the condition $k|d| \prec\prec 1$. Then, the third term of Eq.13 and that of Eq.19 are smaller compared to their respectives first term. The third term of Eq.13 also smaller than the first term. These can be interpreted by the following mathematical relations:

$$\left|\frac{d}{4}\left[\dot{\mu}\times\left(\frac{d}{2}\nabla\right)B\right]\right| = \frac{|d|^2}{8}K^2|\mu|\cdot|E| \qquad (20),$$

$$|(\mu\cdot\nabla)E| \approx |\mu|\cdot K\cdot|E| \qquad (21),$$

$$\left|\dot{\mu}\times B\right| \approx |\mu| \cdot K \cdot |E| \qquad (22).$$

From the following discussions, the net mechanical force and torque giving by Eq.10 and Eq.19 take the expressions Eq.23 and Eq.24.

$$F = (\mu \cdot \nabla)E + \dot{\mu}\times B = F^{inhomo} + F^{Lorentz} \qquad (23),$$

$$N = \mu \times E \qquad (24).$$

Trapping can also be looking as a simple conservation of atoms in bottles which walls are immaterial rather than materials substances. For trapping material, we choosed a magnetic field which we looked as a trap as has suggested Gov and Shtrickman (1999), who also gave an explanation of the physical mechanism underlying the operation of magnetic trap. Our motivation for choosing this type of trap, as similar as did Gov and Shtrickman (1999), comes from the fact that magnetic trap is the natural candidate for trapping both microscopic particles and large scale objects (Harrigan, 1983 ; Hones and Hones, 1995) in one hand and the electromagnetic field can be used to confine particles with less perturbation to their internal structure and minimal heating from the surrounding environment in the other hand. The appropriate way to describe their operation is in terms of classical mechanics in which the particle is realized in the trap by pointing its magnetic moment antiparallel to the direction of the magnetic field. The Hamiltonian for interaction of a magnetic moment μ_B known as Bohr magneton with a homogeneous magnetic field B is given by Eq.25 that fellows, where we suggested the field to be directed by σ_3 which is the Pauli operator in the z direction.

$$H_B = -\mu_B B \otimes \sigma_3 \qquad (25).$$

But, it has been found that, inside the trap, the particle experiences lateral oscillations which are slow compared to their precision. Therefore the particle may be considered as experiencing a slowly rotating magnetic field. As a result, the magnetic moment μ_B points antiparallel to the local magnetic field lines and the Hamiltonian of the system can just take the normal form (Eq.26) which follows;

$$H_B = \mu_B B \otimes \sigma_3 \tag{26}.$$

These expressions for the Hamiltonian of the interacting system correspond to the spin fiability frequency is giving by Eq.27.

$$h\omega_B = \frac{\mu_B}{I} B \otimes \sigma_3 \tag{27},$$

where I is the related spin equal to $1/2$ for polaritons. From the previous relations, the Hamiltonian H_B that characterizes the field-polariton interaction takes the form of Eq.28.

$$H_B = \frac{\omega_B}{2} \otimes \sigma_3 \tag{28}.$$

In the relation above, $\omega_B = \lambda \mu_B B$ is the magnetic field frequency, giving that λ is the gyromagnetic factor, μ_B the Bohr magneton and B the magnetic field defined by Eq.29 bellow:

$$B = \frac{1}{2}\left\{\cos(kz)\cos(\omega_B t) - i\sin(kz)\sin(\omega_B t)\right\} \tag{29}.$$

To clearly understand the effect of magnetic field in laser cooling and trapping of polariton, we consider two important assumptions. At first, we assumed that since laser cooling and trapping processes are always carried on in the real environment, therefore the Hamiltonian of the magnetic trap should be of the real part. Secondly, we consider that for a weak magnetic field with frequency ω_B, $\sin(\omega_B t) \to 0$ as $\omega_B \prec\prec 1$. Thus, the second term to the right hand side of Eq.25 vanishes and the magnetic field expression becomes $B = \frac{1}{2}\left\{\cos(kz)\cos(\omega_B t)\right\}$. The graphical representation for the simplified expression of the magnetic field is illustrated in Figure 19.

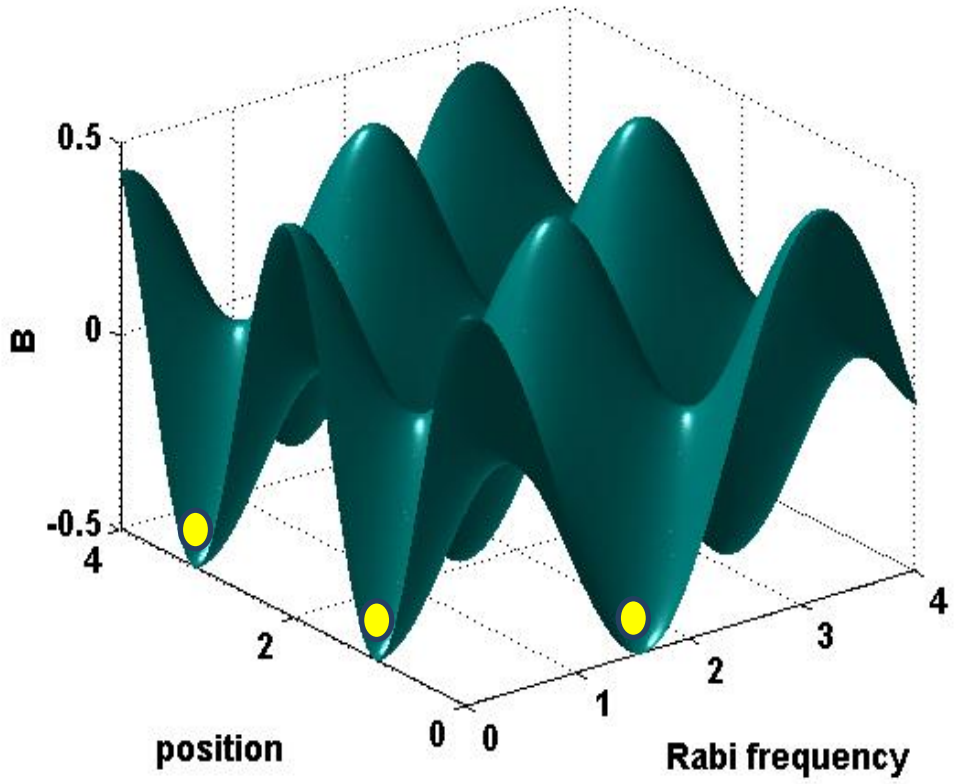

Figure 19. Graphical representation of the magnetic trap used to trap cooled polariton choosing for and schematization of trapped atomic entities.

II.2.2. The semiclassical Jaynes-Cummings Hamiltonian

In this section, we consider an EM wave propagating toward the z-direction with an electric field described by Eq.30.

$$E = E_0 \cos(\omega_l t - kz) \qquad (30).$$

In Eq.30, μ is still the well known electric dipole moment along the direction of the electric field, and E_0 the amplitude of the electric field. ω_l is the laser frequency. The laser light propagating toward the z-direction with an electric field E interacts with the atomic particle (essentially polariton or polaron) at the position $z = 0$. The Hamiltonian of the system, i.e. atomic particle light interaction is giving by Eq.31.

$$H = \overline{H} + H' \quad (31).$$

In Eq.31, $\overline{H} = H_{exc} + H_{ph}$ is a time-independent Hamiltonian of a atomic particle (here a TLS) given that H_{exc} is the exciton Hamiltonian expected as a two-level Hamiltonian and H_{ph} is the photon Hamiltonian. H' is the time-dependent Hamiltonian due to an interaction between TLS and the EM wave. The time dependent Hamiltonian of the radiation field is expressed by Eq.32.

$$H' = -\mu.E_0 \cos w_l t = -\mu E_0 \cos w_l t \quad (32).$$

Since only the electric dipole transition has been considered, the contribution of the magnetic field is neglected. In addition, the effect of the surrounding environment on the system of laser cooled and trapped polariton is taking into account through the interaction Hamiltonian H_I Eq.33.

$$H_I = \hbar g\left(\sigma_+ a + \sigma_- a^+\right) \quad (33).$$

In Eq.33, g is the coupling strength constant between the polariton and photon, a^+ and a are the photon creation and annihilation operators, respectively. The complete Hamiltonian of the system of cooled and trapped polariton (Eq.31) interacting with surrounding environment becomes as given in Eq.34.

$$H = H_{exc} + H_{ph} + H_I + H' = H_{exc} + \hbar\omega a^+ a + \hbar g\left(\sigma_+ a + \sigma_- a^+\right) - \mu E_0 \cos\left(\omega_l t\right) \quad (34),$$

By introducing the magnetic field in the system, characterized by the magnetic field Hamiltonian Eq.28, the total Hamiltonian of the system of laser cooled and trapped polariton with magnetic field is given by Eq.35 in which all the parameters have been identified in the above sections.

$$H_1 = H_{exc} + H_{ph} + H_I + H_B + H' = H_{exc} + \hbar\omega a^+ a + \hbar g\left(\sigma_+ a + \sigma_- a^+\right) + \frac{\omega_B}{2} \otimes \sigma_3 - \mu E_0 \cos\left(\omega_l t\right)$$

(35).

II.2.3. The wavefunction

The wavefunction of the laser cooled and trapped TLS is investigated by solving the time dependent Schrödinger equation (TDSE) (Eq.36) for the giving Hamiltonians Eq.34 and Eq.35.

$$i\hbar\frac{\partial\psi}{\partial t}=H\psi \tag{36}.$$

In general, solution of the above equation, for a TLS Hamiltonian H_0 is given by Eq.37.

$$H_0\psi_{0i}=w_i\psi_{0i}\ ,i=1,2 \tag{37}.$$

In Eq.37 ψ_{0i} and ω_i are eigenfunctions and energies for the eigenstates 1 and 2 respectively $(\omega_1\prec\omega_2)$. From here, it comes that the solution for the Schrodinger Eq.36 considering the total Hamiltonian Eq.35 is a linear combination of the wave function for Eq.37 as in Eq.38.

$$\psi=a_1(t)\psi_{01}\exp\left(-i\frac{\omega_1}{\hbar}t\right)+a_2(t)\psi_{02}\exp\left(-i\frac{\omega_2}{\hbar}t\right) \tag{38},$$

where $a_1(t)$ and $a_2(t)$ in Eq.38 are the probabilities amplitudes of the eigenstates 1 and 2 respectively. In order to obtain the amplitude probabilities transition $a_1(t)$ and $a_2(t)$, we must solve the Schrodinger Eq.36. To avoid difficulties, it's necessary for us to write the total Hamiltonians Eq.34 and Eq.35 in the matrix form. This constitutes the main purpose of the next section.

II.2.4. Matrix representation of the semiclassical Jaynes-Cummings Hamiltonian

The matrix representation for Hamiltonians of kind Eq.34 and Eq.35 is widely explained in reference (Xiao-Guang and Chang-Pu, 1996). In order to find the easiest manner to solve the Schrodinger equation (Eq.36) with the help of Hamiltonians Eq.34 and Eq.35, we decompose the equivalent Hamiltonians in diagonal and off-diagonal parts. We started by making a review of the two-dimensional complex vector space C^2 and complex matrix space $M(2,C)$ within our necessity. Firstly, we introduce the Pauli matrices $\{\sigma_1,\sigma_2,\sigma_3\}$ defined by Eq.39:

$$\sigma_1 = \begin{pmatrix} 0 & 1 \\ 1 & 0 \end{pmatrix},\ \sigma_2 = \begin{pmatrix} 0 & -i \\ i & 0 \end{pmatrix},\ \sigma_3 = \begin{pmatrix} 1 & 0 \\ 0 & -1 \end{pmatrix}. \quad (39);$$

And also set the pseudo-spin matrices σ_+ and σ_- with the unit matrix l_2 as indicated in Eq.40 below:

$$\sigma_+ = \frac{1}{2}(\sigma_1 + i\sigma_2) = \begin{pmatrix} 0 & 1 \\ 0 & 0 \end{pmatrix},\ \sigma_- = \frac{1}{2}(\sigma_1 - i\sigma_2) = \begin{pmatrix} 0 & 0 \\ 1 & 0 \end{pmatrix},\ l_2 = \begin{pmatrix} 1 & 0 \\ 0 & 1 \end{pmatrix} = 1 \quad (40).$$

Let consider now $\{|0\rangle, |1\rangle\}$ a basis of C^2 by use of Dirac's notation (Eq.41):

$$|0\rangle = \begin{pmatrix} 1 \\ 0 \end{pmatrix},\ |1\rangle = \begin{pmatrix} 0 \\ 1 \end{pmatrix} \quad (41),$$

It comes from Eq.41 that,

$$\sigma_1|0\rangle = |1\rangle,\ \sigma_1|1\rangle = |0\rangle \quad (42).$$

Thus, σ_1 is considered as the 'flip operator' an equivalent term with quantum creation and annihilation operators in the classical electromagnetism. Giving that the energies of the ground and excited state are ω_1 and ω_2 respectively with $(\omega_1 \prec \omega_2)$, then we can write the relation in Eq.43, where $\omega_0 = \omega_2 - \omega_1$ is the Bohr's frequency. Since Eq.42 is satisfied, then the time dependent Hamiltonian H' can takes the matrix form Eq.44.

$$\overline{H} = \begin{pmatrix} \frac{\omega_1 + \omega_2}{2} - \frac{\omega_0}{2} & 0 \\ 0 & \frac{\omega_1 + \omega_2}{2} + \frac{\omega_0}{2} \end{pmatrix} \quad (43).$$

$$H' = -\mu E_0 \cos\omega_l t \otimes \sigma_1 = \begin{pmatrix} 0 & -\frac{\mu E_0}{2}\exp\{i\omega_l t\} \\ -\frac{\mu E_0}{2}\exp\{i\omega_l t\} & 0 \end{pmatrix}. \quad (44).$$

From Eq.43 and Eq.44, and following the expression of the interaction Hamiltonian (Eq.33), the total Hamiltonian of the system is then given by Eq.45.

$$H=\begin{pmatrix} \frac{\omega_1+\omega_2}{2}-\frac{\omega_0}{2}+\omega N & ga-\mu E_0\cos\omega_l t \\ ga^+-\mu E_0\cos\omega_l t & \frac{\omega_1+\omega_2}{2}+\frac{\omega_0}{2}+\omega N \end{pmatrix} \quad (45).$$

Since our Hamiltonian has to be hermitian, then Eq.45 becomes Eq.46 which is the most appropriate form of the Hamiltonian Eq.34 in the matrix representation,

$$H=\begin{pmatrix} \frac{\omega_1+\omega_2}{2}-\frac{\omega_0}{2}+\omega N & ga-\frac{\omega_{Rabi}}{2}e^{i\omega_l t} \\ ga^+-\frac{\omega_{Rabi}}{2}e^{-i\omega_l t} & \frac{\omega_1+\omega_2}{2}+\frac{\omega_0}{2}+\omega N \end{pmatrix} \quad (46).$$

Taking into consideration the effect of magnetic trap in the Hamiltonian Eq.46 conducts to the final expression of the total Haimiltonian of laser cooled and trapped two level atomic entity Eq.47.

$$H_1=\begin{pmatrix} \frac{\omega_1+\omega_2}{2}-\frac{\omega_0}{2}+\frac{\omega_B}{2}+\omega N & ga-\frac{\omega_{Rabi}}{2}e^{i\omega_l t} \\ ga^+-\frac{\omega_{Rabi}}{2}e^{-i\omega_l t} & \frac{\omega_1+\omega_2}{2}+\frac{\omega_0}{2}-\frac{\omega_B}{2}+\omega N \end{pmatrix} \quad (47).$$

Unfortunately we cannot solve Eq.36 exactly at the present time using both Hamiltonians Eq.46 and Eq.47. In addition, Eq.36 must be non–integrable. Therefore we must apply some approximate method in order to obtain an analytic approximate solution. For simplicity, we focused our choice to the RWA. The next section is devoted to explain the RWA method.

II.2.5. Rotating wave approximation

Let us recall in this section the Euler formula Eq.48.

$$e^{i\theta}=\cos\theta+i\sin\theta\Rightarrow 2\cos\theta=e^{i\theta}+e^{-i\theta} \quad (48).$$

From Eq.48, its comes Eq.49 below:

$$2\cos\theta=e^{i\theta}+e^{-i\theta}=e^{i\theta}\left(1+e^{-2i\theta}\right)\approx e^{i\theta} \quad (49).$$

Because $e^{-i\theta}$ goes away from $e^{i\theta}$ by two times speed, so we neglect this term. We call this approximation the RWA illustrated in Figure 20.

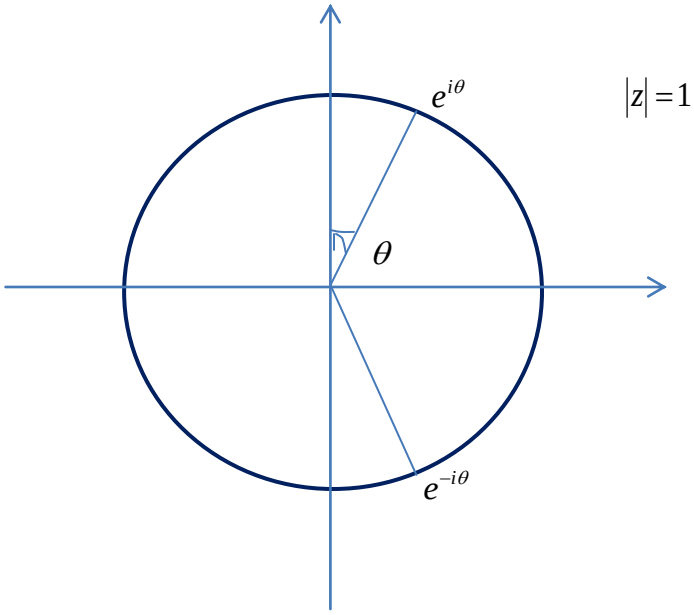

Figure 20. Schematization of the Rotating Wave Approximation (RWA)

Based on the above approximation, it's then possible to solve the Schrödinger equation (Eq.36) using the Hamiltonians Eq.46 and Eq.47 within the RWA. From Eq.40, it's easy to see that

$$H' = \begin{pmatrix} e^{i\frac{\omega_l}{2}t} & 0 \\ 0 & e^{-i\frac{\omega_l}{2}t} \end{pmatrix} \begin{pmatrix} \frac{\omega_1+\omega_2}{2}-\frac{\omega_0}{2} & -\frac{\omega_{Rabi}}{2} \\ -\frac{\omega_{Rabi}}{2} & \frac{\omega_1+\omega_2}{2}+\frac{\omega_0}{2} \end{pmatrix} \begin{pmatrix} e^{-\frac{\omega_l}{2}t} & 0 \\ 0 & e^{i\frac{\omega_l}{2}t} \end{pmatrix} \quad (50).$$

In Eq.50, $\omega_{Rabi} = \mu E_0$ is the Rabi frequency of oscillation of the system. If we set Eq.51 then, the Schrodinger equation $i\frac{d\psi}{dt} = H\psi$ for the total Hamiltonian H at unite $\hbar$ gives Eq.52.

$$\psi = \begin{pmatrix} e^{i\frac{\omega_l}{2}t} & 0 \\ 0 & e^{i\frac{\omega_l}{2}t} \end{pmatrix} \phi . \quad (51),$$

$$i\frac{\partial\phi}{\partial t}=\begin{pmatrix}\frac{\omega_1+\omega_2}{2}-\frac{\omega_0}{2} & -\frac{\omega_{Rabi}}{2}\\ -\frac{\omega_{Rabi}}{2} & \frac{\omega_1+\omega_2}{2}+\frac{\omega_0}{2}\end{pmatrix}\phi \qquad (52).$$

The solution for the equation Eq.48 using the RWA and considering Eq.48 takes the form of Eq.53.

$$\psi=e^{i\left(\frac{\omega_l-\omega_0}{2}\right)}e^{-i\omega_1 t}\psi_{01}\left(\cos\frac{\Omega}{2}t-i\frac{\omega_0-\omega_l}{\Omega}\sin\frac{\Omega}{2}t\right)+i\frac{\omega_{Rabi}}{\Omega}\psi_{02}e^{-i\left(\frac{\omega_l-\omega_0}{2}\right)t}e^{-i\omega_2 t}\sin\frac{\Omega}{2}t \qquad (53).$$

In Eq.53, we considered that $\Omega=\sqrt{(\omega_l-\omega_0)^2-\omega_{Rabi}^2}$. Identifying Eq.47 with Eq.53 taking into account the fact that we have set $\hbar=1$ lead to the Eq.54 and Eq.55 for the transition probabilities amplitudes.

$$a_1(t)=\exp\left\{i\frac{\omega_l-\omega_0}{2}t\right\}\left(\cos\frac{\Omega}{2}t-i\frac{\omega_l-\omega_0}{\Omega}\sin\frac{\Omega}{2}t\right) \qquad (54),$$

and

$$a_2(t)=i\frac{\omega_{Rabi}}{\Omega}\exp\left\{-\frac{\omega_l-\omega_0}{2}t\right\}\sin\frac{\Omega}{2}t \qquad (55).$$

Thus, solution of the Schrödinger equation (Eq.36) based on the Hamiltonian of the type Eq.34 using the RWA conducts to the expression of wavefunction of the cooled and trapped polariton with laser, given that the subscript $'cp'$ stands for cooled polariton:

$$\psi(t)=e^{-i\omega_1 t}e^{it\frac{\Lambda-\omega_0-2\omega N}{2}}\psi_{01}\left\{\cos(\Omega_{cp}t)-i\frac{\delta}{2\Omega_{cp}}\sin(\Omega_{cp}t)\right\}+i\frac{\omega_{Rabi}}{2\Omega_{cp}}e^{-i\omega_2 t}e^{-it\frac{\Lambda-\omega_0+2\omega N}{2}}\psi_{02}\sin(\Omega_{cp}t) \qquad (56),$$

where $\Lambda=\omega_l-\omega,\delta=\omega_l-(\omega_0+\omega),\ \Omega_{cp}^2=\frac{\delta^2}{4}+2g^2+\frac{\omega_{Rabi}^2}{4}$.

Following the same mathematical approach in the case of Hamiltonian Eq.31, then the wavefunction of laser cooled and confined in the magnetic field is expressed in Eq.57. To avoid confusion with that of cooled polariton, the supscript $'cp'$ is changed to $'1'$.

$$\psi(t)=e^{it\frac{\Lambda-\omega_0-2\omega N}{2}}\left\{\cos(\Omega_1 t)+i\frac{\delta_1}{2\Omega_1}\sin(\Omega_1 t)\right\}\psi_{01}e^{-\omega_1 t}+i\frac{\omega_{Rabi}}{2\Omega_1}e^{-it\frac{\Lambda-\omega_0+2\omega N}{2}}\sin(\Omega_1 t)\psi_{02}e^{-\omega_2 t} \quad (57).$$

Here, $\delta_1=\omega_B+\omega_l-(\omega_0+\omega)$, $\varphi^2=\frac{\delta^2}{4}+g^2$, and $\Omega_1^2=\varphi_1^2+g^2+\frac{\omega_{Rabi}^2}{4}$

Even at the present level, complete expressions of the force and corresponding torque can not be obtained without the well known of the dipole moment induced by the radiation field. We then concentrate ourselves in the next section in evaluating the dipole moment induced by laser light.

II.2.6. Dipole moment induced by laser light on the two-level systems

From Eq.54 and Eq.55 above, it's become easy to find the dipole moment induced by electromagnetic wave laser light. The expectation value of such dipole moment is expressed by Eq.58.

$$\mu(t)=a_2^*(t)a_1(t)\mu_{21}\exp\{i\omega_0 t\}+a_1^*(t)a_2(t)\mu_{12}\exp\{-\omega_0 t\} \quad (58).$$

Since $\mu_{12}=\mu_{21}=\bar{\mu}$ then, it comes for the result of Eq.59 bellow,

$$\mu(t)=\bar{\mu}\frac{\omega_{Rabi}}{2\Omega}\left\{-\frac{\omega_l-\omega_0}{\Omega}(1-\cos\Omega t)-i\sin\Omega t\right\}\exp\{i\omega_l t\}+C.C \quad (59).$$

The development of Eq.59 considering the trigonometric relations Eq.60 and Euler's formulas Eq.61, allow the obtention of the final result Eq.62.

$$\sin\alpha\cos\alpha=\frac{1}{2}\sin(2\alpha),\ \sin^2(\alpha)=\frac{1-\cos(2\alpha)}{2} \quad (60),$$

$$2\cos(\alpha)=e^{i\alpha}+e^{-i\alpha},\ 2i\sin(\alpha)=e^{i\alpha}-e^{-i\alpha} \quad (61),$$

$$\mu(t)=-\frac{\overline{\mu^2}}{\Omega}\frac{\omega_l-\omega_0}{\Omega}(1-\cos\Omega t)E_0\cos\omega_l t+\frac{\overline{\mu^2}}{\Omega}E_0\sin\Omega\sin\omega_l t \quad (62).$$

This expression for the dipole moment can also take the form Eq.63,

$$\mu(t) = \alpha^{'} E_0 \cos\omega_l t + \alpha^{''} E_0 \sin\omega_l t \qquad (63),$$

where

$$\alpha^{'} = -\frac{\overline{\mu^2}}{\Omega}\frac{\omega_l - \omega_0}{\Omega}(1-\cos\Omega t), \alpha^{''} = \frac{\overline{\mu^2}}{\Omega} E_0 \sin\Omega t \qquad (64).$$

The first and the second term of Eq.64 are respectively the dispersive and dissipative components of the polarizability of the atom. Achieving calculus on the dipole moment induced by laser light on the atom, the mechanical force and torque calculation looks very simple, from where we easily evaluate the linear and angular momentum and also energy. The dipole moment induced by a system of two opposite charge can just be understood physically as the separation of positive and negative electrical charges within a system; that is a measure of the system's overall polarity. The importance of the evaluation of this parameter in this work comes from the link between a particular force produced by a system of two opposite charge particles, energy and the proper dipole moment induced. For two opposite charges $(-q)$ and $(+q)$ separated with a distance d the dipole moment induced by the system is given by $\mu = qd$ and the force is expressed by $F = qE$. From the Lorentz model of the atomic polarizability, the electric field is replaced by $E = \frac{\mu}{\alpha}$ which means that $\mu = \alpha E$. Also, from the relation between energy and force, i.e $U = W = Fd$, it's comes the importance of performing calculus on the induced dipole moment in the system of cooled and trapped atomic entities with laser light.

We now consider a plane electromagnetic wave E and B, in which the complex electric field vanishes in the z direction as given in Eq.65 bellow , where E_{0x} and E_{0y} are constants.

$$\hat{E} = (E_{0x}\exp(-ikz), E_{0y}\exp(-ikz), 0) \qquad (65),$$

The corresponding complex magnetic field is obtained from Maxwell's relation Eq.66:

$$\hat{B} = -\frac{1}{i\omega_l} curl\,\hat{E} \qquad (66).$$

For $B_{ox} = -\frac{E_{0y}}{c}$ and $B_{oy} = \frac{E_{0x}}{c}$, the appropriate magnetic field takes the form of Eq.67,

$$\hat{B} = \left(B_{0x}\exp(-ikz), B_{0y}\exp(-ikz), 0\right) \tag{67}.$$

Substitution of Eq.61 into Eq.23 and Eq.24 conducts to the final expressions of the average values of the force and its corresponding torque acting on the system of laser cooled and trapped polariton without magnetic field Eq.68 and Eq.69 respectively.

$$\overline{F_z} = \overline{F_z}^{Lorentz} = \frac{\omega_{Rabi}^2}{4\Omega_{cp}} k \sin\left(2\Omega_{cp} t\right) \tag{68},$$

$$\overline{N} = \overline{N_z} = \frac{\overline{\mu^2}}{4\Omega_{cp}} \left(E_x^* E_y - E_y^* E_x\right) \sin\left(2\Omega_{cp} t\right) \tag{69}.$$

When the confinement is introduced in the system, that is the magnetic field with Hamiltonian Eq.28, substitution of Eq.61 into Eq.23 and Eq.24 conducts to the final expressions of the average values of the force and its corresponding torque acting on the system of laser cooled and trapped polariton and confined in the magnetic field which we considered as a trap Eq.70 and Eq.71 respectively.

$$\overline{F_z} = \frac{1}{2}\mathrm{Re}\left\{\dot{\mu}_x^* B_y - \dot{\mu}_y^* B_x\right\} = \frac{\omega_{Rabi}^2}{4\Omega_1} k \sin\left(2\Omega_1 t\right) \tag{70},$$

$$\overline{N} = \overline{\left(\mu \times E\right)_z} = \frac{1}{2}\frac{\overline{\mu^2}}{2\Omega_1}\left(E_x^* E_y - E_y^* E_x\right) \sin\left(2\Omega_1 t\right) \tag{71}.$$

II.2.7. Transition probabilities and energies

From the definition of the transition probability amplitude, for a wave function describes by Eq.72, the probability of founding the system characterizes by the wave function Eq.72 in the state i is usually evaluated using Eq.73.

$$\psi(t) = \sum_i a_i \psi_i \,, \quad i = 1,2,\ldots,n \tag{72},$$

$$p_i = |a_i|^2 = a_i a_i^* \tag{73}.$$

The energy receives by the polariton from the plane wave radiation field when its cool is given by Eq.74 and its average value expressed by Eq.75.

$$\Delta U = \overline{\dot{\mu} \cdot E} = \frac{1}{2}\mathrm{Re}\left\{ \hat{\dot{\mu}}^* E \right\} \tag{74}.$$

$$\overline{\Delta U} = \int_0^t \Delta U dt \tag{75}.$$

From the wavefunction above, the transition probability amplitudes of finding the cooled and trapped polariton in the ground and excited states are defined as in Eq.76 and Eq.77 bellow.

$$a_1(t) = e^{it\frac{\Lambda-\omega_0-2\omega N}{2}}\left\{\cos(\Omega_{cp}t) - i\frac{\delta}{2\Omega_{cp}}\sin(\Omega_{cp}t)\right\} \tag{76},$$

$$a_2(t) = i\frac{\omega_{Rabi}}{2\Omega_{cp}} e^{-it\frac{\Lambda-\omega_0+2\omega N}{2}}\sin(\Omega_{cp}t) \tag{77}.$$

Futhermore, from Eq.77, the transition probability of finding the system in the excited state is expressed by Eq.78.

$$P_2 = a_2 a_2^* = |a_2|^2 \tag{78}.$$

Simple substitution of Eq.çà into Eq.78 yields Eq.79.

$$|a_2(t)|^2 = \frac{\omega_{Rabi}^2}{4\Omega_{cp}^2}\frac{1-\cos(2\Omega_{cp}t)}{2} \tag{79}.$$

From Eq.74, the energy received by the atomic entity from the plane wave radiation field when it is cooled takes the form of Eq.80.

$$\Delta U = c\frac{\omega_{Rabi}^2}{4\Omega_{cp}} k\sin(2\Omega_{cp}t) \tag{80},$$

And the average value is expressed by Eq.81.

$$\overline{\Delta U} = \Lambda\frac{\omega_{Rabi}^2}{8\Omega_{cp}^2}1-\cos(2\Omega_{cp}t) \tag{81}.$$

When a magnetic field, looked as a trap is introduced in the system, similar analysis conducts to the transition probability of finding the system in the excited state Eq.82 and total energy of the system Eq.83.

$$\left|a_2(t)\right|^2 = \frac{\omega_{Rabi}^2}{4\Omega_1^2}\frac{1-\cos(2\Omega_1 t)}{2} \tag{82}.$$

$$\overline{\Delta U} = \int_0^t \Delta U dt = \Lambda \frac{\omega_{Rabi}^2}{4\Omega_1^2}\frac{1-\cos(2\Omega_1 t)}{2} \tag{83}.$$

II.3. Quantum mechanical approach of laser cooling and trapping of two-level systems

II.3.1. Quantum Rabi model of polariton

II.3.1.1. Derivation of the quantum Rabi Hamiltonian of cooled and trapped polariton

We recall to readers that, our choice is due to the fact that polariton is composite exciton and photon wich is relatively free of decoherence that plagues other quantum systems. The purpose therefore in this section is to define the correct Hamiltonian describing the dynamics of a single exciton-polariton interacting with radiation field. To generalize the phenomenon and to set calculations which will be usefull in the next section where we introduce our model, we consider that our exciton-polariton is embeded inside a microcavity. We leave out the procedure of quantization of the field, which can be find in any book of quantum optics (Scully and Zubairy, 1997). The full Hamiltonian describing an atom interacting with an EM field is given by Eq.84.

$$H = \frac{1}{2m}\left[p - qA(x)\right]^2 + U(x) + \hbar\omega\left(a^+ a + \frac{1}{2}\right) + H_{el} \tag{84}.$$

In Eq.84, the parameters p , q , x and m are respectively momentum, charge, position and mass of the atom. a^+ and a are the photon creation and annihilation operators for microwaves photons of frequency ω respectively and H_{el} is the Hamiltonian describing the electronic state of the atom. The vector potential $A(x)$ is expressed in Eq.85, where $\bar{\varepsilon}$ is the polarization vector and $f(x)$ is a function describing the field along the mode in the cavity.

$$A(x) = A_0\left[\bar{\varepsilon} f(x) a + \bar{\varepsilon}^* f^*(x) a^+\right] \tag{85}.$$

It gives the effective mode volume Eq.86 which is related to the constant A_0 as it's in Eq.87.

$$V = \int |f(x)|^2 d^3x \tag{86},$$

$$A_0 = \sqrt{\frac{\hbar}{2\varepsilon_0 \omega V}} \tag{87}.$$

Under the assumption that only one polaritonic transition couples to the mode, the electronic states may be labeled $|\pm\rangle$ and the electronic hamiltonian in Eq.88 can be written as given in Eq.88, where $\Delta_0 = \omega_2 - \omega_1$ is the transition frequency and σ_z is the $z-$ Pauli's operator.

$$H_{el} = \frac{\hbar\Delta_0}{2}\sigma_z \tag{88}.$$

By neglecting the multi-photon processes and assuming that the external atomic potential is zero, the complete Hamiltonian of the system is therefore (see Eq.89):

$$H = H_{exc} + H_{Ph} + H_{Int} \tag{89},$$

$$H_{exc} = \frac{p^2}{2m} + \frac{\hbar\Delta_0}{2}\sigma_z \tag{90},$$

$$H_{Ph} = \hbar\omega\left(a^+ a + \frac{1}{2}\right) \tag{91},$$

$$H_{Int} = -\frac{q}{m}A_0\left[(p\cdot\hat{\varepsilon})f(x)a + (p\cdot\hat{\varepsilon}^*)f^*(x)a^+\right] \tag{92}.$$

In matrix representation, within the atomic basis states, the interaction Hamiltonian Eq.92 is (Scully and Zubairy, 1997) $H_{Int} = g(x)(a^+\sigma_- + a\sigma_+)$, where $\sigma_\pm = \frac{1}{2}(\sigma_1 \pm i\sigma_2)$ are defined in the previous section as pseudo-spin operators used so as to satisfy the commutation relations $[\sigma_+, \sigma_-] = \sigma_3$; $[\sigma_3, \sigma_\pm] = \pm 2\sigma_\pm$ and the parameter $g(x)$ known as the coupling strength constant is given in Eq.93.

$$g(x) = -\frac{q}{m}\langle + |(p \cdot \hat{\varepsilon})| - \rangle f(x)\sqrt{\frac{2}{\hbar\omega\varepsilon_0 V}} \quad (93).$$

In deriving Eq.75, we adjusted the phases of the states $|\pm\rangle$ such that $g(x)$ is real. If we further assume that $g(x)$ is to a good approximation independent of x, the atomic kinetic energy operator is a constant of motion and can be omitted, as may the constant vacuum term $\hbar\omega/2$. We then arrise at unit $\hbar$ to the resulting Hamiltonian Eq.94 which corresponds to the quantum Rabi Hamiltonian.

$$H = \frac{\Delta_0}{2}\sigma_z \otimes 1 + \omega \otimes N + g(\sigma_+ + \sigma_-) \otimes (a + a^+) \quad (94).$$

Solution of TDSE (Eq.36) using the above hamiltonian (Eq.94) is not possible if we do not perfom some approximation. Here again, our interest is turned to the RWA which constitute the purpose of the next section.

II. 3.1.2. Rotating wave approximation and Jaynes Cummings Hamiltonian

As compared to the semiclassical approach, there is a litle difference of applying the RWA in quantum mechanical approach. Let consider the fundamental relations of the Heisenberg algebra in the Fock space:

$$\lfloor N, a^+ \rfloor = a^+, \ [N, a] = -a, \lfloor a, a^+ \rfloor = 1 \quad (95).$$

Here the Fock space F is a Hilbert space over C, given by Eq.96, where $|0\rangle$ is the vacuum and $|n\rangle$ is given by Eq.97.

$$F = vect\{|0\rangle, |1\rangle\} \quad (96),$$

$$|n\rangle = \frac{(a^+)^n}{\sqrt{n!}}|0\rangle, \text{ for } n \geq 0 \quad (97).$$

On this space, the operators a, a^+ and N are represented in their matrix forms by Eq.98, using Eq.95.

$$a=\begin{pmatrix}0 & 1\\ 0 & 0\end{pmatrix},\ a^+=\begin{pmatrix}0 & 0\\ 1 & 0\end{pmatrix},\ aa^+=a^+a+1=N=\begin{pmatrix}0 & 0\\ 0 & 1\end{pmatrix} \quad (98).$$

We can add a phase to $\{a,a^+\}$ and thus, $b=e^{i\theta}a$, $b^+=a^+e^{-i\theta}$, $N=b^+b=a^+a$ where θ is constant. We then have Heisenberg algebra:

$$\left[N,b^+\right]=b^+,\ \left[N,b\right]=-b,\left[b,b^+\right]=1 \quad (99).$$

The main problem at this stage is to solve the TDSE (Eq.100) exactly.

$$i\frac{\partial}{\partial t}\left|\Psi\right\rangle=H\left|\Psi\right\rangle=\left\{\frac{\Delta_0}{2}\sigma_z\otimes 1+\omega\otimes N+g\left(\sigma_+ +\sigma_-\right)\otimes\left(a+a^+\right)\right\}\left|\Psi\right\rangle \quad (100).$$

Based on the fact that Eq.101 is satisfied, we neglect the middle terms to the right hand side of Eq.101 and set Hamiltonian Eq.102.

$$\left(\sigma_+ +\sigma_-\right)\otimes\left(a+a^+\right)=\sigma_+\otimes a+\sigma_+\otimes a^+ +\sigma_-\otimes a+\sigma_- +a^+ \quad (101),$$

$$H=\frac{\Delta_0}{2}\sigma_z\otimes 1+\omega\otimes N+g\left(\sigma_+\otimes a+\sigma_-\otimes a^+\right) \quad (102).$$

Such an approximation is called the RWA in quantum mechanical formalism and the resulted Hamiltonian Eq.102 is called the JCH. It is then possible for us to solve the TDSE (Eq.100) using Hamiltonian (Eq.102) following the Jaynes-Cummings approach.

II.3.2. Jaynes-Cummings model

II.3.2.1. Matrix representation of the Jaynes-Cummings Hamiltonian

Hamiltonian Eq.102 can simply takes the form of Eq.103.

$$H=\frac{\Delta_0}{2}\sigma_z+\omega a^+a+g\left(\sigma_+a+\sigma_-a^+\right) \quad (103).$$

Based on Eq.103 and following the analysis of Larson (2005), we observed that the form of the coupling term is such that the number of excitation $N = aa^{+} + \frac{1}{2}\sigma_3$ in the system is preserved and is customary to work within the interaction picture Eq.104 where $\Delta = \Delta_0 - \omega$ is the atom-field detuning.

$$\overline{H} = H - \omega N = \frac{\Delta_0}{2}\sigma_z + g\left(\sigma_+ a + \sigma_- a^{+}\right) \tag{104}.$$

Since N is a constant of motion, it is enough to solve the system for one particular value $n \pm \frac{1}{2}$ of N. Thus, in the interaction picture, the Hamiltonian is of block-diagonal form with 2×2 blocks Eq.105 with eigenvalues given in Eq.102.

$$H_n = \begin{bmatrix} \frac{\Delta}{2} & g\sqrt{n} \\ g\sqrt{n} & -\frac{\Delta}{2} \end{bmatrix} \tag{105}.$$

$$E_{\pm} = \pm\sqrt{\left(\frac{\Delta}{2}\right)^2 + g^2 n} \tag{106}.$$

II.3.2.2. The Von neumann entropy

In cooling and trapping process, the level of disorder of a system is well observed by evaluating its entanglement which is a phenomenon, as a non local between two (or more) quantum systems. In most cases, specification of amount of entanglement is achieved by use of appropriate mathematical models. For TLSs, various acceptable models for entanglement measurement have been proposed. That is entanglement formation and distillation (Woolters, 1998), concurrence, negativity (Vidal and Werner, 2002) and Von Neumann entropy. In the present study, we focused our attention to the Von Neumann entreopy. We justify our choice by the fact that it's introduced in the system a weak magnetic field. Moreover, its seems more appropriate the use of Von Neumann entropy, a very useful operational measure of the disorder of a system of a qubit. For a given density operator ρ the Von Neumann entropy is expressed by

Eq.107 where the symbol 'Tr' stands for trace as indicated above, and $S(\rho)$ranges from 0 (for a separable state) to 1 (for a maximally entangled state).

$$S(\rho)=Tr(\rho\ln\rho) \tag{107}$$

Based on the previous section, the density matrix in Eq.107 has the form of Eq.108 where $a_1(t)$ and $a_2(t)$ are the transition amplitude of finding the cooled and trapped system in both ground and excited states respectively, assuming the system as a TLS. The transition amplitude values $a_1(t)$ and $a_2(t)$ are obtained by solving the Schrödinger Eq.104 using the JCH Eq.102.

$$\rho=\begin{pmatrix}|a_1(t)|^2 & 0\\ 0 & |a_2(t)|^2\end{pmatrix} \tag{108}$$

From Eq.57, and given the expressions of wavefunction Eq.56 and Eq.57, the entropy of the system takes the form of Eq.109 given that the transition probability amplitudes are described in Eq.110 in the case of laser cooled and trapped polariton without magnetic trapping and Eq.111 in the case of laser cooled and trapped polariton with magnetic field.

$$S=-|a_1(t)|^2\ln|a_1(t)|^2-|a_2(t)|^2\ln|a_2(t)|^2 \tag{109}$$

$$\begin{cases}a_1(t)=\exp\left\{i\dfrac{\omega_l-\omega_0}{2}t\right\}\left(\cos\dfrac{\Omega_{cp}}{2}t-i\dfrac{\omega_l-\omega_0}{\Omega_{cp}}\sin\dfrac{\Omega_{cp}}{2}t\right)\\ a_2(t)=i\dfrac{\omega_{Rabi}}{\Omega_{cp}}\exp\left\{-\dfrac{\omega_l-\omega_0}{2}t\right\}\sin\dfrac{\Omega_{cp}}{2}t\end{cases} \tag{110}$$

$$\begin{cases}a_1(t)=\exp\left\{i\dfrac{\omega_l-\omega_0}{2}t\right\}\left(\cos(\Omega_1 t)+i\dfrac{\delta_1}{2\Omega_1}\sin(\Omega_1 t)\right)\\ a_2(t)=i\dfrac{\omega_{Rabi}}{2\Omega_1}\exp\left\{-\dfrac{\omega_l-\omega_0}{2}t\right\}\sin\dfrac{\Omega_1}{2}t\end{cases} \tag{111}$$

II.3. 3. Landau-Zener model

II.3.3.1. Landau-Zener problem in cooling and trapping of polariton

To introduce the LZ problem in cooling and trapping of polariton, we reconsider the Hamiltonian of block-diagonal form with 2×2 blocks Eq.105.

$$H_n = \begin{bmatrix} \frac{\Delta}{2} & g\sqrt{n} \\ g\sqrt{n} & -\frac{\Delta}{2} \end{bmatrix} \tag{112}.$$

Eq.112 is similar to that described by Avishai (2014) after performing two different types of changes; i.e. $\alpha t/2 \to \Delta/2$ and $V \to g\sqrt{n}$ nomatter the difference in sign. The Hamiltonian Eq.112 is also similar to that had obtained Liu et al. (2001) if one does not consider any energy difference in the level bias (see Yan and Wu, 2008). This means that the nonlinear parameter describing the level energy dependence on the population transfer vanishes. Similar transformations can be applied in case of Hamiltonians defined by Hicke et al. (2005), Yang et al. (2017) and Dodonov et al. (2016) to cite a few, who analyzed some physical phenomena with the aid of LZ model. It comes clear that, after we emphasized substitution describes in this paragraph, our problem coincides with that of LZ described by Avishai (2014). Thereby arizes LZ problem in cooling and trapping of polariton. To go further, eigenvalues of Hamiltonian Eq.112 are giving in Eq.113.Graphical representation of these eigenvalues (Figure 21) presents crossing and avoided crossing of energy levels for two different values of the detuning Δbetween exciton and photon, i.e. $\Delta = 0$ (crossing) and $\Delta = 2$ (avoided crossing). The figure appears more appropriate to jusitfy the apprearence of LZ problem in cooling and trapping of polariton.

$$E_{\pm} = \pm\sqrt{\left(\frac{\Delta}{2}\right)^2 + g^2 n} \tag{113}.$$

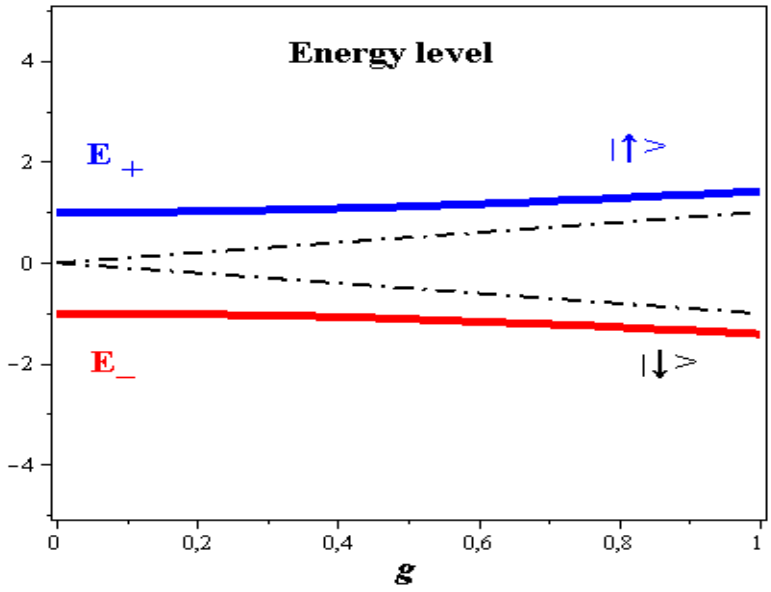

Figure 21. Eigenvalues of Hamiltonian are plotted as a function of the coupling strength. Avoided crossing of energy levels is observed for n = 1 and Δ = 2. The dashed black lines correspond to the diabatic transition and the solid blue and red lines are the adiabatic transition. The figure shows that, for low coupling strength constant $(g \approx 0)$, crossing and avoided crossing are well observable; as the coupling increases, the similitude diminishes and tends to identity for very important values g .

II.3.3.2. Adiabatic-impulse approximation and Landau-Zener Hamiltonian

Nomatter we successfully formulated LZ problem in cooling and trapping of polariton, it is not yet possible to arize to the LELs with Hamiltonian Eq.160. The Hamiltonian has to be writen in the best and well accepted form. In order to get the best equation for theoretical and numerical calculations, we rewrite Eq.112 in term of pseudo-spin operators σ_i $(i = 1,2,3)$(see Eq.114)

$$H_1 = -\frac{\Delta}{2}\sigma_3 + g\sqrt{n}\sigma_1 . \qquad (114).$$

In addition, we introduce the laser light Hamiltonian for cooling process. The Hamiltonian of radiation field is given by Eq.115.

$$H_{Laser} = -\mu E_0 \sin(\omega_l t)\sigma_1 \qquad (115).$$

Therefore, the model Hamiltonian for the system takes the form of Eq.116 where $\eta_0 = g\sqrt{n}$.

$$H = -\frac{\Delta}{2}\sigma_3 + \left(\eta_0 + A\sin\left(\omega_l t\right)\right)\sigma_1 \tag{116}.$$

We have already mentioned above that the subscript *l* indicates the laser light. For the model to be simple, we assume that $A = -\Omega$, where the quantity $\Omega = \mu E_0$ is known as the Rabi frequency. We can then construct the polariton-field Hamiltonian by introducing a time-dependent parameter. The total Hamiltonian of Eq.116 changes to the appropriate form Eq.117 below.

$$H = -\frac{\Delta}{2}\sigma_3 + \eta(t)\,\sigma_1 \tag{117}.$$

In Eq.117, $\sigma_i (i = 1,2,3)$ and Δ are similar parameters well defined above. There have been several works (Buluta et al., 2011) in which the parameter $\eta(t) = \eta_0 + A\sin\left(\omega_l t\right)$ is introduced for a TLS. The parameter is identified as the bias, which is the total environment coupled to the single qubit. The corresponding instantaneous eigenvalues are expressed in Eq.118 and depicted in Figure 22. The figure shows that the laser frequency ω_l can be strongly influenced by the avenue of the multi-crossing, which manifests itself as stronger of the energy levels [Figure (22d)]. In Figure (22b), one can see the anti-crossing points between the adiabatic energy levels (the red and blue solid curves) corresponding to the LZ transition to the region. An important point to note here is that, because of the relation in Eq.118, there are two ways to obtain a large effective driving field in the quantum model, namely by having a multi-crossing scenario. The accumulated Stückelberg phases increase with the laser amplitude, point out the LZS interferometry transition [see Figure 22].

$$E_{\pm} = \pm\sqrt{\left(\frac{\Delta}{2}\right)^2 + \eta(t)^2} \tag{118}.$$

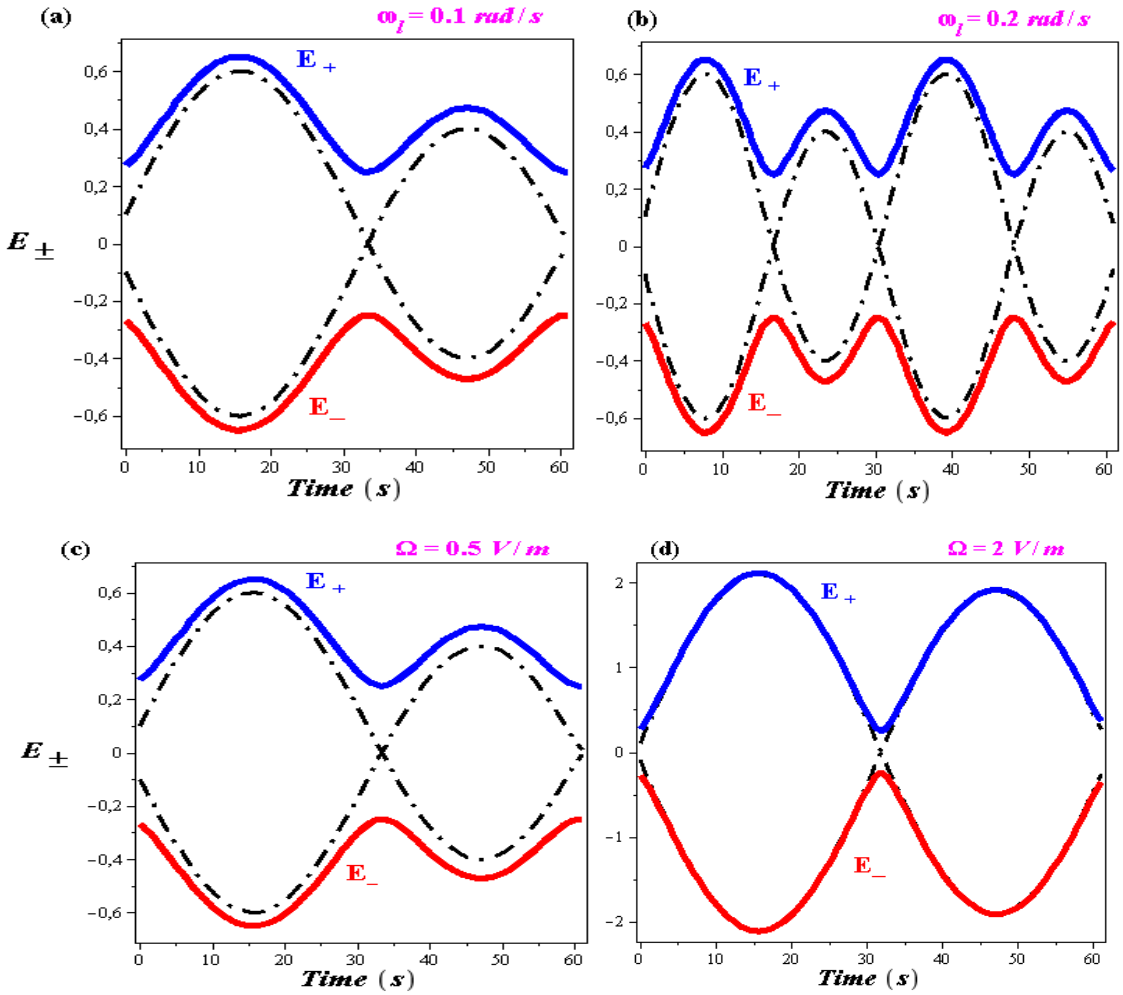

Figure 22. Eigenvalues of Hamiltonian are plotted versus time Eq.118. Multilevel crossing of energy level for different values of laser frequency: (a) $\omega_l = 0.1$ rad/s and (b) $\omega_l = 0.2$ rad/s. Modulation dynamic phase for different values of amplitude of laser field: (c) $\Omega = 0.5$ V/m and (d) $\Omega = 2$ V/m. Here, the following values have been choosed: $\Delta = 0.5$ eV and $g\sqrt{n} = 0.1$.

Nomatter Eq.117 is as similar as that of LZ after performing some changes, it is not yet appropriate in determining cooled and trapped polariton parameters within the formalism such as, and particularly, LELs. In general, concrete calculations of LELs using Hamiltonian of Eq.117 present significant difficulties, nomatter the corresponding Hamiltonian is that of TLS. Part of those difficulties regroups the Schrodinger equation which can be written as a second-order differential equation with periodic coefficients and the Hill equation which is not solvable in analytic closed form (Buluta et al., 2011 ; Grifoni and Hänggi, 1998). Yet, different theoretical

approaches can be used to obtain approximate analytical results of various parameters, such as transition probability, entropy, entanglement and so on. Some of those methods include traditional method, such as Landau method (Kami and Nikitin, 1994) that uses perturbation theory and complex integral method to express non-adiabatic transition probabilities. The group consists also of Stenholm's method in which the Hamiltonian is written in term of Pauli matrices and the London phase operator method that consists to carry calculations on Eq.117 by writing it in term of London phase operator. Another interesting method consists to apply various approximations such as linear diabatic potentials, constant diabatic coupling and the straight-line trajectory with constant velocity for the relative notion to Landau's expression of non-adiabatic transition probability, known as LZ method.

One key relation for purposes of deciding the suitability of a given method or approach is the link between the laser frequency ω_l and the energy splitting Δ (Sillanpää et al., 2005 ; Oliver et al., 2005). The link is $\omega_l \prec\prec\prec \Delta$ (Sillanpää et al., 2005) and $\omega_l \succ\succ\succ \Delta$ (Oliver et al., 2005) for a qubit. Similarly, the velocity of passing the avoided level region should be such that $A\omega_l \le \Delta^2$ and $A\omega_l \ge \Delta^2$ for slow and fast driving regime, respectively. For our model, a theoretical approach that can be used is the adiabatic impulse approximation (AIA) which is the commonless method weither the polariton is driven through the avoided crossing or not. The method does not depend on the nature of particles studied. Perharps, the model is an intuitive mathematical tool which describes the dynamic of a TLS driven by a radiation field. Based on the AIA formalism, Hamiltonian Eq.117 has to be linearized. Doing it, we assume that the energy levels $E_\pm$ obtained from Eq.117 has minimum distance of Δ which is realized at a particular time $t_\pm + 2\pi k/\omega_l \ \ (k \in Z)$. Accordingly, it follows the two expressions $\omega_l t_+ = \arcsin(-\eta_0/A)$ and $\omega_l t_- = \pi - \arcsin(-\eta_0/A)$. The phases acquired during the adiabatic stages are giving by $\nu_1 = \int_{t_1}^{t_2} E_+(t)dt$ and $\nu_2 = \int_{t_2}^{t_1+2\pi/\omega_l} E_-(t)dt$. Considering the non-adiabatic region in the vicinity point $t_{1,2}$ such that $t_1 = t_{1,2} + t'$, $\omega_l t' \prec\prec 1$, then the bias $\eta(t)$ can be linearized as $\eta(t_{1,2}+t') \cong \upsilon t'$, where

$$\upsilon = A\omega_l \left|\cos\omega_l t_{1,2}\right|, \qquad (119),$$

with $\left|\cos\omega_l t_{1,2}\right| = \sqrt{1-(\eta_0/A)^2}$.

From here, the linearized expression for the Hamiltonian Eq.117 is exactly that of LZ problem after performing the sweep velocity or LZ velocity υ. The convenient Hamiltonian is rewritten as given in Eq.120 and stands as the best formulation (Hamiltonian) of LZ problem in laser cooling and trapping of polariton. From Hamiltonian Eq.120, it can be then possible to investigate the most important laser cooled and trapped polariton parameters such as LELs and transition probabilities. LELs of the system are theoretically expressed as $E_{\pm}\left(t^{'}\right)=\sqrt{\left(\upsilon t^{'}\right)^{2}+\Delta^{2}}$. In Eq.120, $\sigma_{1,3}$ are Pauli matrices, $\upsilon t^{'}$ is the energy difference between the two diabatic (crossing) basis states (i.e. the eigenstates $\left|\uparrow\right\rangle$ and $\left|\downarrow\right\rangle$ of σ_3 operator), controlled by the surrounding environment which depends linearly on time $t^{'}$, and Δ is the constant gap between the two instantaneous eigenenergy states $\left|+\right\rangle$ and $\left|-\right\rangle$ at the center of the avoided crossing $\upsilon t^{'}=0$.

$$H\left(t^{'}\right)=-\frac{\Delta}{2}\sigma_1+\frac{\upsilon t^{'}}{2}\sigma_3 \qquad (120).$$

II.3.3.3. Transition probabilities

II.3.3.3.1. Transition probabilities in the diabatic basis

Through the AIA, we get the best Hamiltonian describing the laser cooling and trapping polariton process. Therefore, it becomes important to investigate the cooled and trapped polariton wavefunction. We find more interesting the use of LZ approach since we face the LZ problem. Theoretical analysis of LZ problem is studied in detail by Zener (1932), Shevchenko et al. (2010) and Keeling and Gurarie (2008) to cite a few. We begin by introducing the wavefunction $\psi(t')$ (Eq.121) which represents the variable indicating how the polariton manifests itself when it is cooled and trapped using laser light. In Eq.(121), the parameters $C_1\left(t'\right)$ and $C_2\left(t'\right)$ are superposition coefficients in the diabatic basis.

$$\Psi\left(t^{'}\right)=C_1\left(t^{'}\right)\left|0\right\rangle+C_2\left(t^{'}\right)\left|1\right\rangle \qquad (121).$$

The Hamiltonian of the system of cooled and trapped polariton Eq.120 can be expressed by a 2×2 matrix that is quite concise and convenient to deal with (Eq.122). Without loss of generality, Δ and υ are assume positive and have both the dimension of frequency.

$$H(t')=-\frac{\Delta}{2}\sigma_1+\frac{\upsilon t'}{2}\sigma_3=\frac{1}{2}\begin{bmatrix}\upsilon t' & -\Delta\\ -\Delta & -\upsilon t'\end{bmatrix} \qquad (122).$$

The Schrödinger equation (Eq.104) takes then the following form Eq.123.

$$i\frac{d}{dt'}\begin{bmatrix} C_1(t') \\ C_2(t') \end{bmatrix} = \frac{1}{2}\begin{bmatrix} \upsilon t' & -\Delta \\ -\Delta & -\upsilon t' \end{bmatrix}\begin{bmatrix} C_1(t') \\ C_2(t') \end{bmatrix} \quad (123).$$

Eq.123 can be decomposed in the following two differencial equations (Eq.124).

$$\begin{cases} i\frac{d}{dt'}C_1(t') = \frac{1}{2}\upsilon t' C_1(t') - \frac{\Delta}{2}C_2(t') \\ i\frac{d}{dt'}C_2(t') = -\frac{\Delta}{2}C_1(t') - \frac{1}{2}\upsilon t' C_2(t') \end{cases} \quad (124).$$

From the second expression of Eq.124, it follows that,

$$C_1(t') = -\frac{2}{\Delta}i\frac{dC_2(t')}{dt'} - \frac{\upsilon t'}{\Delta}C_2(t') \quad (125),$$

And simple substitution of Eq.125 into the first equation of system Eq.124 conducts to Eq.126 ;

$$\frac{d^2C_2(t')}{dt'^2} - \left[i\frac{\upsilon}{2} - \frac{(\upsilon t')^2 + \Delta^2}{4} \right]C_2(t') = 0 \quad (126).$$

Following the notation of Danga et al. (2016), we introduce for convenience the scale dimensionless quantities $\tau = -\sqrt{\upsilon}t'$ and $\nu = -\frac{\Delta}{\sqrt{\upsilon}}$. It comes relation in Eq.127.

$$\frac{d^2C_2(\tau)}{d\tau^2} - \left[-\frac{\nu^2}{4} + \frac{1}{2}i - \frac{1}{4}\tau^2 \right]C_2(\tau) = 0 \quad (127).$$

It is evident to observe from Eq.127 that the two first term in the cote correspond to a complex number. Thus, one can writes $Z = -\frac{\nu^2}{4} + \frac{1}{2}i = a + ib$ given that $a = -\frac{\nu^2}{4}$ and $b = \frac{1}{2}$; and finally, Eq.127 becomes as illustrated in Eq.128.

$$\frac{d^2C_2(\tau)}{d\tau^2} - \left[Z - \frac{1}{4}\tau^2 \right]C_2(\tau) = 0 \quad (128).$$

Eq.128 is the well known ordinary differential equation, which solutions are also well known parabolic cylinder functions (PCFs). PCFs are also known as Weber parabolic cylinder functions: $U(a,z), V(a,z), \bar{U}(a,z)$ and $W(a,z)$. These notations are due to Miller (1952, 1955). An older notation, due to Whittaker (1902), for $U(a,z)$ is $D_\nu(z)$. The notations are related by $U(a,z) = D_{-a-\frac{1}{2}}(z)$. Whittaker's notation $D_\nu(z)$ is useful when ν is a nonnegative integer

(Hermite polynomial case). Similar analysis is carried in case of amplitude $C_1(t')$. Following the approach of Zener (1932), we carefully introduce the boundary conditions defined by $C_1(-\infty)=1$ and $C_2(-\infty)=0$. Then, the amplitude value of the corresponding laser cooled and trapped polariton wave function is expressed via the parabolic cylinder function $D_\nu(z)$ (Gradshteyn and Ryzhik, 1994 ; Beals and Wong, 2010) Eq.129.

$$\begin{cases} C_1(\tau)=e^{-\pi\nu^2/8}D_{i\nu^2/2}\left(\tau e^{3i\pi/4}\right) \\ C_2(\tau)=e^{-\pi/4}\dfrac{\nu}{\sqrt{2}}e^{-\pi\nu^2/8}D_{-1+i\nu^2/2}\left(\tau e^{3i\pi/4}\right) \end{cases} \quad (129).$$

Thus, the transition probability in the diabatic basis is given by Eq.130.

$$P_d(\tau)=\frac{\nu^2}{2}e^{-\pi\nu^2/4}\left|D_{-1-i\nu^2/2}\left(\tau\sqrt{2}e^{i3\pi/4}\right)\right|^2 \quad (130).$$

II.3.3.3.2. Transition probabilities in the adiabatic basis

In the adiabatic basis, we introduce the instantaneous eigenstates $\varphi_i \ (i=1,2)$ of the time varying Hamiltonian matrix Eq.122, defined by Eq.131.

$$H\varphi_i(t')=E_i\varphi_i(t') \ \ (i=1,2). \quad (131).$$

Since the Hamiltonian changes in time, then the eigenvectors and the adiabatic states $\varphi_{1,2}$ will change with the same parameter. For theoretical simplifications, we express the state vector $\Psi(t')$ in Eq.121 as a superposition of the adiabatic states $\Psi(t')=C_{\mp}\varphi_i(t')$, $(i=1,2)$ where $C_{\mp}$ are coefficients or transition amplitudes. A strict comparison between $C_{1,2}(t')$ and $C_{\mp}(t')$ leads to the conclusion that the adiabatic states appear as an orthogonal rotation of the original diabatic states. This assumption is mathematically expressed by Eq.132 which follows:

$$\begin{bmatrix} \varphi_1(t') \\ \varphi_2(t') \end{bmatrix}=R^{-1}\left(\vartheta(t')\right)\begin{bmatrix} C_1(t') \\ C_2(t') \end{bmatrix}. \quad (132).$$

The first term to the right hand-side of Eq.132 is giving by Eq.133 and the mixing angle $\vartheta(t')$ is defined by Eq.134.

$$R^{-1}\left(\vartheta\left(t^{'}\right)\right)=\begin{bmatrix}\cos\vartheta\left(t^{'}\right) & -\sin\vartheta\left(t^{'}\right)\\ \sin\vartheta\left(t^{'}\right) & \cos\vartheta\left(t^{'}\right)\end{bmatrix}, \tag{133}$$

$$\tan 2\vartheta\left(t^{'}\right)=\frac{\Delta}{\upsilon t^{'}},\quad \left(0\le\vartheta\left(t^{'}\right)\le\frac{\pi}{2}\right). \tag{134}$$

This mixing angle determines the construction of the adiabatic states via the diabatic basis. The link between the superposition coefficients for the diabatic basis $\left(C_1\left(t^{'}\right),C_2\left(t^{'}\right)\right)$ and adiabatic basis $\left(C_{-}\left(t^{'}\right),C_{+}\left(t^{'}\right)\right)$ is labeled in term of $R\left(\vartheta\left(t^{'}\right)\right)$ as shown in Eq.135 below, provided that the transformation matrix $R\left(\vartheta\left(t^{'}\right)\right)$ is expressed as given in Eq.136.

$$\begin{bmatrix}C_1\left(t^{'}\right)\\ C_2\left(t^{'}\right)\end{bmatrix}=R\left(\vartheta\left(t^{'}\right)\right)\begin{bmatrix}C_{-}\left(t^{'}\right)\\ C_{+}\left(t^{'}\right)\end{bmatrix}, \tag{135}$$

$$R\left(\vartheta\left(t^{'}\right)\right)=\begin{bmatrix}\cos\vartheta\left(t^{'}\right) & \sin\vartheta\left(t^{'}\right)\\ -\sin\vartheta\left(t^{'}\right) & \cos\vartheta\left(t^{'}\right)\end{bmatrix}, \tag{136}$$

The unitary matrix $R\left(\vartheta\left(t^{'}\right)\right)$ rotates the polariton system from a diabatic basis to an adiabatic basis. Joining Eq.131 and Eq.137 together, we obtain Eq.137, which represents the most appropriate form in the matrix representation of Hamiltonian Eq.122 in adiabatic basis. According to Eq.135 and Eq.137, the Schrödinger equation in the adiabatic basis, expressed as $i\frac{d}{dt^{'}}\left[R\left(\vartheta\left(t^{'}\right)\right)C\left(t^{'}\right)\right]=H\left(t^{'}\right)\left[R\left(\vartheta\left(t^{'}\right)\right)C\left(t^{'}\right)\right]$, takes the form of Eq.138.

$$R^{-1}HR=\begin{bmatrix}-\sqrt{\nu^2+\tau^2} & 0\\ 0 & \sqrt{\nu^2+\tau^2}\end{bmatrix}. \tag{137}$$

$$i\frac{d}{d\tau}\begin{bmatrix}C_{-}\left(\tau\right)\\ C_{+}\left(\tau\right)\end{bmatrix}=\begin{bmatrix}-\sqrt{\nu^2+\tau^2} & -i\dot{\vartheta}\\ i\dot{\vartheta} & \sqrt{\nu^2+\tau^2}\end{bmatrix}\begin{bmatrix}C_{-}\left(\tau\right)\\ C_{+}\left(\tau\right)\end{bmatrix}. \tag{138}$$

As mentioned by Ostrovsky et al. (2007), the condition for the adiabatic evolution, $\nu\ge 1$, states that $\left|\dot{\vartheta}\left(t^{'}\right)\right|\prec\prec\left|\varepsilon\left(t^{'}\right)\right|$, with $\dot{\vartheta}\left(\tau\right)=-\frac{1}{2}\frac{\Delta}{\tau^2+\nu^2}$ and $\varepsilon\left(t^{'}\right)=\left[\Delta^2+\left(\upsilon t^{'}\right)^2\right]^{1/2}$. Thus, following the methodology used in the previous section for the diabatic representation (Eq.123) and for the same boundary conditions defined by $C_1\left(-\infty\right)=1$ and $C_2\left(-\infty\right)=0$, we carefully obtaine the transition amplitude of the laser cooled and trapped polariton in term of PCFs within the Wittaker representation $D_{\nu}\left[z\right]$ (Beals and Wong, 2010) given by Eq.139.

$$\begin{cases} C_{-}(\tau) = e^{-\pi\nu^2/8}\left\{ D_{i\nu^2/2}\left(\pi e^{i3\pi/4}\right)\sin\vartheta(\tau) - e^{-\pi/4}\,\frac{\nu}{\sqrt{2}}\,D_{-1+i\nu^2/2}\left(\pi e^{i3\pi/4}\right)\cos\vartheta(\tau)\right\} \\ C_{+}(\tau) = e^{-\pi\nu^2/8}\left\{ D_{i\nu^2/2}\left(\pi e^{i3\pi/4}\right)\cos\vartheta(\tau) - e^{-\pi/4}\,\frac{\nu}{\sqrt{2}}\,D_{-1+i\nu^2/2}\left(\pi e^{i3\pi/4}\right)\sin\vartheta(\tau)\right\} \end{cases} \quad (139).$$

The transition probability in the adiabatic basis thus corresponds to the following equation:

$$P_A(\tau) = e^{-\pi\nu^2/4}\left| D_{i\nu^2/2}\left(\pi e^{i3\pi/4}\right)\cos(\tau) - e^{-\pi/4}\,\frac{\nu}{\sqrt{2}}\,D_{-1+i\nu^2/2}\left(\pi e^{i3\pi/4}\right)\sin\vartheta(\tau)\right|^2 \quad (140).$$

II.3.4. Dissipative Landau-Zener model

In physics, one of the most common realizations of strong coupling regime emplies an employement of various low-dimensionnal semi-conductor structures embeded into a microcavity or irradiated by a strong optical field (Shahnazaryan, 2017). To set the stage and to introduce our notation in this section, we recall that the Hamiltonian Eq.118 corresponds to LZ Hamiltonian for an isolated cooled and trapped polaritonic system. While in practices, the cooled and trapped polaritonic system will be influenced by its surrounding environment which may affect the quantum phase of the superposition after the effective interaction between the levels or may cause spontaneous decay. For a polariton cooled and trapped in a solid-state environment, all these processes may occur simultaneously and hinder qubit manipulation. In the context of solid-state quantum information processing, a realistic study of qubit manipulation via LZ transition should include the influence of environmental degrees of freedom. The environment of quantum system can often be described as a bath of harmonic oscillators. In some situations, it is known that the dominant environmental effect can be best modeled as a spin bath instead, for example, for molecular magnets and for josephson-phase qubits.

Due to (i) their unique optoelectronic features in the monolayer limit, (2i) the flexibility of their bandgap energy, (3i) their high oscillator strength, (4i) the fact that they are excellent platform for strong light-matter interactions and quantum confinement and (5i) the possibilities to be studied when embedded in optical microcavities, the surrounding environment is modified and changed to two-dimensional (2D) monolayers TMDs materials. In fact, 2D monolayers TMDs are a certain class of postgraphene 2D materials which stands out as an excellent platform where

strong light-matter interactions (Rahmani and Jagadish, 2018) and quantum confinement at the single layer limit can be studied when embedded in optical cavities. Compounds in the TMDs family exhibit a wide range of electrical properties depending on polytype and the number of transition metal d-electrons, and include metallic (Wilson and Yoffe, 1969), half-metallic (Shishidou et al., 2001), semiconducting (Radisavljevic et al., 2011), superconducting (Ye et al., 2012) and charge density wave (Yoon et al., 2011) behavior. Those of TMDs in quasi-2D geometries have been pointed out by Pu et al. (2012) and Fuhrer and Hone (2013), where electron mobility, symmetry, thickness-dependent evolution of electronic, phonons structures and effect of quantum confinement was recognized as the main ingredient properties that are most relevant in device applications.

We promptly introduce 2D TMDs monolayers into a cavity. In a typical process, the resulting system is mechanically deposited onto a substrate SiO_2. With the help of a laser pump, laser light is directed on the multilayer TMDs through a large orifice, for cooling process (Figure 23a). Within our philosophy, we suppose that on-chip coherent light conducts to ultrafast excitation of the monolayer TMD, leading to the formation of the exciton. We suppose that strong light (on-chip light) matter (exciton) interaction results to microcavity hybrid (half matter and half light) quasiparticle formation called polariton (Figure 23b). The original microcavity polariton is considered as a TLS (Ghoshal et al., 2011; Fujii and Suzuki, 2011) with ground state $|g\rangle$ and excited state $|e\rangle$ (Figure 23c) as we did in the previous sections. In the cavity, each monolayer TMD looks like a spin-oscillator. Thus, the ensemble of multilayer TMDs embedded in the microcavity results to both ensembles of polaritons and spin-oscillators (Figure 23d). The entire system is cooled down by using electromagnetic radiation (laser). The advantage of our model is that the combination of properties inherited from its both counterparts such as ultrasmall effective mass, strong interparticle interactions and enhanced decoherence time, make microcavity polariton unique testbed for observation of various collective quantum phenomena such as BEC, superfluidity, spin currents, optical spin hall effect, quantum transport to cite a few (Shahnazaryan, 2017).

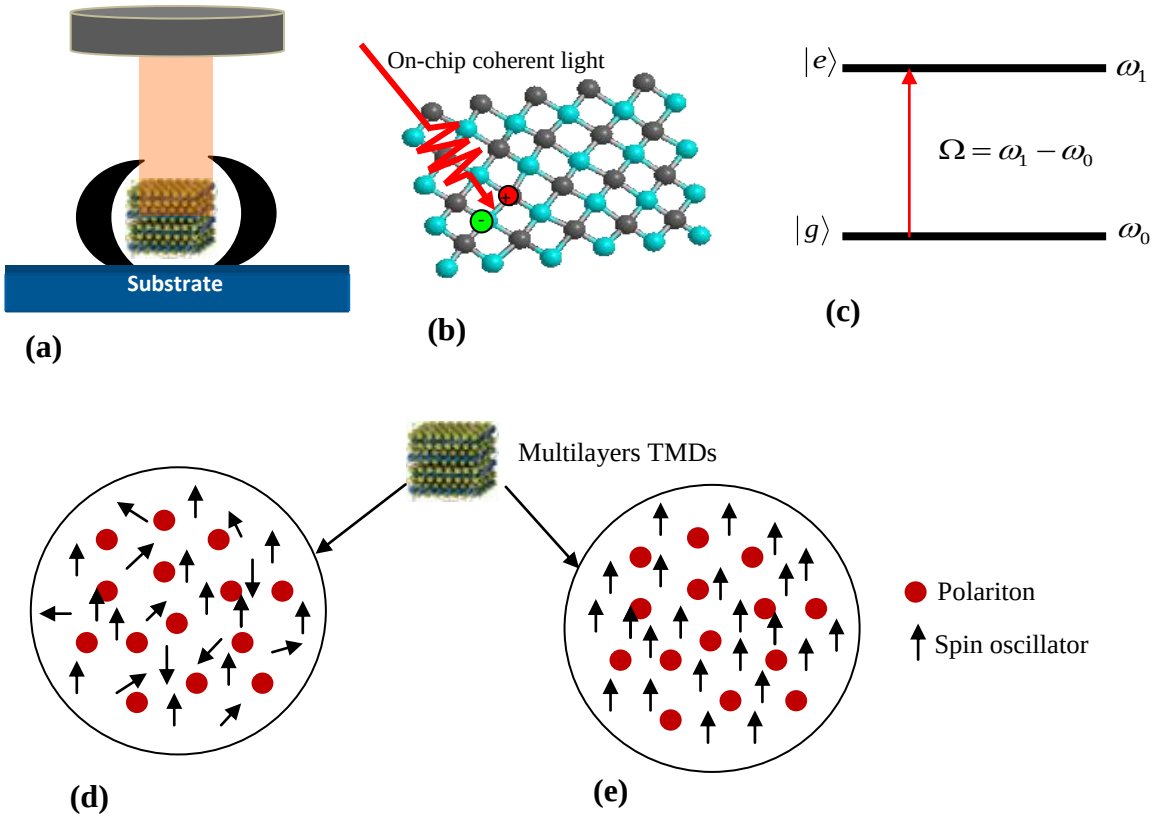

Figure 23. Step by step formalism used in the methodological approach. (a) Multilayer transition metal dichalcogenides embedded in a 2D microcavity and cooled down to zero temperature; the entire system is putted onto a substrate SiO_2. (b) Polariton formation due to strong light (on-chip light) matter (exciton) interaction. (c) Polariton looked as a TLS with ground state $|g\rangle$ and first excited state $|e\rangle$. (d) Spin oscillators and polariton formation at room temperature in 2D microcavity. (e) Coherent state population transfer at zero temperature due to laser light.

II.3.4.1. Hamiltonian of cooled and trapped polariton in Transition Metal Dichalcogenides

Theoretical analysis of the previous model (Figure 23) is performed based on two main considerations. Firstly, we focus our attention only on the polariton at the center of the system. This consideration is inspired from the central spin model investigated and discussed by Prokof'ev and Stamp (2000). Furthermore, we suppose that there is no interaction between the considered polariton in the center of the system with its neighbors due to cooling process. Still, the cooled and trapped polariton is treated here as a TLS (Lopez-Sanchez et al., 2013). We begin with the general Hamiltonian which characterizes the cooled and trapped polariton in 2D TMDs milieu Eq.141, given that the first two terms to the right hand side of Eq.141 represent the LZ

Hamiltonian of hot (no cooled and trapped with laser) polariton in term of Pauli operators and the thirth is that of radiation field (laser light).

$$H = -\frac{\Omega}{2}\sigma_z + \Lambda \mathrm{T}\sqrt{n}\sigma_x - \mu E_0 \sin\left(\omega_l t\right)\sigma_x \tag{141}.$$

In Eq.141, E_0 is the laser amplitude and μ is the laser dipole moment, ω_l been the laser frequency. The parameter Λ is the coupling strength constant between cavity photons and 2D TMDs bands. It's also known as the vacuum Rabi frequency for 2D TMDs at center zone. T is the nearest-neighbor intra-layer hopping or the effective hopping integral. While Ω is the detuning between exciton and photon. Other parameters in Eq.141 are well defined in the previous sections. The Hamiltonian Eq.141 can takes the reduced form of Eq.142 after substitution $\mu_0 = \Lambda \mathrm{T}\sqrt{n}$. We assumed that the Rabi frequency $\Omega_{Rabi} = \mu E_0$. Based on these substitutions, we construct the time dependent Hamiltonian of the polariton embedded in TMD in interaction with laser field. This is expressed in Eq.143:

$$H = -\frac{\Omega}{2}\sigma_z + \left(\mu_0 - \Omega \sin\left(\omega_l t\right)\right)\sigma_x \tag{142},$$

$$H = -\frac{\Omega}{2}\sigma_z + \mu\left(t\right)\sigma_x \tag{143}.$$

In the above equation, the parameter $\mu(t) = \mu_0 - \Omega_{Rabi}\sin\left(\omega_l t\right)$ has been identified by Lopez-Sanchez et al. (20 13) as the bias, which is the total TMDs environment couples to the qubit. In order to get the best mathematical model equation for theoretical analysis, we recall the Hamiltonian Eq.143 and linearized it. Following the AIA as detailed above, we obtained the more appropriate expression of laser cooled and trapped polariton in 2D TMDs materials expressed in Eq.144.

$$H = -\frac{\Omega}{2}\sigma_x + \frac{\eta t'}{2}\sigma_z \tag{144}.$$

LELs are calculated using Hamiltonian Eq.144. In particular, based on quantum mechanic theory, these represent eigenvalues of Hamiltonian Eq.144. Therefore, from relation Eq.144, the corresponding instantaneous LELs are expressed as given in Eq.145,

$$\varepsilon_{\pm} = \pm\frac{1}{2}\sqrt{(\Omega)^2 + (\eta t')^2} \quad (145),$$

where $\sigma_i\,(i = x, z)$ are the same Pauli matrices defined above, $\eta t'$ is the energy difference between the two diabatic basis states $|\uparrow\rangle$ and $|\downarrow\rangle$ of σ_3 of the polariton condensate in TMDs, and Ω is the constant gap between the two instantaneous eigenenergy states $|+\rangle$ and $|-\rangle$ at the center of the avoided crossing $(\eta t' = 0)$ and modulated by the photon's frequency.

II.3.4.2. The Brunsdobler-Elser conjecture

The Brunsdobler-Elser conjecture is a mathematical approximation applied in cooling and trapping system in order to take into account the effect of surrounding environment known here as 2D TMDs. The effect of the surrounding environment is considered through it Hamiltonian H_{env} in the Hilbert space of dimension $M \prec \infty$ and qubit-interaction Hamiltonian H_{q-env}. Eq.144 takes then the form of Eq.146. We assume the most general linear coupling between the qubits operators σ_x, $\sigma_y = -i\left(|\uparrow\rangle\langle\downarrow| - |\downarrow\rangle\langle\uparrow|\right)$ and σ_z and the environment operators $\chi^{\nu}\,(\nu = x, y, z)$. We take the qubit-environment coupling as indicated in Eq.147 and we denote by $|k\rangle$ the eingenstates of the environment operator Hamiltonian H_{env}.

$$H = -\frac{\Omega}{2}\sigma_x + \frac{\eta t'}{2}\sigma_z + H_{env} + H_{q-env} \quad (146),$$

$$H_{q-env} = \sum_{\nu=x,y,z}\sigma_{\nu}\chi^{\nu} \quad (147).$$

An important assumption underlying our model Hamiltonian Eq.146 is that the qubit-environment interaction Eq.147 and the environment itself are not affected by the driving. Then, at very large times $t \to \pm\infty$, the cooled and trapped polariton Hamiltonian is dominated by the time-dependent part, so that all states of the system plus environment belong to one of two bands:

an ‘up cluster’ $\left|\uparrow\right\rangle\left|k\right\rangle$ and a ‘down cluster’ $\left|\downarrow\right\rangle\left|k\right\rangle$, with energies moving upward and downward respectively.

II.3.4.2.1. The Brunsdobler-Elser conjecture in the diabatic basis

The dissipative LZ problem is a scattering problem in the restricted sense that changes in the qubit’s state will occur only during a finite time interval arround $t=0$. In order to exploit the fact that the qubit will not flip for sufficiently large $|t|$, we decompose Hamiltonian Eq.146 into its diabatic states. These are the eigenstates of the total Hamiltonian Eq.146 in the limits $t\to\pm\infty$. Initially and finally, the Hamiltonian is dominated by the term proportional to σ_z, so that the diabatic basis for the qubit is simply given by the states $\left|\uparrow\right\rangle$ and $\left|\downarrow\right\rangle$. For the environment, by contrast, there is no corresponding growing energy scale for large $|t|$. Its diabatic states are influenced by the coupling to the qubit and depend on the qubit’s state. For the up cluster, these diabatic eigenstates of the environment are those which diagonalize the Hamiltonian projected to the subspace $\left|\uparrow\right\rangle$, i.e $\left\langle\uparrow\left|H\right|\uparrow\right\rangle$. They are eigenstates of $H_{env}+\chi^z$ and we denote them by $\left\langle k_+\right|$ and their energies by ε_{k_+}. The diabatic environment sates for the down cluster $\left\langle k_-\right|$ are defined likewise so that Eq.148 is satisfied.

$$\left(H_{env}\pm\chi^z\right)\left|k_\pm\right\rangle=\varepsilon_{k_\pm}\left|k_\pm\right\rangle \qquad (148).$$

The diabetic state of the qubit plus it environment read as given in Eq.149a and Eq.149b.

$$\left|\uparrow k_+\right\rangle\equiv\left|\uparrow\right\rangle\left|k_+\right\rangle \qquad (149a),$$

$$\left|\downarrow k_-\right\rangle\equiv\left|\downarrow\right\rangle\left|k_-\right\rangle \qquad (149b).$$

In the above equations (Eq.149a and Eq.149b), the labels $k_\pm=0,1,2,\ldots$ are assigned such that the energies $\varepsilon_{k_\pm}$ are in increasing order. At asymptotically large times, $t\to\pm\infty$, the diabatic states diagonalize the total Hamiltonian Eq.146 and hence coincide with adiabatic eigenstates which diagonalize $H(t)$ at a given time t. Note that $\left\langle\downarrow k_-\left|\uparrow k_+\right.\right\rangle=0$, although in general $\left\langle k_+\left|k_-^{'}\right.\right\rangle\neq\delta_{kk'}$

. A state of particular interest is the adiabatic ground state $\left|\uparrow 0_{+}\right\rangle$ which has energy $\left(\frac{\eta t'}{2}+\varepsilon_{0_{+}}\right)$. At zero temperature, it is the natural initial state for the LZ dynamics. From here, we can now split the Hamiltonian Eq.146 into two parts, one that is diagonal in the spin index while the other is off-diagonal. The former part consists of all terms proportional to σ_z and is diagonal in the diabatic basis. The latter part corresponds to Eq.150 and will be called the bit-flip interaction, since it contains all interaction terms of the Hamiltonian Eq.146 that induce a population change in the state of the qubit.

$$\nu=\frac{\Delta}{2}\sigma_x+\sigma_x\chi^x+\sigma_y\chi^y \tag{150}.$$

An important feature of the diabatic basis Eq.149 is that all matrix elements of ν vanish within each cluster, i.e., Eq.151 is satisfied.

$$\left\langle\uparrow k_{+}\left|\nu\right|\uparrow k_{+}^{'}\right\rangle=\left\langle\downarrow k_{-}\left|\nu\right|\downarrow k_{-}^{'}\right\rangle=0 \tag{151}.$$

II.3.4.2.2. The Brunsdobler-Elser conjecture in the adiabatic basis

In the above section, we have achieved a useful formulation of the dissipative LZ problem in terms of two groups of diabatic states. If the group of upward moving parallel levels would consist of merely one state, then transition probabilities could be computed with the simple independent-crossing formula, for which Brundobler and Elser (1993) conjectured that it holds even when successive level crossings are not independent. Recent proofs show that the independent-crossing formula indeed holds exactly, even in more general situations (Shytov, 2004; Dobrescu and Sinitsyn, 2006). As stated above, for dissipative LZ transitions, there are two continua of states that cross with constant velocity. For the dissipative LZ problem, if at $t=-\infty$ the system starts in a state $\left|\uparrow k_{+}\right\rangle$ whose diabatic energy is nondegenerate, then the following transition probabilities at $t=\infty$ are exact (see Eq.152).

$$P_{\uparrow k_+ \to \uparrow k_+^{'}} = \begin{cases} \exp\left(-2\pi \dfrac{\left\langle \uparrow k_+ \left| v^2 \right| \uparrow k_+ \right\rangle}{\hbar \eta} \right), k_+^{'} = k_+ \\ 0, k_+^{'} \succ k_+ \end{cases} \quad (152).$$

For the transition to lower states within the initial band of states ($k_+^{'} \prec k_+$), we cannot make any statement. The second line of Eq.152 asserts that, states of the up cluster that lie above the initial state will finally be unpopulated. This no-go theorem was formulated by Sinitsyn (2004) and we think that it is more aptly described by the name 'no-go-up theorem'. A case of particular interest is that of the initial state $\left| \uparrow 0_+ \right|$, which is the ground state of the entire system. For all bath models employed below, the ground state is unique, so that relation Eq.152 applies. Then, final states with $k_+^{'} \prec k_+$ do not exist, while the occupation of final states with $k_+^{'} \succ k_+$ forbidden by the no-go-up theorem. Thus, provided that the final qubit state is $\left| \uparrow \right\rangle$, the environment will end up in its ground state. It is the final transition probabilities $P_{\uparrow \to \uparrow}$ and $P_{\uparrow \to \downarrow}$ for the qubit that interest us most, irrespective of the final state of the environment. By tracing out the environment, i.e., by performing the sum over $k_+^{'}$, we find the Eq.153 below, where the expectation value W^2 is given in Eq.154, recalling that the parameter v is the bit-flip interaction.

$$P_{\uparrow \to \uparrow} = \exp\left(-\frac{\pi W^2}{2\hbar v} \right) = 1 - P_{\uparrow \to \downarrow} \quad (153),$$

$$W^2 = 4\left\langle \uparrow 0_+ \left| v^2 \right| \uparrow 0_+ \right\rangle \quad (154).$$

At this level, the essential steps that remain are first to identify and characterize the diabatic ground state $\left| \uparrow 0_+ \right\rangle$ and to compute the expectation value W^2. We recall to readers that our system consists of the laser cooled and trapped polariton interacting with an ensemble of spin oscillators. This means that, our surrounding environment is a spin bath. The total Hamiltonian of the system is again that of Eq.146, but now with bath Hamiltonian Eq.155 and qubit-bath coupling Eq.156:

$$H_{env} = \sum_{j=1}^{N} \sum_{\nu = x,y,z} B_j^{\nu} \tau_{\nu}^{j} \quad (155),$$

$$H_{q-env} = \sum_{\nu=x,y,z} \sigma_\nu \sum_{j=1}^{N} \gamma_j^\nu \tau_\nu^j \tag{156}$$

where τ_ν^j are the Pauli matrices for the j^{th} bath spin or spin operators and γ_j^ν are coupling constants. The second sum of Eq.156 defines the environment operator χ^ν as a linear combination of the spins operators τ_ν^j with coupling constants γ_j^ν. The bit-flip interaction takes the form of Eq.157.

$$\nu = -\frac{\Omega}{2}\sigma_x + \sum_{j=1}^{N}\left(\gamma_j^x \sigma_x \tau_x^j + \gamma_j^y \sigma_y \tau_y^j\right) \tag{157}$$

We start from here to determine the eigenstates of the qubit plus the spin bath. It has been revealed that (Majorana, 1932), for large $|t|$, the time-dependent term in Eq.175 dominates and so provides the diabatic qubit states $|\uparrow\rangle$ and $|\downarrow\rangle$. Therefore, the diabatic spin-bath states are determined by the operator Eq.158 where, '+' refers to $s = \uparrow$ and '−' to $s = \downarrow$.

$$\langle s|H(t)|s\rangle = \sum_j H_{spin,j}^{\pm} \quad s = \uparrow, \downarrow \tag{158}$$

where

$$H_{spin,j}^{\pm} = \pm\gamma_j^z \tau_z + \sum_{\nu=x,y,z} B_j^\nu \tau_\nu^j \tag{159}$$

is the state of the j^{th} bath spin. The explicit expression for the ground state of $H_{spin,j}^{\pm}$ is not required in determining LZ transition probabilities. Indeed, it suffices to know that the ground state satisfies the eigenvalues equation $H_{spin,j}^{\pm}|g_{j\pm}\rangle = -\mathrm{E}_{\pm}|g_{j\pm}\rangle$. Therefore, we have the following expressions:

$$\langle g_{j\pm}|\tau_x^j|g_{j\pm}\rangle = -\frac{B_j^x}{E_{j+}} \tag{160}$$

$$\langle g_{j\pm}|\tau_y^j|g_{j\pm}\rangle = -\frac{B_j^y}{E_{j+}} \tag{161}$$

$$\langle g_{j\pm}|\tau_z^j|g_{j\pm}\rangle = -\frac{B_j^z}{E_{j+}} \tag{162}$$

Due to the fact that the spins oscillators do not interact with each other, as the entire system is carried to zero temperature with cooling process, then the diabatic ground state $|1\rangle$ is the direct product of the spin diabatic ground state $|g_{j\pm}\rangle$. Therefore, simple substitution of relation Eq.157 into Eq.154 arises to the expression for the ground state expectation value W^2 defined by Eq.163.

$$W^2 = \Omega^2 - 4\Omega\sum_j \left(\gamma_j^x\right)^2 \frac{B_j^x}{\Lambda_{j+}} + 4\sum_j \left[\left(\gamma_j^x\right)^2 + \left(\gamma_j^y\right)^2\right] + 8\sum_j \gamma_j^x \gamma_j^y \frac{B_j^z}{\Lambda_{j+}} + 4\sum_{j\neq j'} \left(\gamma_j^x \gamma_{j'}^x \frac{B_j^x B_{j'}^x}{\Lambda_{j+}\Lambda_{j'+}} + \gamma_j^y \gamma_{j'}^y \frac{B_j^y B_{j'}^y}{\Lambda_{j+}\Lambda_{j'+}}\right) \quad (163).$$

As the system is carried to zero temperature, meaning that interactions between internal elements are very low so that they can be neglected, then we assume that $\gamma_j^x = \gamma_j^y = 0$. The ground state expectation value takes then the form of Eq.164.

$$W^2 = \Omega^2 \quad (164).$$

Such an approximation has been given the name of pure dephasing by Majorana (1932). With such an approximation, Majorana (1932) indicates that the tunneling probability $P_{\uparrow\to\downarrow}$ equals to the standard LZ probability. In the same way, Qiao Chen et al. (2018) in their recent perturbation calculations for dissipative LZ transitions in a spin bath obtained the same bath independent transition probability, assuming that Δ is small. The transition probability in Eq.153 takes the forms of Eq.165 and Eq.166 in both diabatic and adiabatic basis respectively.

$$P_D = \exp\left(-\frac{\pi\Omega^2}{2\hbar\eta}\right) \quad (165),$$

$$P_A = 1 - P_D = 1 - \exp\left(-\frac{\pi\Omega^2}{2\hbar\eta}\right) \quad (166).$$

II.3.5. Fröhlich model of polarons

II.3.5.1. The Fröhlich Hamiltonian

Fröhlich proposed a model Hamiltonian for the “large” polaron through which its dynamics is treated quantum mechanically, the so called Fröhlich Hamiltonian. The polarization,

carried by the longitudinal optical (LO) phonons, is represented by a set of quantum oscillators with frequency ω_{Lo}, the long wavelength LO-phonon frequency, and the interaction between the charge and the polarization field is linear in the field as given by Eq.167 (Fröhlich, 1954).

$$H = \frac{P^2}{2\mu} + \sum_k \hbar\omega_{Lo} a_k^+ a_k + \sum_k \left(V_k^* a_k^+ e^{-ik\cdot r} + V_k a_k e^{ik\cdot r} \right) \qquad (167).$$

In Eq.167, r is the position coordinate operator of the electron with band mass μ, p is its canonically conjugate momentum operator and a_k^+(a_k) is the creation (annihilation) operators for longitudinal optical phonons of wave vector k and energy $\hbar\omega_{Lo}$. The parameters V_k are Fourier components of the electron-phonon interaction and V_k^* their complex conjugates.

II.3.5.2. Optical absorption of Fröhlich polarons and canonical transformation method

The optical absorption of large polarons as a function of the frequency of the incident light is performed using the canonical-transformation formalism by Devreese, Huybrechts and Lemmens (DHL). An introduction of laser radiation in the polaronic system leads to the creation of perpendicular magnetic field. In fact, the electric field $\vec{E}$ and magnetic field $\vec{B}$ are linked through the relation $\hat{B} = -\frac{1}{i\omega_l} curl \hat{E}$. Due to the presence of magnetic field, the entire system is looked as a magneto-polaron. As the system is cooled down with laser, its called, for simplicity, magneto-polaron condensate. A simple calculation, which is developed below in full detail, gives a result for the absorption coefficient. We start from the Hamiltonian Eq.168 of the electron-phonon system interacting with light and written down using the vector potential of an electromagnetic field $A(t)$ at unit h where CC is the acronym of complex conjugate.

$$H = \frac{1}{2\mu}\left[p + \frac{e}{c} A(t) \right]^2 + \sum_k \omega_{Lo} a_k^+ a_k + \sum_k \left(V_k^* a_k^+ e^{-ikr} + CC \right) \qquad (168).$$

The electric field is related to the vector potential as given by Eq.169. Within the electric dipole interaction the electric field with frequency Ω is given by Eq.170 where the vector potential is expresse in Eq.171.

$$E(t) = -\frac{1}{c}\frac{\partial A(t)}{\partial t} \qquad (169),$$

$$E(t) = E\cos(\Omega t) \tag{170},$$

$$A(t) = -\frac{c}{\Omega} E\sin(\Omega t) \tag{171}.$$

II.3.5.3. Time-dependent Schrödinger equation

Within the perpendicular magnetic field B, we adjust the triangular quantum well potential (Figure 24) in the system ellucidated in the above section. The Hamiltonian that clearly describes the magneto-polaron condensate under the influence of a triangular quantum well potential $U(r)$ is encoded in the Fröhlich Hamiltonian and its given by Eq.172, where r and P are still the electron position and momentum operators, $\mu = \frac{m_e}{m_o}$ (giving that m_e is the electron band mass and m_0 is the electron rest mass) is the polaron mass and a_k^+ (a_k) are the creation (annihilation) operators of longitudinal optical (LO) phonon with wave vector q and energy ω_{Lo} at unit $\hbar$. Still, V_k^* and CC are complexe conjugates of the Fourier components of the electron-phonon interactions and complex conjugate.

$$H = \frac{1}{2\mu}\left[p + \frac{e}{c} A(t)\right]^2 + \sum_k \omega_{Lo} a_k^+ a_k + \sum_k \left(V_k^* a_k^+ e^{-ikr} + CC\right) + U(r) \tag{172}.$$

In the above expression, the magnetic field is taken along the Z direction. The first term to the right hand side of Eq.172 is the single electron's Hamiltonian or energy, the second term is the LO phonon Hamiltonian, the third term is the electron-LO interaction term and the last term, the expression $U(r)$, is the potential field Hamiltonian which gives the final expression of the total Hamiltonian of the system and thus dictates that of the energy levels. We choose the triangular quantum well potential with constant electric field Σ and an infinite barrier F at $Z = 0$. Theoretical expression of the corresponding triangular quantum well potential is defined in Eq.173, where Δ is a constant which characterizes the electric field frequency.

$$U(r) = \begin{cases} \Sigma - \frac{\hbar\Delta}{2} + FZ \\ \infty \end{cases} \tag{173}.$$

From this expression of the perturbed system's Hamiltonian Eq.173, the energy is derived and it dependence on the quantum well is depicted in Eq.173. It is important to note that, theoretical investigation of the unperturbed polaron system's energy is presented in detail by Devreese (2015), Tkach et al. (2015) and Fai et al. (2005) and will be used in this paper for more detail analysis and theoretical predictions. Result of Eq.173 has been obtained by solving the Schrödinger Eq.174 given that $\alpha = \Sigma - \frac{\hbar\Delta}{2} = cste$. For further information concerning the Schrödinger equation, readers should refer to Erbil (2017) and McMahon (2006).

$$\frac{d^2\psi(Z)}{dZ^2} - \frac{2\mu}{\hbar^2}(\alpha + FZ - E_Z)\psi(Z) = 0 \tag{174}.$$

The parameter ψ in Eq.174 is the wave function which describes the probability of the system quantum state as a function of position, momentum, time and/or spin. In order to solve the Schrödinger Eq.174, we first consider arrangement in Eq.175 and perform the changes in Eq.176 and Eq.177.

$$\frac{1}{\left(\frac{2\mu}{\hbar}\right)^{\frac{2}{3}}}\frac{d^2\psi(z)}{dz^2} - \left(\frac{2\mu}{\hbar^2}\right)^{\frac{1}{3}} F\left[Z + \frac{\alpha - (E_z)_n}{F}\right]\psi(z) = 0 \tag{175},$$

$$U = \left(\frac{2\mu F}{\hbar^2}\right)^{\frac{1}{3}}\left[Z + \frac{\alpha - (E_z)_n}{F}\right] \tag{176},$$

$$\frac{d}{dz} = \frac{d}{dU}\frac{dU}{dz} \tag{177}.$$

It comes from the above the final expression of Schrödinger equation given in Eq.178, which is the well-known Airy function with solutions given in Eq.179. In Eq.179, the parameter C is the normalized constant, since the wave function has to be zero at the infinite barrier.

$$\frac{d^2U}{dU^2} - U\psi(U) = 0 \tag{178},$$

$$\psi(U) = CA_i(U) \tag{179}.$$

From Eq.179 and considering changes in Eq.176, it comes the expression of the wavefunction for Schrödinger Eq.191 and expressed in Eq.180.

$$\psi(z) = CA_i\left\{\left(\frac{2\mu F}{\hbar^2}\right)\left[Z + \frac{\alpha - (E_z)_n}{F}\right]\right\} \tag{180}.$$

The eigein energies are obtained from the consideration that $\psi(z=0)=0$. This conducts to the relation Eq.181, where a_n expressed in Eq.182 are the zeroes of the Airy function.

$$A_i a_n = 0 \tag{181},$$

$$a_n = \left(\frac{2\mu F}{\hbar^2}\right)^{\frac{1}{3}}\left[\frac{\alpha - (E_z)_n}{F}\right] \tag{182}.$$

Simple analysis of Eq.213 results to the eigein energies Eq.183 of the system.

$$(E_z)_n = \Sigma - \frac{\hbar\Delta}{2} - F\left(\frac{2\mu F}{\hbar^2}\right)^{-\frac{1}{3}} a_n \tag{183}.$$

In contrast, a_n initial estimate for the n^{th} zero of Airy function are given in Eq.184 where $f(z)$ is kindly expressed in Eq.185.

$$a_n = -f\left[\frac{3\pi(4n-1)}{8}\right] \tag{184},$$

$$f(z) = z^{\frac{2}{3}}\left(1 + \frac{5}{48}z^{-2} - \frac{5}{36}z^{-4} + \frac{77125}{82944}z^{-6} - \frac{108056875}{6967296}z^{-8} + \frac{162375596875}{33443020}z^{-10}\right) \tag{185}.$$

Based on Eq.184 and Eq.185 it comes that a_n has the form of Eq.186 and finally, the energy levels take the form of Eq.187. with $n = 0,1$ for both ground and excited state of the system.

$$a_n = -\left[\frac{3\pi(4n-1)}{8}\right]^{\frac{2}{3}} \tag{186},$$

$$\left(E_z\right)_n = \Sigma - \frac{\hbar\Delta}{2} + F\left(\frac{2\mu F}{\hbar^2}\right)^{-\frac{1}{3}}\left[\frac{3\pi\left(4n-1\right)}{8}\right]^{\frac{2}{3}} \quad (187).$$

Within the influence of triangular quantum well potential and perpendicular magnetic field, the complete Hamiltonian describing the sytem takes the form of Eq.188, which is as similar as that of Eq.187. The only difference being the fact that the magnetic field is not equal to zero, thereby conducting to the annulation of the cooling effect.

$$H = \frac{1}{2\mu}\left[p + \frac{e}{c}A(t)\right]^2 + \sum_k \omega_{Lo} a_k^+ a_k + \sum_k \left(V_k^* a_k^+ e^{-ikr} + CC\right) + U(r) \quad (188).$$

From this expression of the perturbed system's Hamiltonian (Eq.188), the energy of the system is derived and it dependence on the quantum well is depicted in Eq.189. In Eq.189, $\Omega_c = eB/\mu c$ is the cyclotron frequency.

$$E = \left(n + \frac{1}{2}\right)\hbar\Omega_c + \left(E_z\right)_n = \left(n + \frac{1}{2}\right)\hbar\Omega_c + \Sigma - \frac{\hbar\Delta}{2} + F\left(\frac{2\mu F}{\hbar^2}\right)^{-\frac{1}{3}}\left[\frac{3\pi\left(4n-1\right)}{8}\right]^{\frac{2}{3}} \quad (189).$$

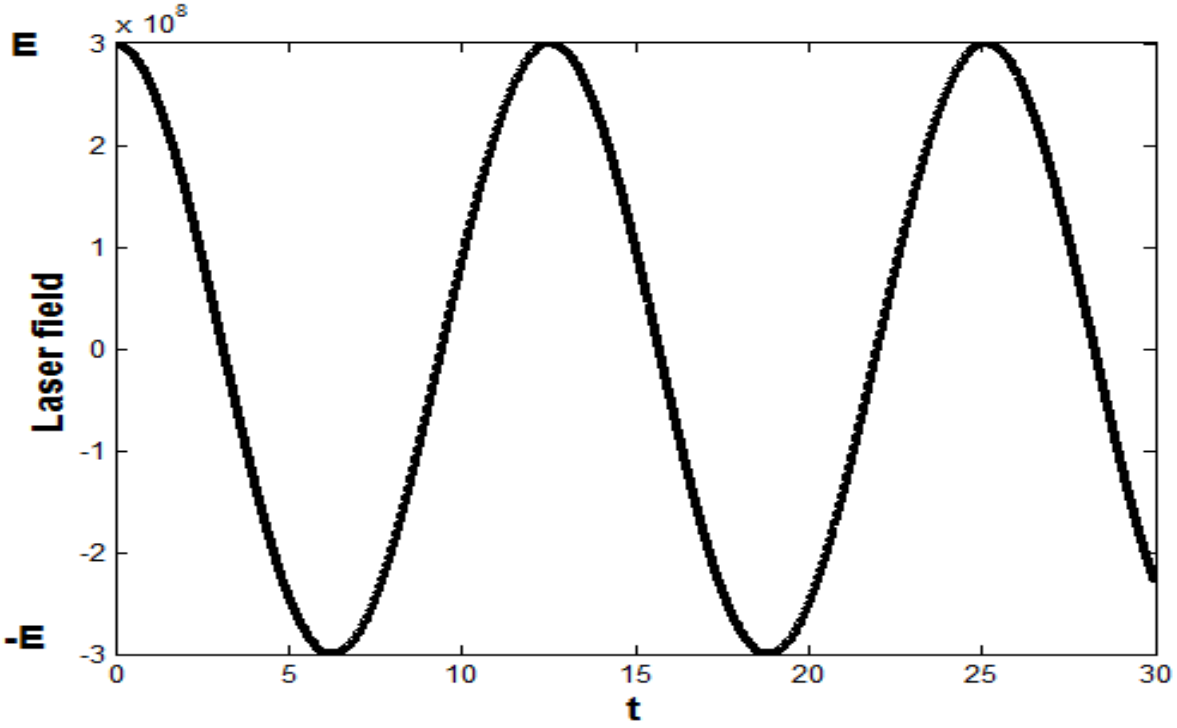

Figure 24. Graphical representation of the laser field amplitude used to cool the system of magneto-polaron at nearest zero temperature as a function of time.

II.3.5.4. Density functional perturbation and improved wigner-brillouin theories

To investigate fundamentals (Fobasso et al., 2019) in a more practical environment thereby open door to possible new features for electronic and optoelectronic devices, we consider that the polaron results from a peculiar coupling which emerges between electron and longitudinal optical (LO) phonons in 2D TMDs. A model Hamiltonian is developed at different levels to present theoretical description of the system. While the laser radiation of amplitude E_0 is introduced in the system, the laser reduces the motion of the entire system of magneto-polaron embedded in 2D TMDs milieu under the influence of triangular quantum well potential. We consider such a phenomenon as the cooling process and the entity arising from it as a cooled magneto-polaron or more appropriately magneto-polaron condensate, no matter the one particle task. We consider the one dimensional cooling process of the system, that is the z-direction, as mentioned in the previous section. Due to the dimensionality of the 2D material, only the two substrates with the highest magnetic quantum numbers are involved in the dynamics, called the ground state $|g\rangle$ and the excited state $|e\rangle$. This assumption stands as the main reason of considering our system as a TLS. The model we employed in this part of the paper is based on the Fröhlich Hamiltonian. Within the framework of the continuum model describing the magneto-polaron condensate interacting with vibrational modes of 2D TMDs materials under the influence of a triangular quantum well potential, the Hamiltonian of the system is theoretically expressed by Eq.190 at unit $\hbar$. Expressions Eq.190 and Eq.172 are alike with the same terms. In contrast, the Fourier components of the electron-phonon interaction V_k are changed to the parameter $G(q)$ which corresponds to the polar-optical coupling with LO phonons in 2D TMDs materials, known elsewhere (Sohier et al., 2016) as the Fröhlich interaction and which is the main purpose of the next section.

$$H = \frac{1}{2\mu}\left(P + \frac{e\overrightarrow{A(t)}}{c}\right) + \sum_q \Omega b_q^+ b_q + \sum_q \left[G(q) b_q e^{iqr} + CC\right] + U(r) \qquad (190).$$

II.3.5.4.1. Density functional perturbation theory calculations

We now present analytical model calls density functional perturbation theory (DFPT) which explains how we get to the best formulation of the Fröhlich interaction $G(q)$ in 2D TMDs. The tensor of Born effective charge is noted by Z_a^m for monolayer. The index a runs over the atoms of the unit cell. The relative dielectric permittivity tensor (simply called dielectric tensors hereafter) for monolayer is noted ε^m. By symmetry, the tensor is isotropic in the plane, but we allow for different properties in the out-of-plane direction. The tensors thus have the generic forms of Eq.191.

$$\varepsilon = \begin{pmatrix} \varepsilon_p & 0 & 0 \\ 0 & \varepsilon_p & 0 \\ 0 & 0 & \varepsilon_z \end{pmatrix},\ Z_a = \begin{pmatrix} Z_{a,p} & 0 & 0 \\ 0 & Z_{a,p} & 0 \\ 0 & 0 & Z_{a,z} \end{pmatrix} \tag{191}.$$

In-plane and out-of-plane, variables are separated according to the notation $r \to (r_p, z)$ and $q \to (q_p, q_z)$. We use Gaussian centimeter-gram-second (CGS) units. We consider LO phonons in a 2D material of thickness d. Its dielectric tensor ε^m has the form of Eq.191, with in-plane and out-of-plane dielectric constants ε_p^m and ε_z^m respectively. Above and below are two semi-infinite spaces with isotropic dielectric properties represented by the dielectric constants ε_2 and ε_1 respectively. The origin of the polar-optical coupling is the polarization density $P(r_p, z)$ Eq.192 generated by the atomic displacement pattern associated with a LO phonon of in-plane momentum q_p (Figure 25), where A is the area of the unit cell, $f(z)$ the outof-plane profile of the polarization (normalized to unity) and M_p the polaron mass. Other parameters in Eq.192 such as e, $e^a_{q_p,LO}$ and $\omega_{q_p,LO}$ denote respectively the electronic charge, eigenvectors of the system of polaron associated with LO-phonon coupling in 2D TMDs under the influence of triangular quantum well potential and the photon frequency associated with LO phonon coupling.

$$P(r_p, z) = \frac{e^2}{A} \sum_a \frac{Z_a^m . e^a_{q_p,Lo}}{\sqrt{2M_p \omega_{q_p,Lo}}} f(z) e^{iq_p . r_p} \tag{192}.$$

Such a polarization density induces a potential $V_{Fr}(r_p,z)=V_{Fr}(q_p,z)e^{iq_p,r_p}$ with the same periodicity. The associated EPC can then be written as given in Eq.193.

$$g_{Fr}^{2D}(q_p)=\int V_{Fr}(q_p,z)\eta_{el}(z)dz \quad (193),$$

where $\eta_{el}(z)$ is the plane-averaged electronic density. By using this expression, we neglect the details of the wave functions and the associated band dependency. In the out-of-plane direction, we consider the electronic density and the polarization to be uniform over the thickness t of the material Eq.194, where θ is the Heaviside function.

$$f(z)=\eta_{el}(z)=\frac{\theta(t/2-|z|)}{d} \quad (194),$$

This approximation should be satisfactory in the long-wavelength limit, since $V_{Fr}(q_p,z)$ varies mildly in the out-of-plane direction. The potential V_{Fr} must fulfill the Poisson Eq.195, where $\varepsilon(z)$ is a position-dependent dielectric tensor.

$$\nabla.[\varepsilon(z)\nabla V_{Fr}(r)]=4\pi\nabla.P(r) \quad (195).$$

The central objects of the problem are the phonon-induced polarization density and the dielectric tensor. As one travels along the out-of-plane direction, both those quantities change. Inside the 2D material, $\varepsilon(z)=\varepsilon^m$ and the polarization density is finite and oscillating in the plane. Outside the 2D material, $\varepsilon(z)=\varepsilon_1 \mathrm{I}$ (where I is the identity matrix) and the polarization density is zero. Other requirements on the potential are that the associated in-plane electric field $E^{//}(r)$ and out-of-plane electric displacement $D^{\perp}(r)$ should be continuous. After performing calculations, it comes the following expression Eq.196.

$$\left|g_{Fr}^{2D}(q_p)\right|=\frac{c_z}{\varepsilon_{eff}(|q_p|)},\ \varepsilon_{eff}(|q_p|)\approx\varepsilon_{eff}^0+r_{eff}|q_p| \quad (196),$$

In the above, the constant c_z corresponds to the magnitude of the bare Fröhlich interaction. It depends on ε_{12} the Born-effective charges and the phonon displacements. The

parameters in Eq.196 that is the effective screening $\left(\varepsilon_{eff}^{0}\right)$ and the effective thickness $\left(r_{eff}\right)$ are expressed by following relations given that ε_{12} is the average dielectric constant.

$$c_z = \frac{2\pi e^2}{A}\sum_a \frac{e_{q_p}.Z_a^m.e_{q_p,Lo}^a}{\sqrt{2M_a\omega_{q_p,Lo}}} \tag{197},$$

$$\varepsilon_{eff}^{0} = \varepsilon_{12}\frac{\varepsilon_z^m\bar{\varepsilon}}{\varepsilon_z^m\bar{\varepsilon}+\varepsilon_{12}\left(\varepsilon_z^m-\bar{\varepsilon}\right)} \tag{198},$$

$$r_{eff} = \frac{\left(\varepsilon_{eff}^{0}\right)}{\varepsilon_{12}}\left(\frac{\varepsilon_{12}}{3\varepsilon_z^m}+\frac{\varepsilon_p^m}{2\varepsilon_{12}}F\right)\times d \tag{199},$$

$$F = 1+\frac{\varepsilon_1\varepsilon_2}{\bar{\varepsilon}^2}+\frac{\varepsilon_{12}}{\bar{\varepsilon}}-\frac{\varepsilon_{12}^2}{\bar{\varepsilon}\varepsilon_z^m}-\frac{\varepsilon_{12}^2}{\bar{\varepsilon}^2}-\frac{\varepsilon_{12}}{\varepsilon_z^m} \tag{200},$$

$$\varepsilon_{12} = \frac{\varepsilon_1+\varepsilon_2}{2}\ ,\ \bar{\varepsilon} = \sqrt{\varepsilon_z^m\varepsilon_p^m} \tag{201}.$$

In the simple effective isotropic model [see Sohier et al.(2016)], the final expression of the polar-optical coupling with LO phonons in 2D TMDs materials or Fröhlich interaction is given by Eq.202.

$$G(q) = \frac{c_z}{\varepsilon_{eff}^{0}+r_{eff}|q|} \tag{202}.$$

In Eq.219, c_z still describes the bare magnitude of the polar-optical coupling which depends on the Born effective charges and the phonon displacement. Other terms in Eq.219 are given in Eq.203 and Eq.204 respectively for TMDs materials, given that ε_{iso} and d_{iso} are dielectric constant and thickness of 2D TMDs materials in the isotropic model. $\varepsilon_i\left(i=1,2\right)$ represents dielectric constant above $\left(i=1\right)$ and below $\left(i=2\right)$ the 2D TMDs material respectively.

$$\varepsilon_{eff}^{0} = \frac{1}{2}\left(\varepsilon_1+\varepsilon_2\right) \tag{203},$$

$$r_{eff} = \frac{1}{2}\varepsilon_{iso} d_{iso} \quad (204).$$

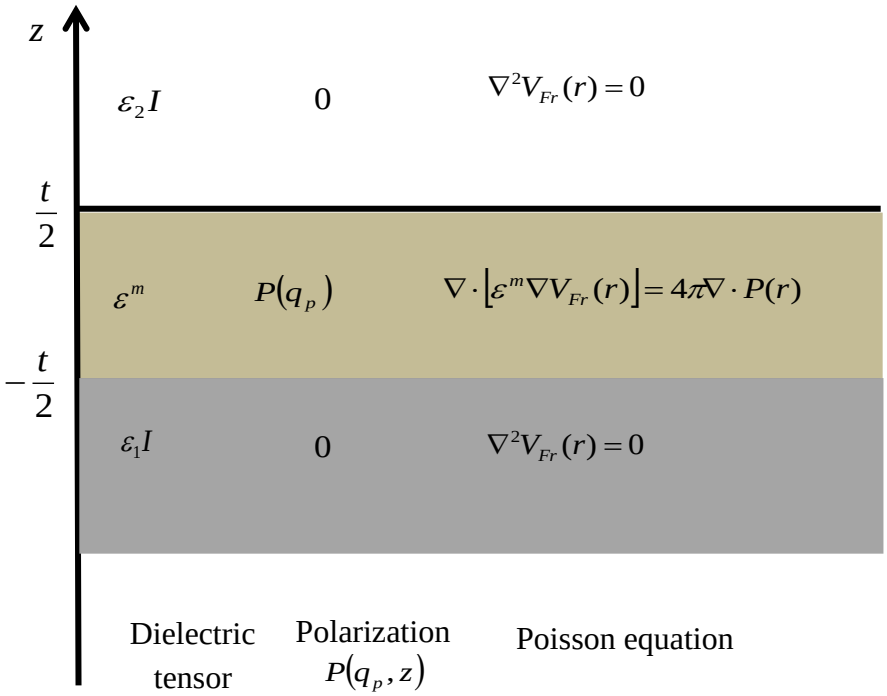

Figure 25. Model of the Fröhlich interaction in a polar 2D material of thickness t . LO phonons generate a periodic polarization density $P(r_p, z) = P(q_p, z) e^{iq_p . r_p}$ inside the 2D material.The dielectric properties of the 2D material are represented by the dielectric tensor ε^m with in-plane and out-of-plane dielectric constant ε_p^m and ε_z^m (denoted for simplicity ε_p and ε_z in the text) respectively. Above and below the two half spaces in which the polarization is zero, and the dielectric constant are ε_2 and ε_1 respectively. The sympbol I denote the identity matrix.The two tick and black horizontal lines represent surfaces charged at the interface of 2D material due to the abrupt variations in the polarization density [from Sohier et al. (2016)].

II.3.5.4.2. Improved Wigner-Brillouin theory

The impoved wigner-Brillouin theory (IWBT) (Chen et al., 2018) is a mathematical tool most suitable in determining LELs of laser cooled and trapped polarons embedded in 2D TMDs materials. Based on Hamiltonian Eq.207, we performed LELs using IWBT. Due to the introduction of laser, energy levels of the system are Landau levels (LLs) shifted over $\overline{\Delta(E_Z)_n}$ by

the interaction of the electron with LO-phonons. Within second-order perturbation theory, the energy shift of the n^{th} LLs is given by Lindemann et al. (1983) (Eq.205).

$$\overline{\Delta E_n} = -\sum_{m=0}^{\infty}\sum_{q}\frac{|M_{nm}(q)|^2}{D_{nm}} \tag{205},$$

where,

$$M_{nm}(q) = \langle m;q|H_I|n;0\rangle \tag{206},$$

is the matrix element of the electron-phonon interaction operator H_I (the third term in Eq.207) between an electron in Landau levels (LLs) m and n and one phonon state with momentum q. The energy denominator in Eq.205 is given by Eq.207;

$$D_{nm} = \hbar\omega_{Lo} - \Delta_n + \hbar\omega_c(m-n) \tag{207},$$

with the energy shift $\Delta_n = \Delta E_n - \Delta E_0$ obtained within the IWBPT. Eq.205 is a non-linear equation which is then solved for Δ_n. For the LLs below the LO-phonon continuum, the energy denominator is D_{nm} and therefore, we insert Eq.208 into Eq.205 thereby resulting to Eq.209, where $r(u)$ is the electron position operator at imaginary time $u = -it$, which has been given by Devreese et al. (1973) and Peeters and Devreese (1982) (see Eq.210).

$$\frac{1}{D_{nm}} = \int_0^{\infty} du e^{-D_{nm}u} \tag{208},$$

$$\Delta E_n = -\sum_q |g_{Lo}(q)|^2 \int_0^{\infty} du e^{-(\hbar\omega_{Lo}-\Delta_n)u}\langle n;0|e^{iq.r(0)}|n;0\rangle \tag{209},$$

$$\begin{cases} x(t) = -\dfrac{\Pi_x}{\omega_c} - \dfrac{1}{\sqrt{2\omega_c}}\left(Ce^{-i\omega_c t} + CC\right) \\ y(t) = \dfrac{\Pi_y}{\omega_c} - \dfrac{i}{\sqrt{2\omega_c}}\left(Ce^{-i\omega_c t} + CC\right) \end{cases} \tag{210}.$$

In Eq.210, Π_x and Π_y are the center of orbit operators and obey the commutation relation $[\Pi_x, \Pi_y] = i\omega_c$. For 2D system, $q.r(u) = q_x x(u) + q_y y(u)$. Following the calculations of Peeters and Devreese (1985), we obtain the result of Eq.211.

$$\langle n;0|e^{iq.r(t)}e^{-iq.r(t)}|n,0\rangle = \exp\left\{-\frac{q^2}{2\omega_c}\left[1-e^{\omega_c u}\right]\right\}\sum_{m=0}^{n}\begin{bmatrix} n \\ m \end{bmatrix}\frac{1}{m!}\left(\frac{2q^2}{\omega_c}\sinh^2\frac{\omega_c u}{2}\right)^m \quad (211).$$

We insert the above result into Eq.209 and substitute $\sum_q(...)$ with $\frac{1}{2\pi}\int qdq$. We obtain the final result for the LLs below the LO-phonon continuum Eq.212.

$$\overline{\Delta E_n} = -\frac{1}{2\pi}\int_0^\infty dq\int_0^\infty duq|g_{Lo}(q)|^2 e^{-(\hbar\omega_{Lo}-\Delta_n)u}\exp\left\{-\frac{q^2}{2\omega_c}\left[1-e^{\omega_c u}\right]\right\}\sum_{m=0}^{n}\begin{bmatrix} n \\ m \end{bmatrix}\frac{1}{m!}\left(\frac{2q^2}{\omega_c}\sinh^2\frac{\omega_c u}{2}\right)^m$$

(212).

For the LLs above the LO-phonon continuum, the denominator D_{nm} can become zero and can even change sign. Therefore, in order to obtain the energy correction, we then take the principal value as given in Eq.213.

$$\overline{\Delta E_n} = -p\sum_{m=0}^{\infty}\sum_q \frac{|M_{nm}(q)|^2}{D_{nm}} \quad (213).$$

Because Eq.208 becomes invalid for LLs above the LO-phonon continuum, we should calculate the explicit expression for the matrix element $M_{nm}(q)$ and then perform the q integral. Inserting the interaction Hamiltonian of electron and phonon H_I into the matrix element, we obtain Eq.214.

$$M_{nm}(q) = g^*_{Lo}(q)\langle m|e^{iq.r}|n\rangle \quad (214),$$

Then

$$|M_{nm}(q)|^2 = |g_{Lo}(q)|^2\left|\langle m|e^{iq.r}|n\rangle\right|^2 \quad (215).$$

Let now insert the electron position operators Eq.210 (Devreese et al., 1973; Peeters and Devreese, 1982) into the above formula, we obtain Eq.216.

$$\langle m|e^{iq.r}|n\rangle = e^{-\frac{q^2}{4\omega_c}}\langle m|e^{\frac{iq_+}{\sqrt{2\omega_c}}c}\, e^{\frac{iq_-}{\sqrt{2\omega_c}}c^+}|n\rangle \tag{216},$$

where $q_\pm = q_x \pm iq_y$. $C^+(C)$ is creation (annihilation) operator for a Landau state, and they obey the commutation relation $\lfloor C, C^+ \rfloor = 1$. In Eq.216, we need the expectation value. Thus,

$$\langle m|e^{a_+C^+}\, e^{a_{-+}C}|n\rangle = \sum_{l=0}^{s}\frac{(a_+a_-)^l\, a_+^{|m-n|}}{(|m-n|+l)!}\sqrt{\delta(m,n)}\begin{bmatrix} s \\ l \end{bmatrix} \tag{216},$$

With $s = m(n \geq m)$, $s = n(n \leq m)$ and $\delta(m,n) = \frac{n!}{m!}(n \geq m); \frac{m!}{n!}(n \leq m)$. Eq.217 with Eq.216 give Eq.218.

$$\langle m|e^{iq.r}|n\rangle = e^{-\frac{q^2}{4\omega_c}}\sum_{l=0}^{s}\frac{\left(-\frac{q^2}{2\omega_c}\right)^l\left(\frac{iq_-}{\sqrt{2\omega_c}}\right)^{|m-n|}}{(|m-n|+l)!}\sqrt{\delta(m,n)}\begin{bmatrix} s \\ l \end{bmatrix} \tag{217}.$$

Inserting Eq.218 into Eq.212, we finally obtain the energy shift in monolayer TMD above the LO-phonon continuum Eq.219.

$$\overline{\Delta E_n} = \frac{1}{2\pi}\, p\sum_{m=0}^{\infty}\frac{\delta(m,n)}{\hbar\omega_c(n-m)-\hbar\omega_{Lo}+\Delta_n}\int dqq|g_{Lo}(q)|^2$$
$$\times e^{-\frac{q^2}{4\omega_c}}\left(\frac{q^2}{2\omega_c}\right)^{|m-n|}\left[\sum_{l=0}^{s}\frac{\left(-\frac{q^2}{2\omega_c}\right)^l\left(\frac{iq_-}{\sqrt{2\omega_c}}\right)^{|m-n|}}{(|m-n|+l)!}\sqrt{\delta(m,n)}\begin{bmatrix} s \\ l \end{bmatrix}\right]^2 \tag{128}.$$

It comes from here that, the final expression of LELs of the system of magneto-polaron condensate, in 2D TMDs materials under the influence of triangular quantum well potential and in the presence of perpendicular magnetic field is given in Eq.220 where the last term to the right

hand side is depicted in Eq.212 below LO-phonon coupling and Eq.218 above LO-phonon coupling.

$$E_n = \left(n+\frac{1}{2}\right)\hbar\Omega_c + \Sigma - \frac{\hbar\Delta}{2} + F\left(\frac{2\mu F}{\hbar^2}\right)^{-\frac{1}{3}}\left[\frac{3\pi(4n-1)}{8}\right]^{\frac{2}{3}} + \overline{\Delta E_n} \qquad (229).$$

Conclusion

We present different mathematical tools needed in order to solve the problem treated in this thesis, namely effect of surrounding environment in laser cooling and trapping of atomic particles and particularly polariton and polaron. We propose several methods and showed how it is possible to investigate the dynamic of a laser cooled and trapped polariton within both SC approach and LZ formalism. In particular, based on classical electromagnetism approach with the help of RWA, we carefully investigate the effect of surrounding environment in laser cooling and trapping of polariton in one hand and decoherence in the system of laser cooled and trapped polariton when it is confined in a magnetic field which we consider as a trap. This is done by theoretical calculations of cooled and trapped polariton parameters which are (i) force and corresponding torque, (2i) transition probabilities of founding the system in the excited state, (3i) total energy of the cooled and trapped polaritonic system and (4i) Von Neumman entropy. Due to the consideration that laser cooled and trapped polariton is a TLS, we formulated LZ problem in laser cooling and trapping of polarion. From the Jaynes-Cumming and LZ models, we used LZSIT based on AIA in order to investigate LELs of cooled and trapped polariton. Later, regarding their physical properties which include (i) their unique optoelectronic features in the monolayer limit, (2i) their high oscillator strength, (3i) the fact that they are excellent platform for strong light-matter interactions and quantum confinement, (4i) the possibility to be studied when embedded in optical cavities and (5i) the flexibility of their band gap energy, we consider that the polariton results from peculiar coupling between exciton and photon in 2D TMDs materials. We use the same LZSI theory based on AIA for the investigation of LELs. Under the influence of a triangular quantum well and permendicular magnetic field, the IWBT is considered in performing LELs calculations of cooled and trapped magneto-polaron. The choice of this entity comes from the fact that, in one hand, the introduction of laser radiation in the system

conducts to the braking down of Pauli exclusion principle thereby makinglaser cooled and trapped polariton to behaves like intermediate particle which satisfies both Fermi-Dirac and Bose-Einstein statistics, and, on the other hand, polaron is a fermion which satisfies Fermi-Dirac statistic.

CHAPTER THREE

RESULTS AND DISCUSSIONS

Introduction

In the previous chapter, we present in detail the general mathematical tools and formalism used in this thesis in order to get to our main objective. In addition, the previous chapter presents analytical results on essential parameters investigated within our study. These include forces and corresponding torques, transition probabilities of laser cooled and trapped polaritons and energy of the system. Throught LZ approach, LELs of both laser cooled and trapped polariton and polaron in both diabatic and adiabatic basis are also investigated in the previous chapter. In this chapter then, numerical results are presented and discussed in otrher to support our analytical results and bring insight to our philosophy.

III.1. Laser cooling and trapping of polariton

III.1.1. Laser cooling and trapping of polariton without magnetic field

III.1.1.1. Force and torque

Laser cooling and trapping is the physical phenomenon that can be used to decrease considerably the motion of atomic particles. Just like momentum, and considering their link, force is a characteristic of motion that can be transferred. This radiation pressure has as origin the interaction between matter and laser light, with exchanges of discrete packets of light usually called photons. Various curves are plotted in Figure 26. For numerical purpose, let $E_x^* = E_y$ and $E_y^* = -E_x$. Then we may write $|E_{ox}| = |E_{oy}|$ and $|E_{0x}||E_{0y}| = |E_{ox}|^2 = |E_{oy}|^2 = |E_0|^2$. We observe that without interaction, when ($g = 0$), the polariton is subjected to a decreasing force, which becomes constant with decreasing coupling constant. It becomes more difficult to cool and trap polariton than electron because the environment strongly affects the process. Compared to the force, the torque increases with coupling strength constant. Also, the torque and force change considerably with the Rabi frequency particularly for weak coupling constant. Therefore, the laser does not

have any effect for strong interaction. Both force and torque change sign but not periodically. Thus, the polariton dynamics does not depend on the laser amplitude but on its frequency.

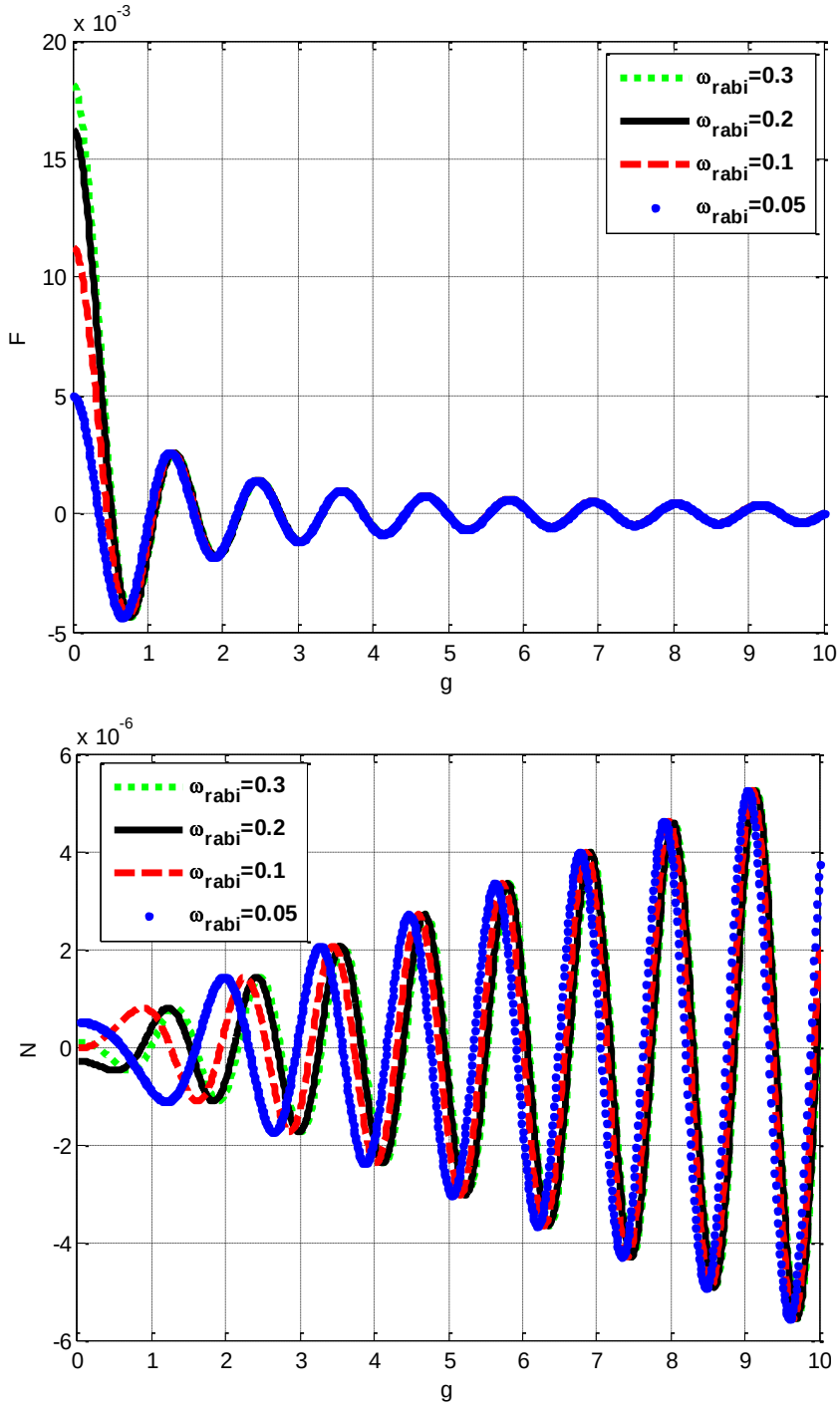

Figure 26. a) Force and b) torque versus coupling constant for different values of Rabi frequency.

We observe that without interaction the particle accelerates ($F > 0$). When the interaction increases, the polariton decelerates and modulates the force, which vanishes for higher coupling constant strength. The Rabi frequency also decelerates the motion of the electron, which is obvious. The physical interpretation is that the environment can be used to cool and trap electrons and also as a control parameter of the cooling and trapping of particle. Negative and positive torque is clearly observed with increasing coupling constant strength. This implies that even if the particle is stable for strong coupling, it has a rotational tendency; perhaps due to state variation of the polariton. It is known that atoms can undergo transitions between different states when a photon with energy is emitted or absorbed.

III.1.1.2. Transition probability and energy

Figure 27 represents the transition probability of finding a cooled and trapped polariton in the excited state as a function of photon frequency for different values of Rabi frequency. Various curves are plotted by setting the oscillating frequencies of the laser radiation at the resonance ($\omega_0 = \omega_{Rabi}$). In Figure 27, it is observed that, with no environmental effects $(\omega = 0)$, the probability is higher and decreases with increasing environmental effects. The probability decreases and collapses for large environment effects. We may also see that the Rabi frequency decreases the probability amplitude. This means that the transition probability for finding the cooled and trapped polariton in the excited state is mostly governed by the environment. Figure 28 shows that strong coupling constant decreases the probability of finding the polariton in the excited state. Compared to the case of weak coupling presented above, the probability to find the polariton in the excited state decreases with Rabi frequency. In addition, in this case compared to weak coupling, the polariton shuttles rapidly between ground and excited states. The coupling strength constant can be used to control electron state under laser radiation.

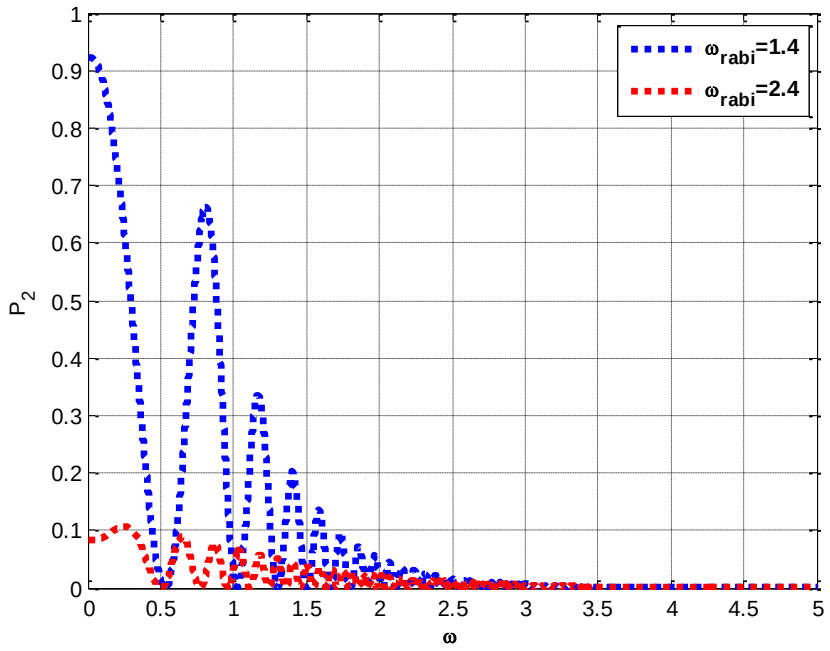

Figure 27. Probabilities of finding the coherently two-level of polariton in the excited state versus photon frequency ω for $g<1$. ω

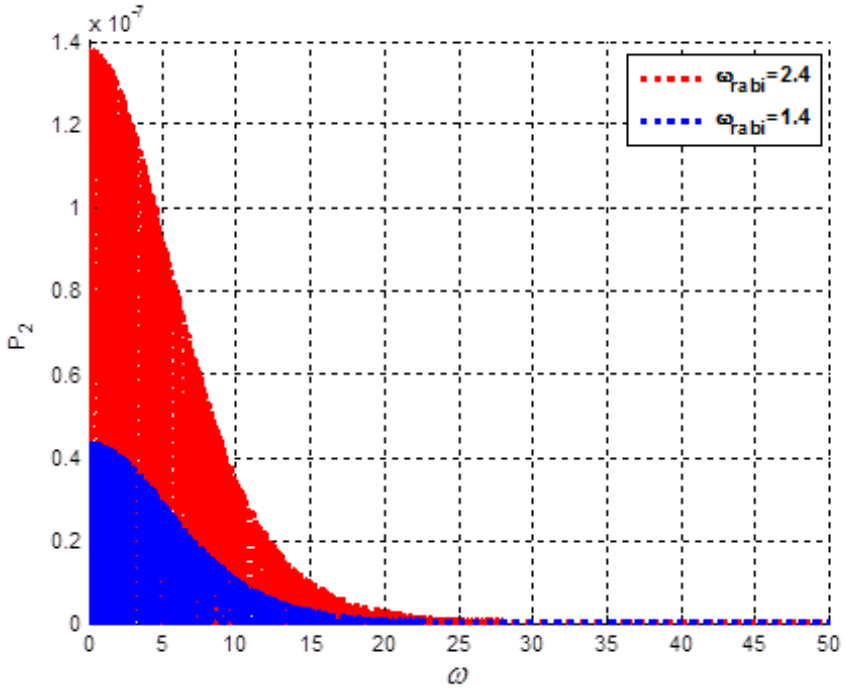

Figure 28. Probabilities of finding the coherently two-level of polariton in the excited state versus photon frequency ω for $g=1.6$.

Energy stands as the most important parameter in laser cooling and trapping phenomena. In Figure 29, we plotted the energy produced by a system of cooled ande trapped polariton against frequency. The results we obtained are similar to those observed in the previous section. The evolution of energy completely depends on the environment. Consequently, considering the case in which the effects of environment are taken into consideration in the system, the energy produced for weak interaction (Figure 29) is similar to that produced without coupling constant in terms of energy amplitude (Figure 30). However, energy is very sensitive to weak environment. Figure 30 shows that, in the absence of environment (g = 0), the amplitude of the energy is minimum. However, the energy increased because of environment effect. This result confirms an existence of transition probability due to environment. For both cases, the atomic particle (exciton) under laser light gains and loses energy. This implies that there is an absorption and emission of photon. This result clearly justifies the transition probability behavior. Previous work (Letokhov et al., 1976) has demonstrated cooling and trapping electron using laser techniques to increase the phase space density of particle beams in storage rings. Therefore, it become interesting to take a moment looking on numerical results for laser cooled and trapped polaritons and confined in magnetic field.

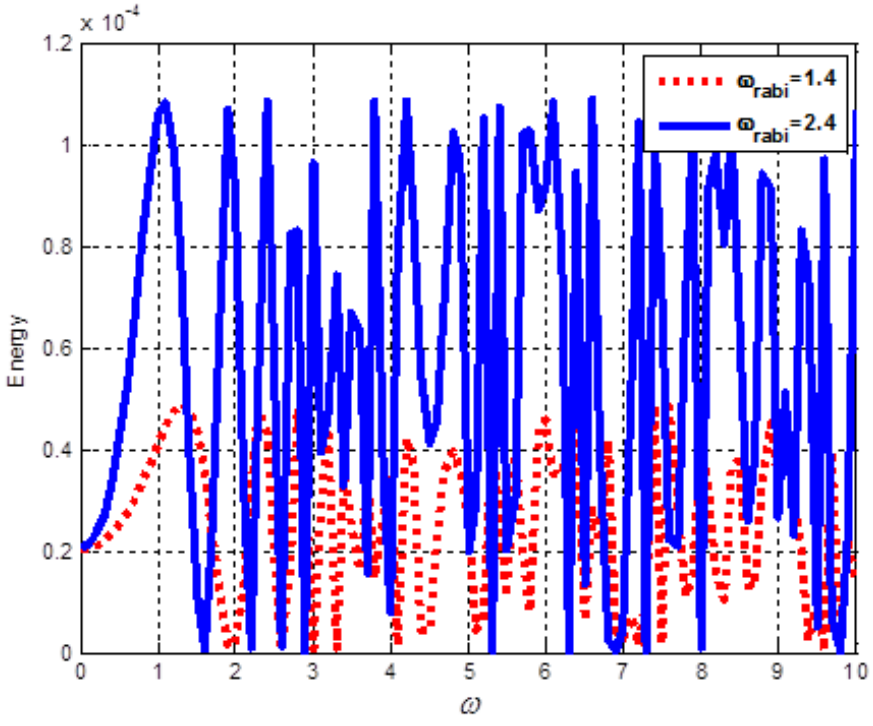

Figure 29. Energy representation of the system of cooled and trapped as a function of photon frequency ω at the limit of weak interaction $(g = 0.35)$.

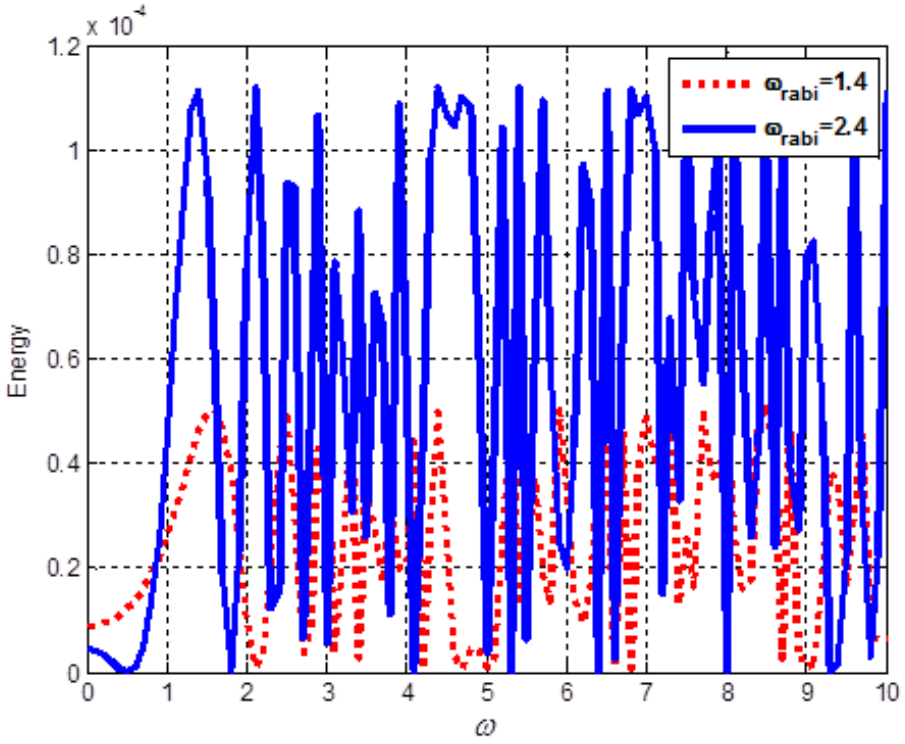

Figure 30. Energy representation of the system of cooled and trapped polariton for different frequency of photon ω and coupling constant $g = 0$

III.1.2. Laser cooling and trapping of polaritons with magnetic field

III.1.2.1. Force and torque

The importance to show variation of the force and its corresponding torque with several parameters of the system as presented in the figures below come from the fact that, force is a characteristic of motion that can be transferred. In this particular case, this force has as origin the interaction between the system of polariton, laser light which exchanges packet of discrete particles usually call photons and the magnetic field considered as a trap. The action of rotational force upon confined particles is perfectly characterized and measured. For the torque to be plotted, we again, as in the case of the force assume that $E_x^* = E_y$ and $E_y^* = -E_x$, yields $|E_{ox}| = |E_{oy}|$ and $|E_{ox}||E_{oy}|| = |E_{ox}|^2 = |E_{oy}|^2 = |E_0|^2$. In Figure 31 and Figure 32, one can perfectly observe how much the magnetic field, choosing here as the trap plays an important role in cooling and trapping phenomenon. It's well seen that, a previous cooled polariton trapped by a magnetic trap is subjected to an increasing force (Figure 31). In contrast, the torque decreases progressively and

tends to be stable at nearest zero point (Figure 32). Also, it is important to note that, either in case of the force or that of the torque, the curves vary considerably with coupling strength constant g proving how much its important to trap a polariton that has interacted with it surrounding environment at low coupling strength constant g. Anyway, the magnetic field added in the system of laser cooled and trapped polariton so as to trap it reduces progressively the effect of surrounding environment and therefore increase in similar way the force necessary to cool the system. As consequence, the torque reduces, meaning that the trap removes rotational tendency behaviour of particles.

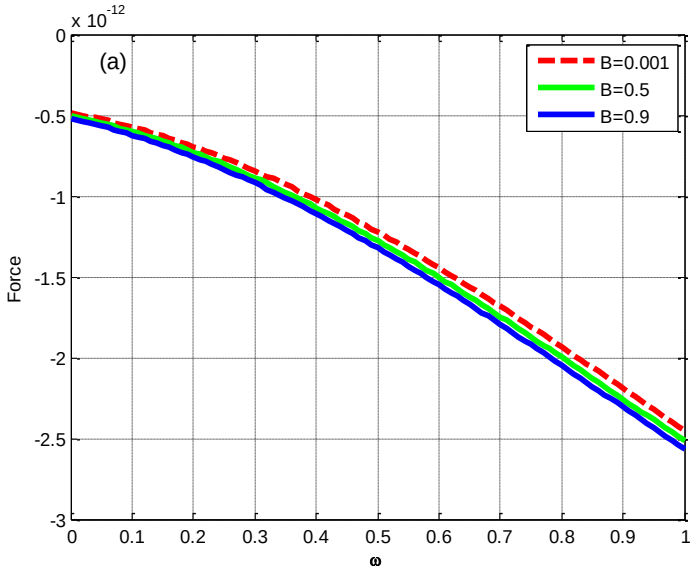

Figure 31. Graphical represention of the force versus Rabi frequency respectivley

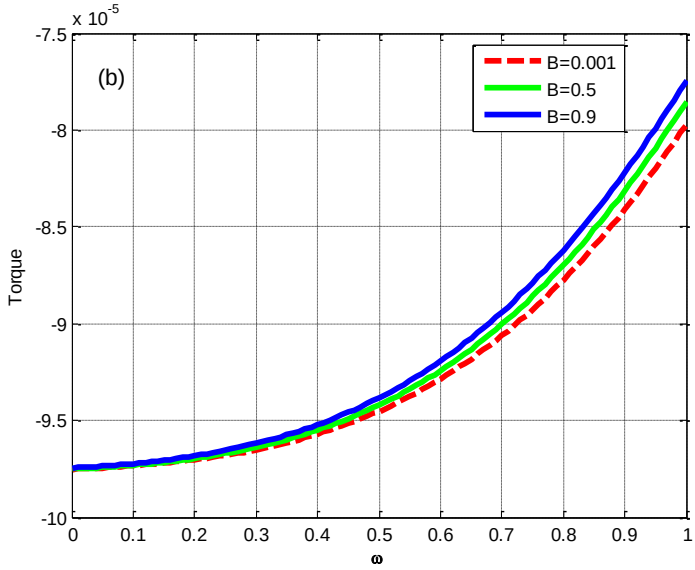

Figure 32. Graphical represention of the torque versus Rabi frequency respectivley

I.1.2.2. Transition probability and energy

The results above, which corresponds to graphical representation of both force and torque as a function of environment, shows how important it is to confined atomic entities, previously cooled and trapped with laser radiation. Here, we simulated the transition probability of finding the polariton in the excited state curve (Figure 33) for both low and strong interaction with surrounding environment, and that for the energy of the system (Figure 34), for some values of magnetic field B. As a fact, we consider the magnetic field frequency $\omega_B = \lambda\mu B$. Choosing the gyromagnetic factor $\lambda = 0.1$ and Bohr magneton $\mu = 0.5$. We then observed that, the probability of founding the system in the excited state has maximum value at the beginning of trapping process. This value of transition probability for the system to be found in the excited state start decreases progressively after a doorway value, $B = 4$, of the magnetic field and tend to collapse for high value magnetic field, $B \succ 20$. We may also see that the surrounding environment decreases the transition probability amplitude of founding the system of cooled polariton in the excited state. In the region $10 \leq B \leq 20$, the slope between the two curves is very weak. Thus, in this region of the magnetic field, the environment has similar effect in cooling and trapping process for both low and strong interaction with the laser cooled and trapped polariton. In addition, the polariton is trapped rapidly, i.e. is shuttles quickly from excited to ground state, in case of low interaction with surrounding environment.

In Figure 34, to investigate energy of the system of cooled and trapped polariton, we choose different types of frequencies in the system. When we compare both Figures 34 (a and b), we observe that when the interaction of the polariton with environment increases, the energy reduces considerably. This result confirms that the polariton under laser light gains energy. Figure 35a shows that surrounding environment reduces the effect of magnetic field in the system of cooled and trapped polariton. It's also found that, weak magnetic field is more appropriate in cooling and trapping processes. In Figure 35b instead, we observe that surrounding environment does not affect cooling and trapping polariton process for very low value of magnetic field ($B \prec 1$). This result confirms that the cooled polariton is well attracted and confines at bottom of the trap with much less perturbation to their internal structure and minimal heating from the surrounding environment.

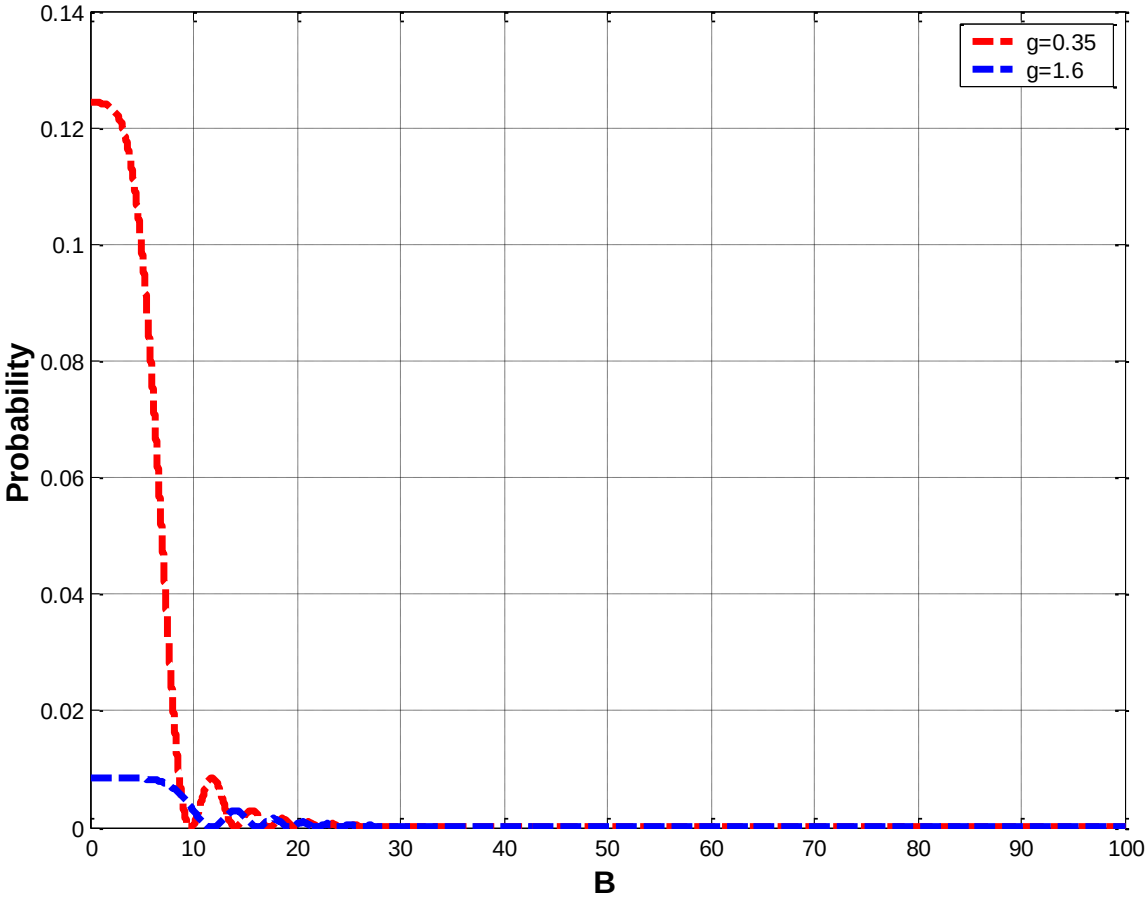

Figure 33. Graphical representation of transition probability versus magnetic field in both low ($g = 0.35$) and strong ($g = 1.6$) interaction with environment respectively.

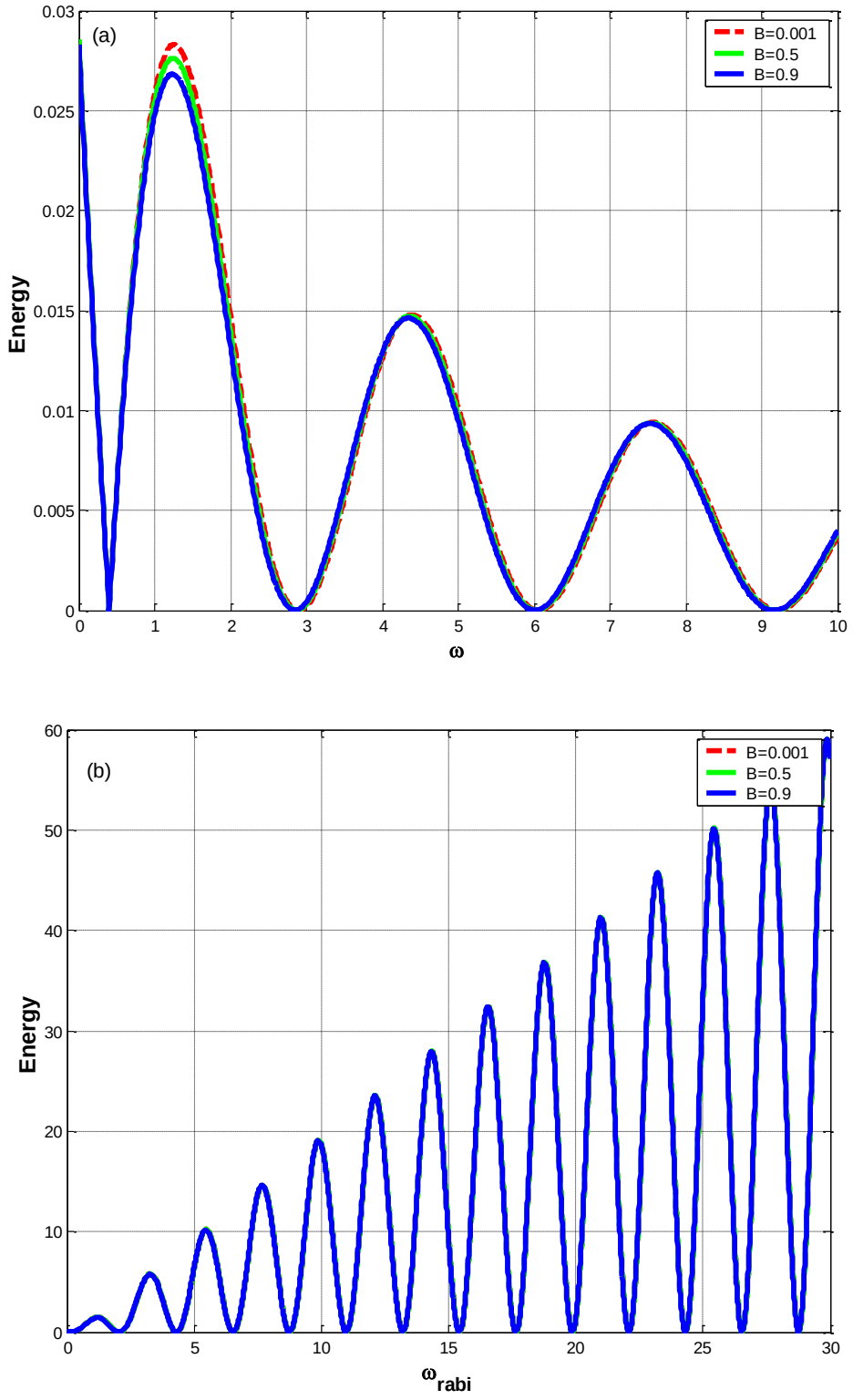

Figure 34. Graphical representation of laser cooled and trapped polariton. a and b: energy versus photon and Rabi frequencies for some values of magnetic field respectively.

III.1.2.3. Entropy

To bring insight to our discussions above, we plot in Figure 35 the Von Neumann entropy S against the induced photon's frequency (Figure 35a) and coupling strength constant g (Figure 35b). We recall to readers that the choice of this parameter has been debated in the previous chapter. Here again, we consider all parameters as addimensionless parameters. We can see that the entropy makes quasi-period oscillation. This means that the deformed field can help to realize and stabilize the degree of entanglement between the atom and the field at a high level. Sometimes (Figure 35b), for low values coupling strength constant (i.e. $g \prec 1$), the atom- field system becomes maximally entangled. We also plotted in Figure 36, the time evolution of the Von Neumann entropy for different values of coupling strength constant g. We observe that in Figure 36a, the entropy S suddenly increases for low values of the magnetic field B (a amount near its maximum value of 0.75) in case of low interaction with environment. In contrast, the rough evolution of the entropy S in case of strong coupling constant g (Figure 36a) is rather observed for high values of the magnetic field B. For various curves, we choose the magnetic field parameter, i.e. the gyromagnetic factor λ and the Bohr magneton μ to be $\lambda = 0.2$ and $\mu = 0.5$.

In the actual system, the atom is steady when it is in the ground state. However, when the atom is in the excited state, some factors such as the spontaneous emission, the collision between atoms and so on, will lead to the decay of the upper-level. In this case, the entropy S attains a stable behavior after some fluctuations at the beginning of the interaction [see Figure 35(a, b)]. As it's seen, the presence of the magnetic trap not only disappears the rapidly oscillations of S in the initial times, but also leads to a reduction of the amount of entanglement. The entanglement decays to the asymptotic value in both larger values of coupling strength constant and photon's frequency. So far, it's observes that, these figures [Figure 36 (a, b)] seems like those obtain by Dehghani et al. (2016), for graphical representation of time evolution of fidelity for a TLS. Bear in mind that entanglement between the atom and field is maximized i.e. the quantum state $\Psi(t)$ becomes maximally entangled, for low value coupling strength constant, its then comes that, the system become more entangled for low value of the fidelity.

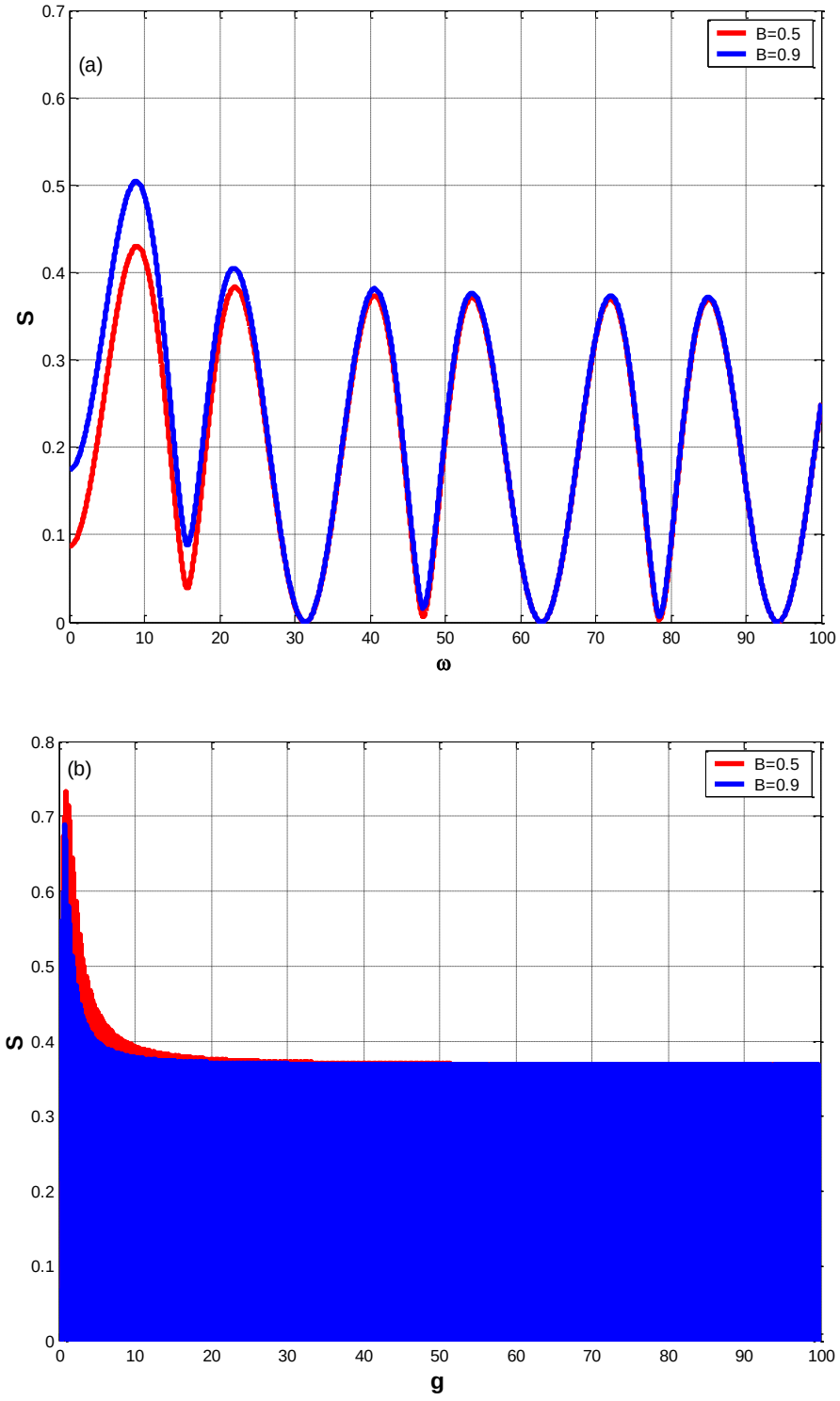

Figure 35. a. Graphical representation of entropy (Von Neumann entropy) in function of photon's frequency for some values of magnetic field B. b. Graphical representation of the entropy in function of coupling strength constant for some value of magnetic field B.

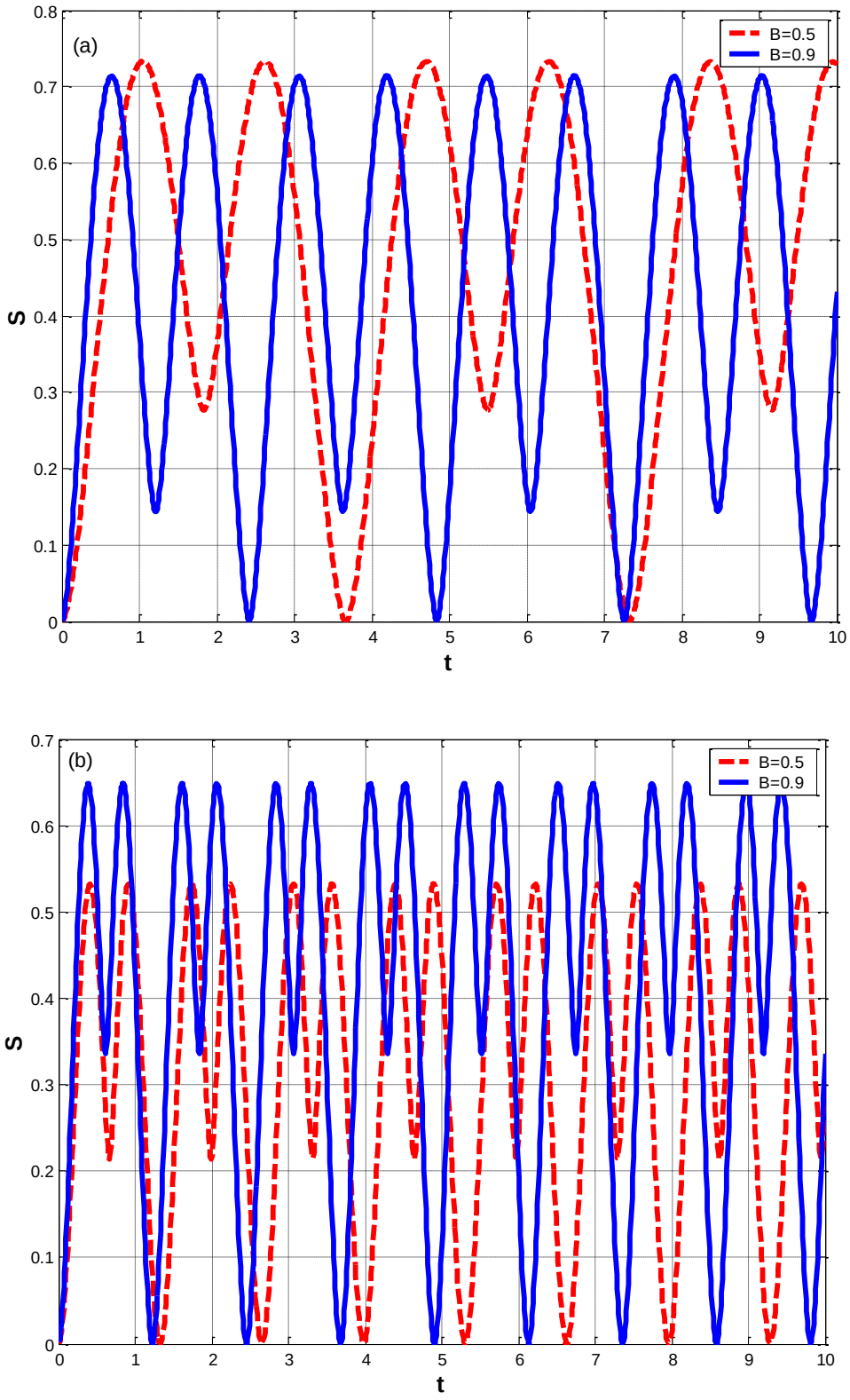

Figure 36. Time evolution of entropy (Von Neumann entropy) for some values of magnetic field B. a and b: case of low and strong interaction with the surrounding environment respectively. In each case, we choose $\lambda = 0.2$ and $\mu = 0.5$

Perharps, nomatter the results above, the entropy of the system (Figure 35) could not attempts the value of 0. Physical interpretation wich arises from such a result is that there still exist in the confinement physical phenomena and particularly collision between atomic entities. This means that the dynamic of the laser cooled and trapped polariton and confined in magnetic field which we considered as a trap, is still controlled by effect of surrounding environment. Due to the above results, we are kindly motivated to look for a more appropriate model which could allow perfect isolation of the system from surrounding environment in order to achieve coherent control of the state of laser cooled and trapped of polariton. A search which conducts to the formulation of LZ problem in laser cooling and trapping of polariton, thereby investigating LELs and transition probability in both diabatic and adiabatic basis. These parameters are numericamlly depicted in the next section in order to justify our hypothesis which consist on formulating LZ problem in laser cooling and trapping of polariton.

III.2. Transition between semiclassical and quantum mechanical theories in laser cooling and trapping of polariton

III.2.1. Landau energy levels

For LELs obtained from Hamiltonian Eq.120, i.e $E_{\pm}\left(t'\right)=\sqrt{\left(\upsilon t'\right)^2+\Delta^2}$, we start with the case of weak coupling ($g\sqrt{n}\prec\prec 1$) between the qubit and the cavity laser, where strong driving would requires a multi-crossing scenario (Figure 37c) as obtained from $g\sqrt{n}=0.1$. In some recent studies (Niemczyk et al., 2010 ; Forn-Diaz et al., 2010), the value $g\sqrt{n}=0.1$ has been identified as being in the ultra-strong-coupling regime in the Rabi model. However, for purposes of this study, this value of $g\sqrt{n}$ can be considered to lie in the weak-coupling regime. The qubit exhibits the characteristic LZS-Rabi oscillation when $g\sqrt{n}=0.1$which is in accordance with the result of Shevchenko et al. (2010). When the coupling between cavity laser and qubit increases [Figure 37 (a-b-c)], the number of pulse of energy decreases, thus strong coupling destroys the interference pattern. In other word, the polariton predicts the decoherence phenomenon. The increase of laser amplitude induces the multicrossing, and then, the cooling of polariton develops the crossings. The weak amplitude of laser alters the crossings and the behavior of the system follows adiabatically.

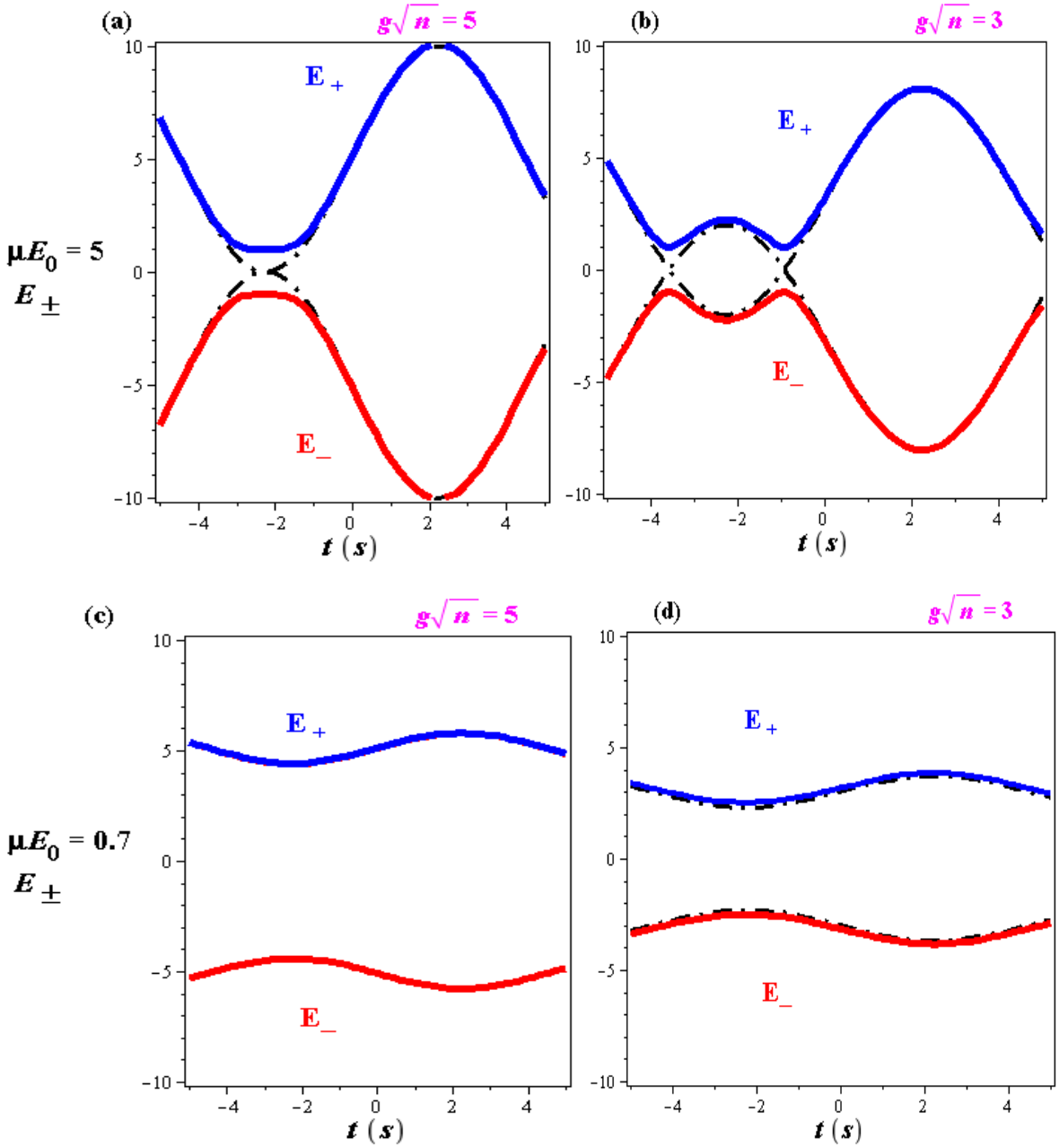

Figure 37. Eigenvalues of Hamiltonian versus time. The dashed black lines correspond to the diabatic transition and the solid blue and red lines are the adiabatic transition. (a)-(b) corresponds to the coupling $g=5$ and $g=3$respectively for strong amplitude of the laser field. (c)-(d) corresponds to the coupling $g=5$ and $g=3$, respectively for a weak amplitude of the laser field. The following parameter values have been chosen: $\Delta=2$ **and** $\omega_l=0.7$.

III.2.2. Transition probabilities

III.2.2.1. Transition probabilities in the diabatic basis

In Figure 39 and Figure 42 the diabatic and adiabatic tunneling probabilities, respectively, p_d and P_A, are plotted for different values of the amplitude of laser Ω/ω_l in both low regime $\left(g\sqrt{n}/\omega_l \prec\prec 1\right)$ and strong regime $\left(g\sqrt{n}/\omega_l \succ\succ 1\right)$ exciton-photon coupling strength. Doing it, we set $\Delta/\omega_l = 1$. In the first case, that is in Figure 39, in the field regime $\mu E_0/\omega_l = 2$, and in the domain $t\sqrt{\upsilon} \prec 0$, almost nothing happens and the ground-state is entirely populated. Around the crossing time $t\sqrt{\upsilon} = 0$, there is a sharp increase in population from a minimum value to a maximum value as the exciton-photon coupling increases. In the strong exciton-photon coupling regime ($g\sqrt{n}/\omega_l \succ\succ 1$), the interference phenomenon alters as it's depicted in Figure 39c (first panel of Figure 39), leading to a dramatic destruction of populations with consequence destruction of coherence state of the entire system. In addition, for the field regime $\mu E_0/\omega_l = 2.3$, as illustrated in the second panel of Figure 39, the coupling does not affect considerably the coherence state of the system, which looks more stable for low exciton-photon coupling. On the other hand, for very high value laser amplitude or very small laser frequency, i.e. by choosing $\mu E_0/\omega_l = 4$, the observed transition clearly exhibits long-period highly regular temporal oscillations through an avoided crossing. This is well shown in the third panel of Figure 39. These oscillations show significant laser frequency and exciton-photon coupling dependence. Despite this fact, there is a striking correlation between the confinement and changes in the population transfer from ground to excited state of the system.

The amplitude evolution of the tunneling probability that the qubit is in state $|\downarrow\rangle$ is depicted in Figure 40 for diabatic basis and Figure 43 for adiabatic basis. It is shown that at intermediate amplitude of the laser, the dynamics depends strongly on the qubit-cooling laser coupling strength $g\sqrt{n}/\omega_l$. By changing $g\sqrt{n}/\omega_l$, the LZ transition switches with a crossing shift at different position of Ω/ω_l. Thus, the LZ dynamics can be manipulated via the qubit-cooling laser coupling strength, at which the qubit levels cross during the above frequency variation in the field. As the amplitude of laser is adjusted (increases progressively at $\Omega/\omega_l = 2$ and $\Omega/\omega_l = 4$), the shifted crossing appear smoothly in such a way that high among of the population is cooled and trapped down; the whole system being transferred from ground to excited state at very strong cooling regime. In contrast, if the system is cooled and trapped down in an environment with whom it's interacts strongly $\left(g\sqrt{n}/\omega_l \succ\succ 1\right)$, important

modifications are observed leading to the splitting polariton states. Low $\left(\Omega/\omega_l = 2\right)$ to strong ($\Omega/\omega_l = 4$) critical amplitude of laser field is analyzed. Analyzing this situation in the adiabatic basis leads to an observation that, in general, higher trapping frequencies lead to larger probability for adiabatic transfer. This can be intuitively understood by imaging that very tight cooling forces the polariton state to overlap and thus increases the interference signal. Typically, the Landau-Zener-Stückelberg interferometry (LZSI) process is observable at the first panel of Figure 39(a) and Figure 42(a) with low exciton-photon coupling $\left(g\sqrt{n}/\omega_l = 0.2\right)$ and moderated amplitude of laser $\left(\mu E_0/\omega_l = 0.5\right)$.

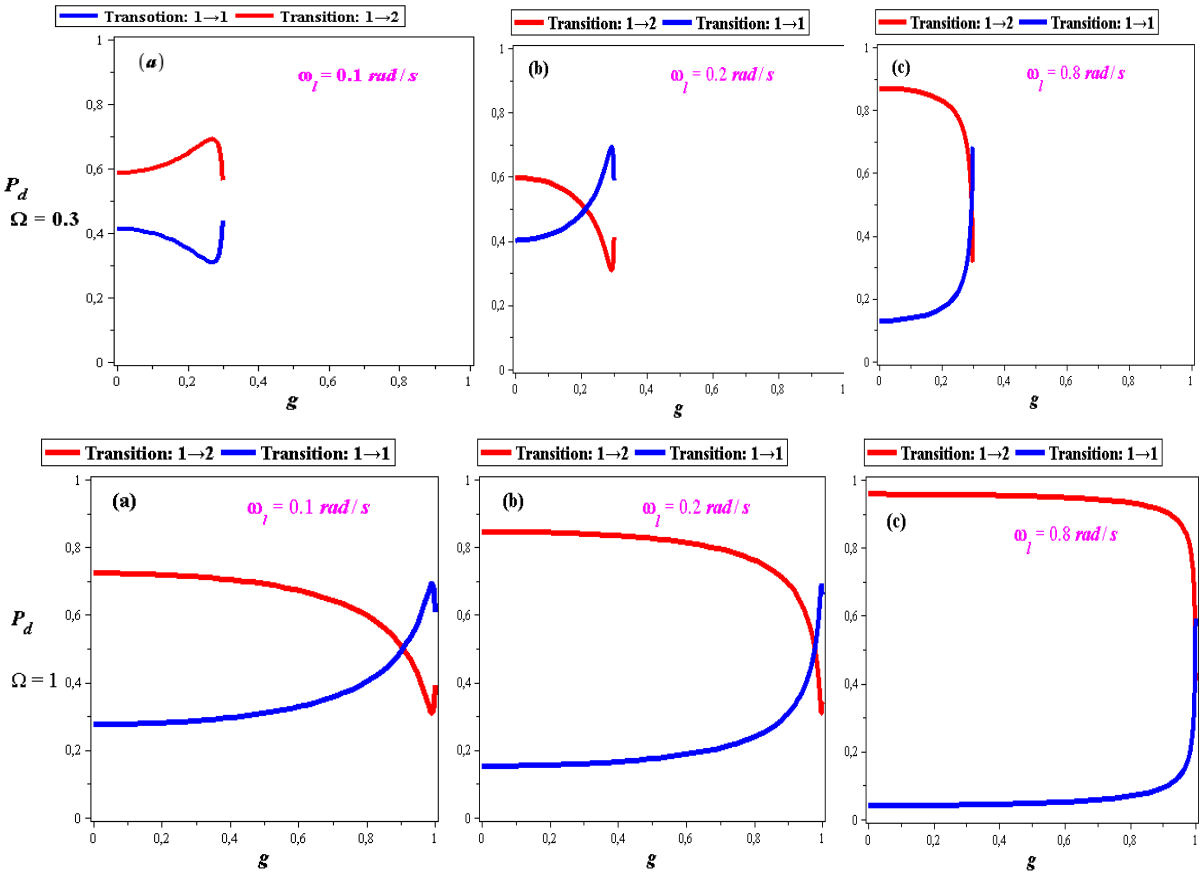

Figure 38. Graphical representation of Landau-Zener probability for the cooled and trapped polariton to be found in both ground and excited states in the diabatic basis for different values of laser frequencies : (a) $\omega_l = 0.1$, (b) $\omega_l = 0.2$ and (c) $\omega_l = 0.8$ for weak $\Omega = 0.3$ and strong $\Omega = 1$ amplitude of electric field, respectively at the upper and down panel. Here, the following parameter values have been chosen: $\Delta = 0.2$, $\sqrt{\upsilon}t = 0.5$ and $n = 1$.

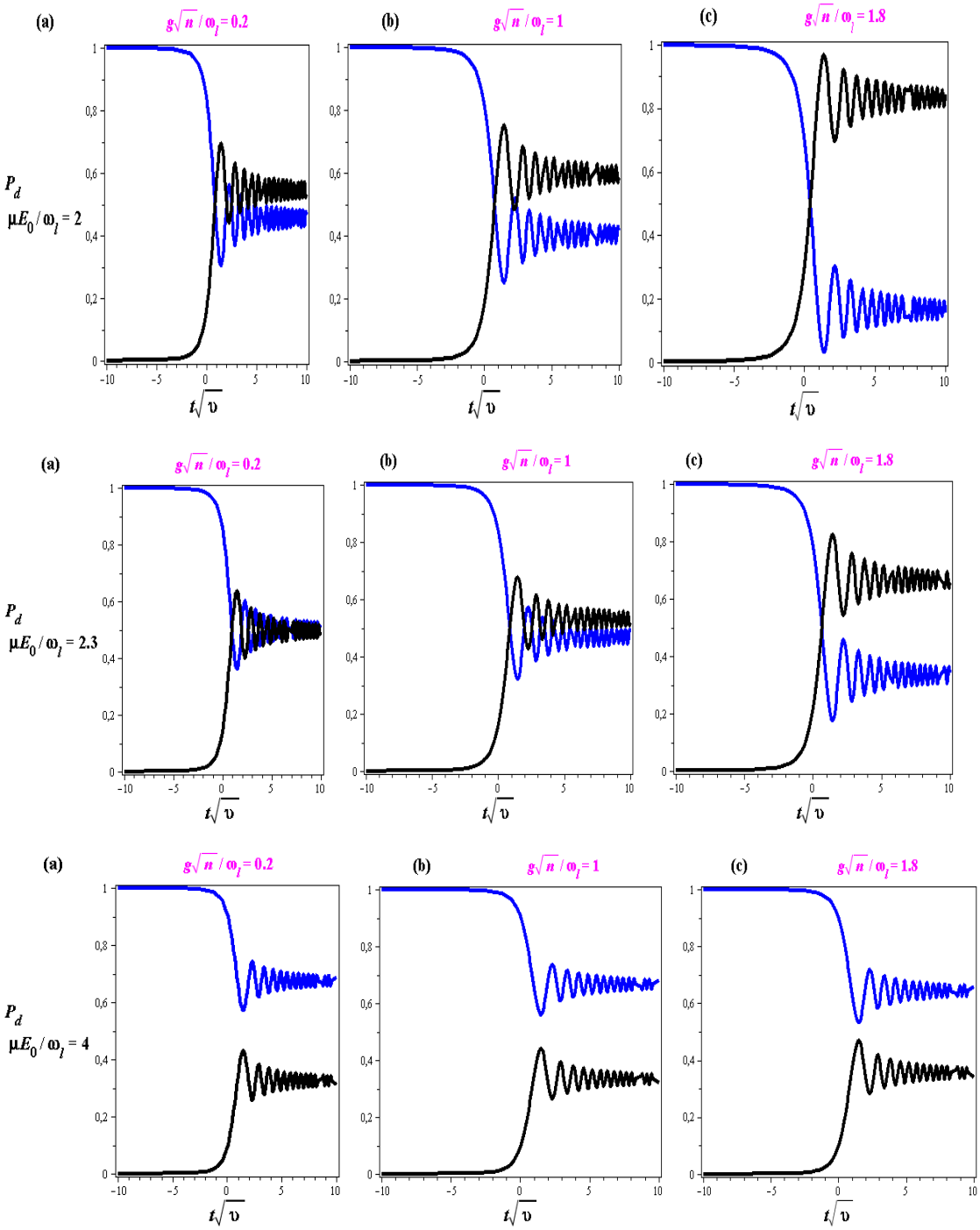

Figure 39. Landau-Zener dynamics in the diabatic basis as a function of time for different values of exciton-photon coupling: (a) $g\sqrt{n}/\omega_l = 0.2$, (b) $g\sqrt{n}/\omega_l = 1$ and (c) $g\sqrt{n}/\omega_l = 1.8$ at low ($\boldsymbol{\mu E_0/\omega_l = 0.2}$.), intermediate ($\boldsymbol{\mu E_0/\omega_l = 2.3}$.) and strong $(\mu E_0/\omega_l = 4)$ amplitude of laser field.. Here, the following parameter value has been chosen: $\Delta/\omega_l = 0.2$

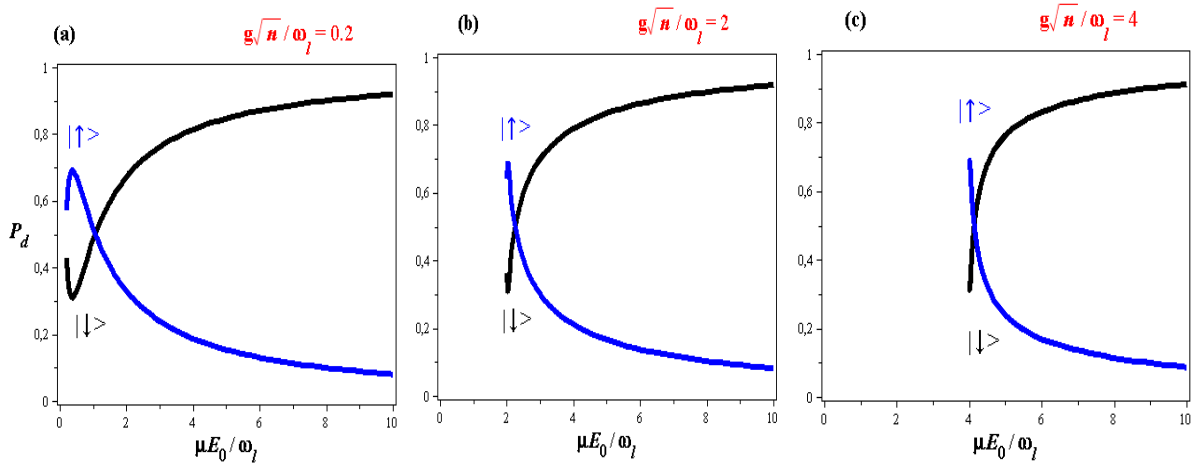

Figure 40. Landau-Zener dynamics in the diabatic basis as a function of the amplitude of laser field for a weak ($g\sqrt{n}/\omega_l = 0.2$) (a), intermediate ($g\sqrt{n}/\omega_l = 2$) (b) and strong ($g\sqrt{n}/\omega_l = 4$) (c). Here, the following parameter values have been chosen: $\Delta/\omega_l = 1$, $t\sqrt{\upsilon} = 0.5$.

II.2.2.2. Transition probability in the adiabatic basis

In Figure 41, the parameters of interest are amplitude of oscillations and laser frequency. The instantaneous transition probability of the upper/lower level as a function of coupling strength is observed at a different laser frequency condition, i.e at Weak $(\omega_l = 0.1 rad/s)$, intermediate $(\omega_l = 0.2 rad/s)$ and Strong $(\omega_l = 0.8 rad/s)$ laser frequencies and in both low $(\Omega = 0.3)$ and strong $(\Omega = 1)$ regime amplitude of oscillation. Collapse and revival of the amplitude of the oscillation between qubit states $|\uparrow\rangle$ and $|\downarrow\rangle$ induces LZ transitions. It is evident that the transition probability is strongly influenced by the avenue of the multi-crossing, which manifests itself as lower of the amplitude of oscillation, as it's depicted in first panel of Figure 41 [see Figure 41(a, b)]. As the laser frequency value increases, the multi-crossing phenomenon alters in Figure 41c (first panel of Figure 41). An important result here is that, the accumulated Stückelberg phases decrease with the laser frequency. In the strong regime of the amplitude of oscillation, as illustrated in the second panel of Figure 41, starting at the crossing point, the qubit state is swept by the laser field. After the LZ transition at the crossing point, the resulting superposition state of ground and excited state accumulates a phase. The qubit state is subsequently driven away from the crossing point and then returns to the starting flux position, i.e at the crossing point (see Figure 41a in the second panel of Figure 41). Such a period of qubit evolution refers to the

Mach-Zehnder (MZ) interferometer. The corresponding qubit transition probability induced by a periodic laser frequency, results in an equivalent optical cascade of MZ interferometer, with no crossing energy levels (Figure 41c of the second panel of Figure 41). The discussions above predict the effect of accumulated phase in the dynamical behavior of the complete system. Yield the coherent measurement of the state of the system.

In Figure 43 for instance, the subscript 'A' indicates the adiabatic basis. From Figure 39 and Figure 42, we see that both diabatic and adiabatic transition probabilities display similar shape before the crossing (anti) time. By varying the laser amplitude, that is by choosing $\mu E_0 / \omega_l = 2$ (firs panel of 42), $\mu E_0 / \omega_l = 2.3$ (second panel of Figure 42) and $\mu E_0 / \omega_l = 4$ (third panel of Figure 42) respectively, we arise at the same interpretation as it was in the case of diabatic basis. This means that the adiabatic transition probability strongly depends on both the exciton-photon coupling and laser frequency. The above discussions show that analysis of cooling and trapping of polariton using LZ theory in the case of diabatic basis is more appropriate in low exciton-photon coupling and in the regime of laser frequency $\mu E_0 / \omega_l = 2.3$. In general, the laser amplitude is properly adjusted to avoid the complete destruction of population of the system for both diabatic and adiabatic analysis.

The ground state polariton of the system changes adiabatically from the last panel of Figure 42, when $\mu E_0 / \omega_l = 4$ and $\Delta / \omega_l = 0.2$. However, the presence of overlapping polariton states can change the situation. If the polariton states are separated, the polariton eigenstates are free with no contribution from the LZS interference. It may be possible to control the ramp exciton-photon coupling to cross one of them diabatically, and the other adiabatically. However, for high exciton-photon coupling, $g\sqrt{n} / \omega_l = 1.8$, both polariton states are clearly broadened and it may no longer be possible to do it. Consequently, the LZ theory is applicable. The numerical results also reveal progress increase of population in excited state as the laser field increases. Hence, the total population found in the excited state is controlled by laser light. Thus, Figure 39 and Figure 42 nicely demonstrate how tight amplitude of laser effectively makes the LZSI wider.

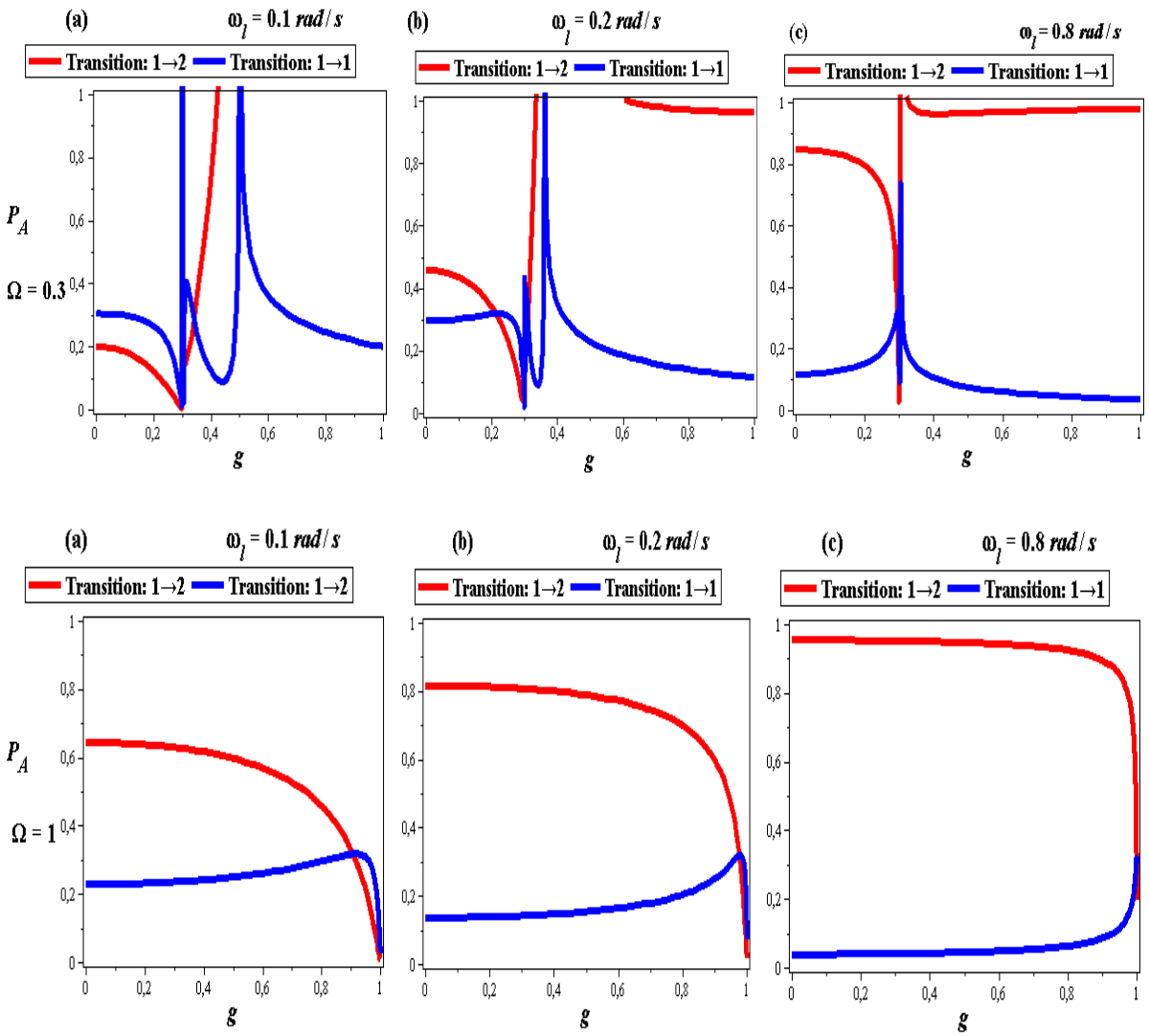

Figure 41. Transition probabilities versus coupling strength constant (g) in both Weak $(\omega_l = 0.1 rad/s)$, intermediate $(\omega_l = 0.2 rad/s)$ and Strong $(\omega_l = 0.8 rad/s)$ laser frequencies regime. Here, the following parameter values have been chosen: $\Delta / \omega_l = 2.3$.

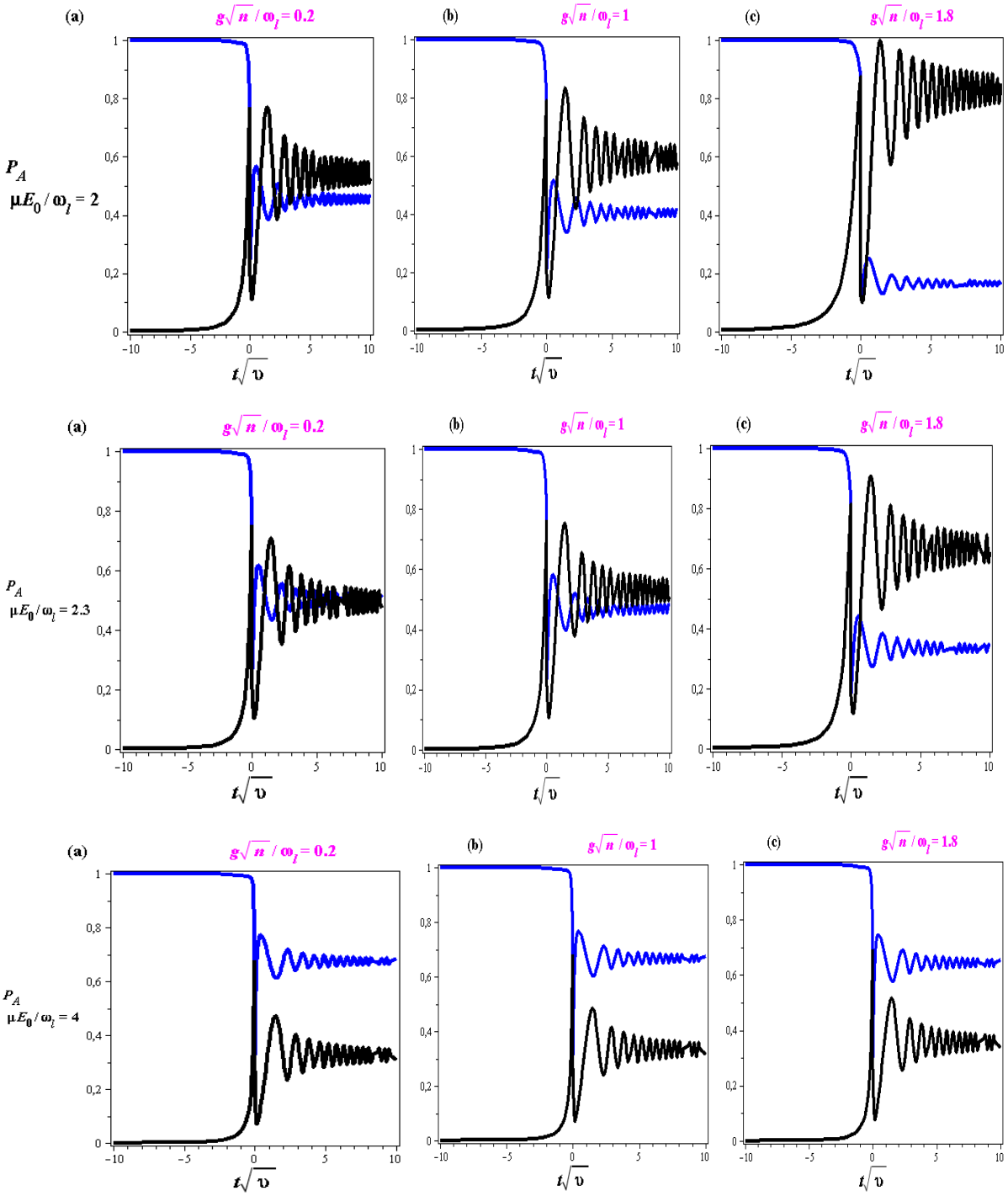

Figure 42. Landau-Zener dynamics in the adiabatic basis as a function of time for different values of exciton-photon coupling: (a) $g\sqrt{n}/\omega_l = 0.2$, (b) $g\sqrt{n}/\omega_l = 1$ and (c) $g\sqrt{n}/\omega_l = 1.8$ at low ($\boldsymbol{\mu E_0/\omega_l = 0.2}$.), intermediate ($\boldsymbol{\mu E_0/\omega_l = 2.3}$.) and strong ($\boldsymbol{\mu E_0/\omega_l = 4}$.) amplitude of laser field. Here, the following parameter value has been chosen: $\boldsymbol{\Delta/\omega_l = 0.2}$.

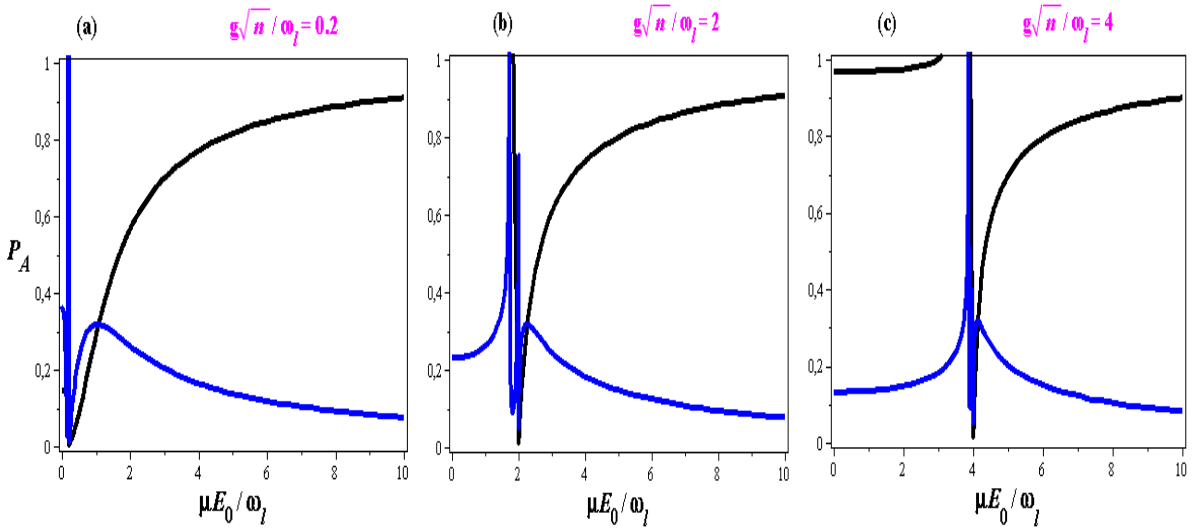

Figure 43. Landau-Zener dynamics in the adiabatic basis as a function of the amplitude of laser field for a weak ($\boldsymbol{g\sqrt{n}/\omega_l = 0.2}$ (a), intermediate ($\boldsymbol{g\sqrt{n}/\omega_l = 2}$) and strong ($g\sqrt{n}/\omega_l = 4$) (c) coupling. Here, the following parameter values have been chosen: $\Delta/\omega_l = 1$,

Moreover, since both states $|g\rangle$ and $|e\rangle$ contribute to the Stückelberg oscillations, it's possible to conclude at posteriori that for the qubit-oscillator coupling, a RWA is justified (Saito et al., 2006). In fact, all those graphical representations for LZS transition probabilities of the polariton in both diabatic and adiabatic basis indicate that the dynamic of the system consists of two transitions. In the specific regime with corresponding value laser frequency, as presented in the above discussions, the two transitions are essentially independent of each other. Therefore, one can investigate analytical expressions of same transition probabilities within the RWA. This means that, we pursued the main objective of the present thesis with another concise end precise mathematical approach thereby allowing arising to quantum error corrections requierement. This indicate that our theoretical formulation allow coherent control and precise measument. It is nice that the argument can be turned around, and from the same Hamiltonian Eq.61, we arize to the same dynamical behavior with the help of LZ theory is investigated. The present theoretical formulation provides an independent and simple method to determine LZ transition probabilities for a system of cooled and trapped polariton, taking into account the effect of surrounding environment in a particular regime (low or strong coupling). Due to its suitability, our formalism can then be used to investigate the effet of surrounding environment in the dynamic of laser cooled and trapped polariton.

III.3. Laser cooling and trapping of polariton in 2D transition metal dichalcogenides

Due to their physical properties including (i) their unique optoelectronic features in monolayer limit; (2i) their high oscillator strength; (3i) the fact that they are excellent platform for strong light-matter interaction and quantum confinement; (4i) the fact that they can be studied when embedded in optical microcavities and (5i) the flexibility of their band-gap energy, we found interesting the use of two dimensional (2D) transition metal dichalcogenides (TMDs) materials of MX_2 types as new playground for laser cooling and trapping of polariton. We suppose that the polariton results form a peculiar coupling between exciton and photons in 2D TMDs. Yields the necessity to investigate LELs of laser cooled and trapped of polariton in 2D TMDs materials and transition probabilities in both diabatic and adiabatic basis. The next section is devoted to present numerical results to bring insight on our philosophy.

III.3.1. Landau energy levels

For numerical purpose, we consider 2D TMDs materials of 2H types. These include: molybdenum disulfide (MoS_2), molybdenum diselenide ($MoSe_2$), tungsten disulfide (WS_2), and tungsten diselenide (WSe_2). The 2D TMDs parameters used are widely indicated in Table 2.

Table 2. Transition metal dichalcogenides parameter constants such as energy band gaps and interlayer Hopping integral.

2D Materials	MoS_2	WS_2	$MoSe_2$	WSe_2
$\Delta(eV)$	1.860	2.080	1.640	1.742
$\mathrm{T}(eV)$	1.137	1.436	0.951	1.233

In Figure 44, graphical representations of LELs are plotted without laser radiation in the system. The figures present crossing and avoided crossing of energy levels for two different values of the detuning between exciton and photon. For the control of dynamic state where $\Delta = \omega$, the level crossing can results in trivial dynamics at $\Omega = 0$ and when the photon frequency is twice that of the band gap value of the corresponding material. This is an

indication that, as $\Omega \neq 0$, the spatial crossing between interspin levels becomes spatial anticrossing.

Despite the difference observed between avoided crossings of energy levels, the figures present identical behavior each other's. This difference is based on the difference in the energy band gap within several materials. In the avoided crossing region, LELs present ground state energy level (red curves) and excited state energy level (blue curves). These features are signatures of the lower polariton (LP) and upper polariton (UP) quasiparticle eigenstates in the 2D microcavity. A result which is not surprising since it corresponds to the properties of microcavity polaritons as presented by Sanvitto and Kéna-Cohen (2016). The anti-crossing between LP and UP branches is the consequence of strong light matter coupling in 2D microcavity. Similar result has been reported by Anderson et al. (1995). Based on this assertion and following the analysis of Anderson et al. (1995), it's then comes that, such a behavior for LELs indicates that the 2D microcavity is populated with polaritons at room temperature (hot polaritons), in the regime dominated by coherent exchange between coherent on-chip light and matter excitations.

Figure 45 illustrates that LELs are modified due to cooling process in the system. The crossing (avoided crossing) points are shifted in front of the initial place of occurrence [compared on that of hoot polaritons (Figure 44)] with an important value displacement d which depends to the material type. The shift d in $MoSe_2$ is larger than in other 2D TMDs materials of our choice, i.e. MoS_2, WS_2 and WSe_2. The result illustrates hypersensitivity of the material $MoSe_2$ with laser. Physical interpretation of such a result is that, $MoSe_2$ is the more indicated 2D TMD material for cooling process.

In Figure 46, we depicted graphical representation of LELs versus laser frequency for particular values of coupling strength constant or vacuum Rabi frequency Λ. The values of $\Lambda \prec 1$ (considered here as low interaction) and $\Lambda \succ 1$ (strong interaction) are choosing. Result indicates the modification of LELs due to radiation field. In general, the plots in Figure 46 illustrate that the energy of the system increases with laser field. Moreover, the general state of the system is progressively condensate to zero temperature. Such a state of the system is the evidence that LELs are strongly influenced by the laser frequency ω_l, which conducts to a complete population transfer from excited state to ground state. The results are indications that one assists to the formation of the coherent state of the system due to cooling with laser. This is the proof that the internal structure of the cooled and trapped polariton is less

perturbed. Yield possibility for successful implementation of quantum computation and simulation devices using the resulted microcavity cooled polariton in 2D TMDs materials. In addition, the complete population transfer from excited state to ground state, thereby indicating that only the ground state becomes efficiently populated, means that nonlinear growth of the ground state is driven by Bose stimulation. A result which has also been revealed by Sanvitto and Kéna-Cohen (2016). Thus, in contrast to organic materials and wide-bandgap semiconductors whose do not seem to offer feasible road toward number of quantum polariton features, hybrid materials or monolayers TMDs offer fascinating possibility which consist to exploit defect states at the edge of dichalcogenide flakes (Liu et al., 2015).

Cooled and trapped polariton in microcavities 2D TMDs material found their applications not only in quantum computation and simulation devices implementation, but also in the realization of interferometers. In fact, in low regime polariton laser coupling, LELs are influenced by the avenue of multi-crossing scenarios, with consecutive LZ transition. This shows the possibility to investigate local interferometry application. Cooled and trapped polaritons in 2D TMDs are therefore candidate for interferometers fabrication. Figure 48 depicts the time dependent LELs for some values of laser frequency and in both low [fist panel of Figure 48, i.e. Figure 48(a, b)] and strong [second panel of Figure 48, i.e. Figure 48 (c, d)] coupling constant or vacuum Rabi frequency Λ.

Because we already argued that laser cooled and trapped polariton is more substantial in 2D $MoSe_2$, then we focus our investigations in Figure 47 only for this material. The figures [Figure 47 (a and b)] illustrate that the system undergo Rabi oscillations between ground and excited states. Such a phenomenon, in the quantum regime is an indication that the polariton condensate can be used as a quantum bit. In addition, the essential components of quantum computers, for instance, is the controlled NOT gate (CNOT) (Monroe et al., 1995). Therefore, laser cooled polariton in microcavities 2D TMDs material can readily undergoes large nonlinearities thereby opening up the possibility of realizing completely passive quantum gates (Sanvitto and Kéna-Cohen, 2016).

In general, the time-dependent LELs of laser cooled and trapped polariton for different values laser frequencies in low coupling regime are very different to that in strong coupling regime. Muti-crossing scenario is slightly influenced by laser frequency in low coupling regime. At strong coupling regime, Figure 47 (c, d) illustrates two different possibilities that correspond to diabatic from adiabatic transition between consecutive crossings, which is

expected due to LP and UP quasiparticle eigenstates in the 2D microcavity. Physically, the difference observed in both panel of Figure 47 [first panel (low regime) and second panel (strong regime)] is explained as a valley-sensitive cavity rate model due to coherent exchange and incoherent scattering. This confirms the presence of valleys zones namely K and K'. In addition, for a perfect coherent state of the system, the figure [Figure 47 (a, b)] indicates that it is of particular interest to investigate polariton condensate in 2D TMDs materials at low coupling with surrounding environment.

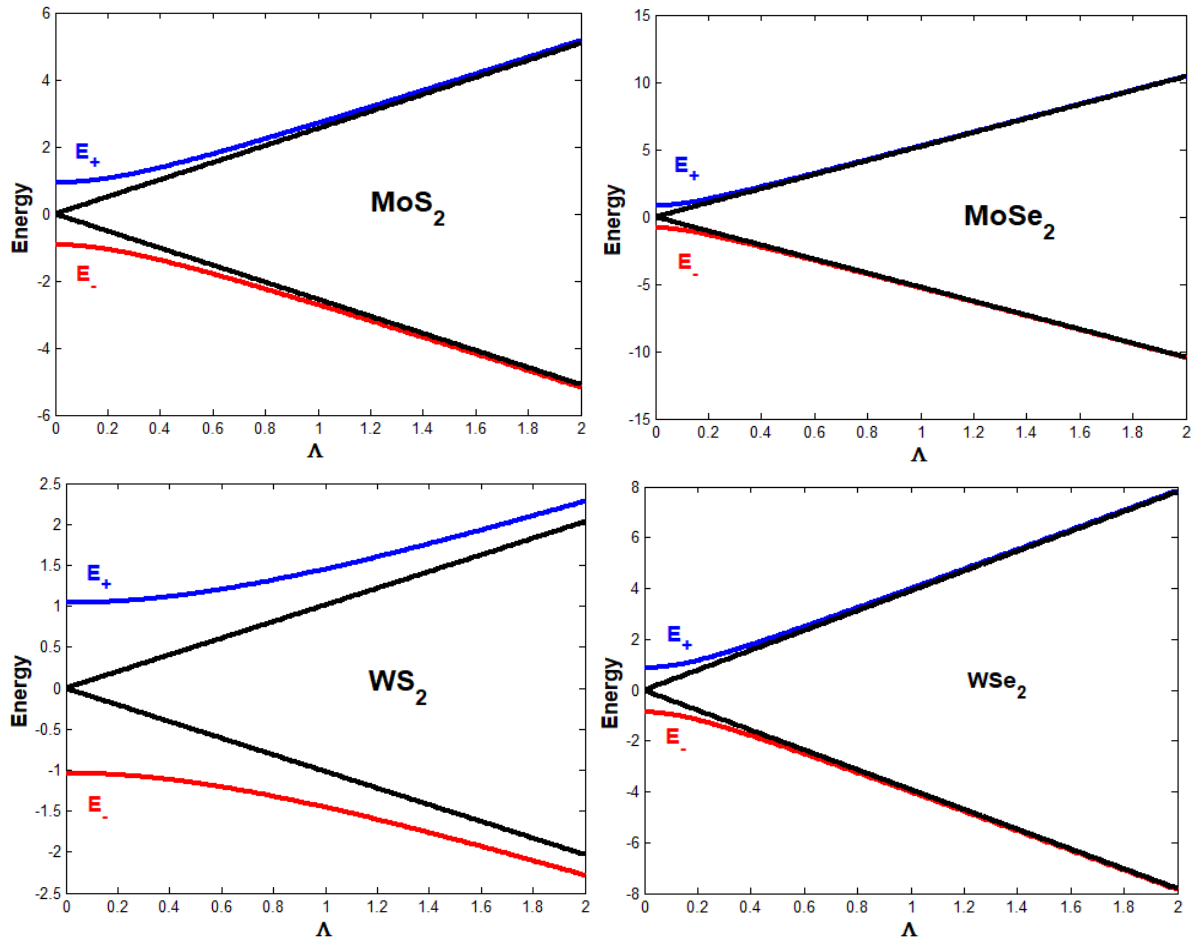

Figure 44. Graphical representation of LELs versus vacuum Rabi frequency Λ. Crossing and avoided crossing of energy levels are observed for $\omega = \Delta$ (resonance) and $\omega = 2\Delta$ respectively. These figures are plotted for $n = 30$. The crossed energy levels, solid black lines, correspond to the diabatic transitions; while the avoided crossed energy levels, the solid red and blue lines, indicate adiabatic transitions. The figure shows that, for a hot polariton, there is no important difference on LELs behavior for different surrounding environment. The figure well illustrates that for low value vacuum Rabi frequency, crossing and avoided crossing are perfectly distinguished; while for high value vacuum Rabi frequency, such a difference diminished and crossing and avoided crossing energy levels come more closer each other.

To go further, 2D map of LELs as a function of coupling strength constant between cavity photons and 2D TMDs bands with photon frequency is illustrated in Figure 49 for $MoSe_2$ 2D material. We identify two main regions with antibunching on the diagonal [blue coloration and yellow colloration)] and bunching on the anti-diagonal (green region). When we move away both below and above the green region, the brightness decreases considerably leading to complete destruction of yellow coloration thereby resulting to the red coloration observed above the anti-digonal. This means that the population of polariton condensates dramatically changes with radiation field in 2D TMDs embedded in 2D microcavity. At zero laser field, the upper valley (K) is highly populated. When laser field is applied, the population decreases in the upper valley (K) and increases in the opposite valley, i.e. the lower valley (K'). Thus, the contribution of laser light from the valley electric dipole moment results in an additional downshift of the population in the K' valley. The applied laser field induces unequal population transfer within the two valleys, yielding an augmentation of energy in the valley K', which is the origin of the fine structure observed in Figure 49. The bunching region on the anti-diagonal (green coloration) stands as the Brillouin zone or the equilibrium region. It's the interband between the K valley (blue coloration) and the K' valley (yellow til red colorations). In general, the curve of Figure 49 does not show the interference fringes, but the oscillatory bands describe the periodic phenomena which can induce the interference fringes. Another important issue based on the observation above, the antibunching behavior of polariton condensate in microcavities 2D TMDs which is a distinct signature of non-classical effects, corresponds to the measure of intensity correlations as a function of time delay. Based on the formulation of Shevchenco et al. (2010), the measurement reflects the coherence character of the states of polariton condensates in 2D TMDs microcavities. These distinguishable K and K' valleys due to population transfer from the excited to ground state of the polariton condensate in 2D TMDs material give access to valley-selective excitation and detection schemes and the outlook for optical valleytronics as indicated by Maragkou (2015). This study which permits to access and manipulate polariton condensates in 2D TMDs embedded in 2D microcavities allow us to understand the limit of the dynamics of the states of spin, the robustness of the spectroscopy of the information and the calibration of the states in the significant zones. The study also stands as a road toward probing others fundamental laser excitations in 2D TMDs materials and the interplay between cooled and trapped polariton particles.

As we move progressively from low to strong coupling regime, LELs crossing disappears in the same manner. This result confirms signature of quantum chaos in the system. Such a result has been debated by several authors like Prokof'ev and Stamp (2000) and Bose (1924). The result predicts the appearance of the butterfly effect in cooling and trapping of polariton process in 2D TMDs materials embedded in 2D microcavity. In contrast to the result of Einstein (1925), high among of avoided level crossing observed in WS_2 TMDs does not mean high energy LZ transition. This is not surprising since there is no universal definition of what one means by avoided crossing (Amo et al., 2009a). In general, crossing and avoided crossing of energy values can be understood in terms of time independent perturbation theory at the textbook level. Thus, energy levels have the tendency to avoid crossing in other to preserve the interference pattern and diverse from each other as the perturbed parameter varies. Figure 47 presents multi crossing of energy levels, with an accumulated phase for the system coupled in both low and strong regime coupling. An important point to note here is the double LZ transition accompanied with two avoided crossing points in the strong driven. Each avoided crossing point is equivalent to a "mirror" characterized by a transparency determined by LZ probability, leading to LZS interferometry. This interference result is a pronounced super-polariton cooling in the time evolution of the probability. Typically, interferometry process is amplified with laser frequencies, particularly matching in Figure 46. The left avoided crossing therefore splits the state into two half parts while the right crossing can either plays a role of another splitter or detects interference between transmitted (diabatic) and reflected (adiabatic) paths. Must favorable, as the LZS interferometry of the microwave dressed states is discussed in 2D TMDs, one can create and/or adjust the position and gap size of the avoided crossings as one desires. Generally, it is noticeable that, cooled and trapped polariton can leads to a broad range of phenomena related to BEC such as superfluidity (Amo et al., 2009a; Amo et al., 2009b), vortex formation (Byrnes et al., 2014) and the possibility to observe Berezinskii-Kosterlitz-Thouless and Barden-Cooper-Schrieffer physics (Carusotto and Ciuti, 2013).

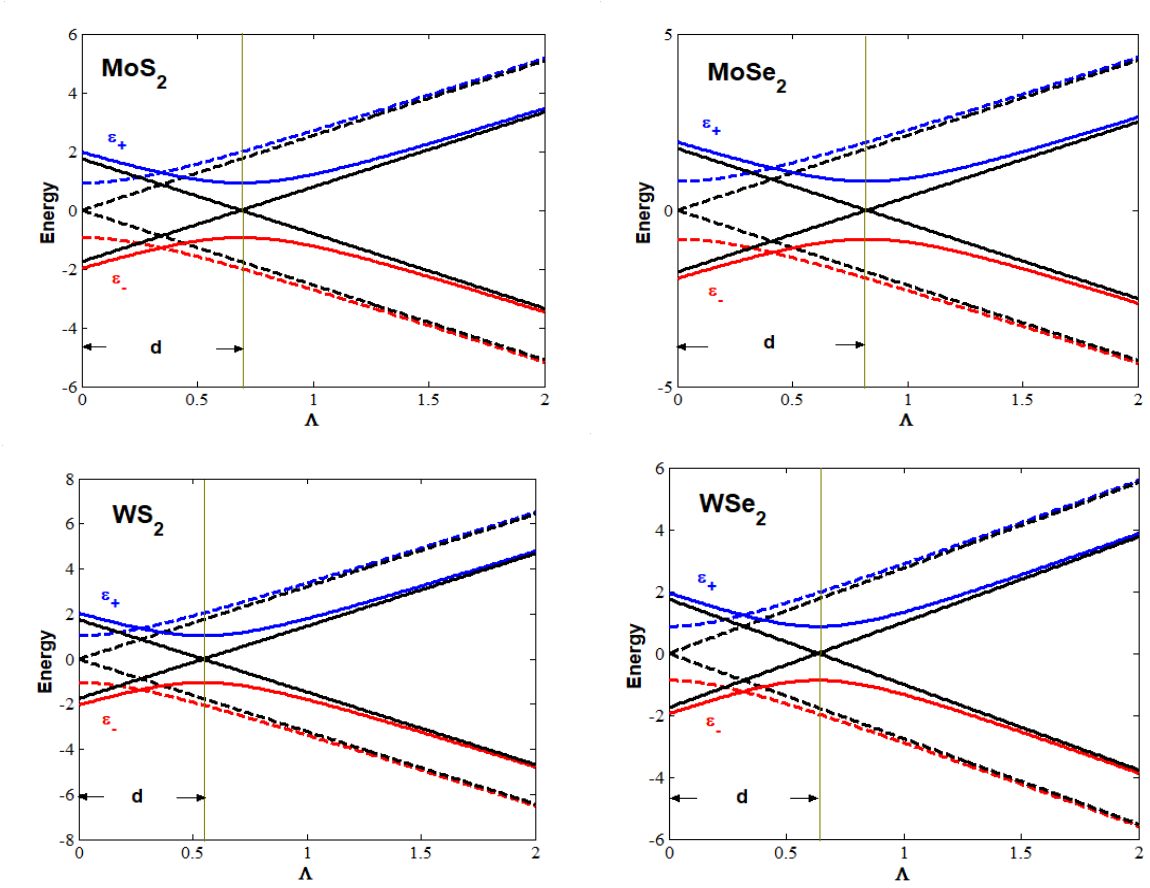

Figure 45. Graphical representation of energy versus vacuum Rabi frequency or coupling strength constant. The tick lines correspond to Landau energy levels of cooled poariton and the dashed lines are Landau energy levels of hoot polariton. The figures are plotted for corresponding band gap values of each transition metal dichalcogenide materials. Here, we choose $n = 5$.

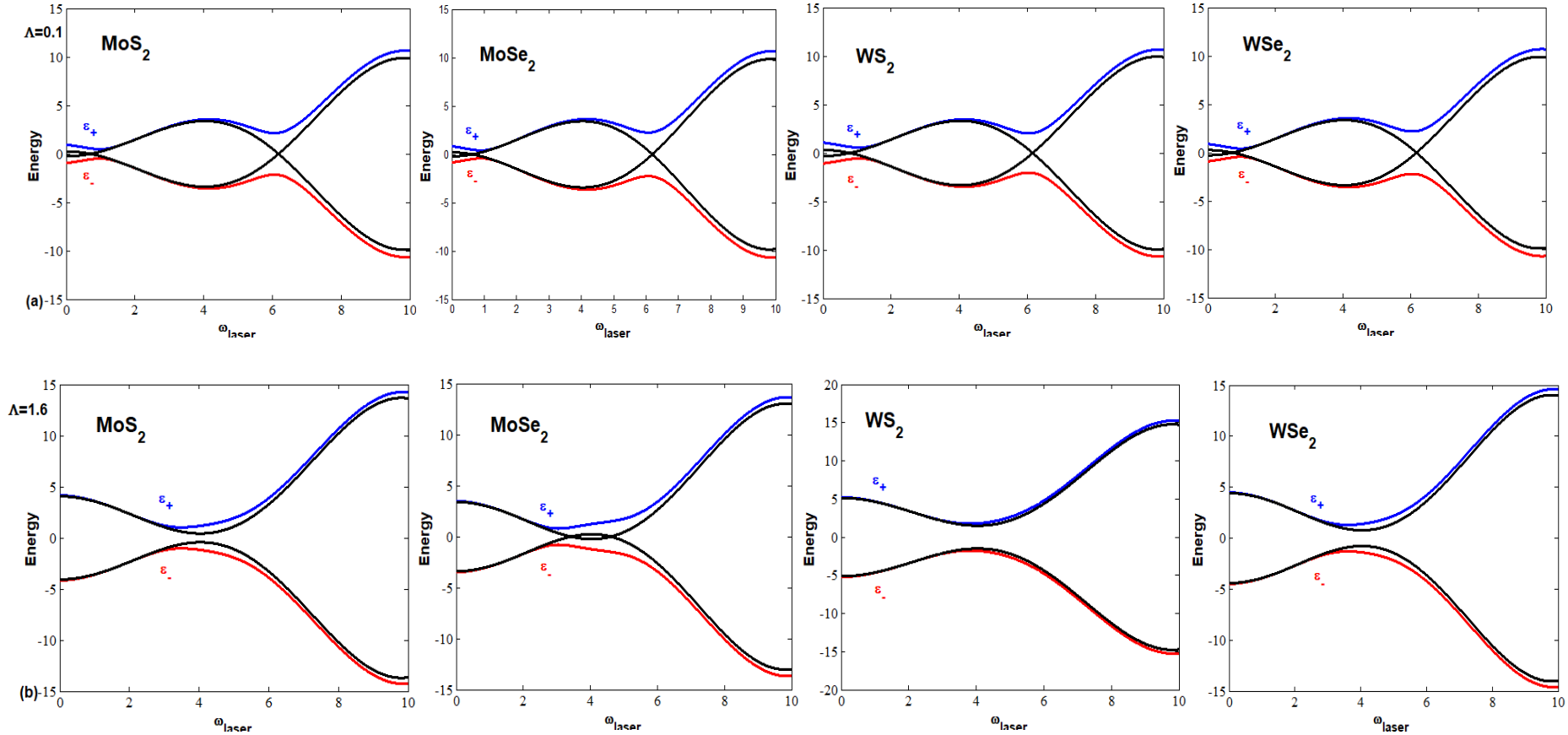

Figure 46. Graphical representation of LELs versus laser frequency for particular values of coupling strength constant or vacuum Rabi frequency Λ. The values of $\Lambda = 0.1$ corresponds to low interaction, while $\Lambda = 1.6$ corresponds to strong interaction.

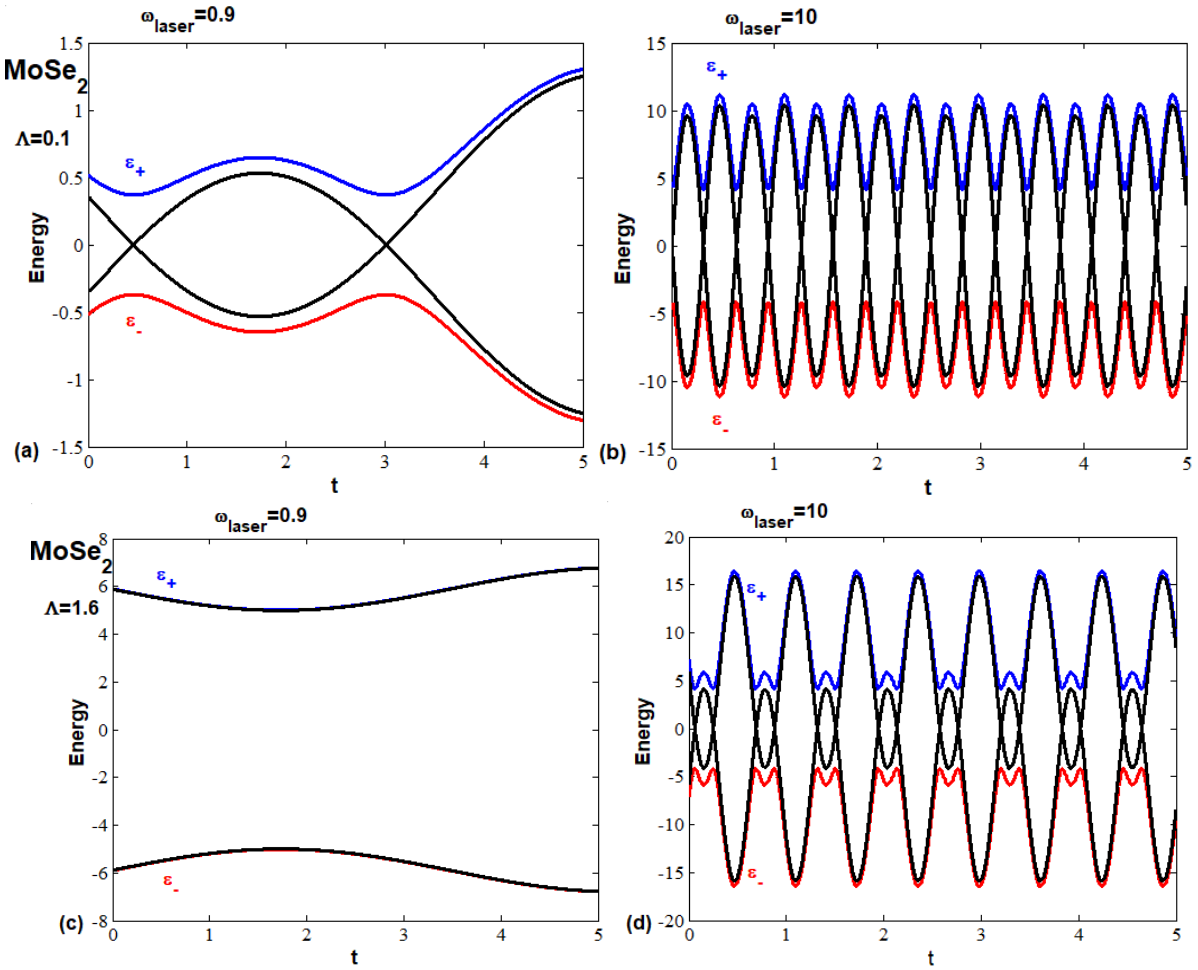

Figure 47. Graphical representation of energy as a function of time, for some values of laser frequency, for both low coupling regime (a, b) and strong regime (c, d). Here, the value of $n = 5$ is choose. For others parameters value such as the Hopfield integral and energy band gap (Hopfield, 1958) , we focus ourselves to the 2D material $MoSe_2$.

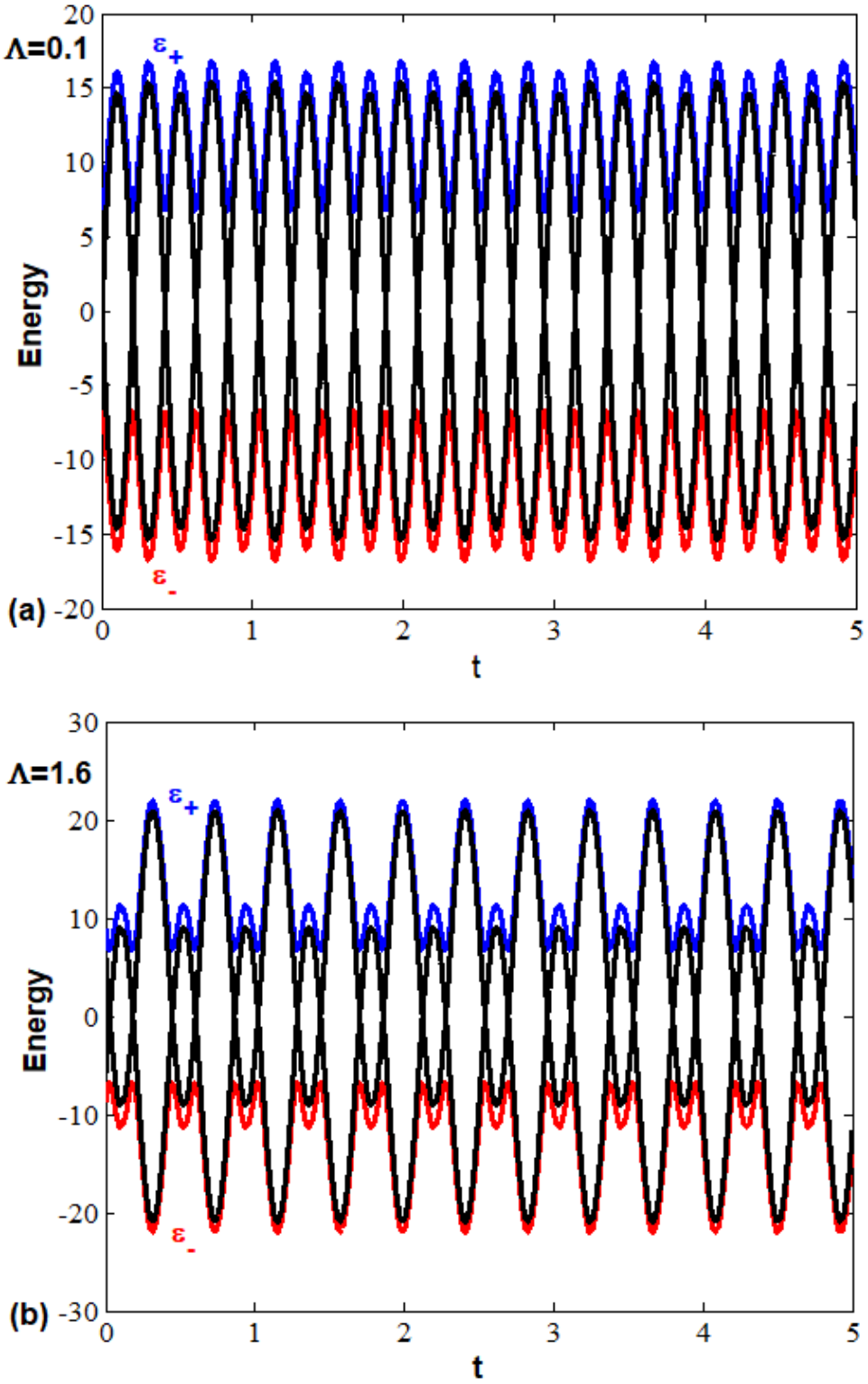

Figure 48. Graphical representation of energy as a function of time, for very important value of laser frequency $\omega_{laser} = 15$, for both low coupling regime (a) and strong regime (b). Here, the value of $n = 5$ is choose. For others parameters value such as the Hopfield integral and energy band gap, we focus ourselves to the 2D material $MoSe_2$.

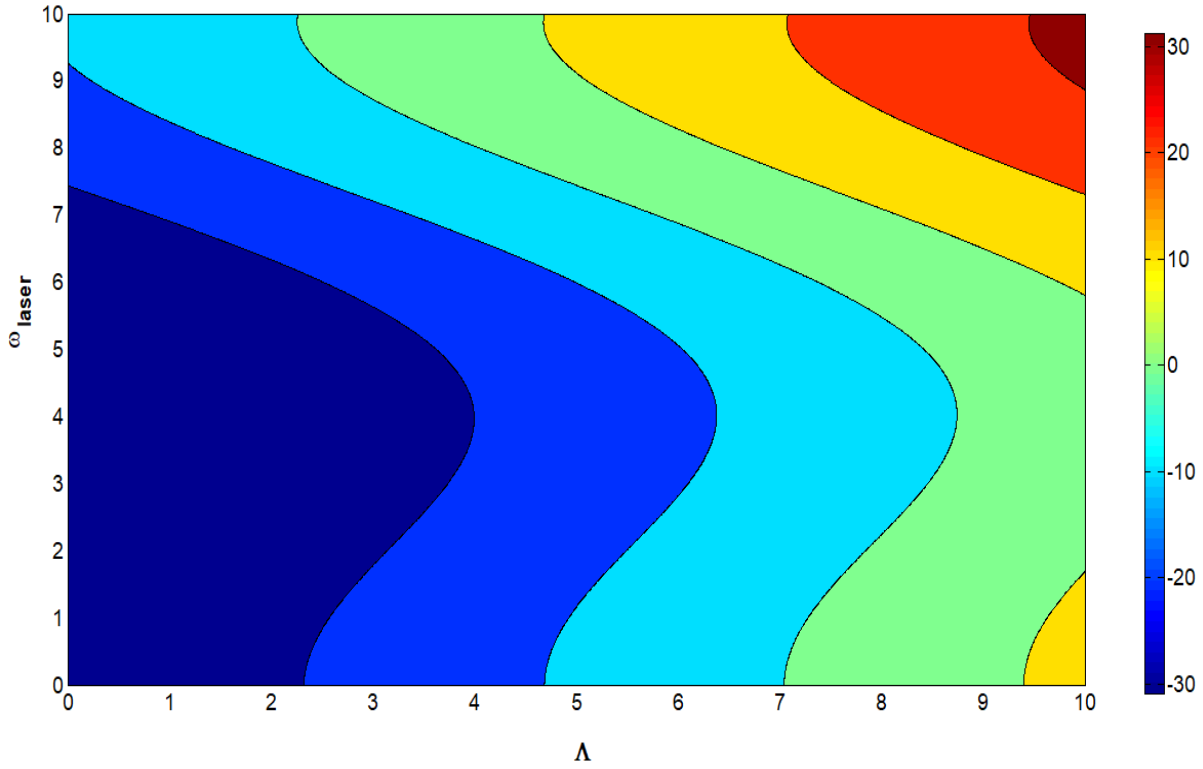

Figure 49. 2D map of LELs as a function of coupling strength constant (Λ)-and laser frequency.

This figure shows oscillatory bands describing periodic phenomena which can induce the interference fringes in 2D TMDs due to crossing (avoided crossing) of LELs. For any value of laser frequency and small value of coupling strength the LEL is low. On the contrary the LEL is strong for large coupling strength and strong laser frequency values. Both parameters present similar effects on the LELs. The colobar scale has the units of energy.

III.3.2. Transition probabilities

In Figure 50, we depicted graphical representation of transition probability versus coupling constant (Figure 50a) and versus laser frequency (Figure 50b). Figure 50a presents consistent modification of the transition probability that the system is been found in the excited state with laser light. The red line in the figure characterizes the transition probability for the hot polariton, that is the probability of the polaritonic system in TMDs $MoSe_2$ without laser light. The blue line for instance characterizes the transition probability of the polaritonic system in 2D $MoSe_2$ embedded in microcavity and cooled down to zero temperature with laser, in such a way that its form a polariton condensate.

As the laser light is introduced in the system, one assists therefore to a population transfer from excited state to ground state. This assertion is shown on the Figure 50a by a final transition probability which undergoes abrupt, nearly vertical jump down to $P_D = 0$ (red

curve) and up to $P_D = 1$(blue curve). In the former, the probability is varied to the minimum from the maximum value, indicating complete population transfer to the ground state. This means that all particles in the system are cooled down to zero temperature. As an important assumption based on this result, $MoSe_2$ is appropriate 2D TMDs material for optoelectronic and photonic devices construction.

Both transition probability curves cross with each other with certain symmetry. The symmetry observed means a reversible process. So, as the laser field is removed in the system, particles become again free and regain their mobility thereby jumping from ground to excited state progressively. Moreover, the figure shows that complete population transfer from excite to ground state and vice-versa is possible in 2D material $MoSe_2$ embedded in 2D microcavity at zero temperature, only at low coupling strength or vacuum Rabi frequency $(\Lambda = 0.1)$. This result confirms our hypothesis labeled in the above section of the present thesis that consist on investigating polariton condensate in 2D TMDs at low coupling strength or vacuum Rabi frequency.

In the adiabatic basis, we concentrated mostly on the transition probability for the polariton condensate. We then plot graphical representation of the polariton condensate in the adiabatic basis as a function of laser frequency. Such a consideration arises from the fact that Figure 50a allows us to get important features which arise from hot and cool polariton (Klembt et al., 2015; Keeling and Marchetti, 2017).

At this level of presentation, in order for readers to be more familiar to our theory, two essentials results are considered. Firstly, the performance of our theory does not modified within the effect of 2D material TMDs environment. For instance, almost all important physical mechanism observed out of 2D TMDs material are still observed in 2D TMDs materials milieu. This means that the 2D TMDs materials are appropriate candaites for the conservation of mathematical formalism. Secondly, within all 2D TMDs material of 2H-types, including (i) molybdenum disulfide (MoS_2), (2i) molybdenum diselenide ($MoSe_2$), (3i) tungsten disulfide (WS_2), and (4i) tungsten diselenide (WSe_2), material molybdenum diselenide ($MoSe_2$) is the best 2D TMD in the preservation of mathematical formalism with high precision. As consequence, material molybdenum diselenide ($MoSe_2$) is the most preferable 2D material to investigate laser cooling and trapping of polariton processes so as to acheve coherent control of the state of the system for practical applications and particularly quantum computers implementation.

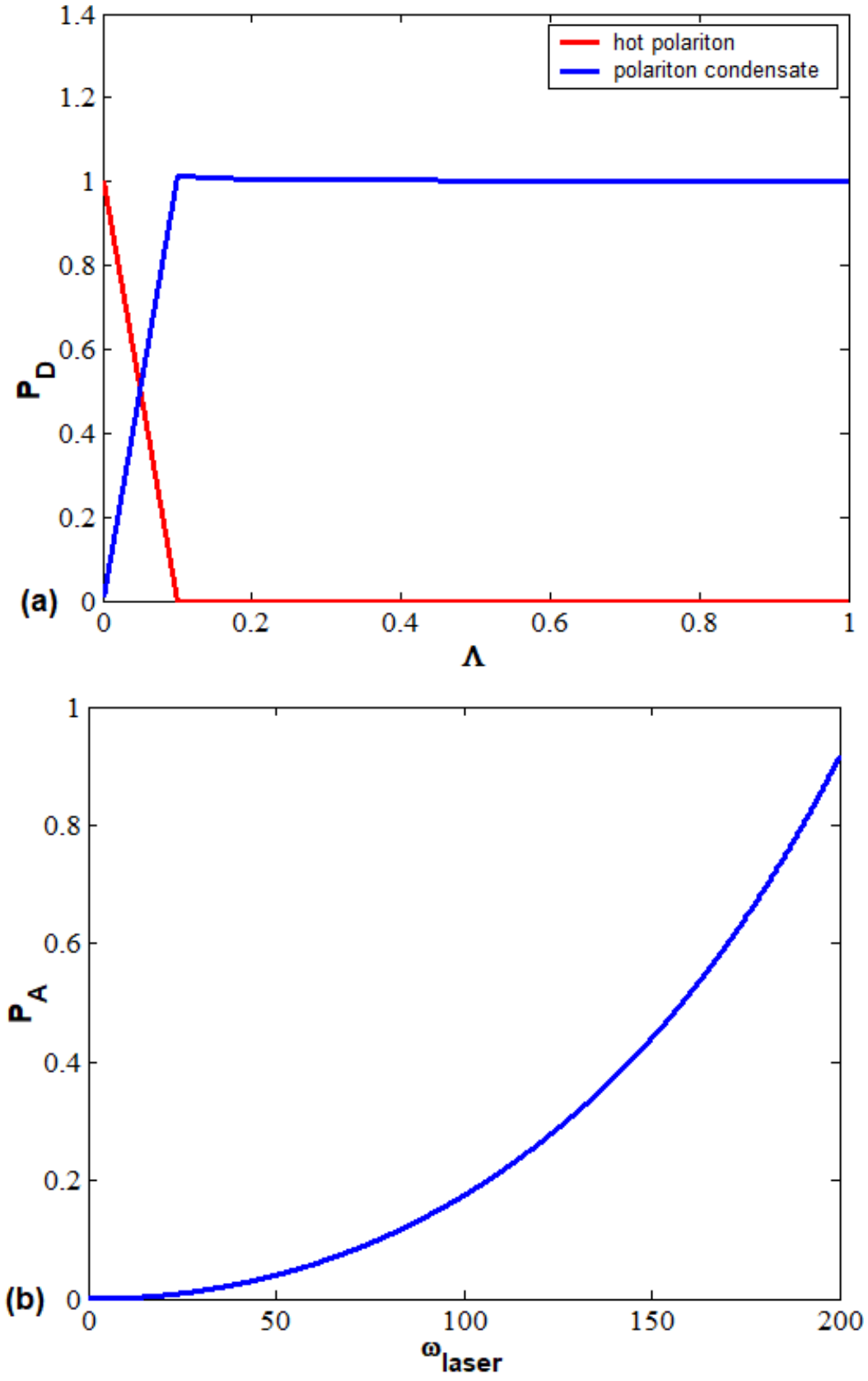

Figure 50. Graphical representation of transition probability versus vacuum Rabi frequency.

III.4. Laser cooling and trapping of polaron

The polaron problem has not yet been solved and continues to attract much attention despite the apparent simplicity of its formulation. It plays an important role in solid state physics, statistical mechanics and quantum field theory because it can be considered as the simplest example of a non-relativistic quantum particle interacting with a quantum field. Many sophisticated mathematical techniques have been tested for the first time using this problem as a model. A brilliant example of this is Feynman's functional integration method, which was first applied to the polaron problem, before becoming one of the main methods used in statistical mechanics and quantum field theory. In addition, the polaron theory is an expanding field of investigation in solid state physics because polarons are not only theoretical constructions but also practically observable physical objects (Devreese, 1976). More generally, electron-phonon interactions of Polaron-type play a very important role in the properties of small-scale quantum systems.

As we have mentioned already elsewhere in the present thesis, in quantum information science, the construction and manipulation of a qubit in nanostructures are two important subjects. Investigating those subjects is necessary and valuable not only to understand quantum mechanics but also to exploit additional information processing methods (Cuilan, 2013). For reminder, a single qubit can be realized by a TLS such as a spin-half particle or a two-level atom. We recall that it is very important for a quantum system to be well isolated from any environmental interaction which would destroy its states. However, quantum systems are very frail and the interaction of a quantum memory with its environment destroys the quantum coherence of the stored information. A phenomenon which is called decoherence. So a great deal of considerable efforts (Barnes, 1999 ; Tolkunov, 2004 ; Grodecka, 2006 ; Lovric, 2007) have been made to investigate the quantum decoherence and how to prolong decoherence time, in recent years for successful quantum computers implementation. Several schemes have been proposed for realizing quantum computer.

Motivated by the fact that (i) polaron can be considered as TLS, (2i) polaron is fermion which satisfied the Fermi-Dirac statistics and (3i) polariton becames intermediate particles due to laser cooling and trapping process thereby satisfying Fermi-Dirac statistics (nomatter being bosons) yields our interest to study these atomic entities using the same mathematical formalism applied to polariton. The objective being to investigate decoherence issues when embedded in a practical environment, i.e 2D TMDs for successful implementation of quantum computers.

For numerical considerations, we adjust the triangular quantum well potential in the system. Therefore, we suppose that the entire system is influenced by a triangular quantum well potential with constant electric field Σ and an infinite barrier F at $Z = 0$. We turned our attention to the energy of the system as its cooled and trapped with laser light. In general, for graphical representations, the $x-axis$ ranges within the values 0 and ∞. But in this thesis, we calibrate the $x-axis$ within the interval $[2;4]$ so that the curves could be more appreciated. In both graphical implementations, LLs are shifted and undergo diabatic and adiabatic transitions because of a quantum potential well in the limit of large magnetic field.

III.4.1. Laser cooling and trapping of polarons without magnetic field

Without cooling process, the system avoids magnetization since the magnetic and electric fields are linked by the relation $E = \frac{B}{c}$, given that c is the light velocity. Figure 51, which depicts graphical representation of LELs versus potential barrier F, presents a crossing of LELs at very low value potential barrier. This means that, the potential barrier dictate the dynamic behavior of the system of polariton. As the potential barrier incrases, energies levels avoid crossing.

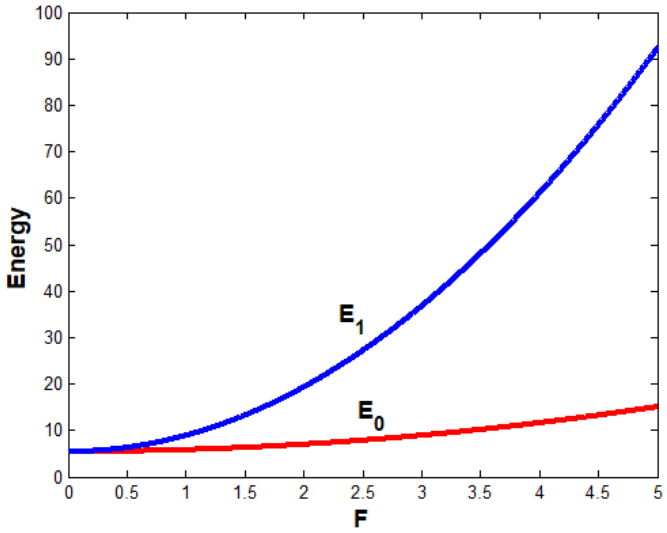

Figure 51. Graphical representation of energy levels versus potential field barrier F.

III.4.2. Laser cooling and trapping of polarons with magnetic field

In Figure 52, we depict LELs versus laser frequency for some values of laser amplitudes E and triangular quantum well potential barrier F .

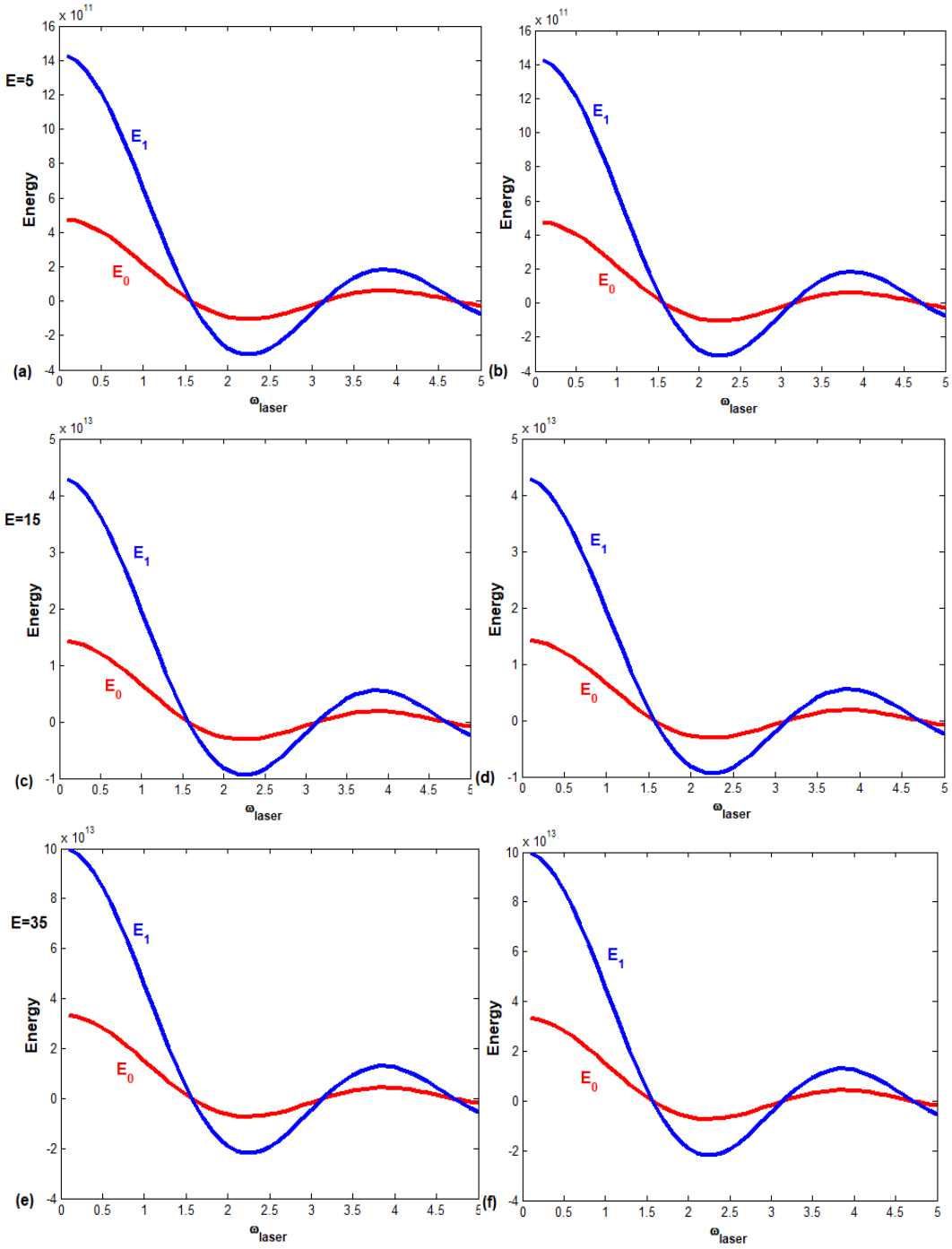

Figure 52. Graphical representation of Landau energy levels versus laser frequency for some values of triangular quantum well potential $F=15$ [Figure 49 (a,e,e)] and $F=25$ [Figure 49 (b,d,f)] and for some values laser amplitude $E=5$ (first panel of Figure 49), $E=15$ (second panel of Figure 49) and $E=35$ (Third panel of Figure 49).

In the first panel [Figure 52 (a,b)] the value of $E = 5$ of laser amplitude is choosed. In the second panel [Figure 52 (c,d)], we choosed the laser amplitude value of $E = 15$while in the third panel [Figure 52 (e, f)], the laser amplitude value of $E = 35$ is choosed. In all cases, the triangular potential barrier is choosing to be $F = 15$ [Figure 52 (a, c, e)] and $F = 25$ [Figure 52 (b, d, f)]. The figure well indicates crossing and avoided crossing of LELs. In presence of laser radiation and thus magnetic field, there is no consistent modification of energy of the system due to triangular quantum well potential. This means that, there is a modification of the state of the system with increasing values of F . In contrast, we observe few modification of the dynamic behavior of the system as the laser amplitude increases. In general, nomatter the introduction of triangular quantum well potential and low magnetic fields acting as traps in the system, no complete population transfer from excited state to ground state is observed. Therefore, the system still influenced by surrounding environnement.

III.5. Laser cooling and trapping of polarons in 2D transition metal dichalcogenides

2D TMDs (Chang and Chen, 2011) constitute a class of layered 2D material that has gained theoretical and experimental popularity since they constitute a perfect environment where bandgap energy of TLSs such as polarons can be studied. Thus, a variety of techniques have been proposed and include alteration of chemical composition (Yin et al., 2012), tailoring of the geometrical shapes of materials (Lee et al., 2012) and changing of lattice constant with mechanical stain (Shi et al., 2013; Lee et al., 2012). Most of polarons based studies have concentrated on electron transport properties. Among the properties requiring further investigations, attention is focused on the crucial aspect of electron-phonon coupling (EPC). Models of EPC have been proposed in 2D TMDs (Sakar and Pal, 2017). When a magnetic field is applied across the 2D TMDs monolayer, a nonlocal magneto-polaron is found and the effects related to the EPC increases.

Recently, LLs calculations based on the IWBT has conducted to the bandgap energy modulation in monolayer 2D TMD MoS_2 by engineering EPC in the presence of perpendicular magnetic field. In our group (Fobasso et al., 2019), we examined the possibility of controlling the dynamic of polaron in an asymmetric quantum dot using laser light in the presence of external magnetic field. Fundamental as well as first state energies investigations have shown that Landau energies are kindly influenced by laser parameters and particularly

laser frequency. In the present thesis, we joined both ideas to bring insight in laser cooling and trapping of polaron in 2D TMDs materials under the influence of a triangular quantum well potential. The main reason of introducing such a potential in our analysis is mentioned in the previous chapter. In addition, the considered polaron results from a peculiar coupling which emerges between electron and longitudinal optical (LO) phonons in monolayer 2D TMDs. The main reason which constitutes the center of interest of these changes is to investigate fundamentals (Fobasso et al., 2019) in a more practical and experimental environment thereby open door to possible new features for electronic and optoelectronic devices. In contrast to the modified Lee-Low Pines (LLP) method used (Fobasso et al., 2019), we perform 2D TMDs parameters analysis, that is LELs, using both QMSA and the IWBT.

III.5.1. Landau energy levels

We now present numerical results for the Landau energy of the magneto-polaron condensate in 2D TMDs under the influence of triangular quantum well potential using LELs specified in Eq.220. Physical aspects that gained our attention are: (i) effects of triangular quantum well potential on the magneto-polaron; (2i) effects of cooling and trapping due to laser radiation and magnetic trap respectively on the magneto-polaron under the influence of triangular quantum well potential. As we did in the case of polariton, for numerical implementations, we focus ourselves on monolayer 2D TMDs of $2H$ types (MoS_2, $MoSe_2$, WS_2 and WSe_2). The material parameters used are presented in Table 3 (Chen et al., 2018). We promptly replaced the light velocity c by the bare Fröhlich interaction c_z. We find this change more instructive in order to inspect a more realistic result. We choose a very small value of the imaginary time u $(u \to 0)$and large value cyclotron frequency Ω_c $(\Omega_c \to \infty)$. These approximations simplified our results and we do not find necessary to investigate analysis in a particular LO-phonons continuum, since the resulted expression of $\overline{\Delta(E_z)_n}$ is a constant either below or above LO-phonons continuum with a perfect choice of ω_{LO} at unit $\hbar$. It comes the final expression of LELs of magneto-polaron condensate in 2D TMDs materials under the influence of triangular quantum well potential Eq.230 below.

$$E_n = \left(n+\frac{1}{2}\right)\hbar\Omega_c + \Sigma - \frac{\hbar\Delta}{2} + F\left(\frac{2\mu F}{\hbar^2}\right)^{-\frac{1}{3}}\left[\frac{3\pi(4n-1)}{8}\right]^{\frac{2}{3}} + Const \qquad (230).$$

We then begin our discussions with a series of numerical results providing LELs versus triangular quantum well potential's parameter F (Figure 53 and Figure 54). In Figure 54, LELs are plotted versus triangular quantum well potential's parameter F for some arbitrary values of magnetic field B $\left(B=0.5; B=0.7; B=0.9\right)$. The energy diagrams reveals two distinct group of 2D materials including less and most influenced materials by triangular quantum well potential. The first one regroup MoS_2 and $MoSe_2$ [first and second panels of (Figure 54)] while the other consist of WS_2 and WSe_2 [third and fourth panels of (Figure 54)]. Clearly, the dynamical behavior of 2D WX materials is more affected within the surrounding effect of the triangular quantum well potential than that of MoX where $X=S_2, Se_2$. Indeed, in almost all cases, crossing disappears progressively to an avoided crossing profit with large magnetic field. The result indicates the appearance of quantum chaotic effect as has been mentioned by Prokof'ev and Stamp (2000) and Bose (1924) thereby predicting the appearance of butterfly effect, which is the popular embodiment of chaos theory as presented by Devane (2008). We predicted such a result also by studying cooling and trapping of polaritons in 2D TMDs in the previous sections LZS theory. Thus, one can expected that, in the presence of triangular quantum well potential, the magnetic field reacts on a polaronic system as similar as the laser affects a polaritonic system, both systems being embedded in 2D TMDs materials.

Hight among of avoided level crossing observed in $WX\,(X=S_2, Se_2)$ 2D TMDs materials predicts the preservation of the conserved magneto-polaron condensate. We interpreted this transition as the onset of dynamic where the influence of surrounding triangular potential well slows down the motion of electrons and eventually freeze the system. However, at the same time, our numerical simulations clearly reveal that the dynamic of the polaron in MoX is not modified enough in the presence of surrounding triangular quantum well potential. This implies that, in the presence of a triangular quantum well potential, it's preferable to study the dynamic of a polaron in 2D TMD $MoSe_2$ material. In order to address effect of laser on the system under the influence of triangular quantum well potential, we depicted LELs as a function of triangular quantum well potential's parameter F for some arbitrary values of laser amplitude E_0 (0.5, 1.5 and 3) (Figure 55). Doing it, we assumed that $\Omega_c=\dfrac{eB}{\mu}=\dfrac{eE_0}{\mu}\cos\left(\Omega_l t\right)$. As similar as in case of Figure 54, crossing and avoided crossing are observed, thereby induces diabatic and adiabatic transition, respectively. LELs increase

with triangular quantum well potential's parameter F . This result is a proof that the system is progressively cooled down to zero temperature.

There is a shift of LELs in 2D TMDs within the confinement well observed through the displacement of the crossing point, with value directly proportional to the laser amplitude. There is a shift in the energy in both $MoSe_2$, MoS_2 and WS_2 with laser field amplitude. The shift in WS_2 is larger than in $MoSe_2$ and MoS_2 , which indicates that the bare Fröhlich interaction in $MoSe_2$ and MoS_2 is larger than in WS_2 . In the third panel of Figure 54, the crossing point is completely disappears, resulting in complete destruction of the coherent state of the system. As an important result, it's come that laser cooling of polarons in 2D TMDs in the presence of magnetic field is more indicated with laser of low amplitude to expect the degeneracy point. Moreover, if we apply a triangular quantum well potential, then one has to consider the triangular quantum well potential of low confinement.

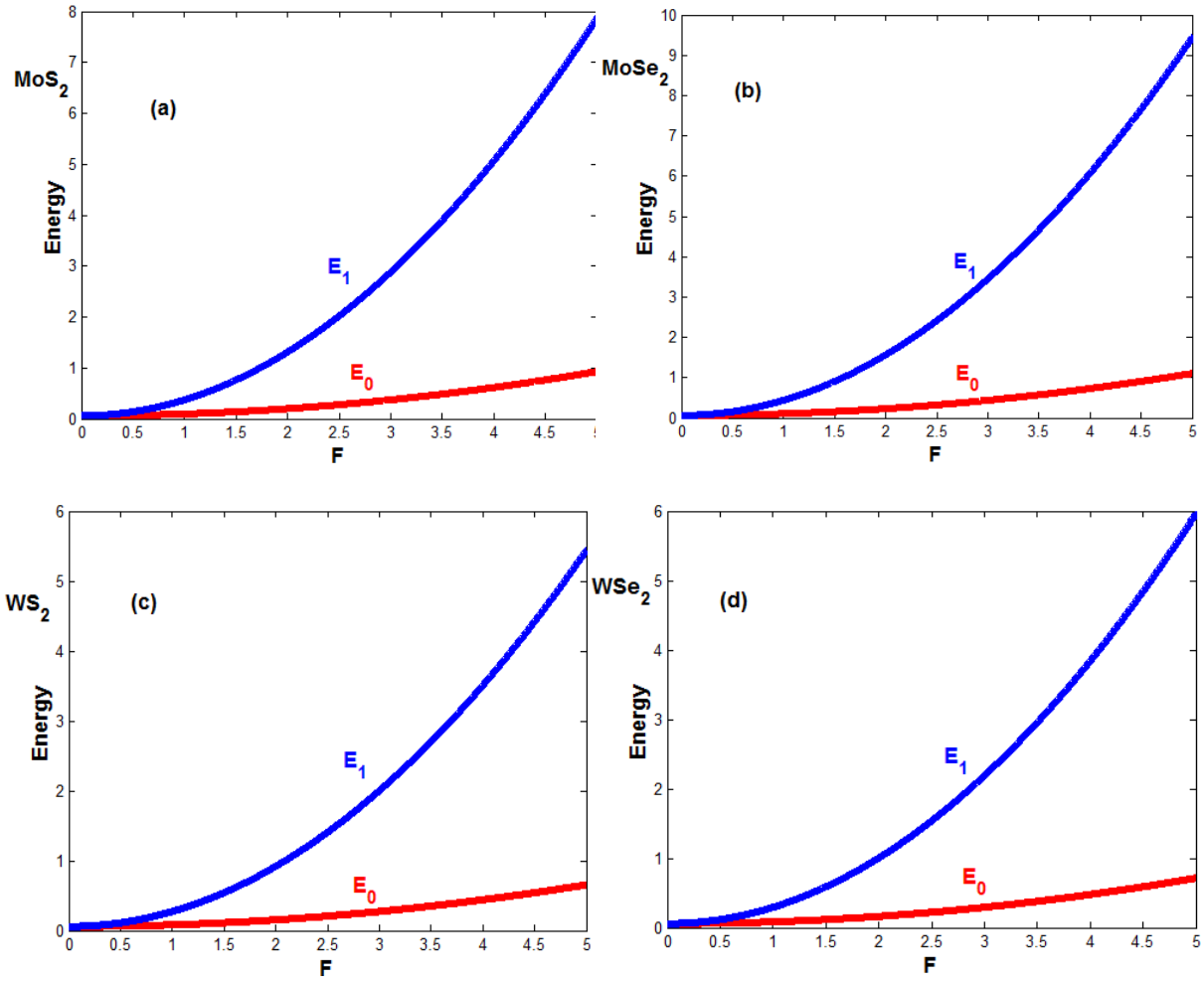

Figure 53. Graphical representation of Landau energy levels versus triangular quantum well's parameter F without the effect cooling process account.

In Figure 56 and Figure 57, the main features observed are as follow: (i) rapid stückelberg oscillations whose amplitudes diminish with laser frequency, yields interference phenomenon and possibilities to realize interferometers with such a system; (2i) energy levels suddenly decreases up to nearest zero value, when the laser frequency reaches the value of $\omega_{laser} = 0.7$; (3i) as the laser frequency increases (far from the value $\omega_{laser} = 0.7$), Stückelber oscillations approach a stable value close to zero. This is an indication that the system is completely cooled down. Thus, the population of the excited state (blue solid curve) is completely transferred to the ground state which becomes the cooled and trapped magneto-polaron. It follows that, for important value laser frequency, the sensitivity of the magneto-polaron under the influence of triangular quantum well potential decays significantly. Indeed, each absorbed photon causes recoil that reduces energy of the system without any modification of its physical characteristics. Thus, it is more suitable to carry cooling and trapping process with a critical value laser frequency.

As the triangular quantum well potential's parameter F increases, one assists to the destruction of the coherent state of the system. In fact, the figures (Figure 56 and Figure 57) well illustrate that, as the parameter F increases, excited state energy level shifts upward. This means that the probability that the system is found in the excited state increases. The physical interpretation which arises from this result is that, the entropy of the system increases interestingly. It then follows a sharp increase in population transfer from ground state to excited state. So, yield the alteration of interference patterns due to strong dephasing. Consequently, for extremely strong quantum well's parameter F, it becomes more difficult to control the dynamic of the magneto-polaron, no matter it's cooled down with laser.

For a better appreciation of the effect of laser on the system, LELs versus laser frequency are plotted for ground state $|g\rangle$ (Figure 58a) and excited state $|e\rangle$ (Figure 58b) energy levels. We use the same parameters values as in case of Figure 56 and Figure 57, except that now we adjusted the curves of all 2D TMDs of our choice in one figure for a particular state system. In both figures, i.e. in Figure 58a and Figure 58b, the coherence of the system's state is more appreciated within the material $MoSe_2$. This indicates once more hypersensitivity of the system with laser. Thus, as similar as the case of polaritonic system, 2D TMD material $MoSe_2$ is the more appropriate 2D TMD environment to form polaron condensate with laser. Therefore, either for polaritonic or polaronic system, laser cooling and trapping phenomenon is more appreciable if the system is embedded in 2D TMD $MoSe_2$.

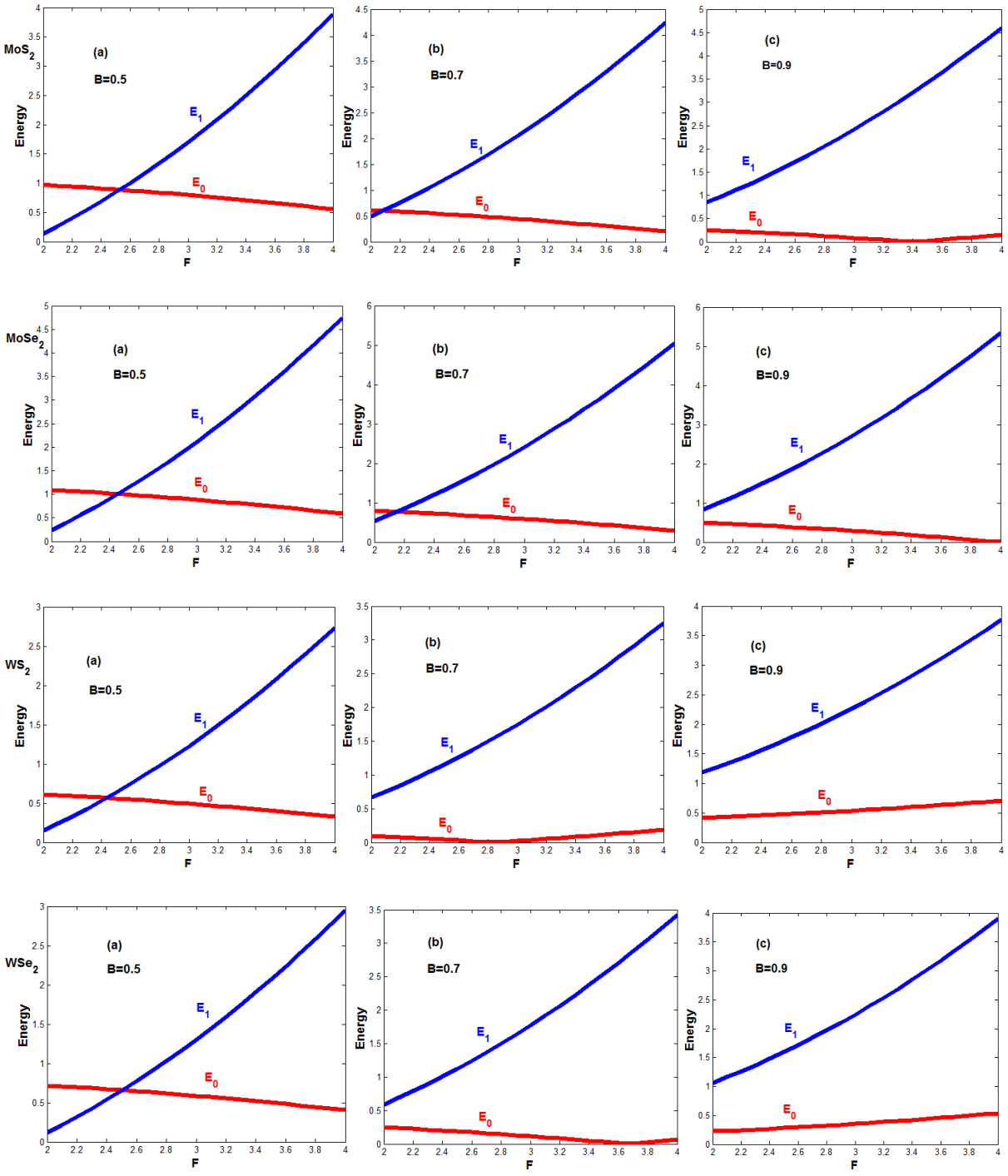

Figure 54. Graphical representations of Landau energy levels as a function of triangular quantum well's parameter F for some arbitrary values of magnetic field B $\left(B=0.5; B=0.7; B=0.9\right)$. Here, other parameters used are $\varepsilon=2$, $e=1.6\times10^{-19}$ and $c=3\times10^{8} m/s$.

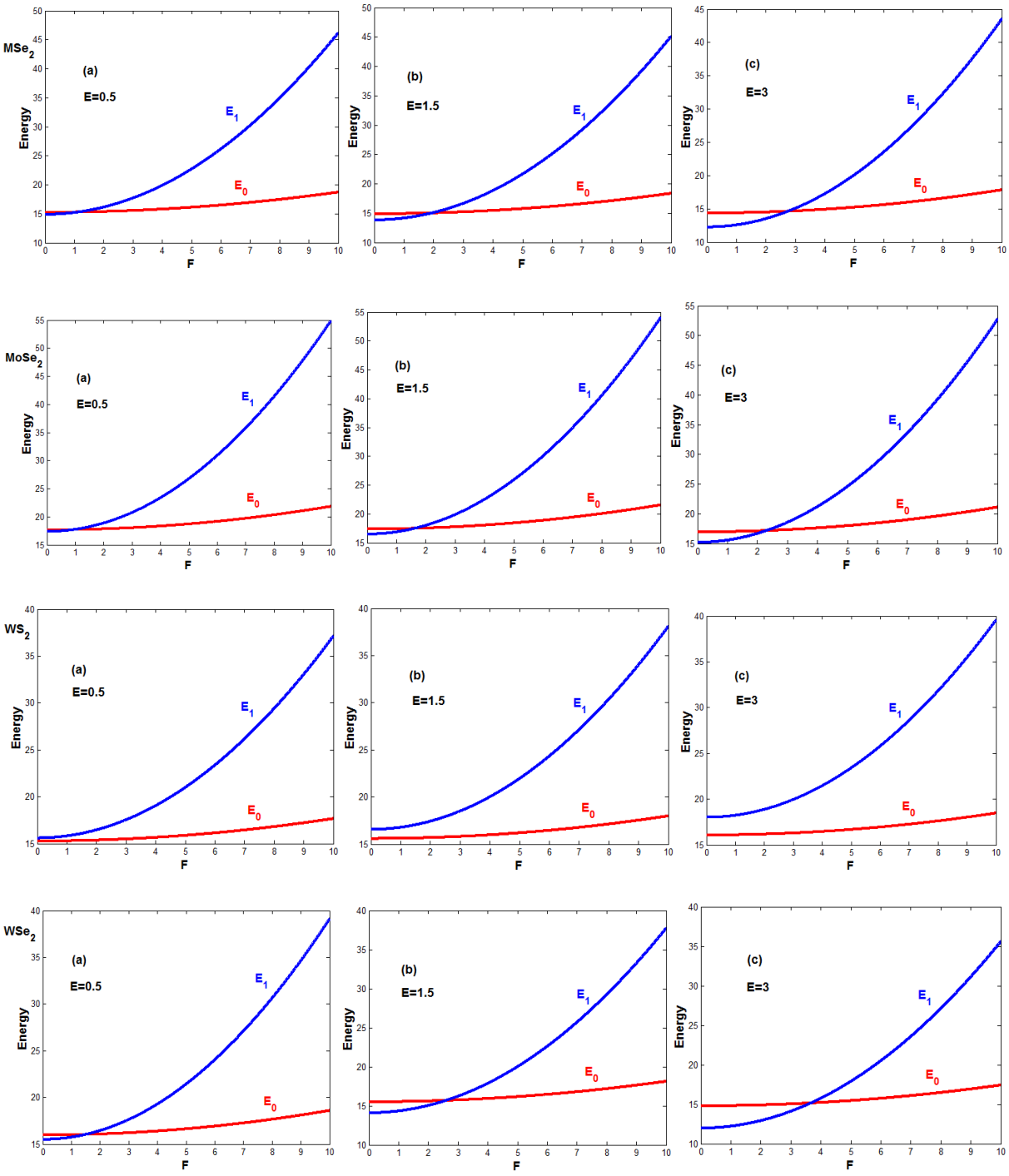

Figure 55. Landau energy levels versus triangular quantum well's parameter F for some arbitrary values of laser field amplitude E $\left(E=0.5; E=1.5; E=3\right)$.

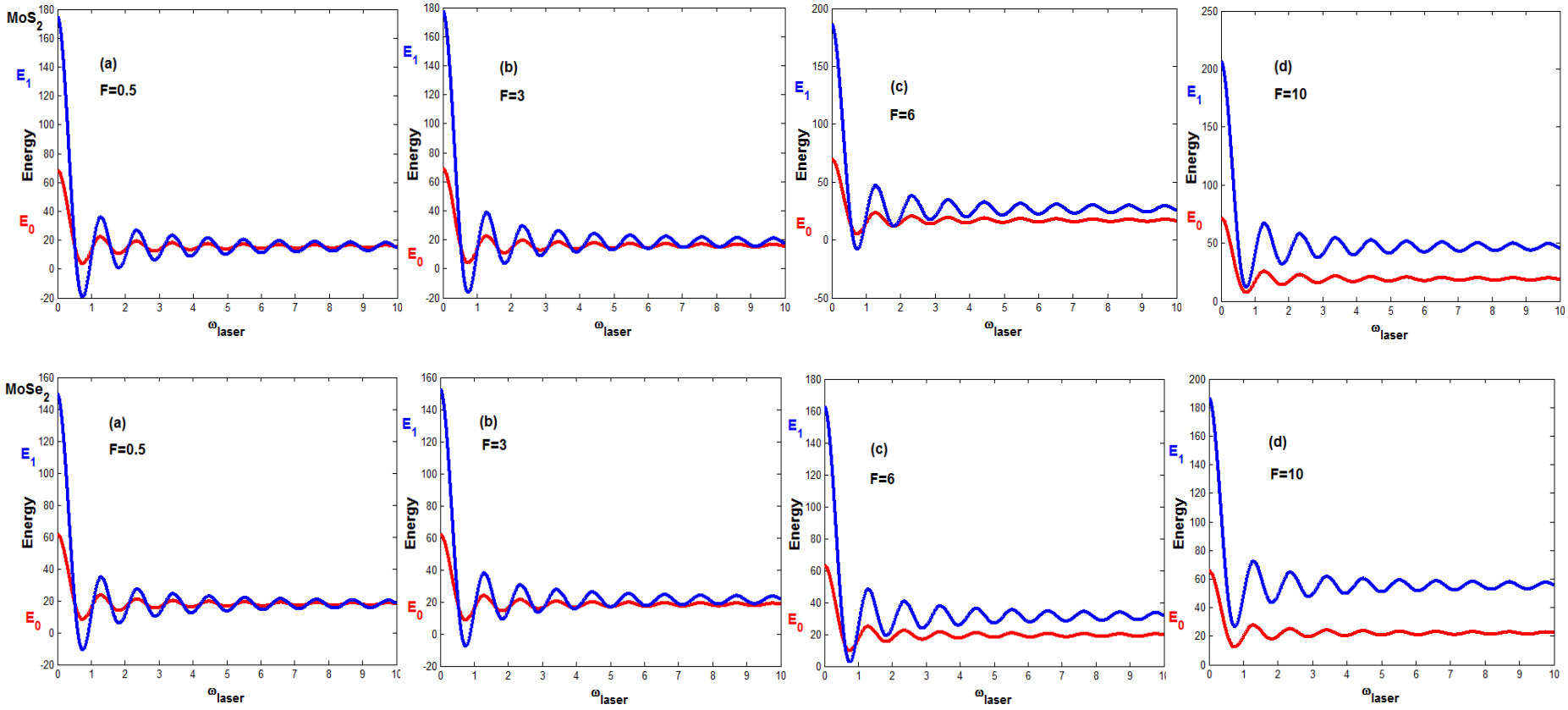

Figure 56. Landau energy levels as a function of laser frequency for some values of triangular quantum well's parameter F . Case study of 2D TMDs materials MoX , giving that $X = S_2, Se_2$.

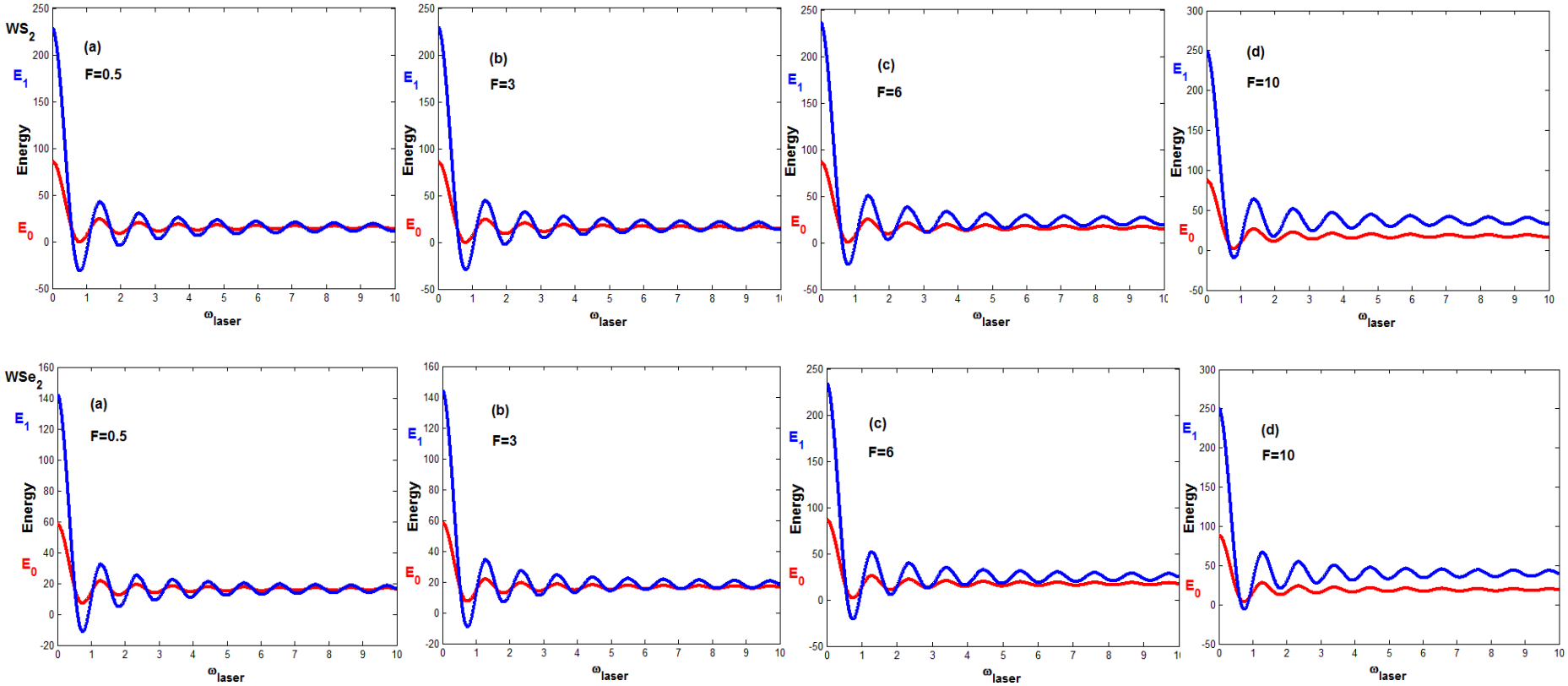

Figure 57. Landau energy levels as a function of laser frequency for some values of triangular quantum well's parameter F. Case study of 2D TMDs materials WX, giving that $X = S_2, Se_2$.

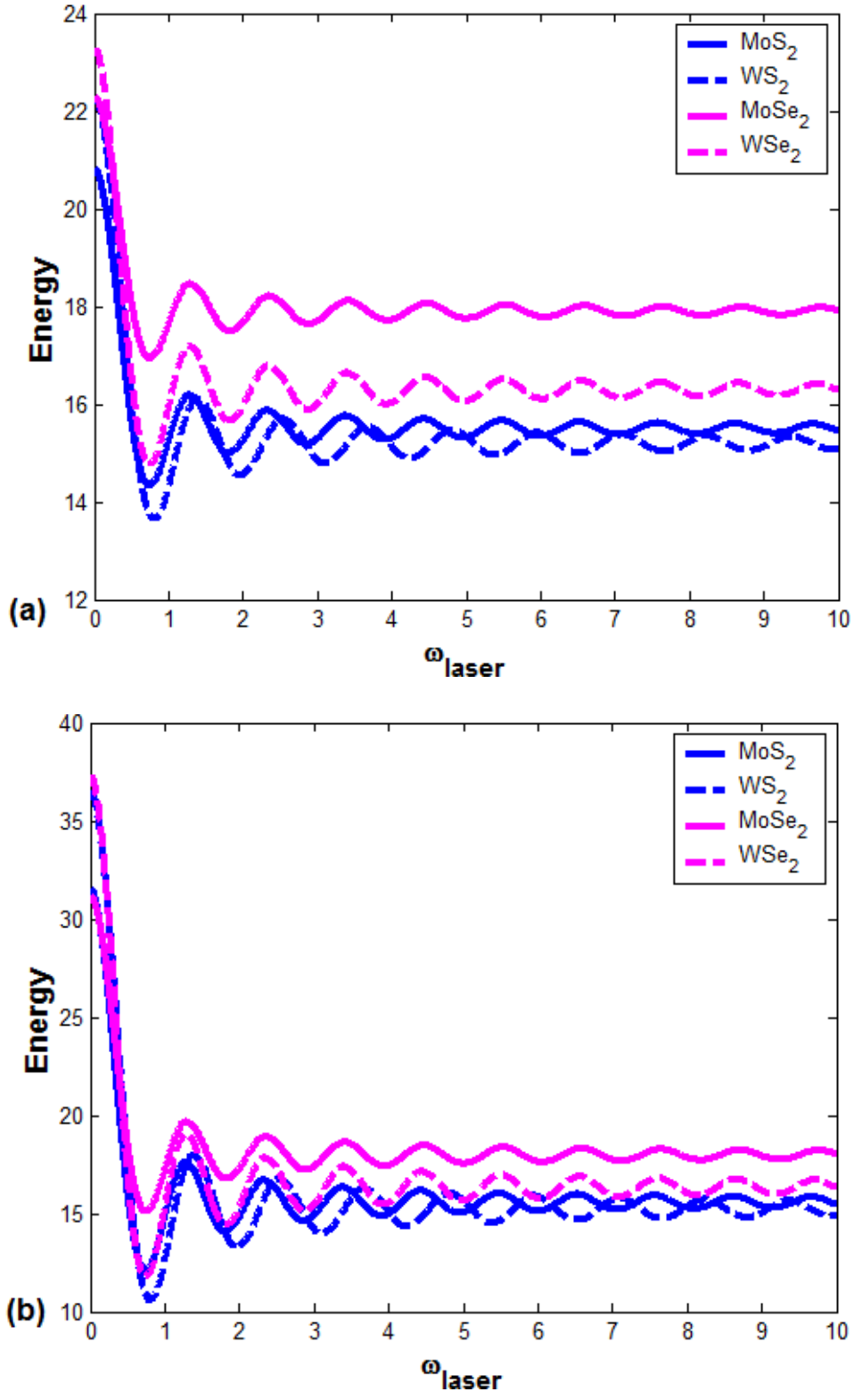

Figure 58. Ground state (a) and first excited state (b) Landau energy levels of magneto-polaron condensate under the influence of triangular potential field.

Conclusion

In the present chapter, we have presented the results obtained from our study. Considering the effect of surrounding environment in laser cooling and trapping processes, we investigated laser cooled and trapped polariton parameters including force and it corresponding torque, transition probability of finding the system in the excited state and the system's energy using semi-classical approach. We observed that the probability of finding cooled and trapped polariton in the excited state is controlled by the surrounding environment even when the system is confined in a magnetic potential which we consider as a trap. Looking for ways to avoid or minimize effect of surrounding environment in laser cooling and trapping of both polariton and polaron entities, we reconsider the approach used and through the system's Hamiltonian, we found a very close connection between semi-classical and quantum mechanical approaches. Doing it, we successfully formulate the LZ problem in laser cooling and trapping polaritonic system. In addition, 2D TMDs materials of 2H types, and particularly $MoSe_2$, MoS_2, WS_2 and WSe_2, are considered as appropriate milieu where to carry laser cooling and trapping phenomena due to their physical properties for practical applications of laser cooled and trapped atomic particles and particularly polaritons and polarons. To go further and to open door to novel applications of laser cooled and trapped atomic particles with concise and precise theoretical formulation and analysis, we introduce polarons as new atomic particles in cooled and trapped processes using LZ formalism. Based on combined QMSA and IWBT, LELs of laser cooled and trapped polaron in monolayer 2D TMDs are investigated within additional influence of perpendicular magnetic field.

GENERAL CONCLUSION

The research work reported in the present thesis is focused on investigating the effect of surrounding environment on the dynamic of laser cooled and trapped polariton and polaron in nanostructures.

Considering the system of interest as a TLS with ground state $|g\rangle$ and first excited state $|e\rangle$, we begin our analysis studying the dynamical behavior of a system of laser cooled and trapped polariton within semi-classical approach. Later, we introduce a magnetic field in the system which we consider as a trap and perform the Vonn Neumann entropy.We justified our choice by the fact that it's introduced in the system a weak magnetic field. Based on the matrix representation of the system's Hamiltonian, we identified and formulated the Landau Zener problem in cooling and trapping of polariton. Motivated by the fact that (i) polaron can be considered as TLS, (2i) polaron are fermions which satisfied the Fermi-Dirac statistics and (3i) polaritons became intermediate particles due to laser cooling and trapping process thereby satisfying Fermi-Dirac statistics althougth they are bosons, we extended our study to polaron. Due to their physical properties, we found interesting the use of two dimensional (2D) transition metal dichalcogenides (TMDs) of MX_2 types as new playground for laser cooling and trapping of polariton as well as polaron. Using LZSIT in one hand and both the QMSA and the IWBT on the other hand, we investigated LELs and transition probabilities in diabatic and adiabatic basis of the laser cooled and trapped polariton and polaron.

We found that the surrounding environment possesses a fatal effect on the dynamic of laser cooled and trapped polaritonic entity. The effect of the environment in laser cooling and trapping phenomena is well corrected by adding in the cooled system a weak magnetic field, which behaves like a confinement. Although we could not achieved complete population transfer from excited to ground states, the amount of energy produced increases considerably due to the introduction of magnetic trap in the system.

Through LZSMI theory, we proved theoretically and numerically the applicability of LZ theory for the analysis of single laser cooled and trapped polariton's dynamic. Afterward, we introduced the laser field in the system and show that crossing and avoided crossing of energy

eigenstates can be seen as a function of laser amplitude for both diabatic and adiabatic basis. Studying energy levels of the upper/lower channel in both diabatic and adiabatic basis at a different gate voltage condition, we showed certain dissimilarities in the dynamic of cooled and trapped polariton at both weak and strong coupling due to crossing and avoided crossing of multiple LZ transitions. As main result, we pointed out the braking down of the Pauli Exclusion Principle proving the applicability of LZSMI theory for the analysis of polariton's dynamic through a model which satisfies both Bose-Einstein and Fermi-Dirac statistics. The above result unveil novel and plethora applications of laser cooled and trapped polariton. We found the generation of arbitrary waveforms of interferometric signals including signusoidals for weak coupling and strong laser amplitude; thereby come s the possibility to investigate interferometry applications. We also find the use of laser cooled and trapped polariton for applications in optics, quantum computation, communication and simulation.

In 2D TMDs materials of 2H types, LELs of the laser cooled and trapped polaritonic system are investigated under two main mathematical approaches including the AIA and the Brundobler-Elser conjecture. We found that LELs are modified by 2D material environment with consistent conservation of novel interference pattern. Landau energy corrections is higher in $MoSe_2$ material than others 2D TMDs of our choice, that is WS_2 , WSe_2, and MoS_2. The modulation of such Landau energy for multicrossing scenario, due to an interaction between polaritonic state and TMDs materials, has conducted to Raman spectroscopy. We predict the possibility to observe butterfly effect in the system of laser cooled and trapped of polariton in 2D TMDs embedded in 2D microcavity. We adjusted the influence of the 2D TMDs environment in laser cooling and trapping of polaron to that of triangular quantum well potential. Within combined QMSA and IWBT, LELs of the system, called for simplicity magneto-polaron condensate are investigated. We clearly observed that the dynamic of polaron is controlled by triangular quantum well potential swept by a laser radiation field. We observed rapid Stückelberg oscillations and energy gap modulation which amplitude decrease progressively with amplitude of magnetic field and laser frequency up to a value where the system arises to it coherence state. This means that one arrive at a complete population transfer from excited state to ground state. Our numerical results have shown a strong dephasing between the levels under the influence of the triangular quantum well potential's parameter F. Various Landau levels (LLs) are

found with increased magnetic field and laser parameter. The quantum confinement is an important parameter to lift the degeneracy of the LLs resulting in an anticrossing and crossing. The dephasing effect due to the quantum well's parameter plays an important role in the magneto-polaron energy corrections, which are also affected by the amplitude of the laser field. Our results are strictly valid as the whole system riches the magneto-polaron condensation in monolayer material $MoSe_2$ compared to MoS_2, WS_2 and WSe_2, while the magnetic and laser parameters are increasing for strong quantum well confinement. In general, the 2D TMDs environment increases considerably the stability of laser cooled and trapped polariton and polaron called therefore polariton condensate and magneto-polaron condensate (under the influence of perpendicular magnetic field) respectively. This lead to wide array of fundamental phenomena and potential applications that range from Bose-Einstein-like condenstation including superfluidity, vortex formation and the possibility to observe Berezinskii-Kosterlitz-Thouless and Barden-Cooper-Schrieffer Physics to quantum computation, simulation and valleytronics.

In the present thesis, we focus ourvelves on the plane lectromagnetic radiation field. Doing it, we then neglect other laser radiation modes including the plane polarized electric mode, transverse electric mode and transverse magnetic mode laser radiation. In the whole study, we consider that the laser radiation propagates in the $z-$direction and the light-matter interaction takes place at the position $z=0$. While it will be interesting to in vestigate the effect of surrounding environment on the dynamic of laser cooled and trapped polariton and polaron using other polarized laser radiation than the plane electromagnetic mode radiation and in the consideration that the laser radiation propagates in other direction than the $z-$direction such as the $x-$direction, $y-$direction and the entire space [(x,y,z)direction]. In 2D TMDs materials of our choice, theoretical investigation of the dynamic of laser cooled and trapped polariton is discussed under two main assumptions. At first, we focused our attention on the polariton only at the center of the system. At second, we consider that there is not interaction between the polariton in the center of the system with it neighbors due to cooling process. These theoretical assumptions are made just for theoretical simplification. In the case of polaron cooled and trapped in 2D TMDs materials with radiation field under the influence of triangular quantum weel potential, we performed analysis by choosing a very small value of the imaginary time and large value cyclotron frequency in order to focus at the zone center thereby avoiding study

neither below nor above longitunal optical phonons continuum. For instance other type of quantum well potential including the square potential, ellipsoidal potential, quadratic potential to cite a fiew can be considered as additional confinement in laser cooling and trapping of polaron in 2D TMDs materials. The above consideration can also be avoided. These facts can open door to other interesting theoretical formulations based on laser cooling and trapping of polariton and polaron with large variety of applications.

REFERENCES

Abram, I. (1987). Quantum theory of light propagation: linear medium. Phys.Rev. A 35: 4661-4672.

Amo, A., Lefrère, J., Pigeon, S., Adrados, C., Ciuti, C., Carusotto, L., Houdré, R., Giacobino, E., Bramati, A. (2009b). Superfluidity of polaritons in semiconductor microcavities. Nature Physics 5: 805–810.

Amo, A., Sanvitto, D., Laussy, F.P., Ballarini, D., del Valle, E., Martin, M.D., Lemaître, A., Bloch, J., Krizhanovskii, D.N., Skolnick, M.S., Tejedor, C., Viña, L. (2009a). Collective fluide dynamics of a polariton condensate in a semiconductor microcavity. Nature 457: 291–295.

Anderson, M. H., Ensher, J. R., Matthews, M. R., Wieman, C. E., Cornell, E. A. (1995). Observation of Bose-Einstein condensation in a dilute atomic vapor. Science 269: 198-201.

Andrews, D.L., Bradshaw, D.S. (2016). Optical Nanomanipulation (San Rafael, CA: Morgan & Claypool Publishers). IOP Science (4): 1-5

Aqvist, J., Warshel, A. (1993). Simulation of enzyme reactions using valence bond force fields and hybrid quantum/classical approaches. Chem. Rev. 93: 2523-2544.

Artoni, M., Birman, J.L. (1990). Quantum-optical properties of polariton waves. Phys. Rev. B 44:3736 -3756

Aspect, A., Arimondo, E., Kaiser, R., Vansteenkiste, N., and Cohen-Tannoudji, C. (1989). Laser cooling below the one-photon recoil energy by velocity-selective coherent population trapping: theoretical analysis. J. Opt. Soc. Am. B 6 (11): 2112-2124.

Aspect, A., Arimondo, E., Kaiser, R., Vansteenkiste, N., Cohen-Tannoudji, C. (1988). Laser cooling below the one-photon recoil energy by velocity-selective coherent population trapping. Phys. Rev. Lett (61): 826-829.

Avishai, Y. (2014). Landau-Zener problem with decay and dephasing. Phys. Rev A 90, 032116: 1-15

Ball, P. (2014). Focus: high-precision measurements using lots of cold atoms. Physics, 7 (90). Page visite on 18th April 2020. URL

Balykin, V.I., Minogin, V.G., Letokhov, V.S. (2000). Electro: https://physics.aps.org/articles/v7/90magnetic trapping of cold atoms. Rep.Prog.Phys (63):1429–1510.

Barnes, W.L., Dereux, A., Ebbesen, T.W. (2003). Surface plasmon subwavelength optics. Nature 424: 824–830.

Barreiro, J.T., Meschede, D., Polzik, E., Arimondo, E., Illuminatie, F., Lugiato, L. (2011). Atoms, photons and entanglement for quantum information technologies. Procedia computer science 7: 52-55.

Basdevant, J.L. (2016). Chapter 7: Two-Stat Systems. Lectures on quantum mechanics, graduate texts in Physics. Springer International Publishing Switzerland: 147-182

Beals, R., Wong, R. (2010). Special functions (Cambridge: Cambridge Press).

Berthiaume, A., Brassard, G. (1992). The quantum challenge to structural complexity theory. in: Proc. 7th Annual Structure in Complexity Theory Conf., IEEE Computer Society Press, Los Alamitos, CA : 132–137.

Bertolazzi, S., Brivio, J., Kis, A. (2011). Stretching and breaking of ultrathin MoS_2. ACS Nano 5 (12): 9703-9709.

Bhushan, B., Agrawal, G.B. (2003). Finite element analysis of nanostructures with roughness and scratches. Ultramicroscopy, 97: 495–501.

Bleeker, E. A., de Jong, W. H., Geertsma, R. E., Groenewold, M., Heugens, E. H., Koers-Jacquemijns, M., et al. (2013). Considerations on the EU definition of a nanomaterial: science to support policy making. Regul. Toxicol. Pharmacol. 65 : 119–125.

Bloch, I., Dalibard, J., Zwerger, W. (2008). Many-body physics with ultracold gases. Reviews of Modern Physics 3 (80):885-964.

Bolpasi, V., Grucker, J., Morrissey, M.J., von Klitzing, W. (2012). Journal of Physics B-Atomic Molecular and Optical Physics 45, 7.

Bornhop, D.J., Dotson, S. (2006). Micro-scale polarimetry. Chiral Analysis: 343-361

Bose, S. N. (1924). Plancks gesetz und lichtquantenhypothese. Zeitschrift für Physik. 26, 1: 178–181.

Bradley, C. C., Sackett, C. A., Tollett, J. J., Hulet, R. G. (1995). Evidence of Bose-Einstein condensation in an atomic gas with attractive interactions. Phys. Rev. Lett. 75: 1687-1690.

Brundobler, S., Elser, V. (1993). S-matrix for generalized Landau-Zener problem. Journal of physica A : Mathematical and General 26 : 1211-1227.

Buluta, I., Ashhab, S., Nori, F. (2011). Natural and artificial atoms for quantum computation. Rep. Prog. Phys. 74, 104401:1-16

Bunch, B.H, Hellemans, A. (2004). The History of Science and Technology. Houghton Mifflin Harcourt. p. 695. ISBN 978-0-618-22123-3.

Butler, L.J. (1998). Chemical reaction dynamic beyond Ann. Rev. Phys. Chem. 49: 125-171.

Byrnes, T., Kim, N.Y., Yamamoto, Y. (2014). Exciton-polariton condensates. Nature Physics 10: 803–813.

Carusotto, I., Ciuti, C. (2013). Quantum fluids of light. Rev. Mod. Phys.85: 299–366.

Castin, Y., Wallis, H., Dalibard, J. (1989). Limit of Doppler cooling. Journal of Optical Society of America B, 6 (11): 2046-2057

Cavazos, D. (2015). All Coils Ioffe-Pritchard Magnetic Trap. Summer 2015. 44p. Accessed on 20 June 2020. URL: http://dycvz.com/DOCS/allcoilsiptrap-notes.pdf

Chang, K., Chen, W. (2011). In situ synthesis of MoS2/graphenenanosheet composites with extraordinarily high electrochemical performance for lithium ion batteries. Chemical Communications 47: 4252-4254.

Chen, Q., Wang, W., Peeters, F.M. (2018). Magneto-polarons in monolayer transition dichalcogenides. Journal of Applied Physics 123, 214303: 1-7

Chhowalla, M., Shin, H.S., Eda, G., Li, L.-J., Loh, K.P., Zhang, H. (2013). The chemistry of two-dimensional layered transition metal dichalcogenide nanosheets. Nat Chem 5 (4) : 263-275.

Cho, B., Hahm, M.G., Choi, M., Yoon, J., Kim, A.R., Lee, Y..-J., Park, S.-G, Kwon, J.-D., Kim, C.S., Song, M., Jeong, Y., Nam, K.-S., Lee, S., Yoo, T.J., Kang, C.G., Lee, B.H., Ko, H.C., Ajayan, P.M., Kim, D.-H. (2015). Charge-transfer-based Gas sensing using atomic layer MoS_2. Scientific Reports 5(1), 8052: 1-6.

Chu, S. (1995). Laser cooling and trapping of atoms. Proceedings of the 6th International Symposium on Advanced nuclear research, Innovative Laser Technologies in Nuclear Energy: 35-43.

Chu, S. (1998). Nobel lecture: the manipulation of neutral particles. Rev. Mod. Phys. 70: 685-706.

Chung, T., Lee, S-Y., Song, E.Y., Chun, H.G., Lee, B. (2011). Plasmonic nanostructures for nano-scale bio-sensing. Sensors 11: 10907–10929.

Ci, L., Song, L., Jin, C., Jariwala, D., Wu, D., Li, Y., Srivastava, A., Wang, Z.F., Storr, K., Balicas, L., Liu, F., Ajayan, P.M. (2010). Atomic layers of hybridized boron nitride and graphene domains. Nature Materials 9 : 430-435.

Cie. (1987). International Lighting Vocabulary Archived 27 February 2010 at the Wayback Machine. Number 17.4. CIE, 4th edition. ISBN 978-3-900734-07-7. By the International Lighting Vocabulary, the definition of light is: Any radiation capable of causing a visual sensation directly.

Cohen, J.M., Micha, D.A. (1992). Electronically diabatic atom-atom collisions: A self consistent eikonal approximation. J. Chem. Phys. 97: 1038-1052.

Cohen-Tannoudji, C.N. (1998). Nobel lecture: manipulating atoms with photons. Rev. Mod. Phys. 70: 707-719.

Cohen-Tannoudji, C.N. (1997). Manipulating atoms with photons, Nobel Prize Lecture. 8th December: 166-190. Accessed on 6 May 2019. URL: https://www.nobelprize.org/uploads/2018/06/cohen-tannoudji-lecture.pdf

Cong, C., Shang, J., Wu, X., Cao, B., Peimyoo, N., Qiu, C., Sun, L., Yu, T. (2014). Synthesis and optical properties of large-area single-crystalline 2D semiconductor WS_2 monolayer from chemical vapor deposition. Adv. Opt. Mater. 2(2): 131-136.

Cornell, E. (1996). Very cold indeed: the nanokelvin physics of Bose-Einstein condensation. J. Res Natl Inst Stand Technol 101 (4): 419-434.

Cornell, E. A., Wieman, C. E. (2002). Nobel lecture: Bose-Einstein condensation in a dilute gas, the first 70 years and some recent experiments. Rev. Mod. Phys. 74: 875-893.

Dalfovo, F., Giorgini, S. (1999). Theory of Bose-Einstein condensation in trapped gases. Reviews of Modern Physics 3 (71): 463-512

Dalibard, J., Cohen-Tannoudji, C. (1989). Laser cooling below the Doppler limit by polarization gradients: simple theoretical models. J. Opt. Soc. Am. B 6(11): 2023-2045.

Danga, J.E., Kenfack, S.C., Fai, L.C. (2016). Quantum wire and magnetic control of a spin qubit in the Landau-Zener-Stückelberg interferometry transition. J. Phys. A: Math. Theor. 49: 1-16

Debs, J. E., Altin, P. A., Barter, T. H., Doring, D., Dennis, G. R., McDonald, G., Anderson, R. P., Close, J. D., Robins, N. P. (2011). Cold-atom gravimetry with a Bose-Einstein condensate. Phys.Rev. A 84(3),033610 : 1-5.

Dehghani, A., Mojaveri, B., Shirin, S., Amiri Faseghandis, S. (2016). Parity deformed Jaynes-Cummings model : 'robust maximally entangled states'. Scientific Reports 6, 38069: 1-15

Devane, E. (2008). A Tale of mathematicians and Hollywood producers:1-13

Devreese, J.T. (2003). in Lectures on the Physics of Highly Correlated Electron Systems VII, edited by Avella A. and Mancini F. (AIP, Melville): 3-56

Devreese, J.T. (2005). Fröhlich polarons from 3D to 0D : concepts and recent developments (Part I). 186 pges

Devreese, J.T. (2008). In Digital Encyclopedia of Applied Physics, edited by G. L. Trigg. available at cond-mat/0004497v2.

Devreese, J.T. (2014). Polarons. Physics Today, 67(10): 54–54.

Devreese, J.T. (2015). More on polaron history. Physics Today 68, 9: 11–11.

Devreese, J.T., Kartheuser, E.P., Evrard, R., Baldereschi, A. (1973). Effect of internal excitations of polarons on magneto-optcical absorption and cyclotron resonance in polar crystals. Phys. Status Solidi B 59 : 629-640.

Devreese. J.T. (2005). Fröhlich polarons from 3D to 0D : concepts and recent developments (Part I). 186 pges

Dion, C. M., Jonsell, S., Kastberg, A., Sjölund. P. (2016). Bimodal momentum distribution of laser-cooled atoms. In optical lattices. Phys. Rev. A 93(5), 053416: 1-10.

Djelouah, H. (2013). Electromagnetism. Bachelor's note, Faculty of physics, University of Sciences and technologies Houari Boumediene, 32 EL Alia 16111, Bab Ezzouar, Algerie, 48p

Dobrescu, B.E., Sinitsyn, N.A. (2006). Comment on 'exact results for survival probability in the multistate Landau-Zener model'.J. Phys. B 39(5) : 1253-1260.

Dodonov, A.V., Militello, B., Napoli, A., Messina, A. (2016). Effective Landau-Zener transitions in the circuit dynamical Casimir effect with time-varying modulation frequency. Physical Review A 93, 052505: 1-9

Du, G., Guo, Z., Wang, S., Zeng, R., Chen, Z., Liu, H. (2010). Superior stability and high capacity of restacked molybdenulm disulfide as anode material for lithiulm ion batteries. Chem. Commun. 46: 1106-1108.

Dunningham, J., Burnett, K., Phillips, W.D. (2005). Bose-Einstein condensates and precision measurements. Philosophical Transaction of the Royal Society A, (363): 2165-2175

Durfee, D.S. (1999). Dynamic properties of dilute Bose-Einstein condensates, PhD thesis, Massachusetts Institute of Technology

Dzyubenko, M.I., Kamenev, Y.Y., Radionov. (2017). Gas-discharge lasers of the tretrahertz range. Telecommunications and Radio engineering 20 (76): 1797-1821

Einstein, A. (1925). Quantentheorie des einatomigen idealen Gases / Quantum Theory of ide al Monoatomic Gases. Sitzungsberichte der Preussischen Akademie der Wissenschaften. 1: 3

Einstein, A., 1924, Sitzber. Kgl. Preuss. Akad. Wiss., 261.

Erbil, H.H. (2017). General solution of the Schrödinger equation with potential field quantization. arXiv:1712.00610v1 [quant-ph]: 1-42.

Fai, L.C., Teboul, V., Monteil, A., Maabou, S., Nsangou, I. (2005). Polaron in a quasi 1D cylindrical quantum wire. Condensed Matter Physics 3(43), 8: 639-650.

Fobasso, M.F.C., Fotue, A.J., Kenfack, S.C., Ekengue, C.M., Ngoufack, C.D.G., Akay, D., Fai, L.C. (2019). Laser light and external magnetic field control of polaron in asymmetric quantum dot. Superlattices and microstructures 129 (2019): 77-90

Foot, C.J. (1991). Lasr cooling and trapping of atoms. Contemporary Physics 6 (32): 369-381

Fortier, K.M. (2007). Individual trapped atoms for cavity QED quantum information applications. PhD Thesis, the academic faculty, School of Physics, Georgia Institute of Technology. Pges 134.

Fotue, A.J., Djomou, D.R.-J., Kenfack, S.C., Fobasso, M.F., Fai, L.C. (2020). Stability and decoherence of optical bipolaron in symmetric quantum dot. Eur. Phys. J. Plus: 1-14.

Fox, M., Ispasoiu, R. (2006). Quantum Wells, Superlattices, and Band-Gap Engineering. Springer Handbook of Electronic and Photonic Materials. Springer US, pp. 1021–1040. D:10.1007/978-0-387-29185-7_42. ISBN 978-0-387-26059-4

Friedman, J. R., Patel, V., Chen, W., Yolpygo, S. K., Lukens, J. E. (2000). Quantum superposition of distinct macroscopic states. Nature 406 : 43–46.

Fröhlich, H. (1954). Electron in lattice fields. Adv. Phys 3: 325-361

Fu, J., Yin, X., Li, N., Tong, L. (2008). Atom waveguide and 1D optical lattice using a two-color evanescent light field around an optical micro/nano fiber. Chinese Optics Letters 2(6): 112-115

Fuhrer, M.S., Hone, J. (2013). Measurement of mobility in dual-gated MoS_2 transistors. Nat. Nanotechnol. 8 : 146-147.

Fujii, K. (2013). Introduction to the Rotating Wave Approximation (RWA): two coherent oscillations. arXiv: 1301.3585v3 [Quant-Ph]:1-22.

Fujii, K. (2014). Introduction to the rotating wave approximation (RWA) : two coherent oscillations. arXiv:1301.3585v3 [quant-ph] : 1-22

Fujii, K., Suzuk, T. (2012). An approximate solution of the dynamical Casimir effect in a cavity with a two-level atom. International Journal of Geometric Methods in Modern Physics 10(06), 1350035:1- 9.

Fujii, K., Suzuki, T. (2011). An approximate solution of the Jaynes-Cummings model with dissipation. . International Journal of Geometric Methods in Modern Physics 8:1799-1814.

Ghaemi, H.F., Thio, T., Grupp, D.E., Ebbesen, T.W., Lezec, H.J. (1998). Surface plasmons enhance optical transmission through subwavelength holes. Phys Rev B 58: 6779–6782.

Ghoshal, S. K., Sahar1, M.R., Rohani1, M.S., Sharma, S. (2011). Nanophotonics for 21st Century: optoelectronics - devices and applications, ISBN: 978-953-307-576-1

Glauber, R.J., Lewenstein, M. (1989). In Squeezed and non classical light. NATO Advanced study institute series B: Physics. Edited by Tombesi, P and Pike, R.P. Mod. Opt 34 (6):

Goluband, R., Pendlebury, J. (1979). Ultra-cold neutrons. Reports on Progress in Physics 42(3): 439-501.

Gould, R.G. (1959). The LASER, Light Amplification by Stimulated Emission of Radiation. In Franken, P.A., Sands, R.H. (eds.). The Ann Arbor Conference on Optical Pumping, the University of Michigan, 15 June through 18 June (1959). p. 128. OCLC 02460155.

Gov, S., Shtrickman, S. (1999). Magnetic trapping of neutral particles : a study of a physically realistic model. arXiv:quant-ph/9812079v2 : 1-27.

Gradshteyn, I.S., Ryzhik, I.M. (1994). Table of Integrals, Series and Products. Edited by Alan Jeffry and Daniel Zwillinger. 7th Edition, New York, Academic Press. 1220p.

Griffin, A., Snoke, D. W., Stringari, S. (1995). BoseEinstein Condensation (Cambridge University Press, Cambridge). ISBN: 9780511524240

Griffiths, D. J. (2004). Introduction to Quantum Mechanics (2nd ed.), Prentice Hall. ISBN 978-0-13-111892-8

Grifoni, M., Hänggi, P. (1998). Driven quantum tunneling. Physics Reports 304: 229-354

Han, D.-J., Wynar, R. H., Courteille, P.H., Heinzen, D. J. (1998). Bose-Einstein condensation of large numbers of atoms in a magnetic time-averaged orbiting potential trap. Phys. Rev. A 57 (6): R4114-R41117.

Hansch, T. W., Schawlow, A. L. (1975). Cooling of gases by laser radiation. Optics Communications 13(1): 68-69.

Hardesty, L. (2016). Hyperprecise measurement with Bose-Einstein condensates. Massachusetts Institute of Technology (MIT), MIT News offices. Page accessed on 18th April 2020. http://news.mit.edu/2016/technique-could-yield-hyperprecise-gravitational-measurements-1227

Hau, L. V., B. D. Busch, C. Liu, M. M. Burns, and J. A. Golovchenko. (1997). InPhotonic, Electronic and Atomic Collisions, Vol. 1, edited by F. Aumayr and H. P. Winter (World Scientific, Singapore), p. 41.

Hau, L. V., Busch, B. D., Liu, C., Dutton, Z., Burns, M. M., Golovchenko, J. A. (1998). Near-resonant spatial images of confined Bose-Einstein condensates in a 4-Dee magnetic bottle. Phys. Rev. A 58: R54-R57.

He, Q., Wu, S., Yin, Z., Zhang, H. (2012). Graphene-based electronic sensors. Chemical Science 3: 1764-1772.

He, Q., Zeng, Z., Yin, Z., Li, H., Wu, S., Huang, X., Zhang, H. (2012). Fabrication of flexible MoS2 thin-film transistor arrays for practical gas-sensing applications. Small 8, 8(19): 2994-2999.

Hecht, J. (2008). The history of X-ray laser. Optics and photonics. Accessed online on 25th January 2018. URL: https://www.osa-opn.org/opn/media/Images/PDFs/10978_22263_109570.pdf?ext=.pdf

Heer, C.V. (1963). Feasibility of containment of quantum magnetic dipoles. Review of Scientific Instruments 34(5): 532-537.

Hicke, C., Santos, L. F., Dykman, M. I. (2005). Fault-tolerant Landau-Zener quantum gates. Physical Review A 73, 012342: 1-6.

Hopfield, J. (1958). Theory of the contribution of excitons to the complex dielectric constant of crystals. Physical Review, 112(5): 1555-1567.

Hsu, T., Sun, N. (1998). Residual stresses/strains analysis of mems. TechConnect Briefs. Technical proceedings of the 1998 international conference on modelling and simulation of microsystem : 82-87.

Hu, Z., Wu, Z., Han, C., He, J., Ni, Z., Chen. W. (2019). Chem. Soc. Rev: 1-29.

Ichino, T., Gianola, A.J., Lineberger, W.C., Stanton, J.F. (2006). Nonadiabatic effects in the photoelectron spectrum of the pyrazolde-d3 anion: Three-state interactions in the pyrazolyl-d3 radical. The Journal of Chemical Physics, 125(8), 084312: 1-22.

Ioffe it, L. B., Geshkenbein, V.B., Feigel'man, M.V., Fauchère, A.L., Blatter, G. (1999). Environmentally decoupled sds-wave Josephson junctions for quantum computing. Nature 398: 679-681.

Irnova. (2018). Quantum Well Infrared Photon Detectors. IRnova. www.ir-nova.se. Retrieved 2018-09-04. https://irnova.se/products/

Izmalkov, A., Izmalkov, A., Van der Ploeg, S. H. W., Shevchenko, S. N., Grajcar, M., Il'ichev, E., Hubner, U., Omelyanchouk, A. N., Meyer, H. G. (2008). Consistency of ground state and spectroszcopic measurements on flux qubits. Physical Review Letters 101, 017003 : 1-4

Jaynes, E.T., Cummings, F.W. (1963). Comparison of quantum and semi-classical radiation theories with application to beam maser. Procedings of the IEEE 51(1): 89-109.

Jeffry, A. (2002). Advanced engineering mathemetics. (Published by the Academic press. ISBN: 9780080522968)

Jenne, M., Chen, K., Flamm, D., Chen, K., Schaefer, M., Kumkar, M., Nolte, S. (2020). Facilitated glass separation by asymmetric Bessel-like beams. Optics Express 28(5): 6552-6564.

Johansson, S., Schweitz, J.A., Tenerz, L., Tirén, J. (1998). Fracture testing of silicon microelements in situ ijn a scanning electron microscope. Journal of Applied Physics, 63(10):4799–4803.

Joos, E., Zeh, H. D. (1985). The emergence of classical properties through interaction with the environment. Zeitschrift für Physik B Condensed Matter 9: 223–243.

Joos, E., Zeh, H.D., Kiefer, C., Giulini, D.J.W., Kupsch, J., Stamatescu, I.-O. (2003). Decoherence and the Appearance of a Classical World in Quantum Theory (Springer, Berlin, 2003), second ed. ISBN: 978-3-662-05328-7

Kaiser, R., Kastberg, A., Morigi, G. (2003). Laser cooling of matter. Optical Society of America B, 5 (20): 883-883

Kami, Y., Nikitin, E.E. (1994). Recovery of the Landau matrix elements from the classical Fourrier components: one-dimensional dissociating oscillator. Journal of Chemical Physics 100: 2027-2033

Kaminski, A., Das Sarma, S. (2002). Polaron percolation in dilute magnetic semiconductors. Phys. Rev. Lett. 88, 247202: 1-4.

Kang, K., Xie, S., Huang, L., Huan, Y., Huang, P.Y., Mak, K.F., Kim, C.-J., Muller, D., Park, J. (2015). Nature 520: 656-660.

Keeling, J., Gurarie, V. (2008). Collapse and revivals of the photons field in a Landau-Zener process. Phys. Rev. Lett. 101, 033001: 1-4

Keeling, J., Marchetti, F.M. (2017). Physics 9, 154

Kenfack, S.C., Fotue, A.J., Fobasso, M.F., Djomou, D.J.-R., Tiotsop, M., Ngouana, K.S.L., Fai, L.C. (2017). Quantum transition and decoherence of levitating polaron on helium film thickness under an electromagnetic field. Indian Journal of Physics:

Kenmoe, M.B., Mkam Tchouobiap, S.E., Danga, J.E., Kenfack Sadem, C., Fai, L.C. (2015). Lie algrebras for some specific dissipative Landau-Zener problems. Physics Letters A 379: 635-642.

Ketterle, W. (2002). Nobel lecture: when atoms behave as waves. Bose-Einstein condensation and the atom laser. Rev. Mod. Phys. 74(4): 1131-11151.

Ketterle, W., Davis, K.B., Joffe, M.A., Martin, A., Pritchard, D.E. (1993). High densities of cold atoms in a dark spontaneous-force optical trap. Phys. Rev. Lett. 70(15): 2253-2256.

Ketterle, W., Durfee, D.S., Stamper-Kurn, D.M. (1999). Making, probing and understanding bose-einstein condensates. Cern document Sever. Document Preprint cond-mat/9904034. 90p.

Kim, Y., Corchado, J.C., Villà, J., Xing, J., Truhlar, D.G. (2000). Multiconfiguration molecular mechanics algorithm for potential energy surfaces of chemical reactions. J. Chem. Phys. 112: 2718-2735.

Klavins, D., Lazov, L., Pacejs, A., Revalds, R., Zaicevs, E. (2019). Research of laser marking and engraving on Brass Alloy 260. Proceedings of the 12th International Scientific and Practical Conference III: 119-123

Klembt, S., Durupt, E., Datta, S., Klein, T., Baas, A. et al. (2015). Phys. Rev. Lett. 114, 186403. 1-5.

Klingshirn, C.F. (2012). Semiconductor Optics. Springer. ISBN 978-364228362-8

Kolpekwar, A., Kellen, C., Blanton, R. D. (1998). MEMS fault model generation using caramel. ITC'98 : Proceeding of the 1998 IEEE international test conference. Accessed online : 10 March 2019. URL : https://dl.acm.org/doi/10.5555/648020.745781

Komai, K., Minoshima, K., Inoue, S. (1998). Fracture and fatigue behavior of single crystal silicon microelements and nanoscopic AFM damage evaluation. Microsystem Technologies : 30– 37.

Kowalski, K., Cao Long, V., Dinh Xuan, K., Glodz, M., Nguyen Huy, B., Szonert, S. (2010). Magneto-optical trap: fundamentals and realization. CMST SI (2): 115-129

Kuznetsov, A.M., Ulstrup, J. (1999). Simple schemes in chemical electron transfer formalism beyond single-mode quadratic forms: environmental vibrational dispersion and anharmonic nuclear motion. Phys. Chem. Chem. Phys. 1 : 5587-5592.

Laloe, F. (2012). Do We Really Understand Quantum Mechanics, Cambridge University Press. ISBN 978-1-107-02501-1

Landau, L. D. (1965). Men of Physics. Phys. Z. Sowjetunion 3, 664 [English translation (1965), Collected Papers, New York: Gordon and Breach, pp. 67-68]

Landau, L. D., Pekar, S. I. (1948). Effective mass of polaon. Zh. Eksp. Teor. Fiz.18, 419: 419-423

Landau, L.D. (1932). Zur theorie der energieubertragung ii. Physikalische Zeitschrift der Sowjetunion. 2: 46–51.

Landau, L.D. (1993). Phys. Z. Sowjetunion. 3: 644–645.

Lawall, J., Kulin, S., Saubamea, B., Bigelow, N., Leduc, M., Cohen-Tannoudji, C. (1995). Three-dimensional laser cooling of Helium beyond the single-photon recoil limit. Phys. Rev. Lett 75(23): 4194-4197

LeBlanc, M. (2012). The use of Fock spaces in quantum mechanics. Department of Mathematics, the University of Georgia. Lecture notes : 1-22

Lee, H.S., Min, S.W., Chang, Y.G., Park, M.K., Nam, T., Kim, H., Ryu, S., Im. S. (2012). MoS_2 Nanosheet phototransistors with thickness-modulated optical energy gap. Nano. Lett. 7: 3695-3700

Lee, Y.-H., Zhang, X.-Q., Zhang, W., Chang, M.-T., Lin, C.-T., Chang, K.-D., Yu, Y.-C., Wang, J.T.-W., Chang, C.-S., Li, L.-J., Lin, T.-W. (2012). Synthesis of large-area MoS_2 atomic layers with chemical vapor deposition. Adv. Mater. 24(17): 2320-2325.

Letokhov, V.S., Minogin, V.G., Pavlik, B.D. (1976). Cooling and trapping of atoms and molecules by resonant laser field. Optics communication, 19 : 72-75

Lett, P.D., Watts, R.N., Westbrook, C.I., Phillips, W.D., Gould, P.L., Metcalf, H.J. (1988). Observation of atolms laser cooled below the Doppler limit. Phys. Rev. Lett. 61(2):169-172.

Li, H., Yin, Z., He, Q., Li, H., Huang, X., Lu, G., Fam, D.W.H., Tok, A.I.Y., Zhang, Q., Zhang, H. (2012). Fabrication of single-and multilayer MoS_2 film-based field-effect transistors for sensing NO at room temperature. Small 8(1): 63-67.

Li, H., Yin, Z.Y., He, Q.Y., Huang, X., Lu, G., Fam, D.W.H., Tok, A.I.Y., Zhang, Q., Zhang, H. (2012). Small 8 (1): 63-67.

Li, T., Galli, G. (2007). Electronic properties of MoS_2 Nanoparticles. J. Phys. Chem. C, 111(44):16192-16196.

Li, X., Bhushan, B., Takashima, K., Baek, C.W., Kim. Y.K. (2003). Mechanical characterization of micro/nanoscale structures for MEMS/NEMS applications using nanoindentation techniques. Ultramicroscopy, 97:481–494.

Lindemann, G., Lassnig, R., Seidenbusch, W., Gornik, E. (1983). Cyclotron resonance study of polarons in GaAs. Phys. Rev. B 28(8) : 4693-4703.

Lipi, M., Xiaoming, Y., Stephen, W. (2012). Solar Energy 86(1)

Liu, C-H., Kim, I.S., Lauhon, J. (2015). Optical control of mechanical Mode-coupling withing a MoS_2 Resonator in the strong-coupling regime. Nanoletters 15(10): 6727-6731.

Liu, J., Fu, L-B., Ou, B-Y., Chen, S-G., Niu, Q. (2001). Theory of nonlinear Landau-Zener tunneling. Physical Review A 66(2), 023404: 1-17

Lo Franco, R., Compagno, G. (2016). Quantum entanglement of identical particles by standards infromation-theoretic notions. Scientific Reports 6, 20603 : 1-10.

Loan, P.T.K., Zhang, W., Lin, C.T., Wei, K.-H., Li, L.-J., Chen, C.-H. (2014). Graphene/MoS2 heterostructures for ultrasensitive detection of DNA hybridisation. Advanced Materials, 26(28): 4838-4844.

London, F. (1938). The $\lambda-$phenomenon of liquid Helium and the Bose-Einstein degeneracy. Nature 141: 643-644.

Lopez-Sanchez, O., Lembke, D., Kayci, M., Radenovic, A., Kis, A. (2013). Ultrasensitive photodetectors based on monolayer MoS_2. Nature Nanotechnology 8, 7: 497–501.

Luo, Y., Chamanzar, M., Apuzzo, A., Salas-Montiel, R., Nguyen, K. N., Blaize, S., Adibi, A. (2015). On-chip hybrid photonic-plasmonic light concentrator for nanofocusing in an integrated silicon photonic Plattform. Nano Lett 15: 849–856.

Mahapatra, S., Köppel, H., Cederbaum, L.S. (2001). Reactive scattering dynamics on conically intersecting potential energy surfaces : the H + H2 exchange reaction±. J. Phys. Chem. A 105: 2321-2329.

Majorana, E. (1932). Atomi orientati in campo magnetico variabile. Il Nuovo Cimento. 9 (2): 43–50.

Manceau, J-M., Biasiol, G., Tran, N.L., Carusotto, I., Colombelli, R. (2017). Immunity of intersubband polaritons to inhomogeneous broadening. Physical Review B 96, 235301: 1-6

Maragkou, M. (2015). Dielectric nanostructures: ultrafast responses. Nature Mater.14, 11 (2015): 1086-1086. DOI: https://doi.org/10.1038/nmat4467

McMahon, D. (2). Quantum mechanics demystified. ISBN-13: 978-0071765633

Meekhof, D.M., Monroe, C., King, B.E., Itano, W.M., Wineland, D.J. (1996). Generation of nonclassical motional states of a trapped atom. Phys. Rev. Lett. 76: 1796-1799.

Menz, M.D., Ye, P., Firouzi, K., Nikoozadeh, A., Pauly, K.B., Khuri-Yakub, P., Baccus. S.A. (2019). Radiation force as a physical mechanism for ultrasonic neurostimulation of the Ex Vivo retina. Journal of neuroscience, 39(32): 6251-6264.

Mewes, M.O., G. Ferrari, F. Schreck, A. Sinatra, C. Salomon. (1999). Simultaneous magneto-optical trapping of two lithium isotopes. Physical Review A 61, 011403:1-4.

Meystre, P., Stenholm, S. (1985). Introduction to feature on the mechanical effects of light. The Jounal of Optical Society of America B (2): 1705-1860

Migdal, A.L., Prodan, J.V., Phillips, W.D., Bergeman, T.H., Metcalf, H.J. (1985). First observation of magnetically trapped neutral atoms. Phys. Rev. Lett.54(24): 2596-2599.

Miller, J.C.P. (1952). On the choice of stndard solutions to weber's equation. Mathematicl Proceedings of the Cambridge Philosophical Society, 48(3) : 428–435.

Minogin, V.G., Letokhov, V.S. (1987). Laser light pressure on atoms. CRC press. 260 P. ISBN: 9782881240805

Minucci, M.A.S., Oliva.J.L.S. (1993). AIAA PAPER 93-3187, 24 th Plasmadynamics and Lasers Conference On the development of a gas generator for CO2-N2 gas dynamic lasers utilizing liquid fuel and liquid oxidizer

Mishchenko, M.I., Yatskiv, Y.S., Rosenbush, V.K., Videen, G. (2011). Polarimetric Detection, Characterization and Remote Sensing. Proceedings of the NATO Advanced Study NATO Science for Peace and Security Series C: Environmental Security (1st ed.). Springer. ISBN 9789400716353

Monroe, C., Meekhof, D.M., King, B.E., Itano, W.M., Wineland, D.J. (1995). Demonstration of a fundamental quantum logic gate. Phys.Rev.Lett.75(25): 4714–4717.

Mooij, J.E., Orlando, T.P., Levitov, L., Tian, L., Van der Wal, C.H., LIoyd, S. (1999). Josephson persistent-current qubit. Science, 285(5430): 1036-1039.

Müller, U., Stock, G. (1997). Surface-hopping modeling of photoinduced relaxation dynamics on coupled potential-energy surfaces. The Journal of Chemical Physics, 107(16): 6230-6245.

Nahata, A., Linke, R.A., Ishi, T., Ohashi, K. (2003). Enhanced nonlinear optical conversion from a periodically nanostructured metal film. Optics Letters, 28(6): 423–425.

Nguenang, P., Jipdi, N.M., Louodop, P., Tchoffo, M., Fai, L.C., Cerdeira, H.A. (2020). Quantum interferometry for different energy Landscape in a tunable Josephson-junction circuit. Journal of Applied Mathematics and Physics, 8: 2569-2600.

Ni, Z., Liu, Q., Tang, K., Zheng, J., Zhou, J., Qin, R., Gao, Z., Yu, D., Lu, J. (2011). Tunable bandgap in Silicene and Germanene. Nano Lett. 12(1): 113-118.

Niehues, N. (1976). Thesis,Universitat Bonn Report No. Bonn-IR-76-35 (unpublished).

Nisar, S., Li, L., Sheikh, M.A. (2013). Laser glass cutting techniques. Journal of Laser Applications 4 (25), 042010: 1-11

Novotny, L., Bian, R.X., Xie, X.S. (1997). Theory of nanometric optical tweezers. Phys Rev Lett 79: 645–648.

Ol'shanii, M.A., Ovchinnikov, Y.B., Letokhov, V.S. (1993). Laser guiding of atoms in a hollow optical fiber. Optics Communications, 98(1): 77-89.

Oliver, W. D., Yu, Y., Lee, J.C., Berggren, K.K., Levitov, L.S., Orlando, T.P. (2005). Mach-Zehnder interferometry in a strongly driven superconducting qubit. Science, 310(5754): 1653-1657

Ostrovsky, V.N., Volkov, M.V., Hansen, J.P., Selstø, S. (2007). Four-state non stationary models in multistate Landau-Zener theory. Phys. Rev. B, 75(1), 014441: 1-7

Ovchinnikov, Y.B., Shul'ga, S.V., Balykin, V.I. (1991). An atomic trap based on evanescent light waves. Journal of Physics B: Atomic, Molecular and Optical Physics,24(14) : 3173-3178.

Patent, U.S. (1986). Apparatus for ptodution of three-dimensional objects by stereolithography. Justia Patents Search 4(575). Retrived. (2019).

Paz, J. P., Zurek, W. H. (2001). In: R. Kaiser, C. Westbrook, F. David (Eds.), Coherent Atomic Matter Waves, LesHouches Session LXXII, Vol. 72 of Les Houches Summer School Series, Springer, Berlin, pp.533–614.

Pedernales, J.S., Lizuain, I., Felicetti, S., Romero, G., Lamata, L., Solano, E. (2015). Quantum Rabi model with trapped ions. Scientific Report 5, 15472: 1-7.

Peeters, F.M., Devreese, J.T. (1982). Statistical properties of polarons in a magnetic field. I. Analytic results. Phys. Rev. B, 25(12) : 7281-7301.

Pekar, S.I. (1958). Theory of electromagnetic waves in a crystal with excitons. Journal of Physics and Chemistry of Solids, 5 (1–2): 11–22.

Perkins, F.K., Friedman, A.L., Cobas, E., Campbell, P.M., Jernigang, G.G., Jonker, B.T. (2013). Chemical vapor sensing with monolayer MoS_2. Nano Lett. 13(2) : 668-673.

Phillips, W., Metcalf, H. (1982). Laser deceleration of an atomic beam. Phys. Rev. Lett. 48: 596-599

Phillips, W.D. (1998). Nobel lecture: laser cooling and trapping of neutral atoms. Rev. of Mod. Phys. 70(3): 721-741.

Preskill, J. (2015). Lecture notes for Ph219/CS219: quntum iformation. Chapter 2: 1-53. Accessed online on 10th July 2019. URL: http://theory.caltech.edu/~preskill/ph219/chap2_13.pdf

Pritchard, D. E., Hermerson, K., Bagnato, V. S., Lafyatis, e., and Martin, A. G. (1987). Laser Spectroscopy VIII, ed. by Persson, W., and Svanberg, S., Berlin, Springer, 1987.

Prokof'ev, N.V., Stamp, P.C.E. (2000). Theory of the spin bath. Rep. Prog. Phys. 63(4):559-726.

Pu, J., Yomogida, Y., Liu, K-K., Li, L-J., Iwasa, Y., Takenobu, T. (2012). Highly flexible MoS2 Thin-film transistors with ion Gel dielectrics. Nano Lett. 12(8): 4013-4017.

Rabi, I.I. (1936). On the process of space quantization. Phys. Rev. 49(4) : 324-328.

Radisavljevic, B., Whitwick, M.B., Kis, A. (2011). Integrated circuit and logic operations based on single-layer MoS_2. ACS Nano 5(12): 9934-9938

Rahmani, M., Jagadish, C. (2018). Light-matter interactions on the nanoscale. Beilstein J Nanotechnol 9: 2125-2127.

Ramrakhiani, M. (2012). Nanostructures and their applications. Recent Research in Science and Technology, 4(8): 14-19

Reed, M.C., Simon, B. (1975). Methods of Modern Mathematical Physics. Volume II, Academic Press 1975. 328p.

Roszak, K., Filip, R., Novotny, T. (2015). Decoherence control by quantuim quantum decoherence itself. Scienfic Reports, 5(9796): 1-10

Saito, K., Wubs, M., Kohler, S., Hänggi, P., Kayanuma, Y. (2006). Quantum state preparation in circuit QED via Landau-Zener tunneling. Europhys. Lett. 76(22): 1-7

Sakar, A.S., Pal, S.K. (2017). Electron-phonon interaction in organic/2D-transition metal dichalcogenide heterojunctions: A temperature-dependent Raman pectroscopic study. ACS Omega, 2(8): 4333-4340

Sanvitto, D., Kéna-Cohen, S. (2016). The road towards polaritonic devices. Nature Materials 4668: 1-13

Sayed, I., Bedair, S. M. (2019). Quantum Well Solar Cells: Principles, Recent Progress, and Potential. IEEE Journal of Photovoltaics, 9 (2): 402–423.

Schlosshauer, M. (2004). Decoherence, the measurement problem, and interpretation of quantum mechanics. Rev. Mod. Phys. 76(4): 1267–1305.

Schlosshauer, M. (2007). Decoherence and the Quantum-to-Classical Transition (Springer, Berlin, 2007), second ed

Schneider, S., Milburn, G. J. (1999). Decoherence and fidelity in ion traps with fluctuating trap parameters. Phys. Rev. A 59(5): 3766-3774.

Sciara, S., Lo Franco, R., Compagno, G. (2017). Universality of Sschmidt decomposition and particle identity. Scientific Reports 7, 44675 : 1-11.

Scully, M.O., Zubairy, M.S. (1999). Amercan Journal of Physics, 67(7) :648-648.

Shahnazaryan, V. (2017). Collective quantum phenomena in the strong light-matter coupling regime. 180 ECTS Thesis submitted in partial fulfillment of a PhD Scientarium Degree in Physics. Faculty of Physical Science, Universtity of Iceland. Pges 145.

Shevchenco, S.N., Ashhab, S., Nori, F. (2010). Landau-Zener-Stückelberg interferometry. Physics Reports 492, 1: 1-30

Shi, H., Pan, H., Zhang, Y-W., Yakobson, B.I. (2013). Quasiparticle band structures and optical properties of strained monolayer MoS_2 and WS_2. Phys. Rev. B. 87(15), 155304: 1-8

Shi, Y. (1999). Quntum computation with Bose-Einstein condensates and capable of solving NP-complete and $\neq$ P problems. Accessed online on 15th June 2017. URL: https://cds.cern.ch/record/403945/files/9910073.pdf

Shimizu, Y., Sasada, H. (1998). Mechanical force in laser cooling and trapping. American journal of physics 66, (11): 960-967

Shishidou, T., Freeman, A.J., Asahi, R. (2001). Effect of GGA on the half-metalliticity of the

Shore, B. W., Knight, P.L. (1993). Topical review: The Jaynes-Cummings model. Jounal of Modern Optics, 40(7): 1195-1238.

Shytov, A. V. (2004). Landau-Zener transitions in a multilevel system : an exact result. Phys. Rev. A 70(5), 052708 :1-3.

Sicker, C., Heber, J., Berndt, B. (2016). Spatially resolved scatter measurement of diffractive micromirrors arrays. Applied Optics, 55 (16): 4467-4477

Sidis, V. (1992). Diabatic potential energy surfaces for charge-transfer processes. Advanced in Chemical Physics: state selected and state-to-state ion-molecule reaction dynamics, part II, theory, 82: 73-134.

Sillanpää, M., Lehtinen, T., Paila, A., Makhlin, Y., Hakonen, P. (2005). Continuous-time monitoring of Landau-Zener interference in a Cooper-pair box. Phys. Rev. Lett.96(18), 187002: 1-4.

Simon, D. (1994). IEEE Computer Society Press, Los Alamitos, CA : 124–134.

Sinitsyn, N. A. (2004). Counterintuitive transitions in the multistate Landau-Zener problem with linear level crossings. J. Phys. A : Math. Gen. 37(44) : 10691-10697.

Sohier, T., Calandra, M., Mauri, F. (2016). Two-dimensional Fröhlich interaction in transition-metal dichalcogenide monolayers: theoretical modeling and first-principles calculations. Phys. Rev. B 94, 085415: 1-13.

Sokol, P. (1995). In Bose Einstein Condensation, edited by A. Griffin, D. W. Snoke, and S. Stringari (Cambridge University Press, Cambridge). 51p. ISBN: 9780511524240

Stenholm, S. (1985). The semiclassical theory of laser cooling. Rev. Mod. Phys. 58(3): 699-739.

Stickney, J. (2007). A theoretical analysis of Bose-Einstein condensate basedbeamsplitters, interferometers, and transistors. PhD Thesis. 233p.

Tang, L., Kocabas, S.E., Latif, S., Okyay, A.K., Ly-Gagnon, D.-S., Saraswat, K.C., Miller, D.A.B. (2008). Nanometre-scale germanium photodetector enhanced by a near-infraed dipole antenna. Nature Photonics 2: 226–229.

Tao, R., Kamide, K., Arita, M., Kako, S., Arakawa, Y. (2016). Room-temperature observation of trapped exciton-polariton Emission in GaN/AIGaN microcavities with Air-Gap/III-Nitride distributed Bragg reflectors. J ACS Photonics, 3(7): 1182–1187.

Taylor, N. (2000). Laser: The Inventor, The Nobel Laureate, and The Thirty-Year Patent War. Simon & Schuster. ISBN 978-0684835150.

Tkach, M.V., Seti, J.O., Voitsekhivska, O.M., Pytiuk, O.Y. (2015). Renormalized energy of ground and first excited state of Fröhlich polaron in the range of weak coupling. Condensed Matter Physics, 3(18): 1-12.

Tully, J.C. (2000). Chemical dynamics at metal surfaces. Ann. Rev. Phys. Chem. 51: 153-178.

Van der Wal, C. H., Ter Haar, A. C. J., Wilhelm, F. K., Schouten, R. N., Harmans, C. J. P. M., Orlando, T. P., Lloyd, S., Mooij, J. E. (2000). Quantum superposition of macroscopic persistent-current. Science 290 : 773–777

Vidal, G., Werner, R. F. (2002). Computable measure of entanglement. Phys. Rev. A 65, 032314: 1-11

Vubangsi, M., Migueu, F.B., Kamsu, B.F., Yonya, Tchapda, L.S., Tchoffo, M., Fai, L.C. (2021). A model effective mass quantum anharmonic oscillator and its thermodynamic characterization. Journal of Applied Mathematics and Physics, 9: 306-316.

Wang, X., Deng, Y., Li, Q., Huang, Y., Gong, Z., Tom, K. B., Yao, J. (2016). Official journal of the CIOMP 2047-7538/16. Light: Science & Applications 5, e16179: 1-6

Whittaker, E. T. (1902). On the functions associated with the parabolic cylinder in Harmonic analysis. Proc. London Math. Soc. 35 : 417–427.

Wilson, C. J., Beck, P. A. (1996). Fracture testing of bulk silicon microcantilever beams subjected to a side load. Journal of Microelectromechanical System 5:142–150.

Wilson, C. J., Ormeggi, A., Narbutovskih, M. (1995). Fracture testing of silicon microcantilever beams. J. Appl. Phys., 79: 2386–2393.

Wilson, C. M., Duty, T., Persson, F., Sandberg, M., Johansson, G., Delsing, P. (2007). Coherence time of dressed states of superconducting qubit under extreme driving. Phys. Rev. Lett. 98(25), 25700:1-4

Wilson, J.A., Yoffe, A.D. (1969). The transition metal dichalcogenides discussion and interpretation of the observed optical, electrical and structural properties. Advances in Physics, 18(73): 193-335.

Wineland, D., Dehmelt, H. (1975). Principle of the stored ion calorimeter. Journal of Applied Physics, 46(2): 919-930.

Woolters, W. K. (1998). Entanglement of formation of an arbitrary state of two qubits. Phys. Rev. Lett 80(10): 2245-2248.

Wubs, M., Saito, K., Kohler, S., Kayanuma, Y., Hänggi, P. (2005). Landau-Zener transitions in qubits controlled by electromagnetic fields. New Journal of Physics, 7(218): 1-14.

Xiao-Guang, W., Chang-Pu, S. (1996). Higher-order correction for rotating wave approximation, rabi transformation, and its applications in the Jaynes-Cummings model. Acta Physica Sinica (Overseas Edition), 5(12): 881-889.

Yan, Y., Wu, B. (2008). arXiv:0811.1388v1 [quant-ph]: 1-7

Yang, C. N. (1962). Concept of off-diagonal long-range order and the quantum phases of liquyid He and of superconductors. Rev. Mod. Phys. 34(4): 694-704.

Yang, J., Pang, S., Jordan, A. N. (2017). Quantum parameter estimation with the Landau-Zener transition. Physical Review A, 96(2), 020301(R): 1-5

Ye, H.P., Wang, H.F., Yeo, S.P., Qiu, C.W. (2013). Electromagn Waves 136: 17–27.

Ye, J.T., Zhang, Y.J., Akashi, R., Bahramy, M.S., Arita, R., Iwasa, Y. (2012). Superconducting dome in a gate-tuned band insulator. Science, 338(6111): 1193-1196.

Yoon, Y., Ganapathi, K., Salahuddin, S. (2011). How good can monolayer MoS2 transistors be ? Nano Lett. 11(9) : 3768-3773.

You, J. Q., Nori, F. (2011). Atomic Physics and quantum optics using superconducting circuits. Nature 474: 589-597

Zener, C. (1932). Non-adiabatic crossing of energy levels. Proceedings of the Royal Society of London A. 137 (6): 696–702.

Zenesini, A., Lignier, H., Tayebirad, G., Radogostowicz, J., Ciampini, D., Mannella, R., Wimberger, S., Morsch, O., Arimondo, E. (2009). Time-resolved measurement of Landau-Zener tunneling in periodic potentials. Phys. Rev. Lett. 103(9), 090403:1-4

Zhang, X., Liu, Z.W. (2008). Superlenses to overcome the diffraction limit. Nat Mater 7: 435–441.

Zhong, C., Duan, C., Huang, F., Wu, H., Cao, Y. (2010). Materials and devices toward fully solution processable porganic light-emitting diodes. Chem. Mater. 23(3): 326-340.

Zurek, W. H. (1981). Pointer basis of quantum apparatus: into what mixture does the wave packet collapse? Phys. Rev. D, 24(6): 1516–1525.

Zurek, W. H. (1986). In: Moore, G. T., Scully, M. O. (Eds.), Frontiers of Nonequilibrium Statistical Mechanics, Plenum Press, New York, pp. 145–149, first published in 1984 as Los Alamos report LAUR 84-2750.

Zurek, W. H. (1991). Decoherence and the transition from quantum to classical. Phys. Today 44: 36–44.

LIST OF PUBLICATIONS

The list of publications below is relevant to the current thesis.

I. Kenfack, S.C., **Ekengoue, C.M**., Fotue, A.J., Fobasso, F.C., Bawe Jr, G.N., Fai, L.C. (2017). Laser cooling and trapping of polariton. Computational Condensed Matter 11: 47-54.

II. **Ekengoue, C.M.**, Kenfack, S.C., Fotue, A.J., Fobasso, M.F.C., Bawe, G.N. Jr., Fai, L.C. (2018). Decoherence of cooled and trapped polariton under magnetic field. Computational Condensed Matter 14: 106-113.

III. Kenfack-Sadem, C., **Ekengoue, C.M**., Danga, J.E., Fobasso, M.F.C., Nguepnang, J.V., Fotue, A.J., Fai, L.C. (2020). Laser control of magneto-polaron in transition metal dichalcogenides triangular quantum well. Physics Letters A 384, 126662: 1-11.

IV. Kenfack-Sadem, C., **Ekengoue, C.M.**, Danga, J.E., Fotue, A.J., Fobasso, M.F.C., Fai, L.C. (2020). Laser control of polariton using Landau-Zener-Stückelberg Interferometry theory.The European Physical Journal Plus 135(10): 1-24.